

THESIS

CHANGES IN WATER CHEMISTRY AND FLUVIAL GEOMORPHOLOGY FROM
ARSENIC CONTAMINATED FLOODPLAINS OF WHITEWOOD CREEK AND BELLE
FOURCHE RIVER, SOUTH DAKOTA

Submitted by

Alexander E. Marr

Department of Geosciences

In partial fulfillment of the requirements

For the Degree of Master of Science

Colorado State University

Fort Collins, Colorado

Fall 2023

Master's Committee:

Advisor: Sally Sutton
Co-advisor: John Ridley

Matthew Ross

Copyright by Alexander Marr 2023

All Rights Reserved

ABSTRACT

CHANGES IN WATER CHEMISTRY AND FLUVIAL GEOMORPHOLOGY FROM ARSENIC CONTAMINATED FLOODPLAINS OF WHITEWOOD CREEK AND BELLE FOURCHE RIVER, SOUTH DAKOTA

From 1877 to 1977 the Homestake Gold Mine in Lead, South Dakota released over 100 million megagrams (Mg) of arsenic rich mine waste into Whitewood Creek which joins the Belle Fourche River. The mine waste which contains arsenopyrite and other arsenic bearing minerals, is deposited along the floodplains of Whitewood Creek and the Belle Fourche River as overbank deposits and abandoned meander and channel fill. The introduction of mine tailings into these streams has impacted them chemically and geomorphologically for over 100 years.

This study is a continuation of the work from Ji (2021) who focused on the long-term behavior of arsenic in the mine tailings. Her work involved sequential extractions of the tailings to determine the mineralogical setting of the arsenic and its rate of release. She also used statistical regression on historical data to estimate the physical and chemical removal of arsenic from Whitewood Creek's watershed. The focus of this study is to see how the tailings might have impacted the stream chemistry of Whitewood Creek and the Belle Fourche River by modeling mineral saturation indices of the stream and seep water through the geochemical modeling program, The Geochemist's Workbench. The Geochemist's Workbench was used to model the dissolution rate of arsenopyrite to calculate the rate of dissolved arsenic entering

Whitewood Creek. Suspended arsenic entering Whitewood Creek was calculated using the dimensions of the creek bed, thickness of tailings, and density of arsenopyrite.

In addition to chemistry, this study investigated the changes in the tailings and fluvial geomorphology of Whitewood Creek and the Belle Fourche River from 1948 to 2012. This was performed by using aerial photographs from 1971, which mapped locations of the tailings along the floodplains, and overlaying them with photographs from 1948, 1977, and 2012. Using GIS through ArcMap, the tailings and their portions that have been removed over time were digitized. Other fluvial parameters that have been determined and digitized are stream longitudinal profiles, sinuosity, contaminated floodplain width, channel migration, and total sediment deposition area.

The mineral saturation indices of Whitewood Creek and the Belle Fourche River are similar to each other and differ at the most by around 2-3 orders of magnitude. The minerals that are supersaturated are mainly phyllosilicates (mostly clays), Fe, Cu and Al (hydr)oxides, and carbonates with minor sulfates and phosphates. Seep waters have lower mineral saturation indices, up to 10 orders of magnitude lower for Fe bearing minerals. The only arsenic bearing mineral that is calculated to be supersaturated is $Ba_3(AsO_4)_2$; however, this mineral has not been observed in nature.

Based on the range of possible arsenopyrite concentration in the contaminated sediment (15 to 0.11%), the calculation of dissolved arsenic being discharged out of Whitewood Creek ranges from 52 to 0.39 Mg per year. This range compares to Ji's (2021) daily dissolved arsenic rate range of 3.89-0.33 Mg/year. For a tailings width range of 0.6 to 3.5 m, the calculated rate of suspended arsenic being discharged ranges from 254 to 1.98 Mg per year. Although large, this range encompasses Ji's (2021) suspended arsenic transport rate range of 33 to 70 Mg per year.

The overlap of values from Ji's (2021) statistical approach and this study's geochemical approach indicates that arsenopyrite may be to some degree significant in controlling As transportation in Whitewood Creek.

Based on GIS results, the location and evolution of contaminated floodplains along Whitewood Creek and the Belle Fourche River are very complex. The streams are different from each other and behave as their own systems. In Whitewood Creek, locations with high tailings area and removal are controlled by a possible range of factors such as knickzone geomorphology, bedrock lithology, and changes in stream energy due to topography. In the Belle Fourche River, reaches with high tailings area and removal are found about 7 km from the Whitewood Creek confluence and a 30 km stretch where rapid floodplain reworking occurs due to neotectonics from Precambrian basement adjustments. Tailings removed area and contaminated floodplain width graphs show that the Belle Fourche River has larger storage for tailings and undergoes more floodplain reworking due to higher flood frequency and neotectonics. In contrast, Whitewood Creek has lower storage and erosion due to decreasing mine sediment load at least since 1948 and channel incision into shale bedrock in some reaches. While the reworking of tailings into the stream is lower in Whitewood Creek than the Belle Fourche River, the tailings will remain on the floodplains for many generations.

ACKNOWLEDGEMENTS

I would like to thank my advisor, Dr Sally Sutton, for her guidance, mentorship, and funding for Geochemist's Workbench. I also would like to thank my co-advisor, Dr John Ridley, for suggesting this project, his guidance, patience, and mentorship. I greatly appreciate my thesis committee member, Dr Matthew Ross, for his insightful comments.

I would like to give a big thanks to Anne (Mu) Ji for providing me with the water and sediment chemistry of the study area. I also want to express my gratitude to David Garza and Dedre Henderson from the Environmental Protection Agency for lending me the 1971 aerial photographs of the area. Without the chemistry and photograph data, this project would not have been possible.

I appreciate the faculty and staff, and graduate students at the Colorado State University Department of Geosciences for their kindness and willingness to help others. I want to thank Ellen Wohl for her help on the geomorphology portion of the thesis. I especially want to show my gratitude to my friend and colleague, Christophe Simbo, for helping me out with Geochemist's Workbench and our many geochemistry discussions.

Finally, I would not be here without the support, encouragement, patience, and love of my mom and dad. It's been a long ride on the academic road and the end appears to be in sight. Thank you so much for picking me up in the beginning and walking with me all the way to the end.

TABLE OF CONTENTS

ABSTRACT	ii
ACKNOWLEDGEMENTS	v
LIST OF TABLES.....	ix
LIST OF FIGURES.....	x
LIST OF SUPPLEMENTAL DATA INCLUDED SEPARATELY	xiv
CHAPTER 1. INTRODUCTION	1
1.1. Literature Review.....	1
1.1.1. Geochemistry of Arsenic	2
1.1.2. Arsenic Mobilization.....	3
1.1.3. Immobilization of Arsenic.....	4
1.1.4. Geomorphological-Geochemical Approach to Mine Contaminated Fluvial Systems ..	8
1.2. Purpose of Study	9
CHAPTER 2. STUDY LOCATION BACKGROUND AND HISTORY	11
2.1. Study Area Location.....	11
2.2. Homestake Mine History	11
2.3. Past Environmental and Academic Work	12
CHAPTER 3. GEOLOGICAL SETTING.....	20
3.1. Bedrock Units.....	20
3.2. Regional Geomorphology	20
3.2.1. Neotectonics at the Belle Fourche River	24
3.3. Whitewood Creek.....	25
3.3.1 Whitewood Creek Channel and Floodplain Characterization	26
3.3.2 Discharge of Whitewood Creek	28
3.3.3 Geomorphic and Environmental Changes of Whitewood Creek	28
3.4. Belle Fourche River	29
3.5. Hydrology and Chemistry of Groundwater.....	30
3.6. Geology of Homestake Mine and Contaminated Tailings.....	30
3.6.1. Lithology of Tailings Contamination	33
3.6.2. Chemical Composition of Contaminated Sediments.....	34

CHAPTER 4. GIS METHODS.....	35
4.1. Photograph Extraction.....	36
4.1.1. Georeferencing of Photographs.....	36
4.2. Digitation of Tailings Location and Removal.....	38
4.2.1. Areal Calculation of Tailings and Removed Tailings	38
4.2.2. Limitations of Digitized Tailings	39
4.3. Creation of Fluvial Parameters.....	41
4.3.1. Channel Migration.....	41
4.3.2. Total Sediment Deposition Area	42
4.3.3. Sinuosity	42
4.3.4. Contaminated Floodplain Width	43
4.3.5. Longitudinal (Long Valley) Profiles	43
CHAPTER 5. GEOCHEMISTRY METHODS.....	45
5.1. Water Chemistry from Ji (2021)	45
5.2. Missing analytes and redox potentials	46
5.3. Geochemist’s Workbench	47
5.3.1. pH and Eh Input.....	47
5.3.2. Arsenic Oxidation State Determination.....	48
5.3.3. Determination of Mineral Saturation States (SpecE8)	50
5.3.4. Water-Rock Interaction Application (REACT).....	51
5.3.5. Arsenopyrite Kinetic Dissolution	53
5.4. Determination of Rate of As Dissolution from Tailings into Stream Water.....	55
5.5. Determination of Suspended As and Sediment Transportation in Whitewood Creek.....	58
CHAPTER 6: GIS AND FLUVIAL GEOMORPHOLGY RESULTS	62
6.1. Whitewood Creek Results.....	62
6.1.1. Whitewood Creek Correlations Significance	62
6.1.2. Whitewood Creek Sinuosity and Longitudinal Profile.....	62
6.1.3. Whitewood Creek Contaminated Floodplain Width	63
6.1.4. Whitewood Creek Contaminated Sediment Area.....	64
6.1.5. Whitewood Creek Contaminated Sediment Removed Area	64
6.1.6. Whitewood Creek Channel Migration.....	65
6.1.7. Whitewood Creek Total Sediment Deposition area	65

6.2. Belle Fourche River Results.....	66
6.2.1. Belle Fourche River Correlations Significance	66
6.2.2. Belle Fourche River Sinuosity and Longitudinal Profile	66
6.2.3. Belle Fourche River Contaminated Floodplain Width	67
6.2.4. Belle Fourche River Contaminated Sediment Area	67
6.2.5. Belle Fourche River Contaminated Sediment Removed.....	68
6.2.6. Belle Fourche River Migration.....	68
6.2.7. Belle Fourche River Total Sediment Deposition Area.....	68
CHAPTER 7. GEOCHEMISTRY RESULT	70
7.1. Summary of Water Quality of Whitewood Creek, Belle Fourche River, and Seeps.....	70
7.2. As and Fe Redox Coupling	72
7.3. Minerals Saturation Results	72
7.3.1. Whitewood Creek Mountain Locations (A-E)	73
7.3.2. Whitewood Creek Great Plains Locations (F-H)	74
7.3.3. Belle Fourche River Locations (I-K).....	74
7.3.4. Belle Fourche River before Whitewood Creek (L)	76
7.3.5. <u>Whitewood Creek Seep Locations (B, G, H).....</u>	<u>77</u>
7.4. Dissolved As Transportation Rate into Whitewood Creek Stream Water	77
7.5. Suspended As Transportation Rate in Whitewood Creek Stream Water	77
CHAPTER 8. GIS AND FLUVIAL GEOMORPHOLOGY DISCUSSION	79
8.1. Whitewood Creek Discussion	79
8.1.1 Whitewood Creek Parameters Correlations	79
8.1.2. Controls on Contaminated Sediment Area in Whitewood Creek.....	79
8.1.3. Controls on Contaminated Sediment Removed Area in Whitewood Creek	83
8.2. Belle Fourche River Discussion.....	85
8.2.1. Belle Fourche River Parameters Correlations	85
8.2.2. Controls on Contaminated Sediment Area and Removal in Belle Fourche River	85
CHAPTER 9. GEOCHEMISTRY DISCUSSION	89
9.1. Comments About Mineral Saturation Indices:.....	89
9.2. Mineral Saturations in Stream Water:.....	90
9.2.1 Clay and Phyllosilicate Minerals.....	90
9.2.2. Oxides/Hydroxides	92
9.2.3. Sulfates	93

9.2.4. Carbonates	94
9.2.5. Phosphates	95
9.3. Mineral Saturation States in Seep Water.....	96
9.4. Belle Fourche River Before Whitewood Creek Mineral Saturation Indices (L).....	98
9.5. Similarity of Saturated Species Throughout Study Area	99
9.6. Arsenic Adsorption Capacity in Stream Water through Eh and pH	100
9.7. Arsenic Phases in Stream and Seeps Waters.....	100
9.8. Transportation Rate of Dissolved As in Whitewood Creek.....	103
9.9. Transportation Rate of Suspended As in Whitewood Creek.....	104
9.10. Difference Between Dissolved and Suspended As Transportation.....	105
CHAPTER 10. CONCLUSIONS AND RECOMMENDATION.....	107
TABLES	111
Chapter 5. - Tables.....	111
Table 5.1. Redox potential and average additional species concentration added to Ji (2021) water chemistry.....	111
Table 5.2. Parameters for modeling the kinetic dissolution of arsenopyrite in REACT	112
Chapter 7.- Tables.....	113
Table 7.1. Mineral Saturation Indices for Whitewood Creek Mountain Locations (A-D):.....	113
Table 7.2. Mineral Saturation Indices for Whitewood Creek Great Plains Locations (E-H):	114
Table 7.3. Mineral Saturation Indices for Belle Fourche River Locations (Location I-K):	116
Table 7.4. Mineral Saturation for Location L (Belle Fourche River before Whitewood Creek confluence).....	118
Table 7.5. Mineral Saturation Indices for Seep Locations (Locations B, G, H):.....	119
Table 7.6. Results from average transportation rate of dissolved As calculation in Whitewood Creek.....	120
Table 7.7. Results from average transportation rate of As in suspended sediment in Whitewood Creek.....	121
Chapter 8. - Tables.....	122
Table 8.1. Whitewood Creek R ² correlation of parameters from 1948-2012. Yellow highlights are significant based on Equation 6.1.	122
Table 8.2. Whitewood Creek R ² correlation of parameters from 1977-2012. Yellow highlights are significant based on Equation 6.1.	123
Table 8.3. Belle Fourche River R ² correlation of parameters from 1948-2012. Yellow highlights are significant based on Equation 6.1.	124

Table 8.4. Belle Fourche River R ² correlation of parameters from 1977-2012. Yellow highlights are significant based on Equation 6.1	125
Chapter 9. - Tables.....	126
Table 9.1. Arsenopyrite weight percentage using Ji’s (2021) suspended As 30 year transportation rate.....	126
FIGURES	127
Chapter 1. - Figures.....	127
Figure 1.1. As Eh-pH diagram.....	127
Chapter 2. - Figures.....	128
Figure 2.1. Regional location of the study area	128
Figure 2.2. Detailed view of the Whitewood Creek valley and the Whitewood Creek Superfund site.....	129
Figure 2.3. Aerial photo of the Homestake Gold Mine	130
Figure 2.4. Aerial photograph of the town of Lead, Homestake Gold Mine, Grizzly Gulch tailings impoundment, and Whitewood Creek.....	131
Figure 2.5. Sequential extraction system performed by Ji (2021)	132
Chapter 3. - Figures.....	133
Figure 3.1. Overview of the erosional/knickzone fronts in the Black Hills Region.....	133
Figure 3.2. Hydrograph showing peak discharge from 1946 to 2022 on the Belle Fourche River	134
Figure 3.3. Map of the Belle Fourche and Cheyenne River basins east of the Black Hills showing where basement rock lineaments occur	135
Figure 3.4. View of Whitewood Creek at 194th Street bridge	136
Figure 3.5. 1952 and 2012 aerial photographs of Whitewood Creek near the town of Whitewood (Reach 2).....	137
Figure 3.6. 1948 and 2012 aerial photograph of Whitewood Creek near the Belle Fourche River confluence.....	138
Figure 3.7. View of Whitewood Creek from the Vale Cutoff Road.....	139
Figure 3.8. Whitewood Creek at around the Location G.....	140
Figure 3.9. Aerial photographs of showing the abandonment of a meander between 1948 to 2012	141
Figure 3.10. View of the Belle Fourche River near Highway 34 and the village of Volunteer .	142
Figure 3.11. Field photo of uncontaminated sediment overlaid by contaminated sediment at Whitewood Creek.....	143
Figure 3.12. Auriferous sulfidic chlorite schist from the Homestake Formation.....	144

Chapter 4. - Figures.....	145
Figure 4.1. Workflow process of digitizing contaminated floodplains and their removal	145
Figure 4.2. The location of Whitewood Creek reaches.....	146
Figure 4.3. The location of Belle Fourche River reaches	147
Chapter 5. - Figures.....	148
Figure 5.1. Regional map of Whitewood Creek and Belle Fourche River with the location of Ji (2021) sample sites.	148
Figure 5.2. Arsenic concentration for stream (orange line) and seep water (blue points) for each location from Ji (2021) fieldwork.....	149
Figure 5.3. Dissolved oxygen concentration levels of stream and seep water for each location from Ji (2021).	150
Figure 5.4. pH levels of stream and seep water for each location from Ji (2021).	151
Figure 5.5. Arsenic Eh-pH diagram with stream and seep water conditions from Whitewood Creek and Belle Fourche River.....	152
Figure 5.6. Parameters calculated from initial condition from REACT.....	1533
Figure 5.7. Conceptual illustration of the mine tailings interacting with the hydrology and geology of Whitewood Creek.....	154
Figure 5.8. Example of As concentration dissolving into the stream water from arsenopyrite dissolution	155
Chapter 6. - Figures.....	156
Figure 6.1. Sinuosity index for each reach at Whitewood Creek using the 2012 channel	156
Figure 6.2. Longitudinal profile of Whitewood Creek’s reaches	157
Figure 6.3. Contaminated floodplain widths at Whitewood Creek reaches.....	158
Figure 6.4. Contaminated floodplain widths and their variation (standard deviation) at Whitewood Creek reaches	159
Figure 6.5. Distribution of contaminated sediment area and Whitewood Creek reaches.....	160
Figure 6.6. Contaminated sediment removed area at Whitewood Creek reaches.....	161
Figure 6.7. Result plot from GIS method of the channel migration at Whitewood Creek reaches	162
Figure 6.8. Result plot from GIS method of total sediment gained area at Whitewood Creek reaches.....	163
Figure 6.9. Sinuosity index for each reach at Belle Fourche River using the 2012 channel.	164
Figure 6.10. Longitudinal profile of Belle Fourche River	165
Figure 6.11. Contaminated floodplain widths at Belle Fourche River reaches.	166

Figure 6.12. Contaminated floodplain widths and their variation (standard deviation) at Belle Fourche River reaches.....	167
Figure 6.13. Result plot from GIS method of the distribution of contaminated sediment area and Belle Fourche reaches.	168
Figure 6.14. Result plot from GIS method of the contaminated sediment removed area at Belle Fourche River reaches.....	169
Figure 6.15. Result plot from GIS method of channel migration at Belle Fourche River reaches.	1707
Figure 6.16. Total sediment gained area at Belle Fourche River reaches.....	1717
Chapter 8. – Figures.....	172
Figure 8.1. Comparison of different parameters plots in Whitewood Creek.....	172
Figure 8.2. Comparison of Whitewood Creek’s contaminated sediment area and longitudinal profile.....	173
Figure 8.3. Comparison of different parameters plots in Belle Fourche River.....	174
Figure 8.4. Comparison of Belle Fourche River’s contaminated sediment area and longitudinal profile.....	175
REFERENCES	176
APPENDICES	200
Appendix 5-1. Field parameters collected of in-stream and seep water samples in Whitewood Creek and Belle Fourche River from Ji (2021).....	200
Appendix 5-2. Analytical results from Ji’s (2021) water samples.....	201
Appendix 5-3. Mineralogy of mine tailing and their respective mineral mass in weight percentage.	205
Appendix 5-4. Mean mineral composition for the Pierre Shale	206
Appendix 5-5. Temperature of stream and seep water for each location measured by Ji (2021)	207
Appendix 6-1. 1948 Whitewood Creek parameter statistics	208
Appendix 6-2. 1977 Whitewood Creek parameter statistics	209
Appendix 6-3. 1971 Whitewood Creek tailings statistics from EPA (1972).....	210
Appendix 6-4. 1948 Belle Fourche River parameter statistics	211
Appendix 6-5. 1977 Belle Fourche River parameter statistics	212
Appendix 6-6. 1971 Belle Fourche tailings statistics from EPA (1972) (up to Reach 7).....	213
Appendix 6-7. 1971 Belle Fourche tailings statistics from EPA (1972) (up to Reach 10).....	214
Appendix 7-1. Mineral saturation indices of stream water calculated by Geochemist’s Workbench at Location A (Whitetail Creek).....	215

Appendix 7-2. Mineral saturation indices of stream water calculated by Geochemist's Workbench at Location B	216
Appendix 7-3. Mineral saturation indices of seep water calculated by Geochemist's Workbench at Location B	217
Appendix 7-4. Mineral saturation indices of stream water calculated by Geochemist's Workbench at Location C	2188
Appendix 7-5. Mineral saturation indices of stream water calculated by Geochemist's Workbench at Location D	219
Appendix 7-6. Mineral saturation indices of stream water calculated by Geochemist's Workbench at Location E	220
Appendix 7-7. Mineral saturation indices of stream water calculated by Geochemist's Workbench at Location F.....	2211
Appendix 7-8. Mineral saturation indices of stream water calculated by Geochemist's Workbench at Location G.....	222
Appendix 7-9. Mineral saturation indices of seep water calculated by Geochemist's Workbench at Location G.....	223
Appendix 7-10. Mineral saturation indices of stream water calculated by Geochemist's Workbench at Location H.....	224
Appendix 7-11. Mineral saturation indices of seep water calculated by Geochemist's Workbench at Location H.....	225
Appendix 7-12. Mineral saturation indices of stream water calculated by Geochemist's Workbench at Location I	226
Appendix 7-13. Mineral saturation indices of stream water calculated by Geochemist's Workbench at Location J	227
Appendix 7-14. Mineral saturation indices of stream water calculated by Geochemist's Workbench at Location K.....	228
Appendix 7-15. Mineral saturation indices of stream water calculated by Geochemist's Workbench at Location L	229
Appendix 7-16. Plots of soluble As being released from into stream water from 0.11% arsenopyrite dissolution calculated by Geochemist's Workbench at Whitewood Creek (Locations F, G, and H).	230
Appendix 7-17. Plots of soluble As being released from into stream water from 15% arsenopyrite dissolution calculated by Geochemist's Workbench at Whitewood Creek (Locations F, G, and H).....	231

LIST OF SUPPLIMENTAL DATA INCLUDED SEPARATELY

Dataset 1- Whitewood Creek GIS

Dataset 2- Belle Fourche River GIS

Datasets includes the following:

- 1948, 1952, EPA (1972), and 1977, and 2012 aerial photographs
- Shapefiles of the channel, contaminated sediment, contaminated sediment removed, total sediment deposition, and Ji's (2021) points.

CHAPTER 1. INTRODUCTION

The occurrence of the element arsenic (As) is ubiquitous in a wide range of settings such as the atmosphere, soils, rocks, organisms, and natural waters. The release of arsenic into the environment can occur through a combination of biogeochemical, geogenic processes, and anthropogenic processes. While natural processes can contribute to significant As pollution, anthropogenic activities such as mining, agriculture, and fossil fuel combustion can leave an important impact (Smedley and Kinnibaugh, 2002). The greatest concern with As is contamination, both natural and anthropogenic, of drinking water. Groundwater in major populous regions such as Bangladesh, India, China, and Vietnam, as well as parts of the United States, is known to have high concentrations of arsenic that exceed the World Health Organization (WHO) maximum concentration limits (MCL) of 0.01 mg/l (Smedley and Kinnibaugh, 2002). The effect on people of arsenic in drinking water includes widespread chronic and severe health problems like skin, liver, kidney, and gastrointestinal cancer, as well as reproductive disorders and birth defects (Raham et al., 2009). While the cause of the As pollution in these countries is mostly geogenic (especially in the Asian countries), arsenic sourced through mining activities can damage soil and sediments in the surrounding area, resulting in polluted surface and groundwater. These contaminated soil and sediments or “tailings” can be deposited and/or reworked by rivers and streams along floodplains, increasing the contamination tens to hundreds of miles downstream (Marron, 1992). In addition to the tailings causing dynamic fluvial changes, there are changes in geochemical conditions that control the speciation of As. Knowing the specific speciation is critical since it can dictate whether the As is in solution and mobile, precipitated as a mineral, or adsorbed to another mineral’s surface.

1.1. Literature Review

The information below is an overview of literature and knowledge of As mobility and geomorphological-geochemical approaches to mine contaminated fluvial systems. The following topics includes: 1) geochemistry of arsenic, 2) arsenic mobility, 3) arsenic immobility, and 4) geomorphological-geochemical approach to mine contaminated fluvial systems:

1.1.1. Geochemistry of Arsenic

Arsenic is a metalloid commonly found in rocks, sediments, soil, and water. It is the 47th most abundant element and has an average crustal abundance of 1.5 mg kg⁻¹ (1.5 ppm) (Vaughan, 2006). Common rocks with the highest concentration of As are shale, mudstone, and slate, as well as coal. Arsenic is a chalcophile element that commonly has a strong affinity for sulfur and sulfide minerals (Noll Jr et al., 1996). Common As bearing minerals are arsenopyrite, arsenian (arsenic rich) pyrite, realgar and orpiment. Since metalloids have excess electrons and unfilled orbitals, arsenic has five oxidation states: -3, -1, 0, +3 (arsenite), +5 (arsenate) (O'Day, 2006). However, in oxidizing conditions, arsenic is more cationic in the form of As³⁺ (III, arsenite) and As⁵⁺ (V, arsenate). Due to its tendency to combine with O²⁻ and OH⁻, As will form oxyanion complexes such as AsO₄³⁻ and H₂AsO₄⁻ for As(V) and H₃AsO₃[°], H₄AsO₄⁻, and HAsO₃²⁻ for As (III) (Figure 1.1). As (III) is a concerning speciation due to its mobility, net zero charge, and toxicity (in the form of H₃AsO₃[°]) in a wide range of pH (0-9) and in semi-oxidizing and reducing conditions. As (V) on the other hand is known to have high adsorption to minerals and sediments and is especially dominant in highly oxidizing and neutral-slightly acidic conditions (in the form of H₂AsO₄⁻) (Kocar et al., 2006; Tufano et al., 2008). At near neutral-basic pH levels of 6.5 to 8.5 (which are common for drinking water), small changes in pH and

Eh can lower arsenic adsorption capacity and increase mobility (Dzombak and Morel; 1990; Smedley and Kinniburgh, 2002; Vance and Greenberg, 2010).

1.1.2. Arsenic Mobilization

The mobilization of As can be caused by three different chemical parameters: changes in pH, changes in Eh, and competition for adsorption sites from other ions.

As indicated in the previous paragraph, pH is a major control on the speciation of As and has an important effect on its adsorption, desorption, and precipitation due to pH affecting the charge of sorbent surfaces. Multiple examples of how pH can affect As will be discussed in the immobilization section below.

Changes in the Eh (reduction potential) can have a major impact on As. Changes in Eh can be caused by multiple process such as microbial processes, oxidation of sulfides, and groundwater levels which can result in the depletion of O₂ (reduction). A drop in Eh can lead to the reduction of As (V) to As (III) and/or dissolve away Fe (III) (hydr)oxides which can release As back into the environment. Although, it is debatable which of these two processes contributes the most to As solubility, total As and Fe content have a strong correlation, thus indicating that Fe (III) (hydr)oxide dissolution can impact As sorption sites and retention (Smedley and Kinnibaugh, 2002).

Another cause of As remobilization is ion competition for adsorption sites. Common “competitors” are bicarbonate, silicate, sulfate, phosphate (Gao et al., 2011). Phosphate is the biggest challenger against As due to its similar chemical properties to As(V) and its large pH range for adsorption (pH 3-10) (Jain and Loeppert, 2000). Areas with high fertilizer and pesticide

runoff such as farmlands where phosphorus is largely used are susceptible to As mobilization (Jain and Loeppert, 2000; Peryea and Kammerack, 1997).

Generally, (hydr)oxide minerals can be amorphous (poorly crystalline, i.e., ferrihydrite) and over time they'll become more crystalline (i.e., goethite, hematite) according to the Ostwald's Step Rule. Amorphous minerals have a larger surface area than crystalline minerals, and this results in more adsorption sites. However, amorphous minerals are more thermodynamically unstable than crystalline which leads to the risk of remobilizing As. According to Appelo et al. (2002), ferrihydrite can be dissolved by an incongruent reaction into more crystalline phases in reduced conditions. While dissolving Fe (hydr)oxides through reduction may lead to the release of As, under certain conditions re-mineralization can occur where As desorption is suppressed (Fendorf et al., 2010). Interestingly, As along with phosphate oxyanion complexes has been shown to promote stability instead of dissolution of Fe (hydr)oxides and prevent the transformation from an amorphous phase to a more crystalline phase (Rancourt et al., 2001; Borch et al., 2007).

1.1.3. Immobilization of Arsenic

Arsenic in near surface conditions can be immobilized through adsorption to mineral surfaces and precipitation as secondary minerals. Adsorption is the principal control of As mobilization due to the ability to transfer mobile As to particulate phases (Wang and Mulligan, 2006). Potentially the most important group of sorbents (sediment, mineral surface, and/or collection of minerals like colloids where adsorption occurs) are Al, Mn, Fe (hydr)oxides which are ubiquitous in soil in the form of discrete particles or coatings on mineral surfaces (Wang and Mulligan, 2006). As (III) and As (V) are known to form inner surface complexes on the surfaces of (hydr)oxides by ligand exchange of OH^- and OH_2 . The bonds of these complexes are more

covalent making it difficult for As to mobilize. However, As (III) can form outer-sphere complexes, as well, through electrostatic interactions. In contrast to inner surface complexes, the bonds of outer-sphere complexes are weaker and As is more likely to remobilize (Wang and Mulligan, 2006). In Al (hydr)oxides As (V) and As (III) form inner sphere complexes with gibbsite and Al oxides although As (III) can form outer sphere complexes (Wang and Mulligan, 2006). On an amorphous Al oxide surface, As (V) adsorption increases at pH 7 and decreases significantly at higher pH while As (III) adsorption occurs at pH 6-9.5, and decreases as pH increases or decreases (Ghosh and Teoh, 1985; Cox and Ghosh, 1994). Mn (hydr)oxides are known to oxidize As (III) to As (V) while reducing Mn (III and IV) (Manning et al., 2002; Oscarson et al., 1981). Fe (hydr)oxides are very important sorbents for As due to having a high net positive charge in most geological settings and having high affinities for As species. Both As (III) and As (V) can form inner sphere complexes with these minerals (Wang and Mulligan, 2006). According to Pierce and Moore (1982), As (V) can adsorb optimally between pH 4-7 while As (III) adsorbs optimally between pH 7-10.

Clay minerals are ubiquitous in terrestrial and aquatic environments. Due to their different structures, As adsorption on clay minerals is complex. Around mid-range pH, clay minerals generally have higher As (V) adsorption and while As (III) adsorption increases at higher pH (around high pH, As (III) has a net negative charge, see Figure 1.1) (Lin and Puls, 2000). Arsenic adsorption on 1:1 clays was found to be moderate to high with kaolinite where the greatest adsorption of As (V) was at pH 5 (Goldberg, 2002). It has been suggested by Manning and Goldberg (1997) that the octahedral Al-OH component is more reactive to As(III). Since kaolinite has alternating tetrahedral and octahedral sheets, with exposed Al-octahedral sheets, it should favor adsorbing As (III) (Lin and Puls, 2000). Lin and Puls (2000) suggested

that halloysite (hydrated kaolinite) has greater As (V) adsorption than kaolinite. This is possibly caused by a hydroxy-arsenate interlayer that is formed in the halloysite from precipitation of high As (V) concentrations and helps cause As(V) to be lightly affected by pH increase. For 2:1 clays, montmorillonite and illite have moderate adsorption with the highest adsorption capacity at pH 6.0 for montmorillonite and 6.5 for illite for As (V) (Manning and Goldberg, 1997). These types of clays have higher adsorption for As (V) than As (III). However, Lin and Puls (2000) found that illite and montmorillonite have higher As (III) adsorption than the kaolin minerals due to finer particle sizes that can create more broken Al-OH bonds on the solid's edges. The 2:1:1 clay, chlorite, has greater As (V) adsorption as well as As (III) and is little affected by pH increase. This adsorption is possibly controlled by the Fe content of chlorite, the hydroxide sheet interlayer, and/or the broken Al-OH bonds on the solid's edges. The Fe in the chlorite, as well as impurities in other clays, can form Fe hydroxide complexes, as mentioned above, which can have high affinities for As(V) and As(III).

There is a debate however over the significance clay minerals play in collecting trace metals in aquatic environments (Horowitz and Elrick, 1988; Jeane, 1976). In general, there is a consensus that clay minerals are not as important as As sorbents as organic matter and oxide minerals (Miller and Miller, 2007). Although not entirely demonstrated, Jeane (1976) proposed that clay minerals serve as substrates for the precipitation and accumulation of organic matter, Fe, and Mn hydroxides due to their large specific surface area. These coatings are where the accumulation of trace metals occur that are associated with clay minerals.

The presence of divalent cationic elements such as Ca^{2+} and Fe^{2+} in hydr(oxide) structures can increase As adsorption by increasing positive charge on the adsorbent surface. Ca^{2+} helps increase As (V) adsorption on Al oxides at pH 8, and ferrihydrite at pH 9 (Ghosh and

Teoh, 1985; Wilkie and Hering 1996). However, this will also help promote the adsorption of phosphate (Antelo et al., 2015). In contrast, Ca^{2+} and Mg^{2+} can help decrease the competitive effect of silicate on As (Meng et al., 2000). With the presence of Ca^{2+} and HCO_3^- , calcite is a common precipitate. In addition to buffering the pH, calcite can play an important role as an adsorbent. According to experimental work by Sørensen et al. (2008), As (V) sorbs to calcite in oxidizing conditions in the form of H_2AsO_4^- and CaHAsO_4^0 while As (III) cannot sorb in reducing conditions. They also found that in conditions with decreasing alkalinity, the sorption of As (V) on calcite can increase, however competition with As (V) and (bi)carbonate can also increase. On the other hand, an increase in alkalinity can increase As (V) and phosphate adsorption on calcite as well (House and Donaldson, 1986; Goldberg and Glaubig, 1988). In addition to promoting As adsorption, some cations such as V and Se adsorb similarly to As, which increases competition for sites (Vance and Greenburg, 2010).

Another way to reduce the mobility of arsenic is through precipitation. There are more than 300 As bearing minerals of which 60% are in the form of arsenates, 20% sulfides and sulfosalts, 10% oxides, and the rest as arsenites, arsenides, native, and metal alloys (Bowell and Parshley, 2001). The most common secondary As bearing mineral is Fe-arsenate scorodite ($\text{FeAsO}_4 \cdot 2\text{H}_2\text{O}$) under acidic Fe (III)-As(V) conditions, usually formed as a product from weathered arsenopyrite and arsenic rich pyrite (Drahota and Filippi, 2009). In addition to Fe, arsenates can form precipitates with Ca and Mg. Common Ca-arsenates include pharmacolite ($\text{Ca}(\text{HAsO}_4) \cdot 2\text{H}_2\text{O}$), weilite (CaHAsO_4), and hornesite ($\text{Mg}_3(\text{AsO}_4)_2 \cdot 8\text{H}_2\text{O}$) (Drahota and Filippi, 2009). Arsenate can also substitute for other anion complexes with “O₄” such as SO_4^{2-} in jarosite ($\text{KFe}_3(\text{SO}_4)_2(\text{OH})_6$) (Savage et al., 2000) and PO_4^{3-} in apatite ($\text{Ca}_5(\text{AsO}_4)_3\text{-OH}$) (Bothe and Brown, 1999). Another relatively common secondary arsenic mineral is the cubic oxide

arsenolite (As_2O_3) and its monoclinic dimorph, claudetite. These minerals are often oxidation products of arsenopyrite and weathered scorodite (Drahota and Filippi, 2009). According to an experiment by Pokrovski et al. (1996), arsenolite and claudetite can dissolve at pH levels <8 (at temperature $90\text{ }^\circ\text{C}$) and Nordstrom and Archer (2003) found that these oxides are stable in equilibrium with high pH waters. Haffert and Craw (2008) suggested that due to the high solubility of these minerals in water and acid, they may strongly influence As concentration in waste water from acid mine drainage. In addition to arsenic bearing minerals, arsenic can be precipitated in ferric oxyhydroxide minerals such as goethite and ferrihydrite. These minerals can form weathering crusts as well as coatings on As primary minerals like arsenopyrite, which can help reduce the dissolution of arsenic into the environment (Bowell, 1994; Matera et al., 2003; Larios, et al., 2012).

1.1.4. Geomorphological-Geochemical Approach to Mine Contaminated Fluvial Systems

Since the 1970s, a large amount of research in North America and Europe identified the spreading, storage, and remobilization of metal rich sediments in fluvial systems and how they can be directly related to sediment transportation, river channel and floodplain sedimentation styles, and flooding regime (refer to Macklin et al. (2006) for complete sources). The rise of such research is due to the transportation of 90% metal contaminants in rivers as particulate forms, which follow the same transport pathways as natural sediment load (Martin and Meybeck, 1979). This coins the idea that if the spatial and temporal dynamics of river sediment can be modeled and understood, then the long term and large-scale distribution of metal rich sediments in a river system can be predictable. This approach to environmental management is coined by Macklin et al. (1999) as “geomorphological–geochemical”. The first systematic review of metal mining in a river system through a geomorphological viewpoint was by Lewin and Macklin (1987). This

research included documents of physical and chemical factors that control the dispersal and storage of metal contaminated sediments on spatial and temporal scales. They also recognized that the mining material can be transported as sediment in the river and not disrupt the channel and floodplain processes. The term for this is “passive dispersal” in contrast to “active transformation” where the fluvial system is altered by the mining sediment input (Lewin and Macklin, 1987). According to Macklin et al. (2006), these two terms are end members of a continuum involving mining related channel changes. This classification scheme has been used worldwide (Benito et al., 2001; Miller 1997; Marron; 1992; Knighton, 1991) to model the distribution of heavy metal rich sediments by fluvial processes and predict patterns and rates in river basins affected by mining. Hudson-Edwards (2003) emphasized the long-term impact of mining on the fluvial environment and the mineralogy and chemistry of heavy metal sediments. The frequency and severity of flooding and droughts are important controls on river dynamics which in turn can significantly affect metal bearing deposits through floodplain reworking (Goudie, 2006; Macklin et al., 2006).

1.2. Purpose of Study

The purpose of this study is to investigate how As rich mine tailings on floodplains are spatially distributed and reworked over time; what is the fate of the As when it is introduced to the stream water; and what potential minerals may be in equilibrium in the stream and seep water. This project is a geomorphologic-geochemical approach to the continuation of Ji’s (2021) study of historic mine tailings on Whitewood Creek and the Belle Fourche River in South Dakota. Ji’s (2021) recommendation for additional work that is incorporated into this project includes the following:

- Identify and monitor floodplains contaminated sediment and their erosion on Whitewood Creek and the Belle Fourche River to identify future movement of contaminated sediments and where bank stability can be developed.
- Model mineral saturation indices in the waters of Whitewood Creek and Belle Fourche River to see what minerals and As bearing minerals are thermodynamically predicted to precipitate.
- Model the daily release of dissolved and suspended As as a result of contaminated sediment being added to the waters of Whitewood Creek.

CHAPTER 2. STUDY LOCATION BACKGROUND AND HISTORY

This chapter will present the history of the Homestake Gold Mine and the environmental and research work on its pollution of the Cheyenne River Basin.

2.1. Study Area Location

The study area is located at the northeastern base of the Black Hills in Western South Dakota (Figure 2.1). The mine tailings originated at the Homestake Gold Mine in the town of Lead in the northern Black Hills. This research will focus on portions of Whitewood Creek from Lead to the confluence with the Belle Fourche River and 30 km of the Belle Fourche River downstream from the confluence.

2.2. Homestake Mine History

The Homestake Mine was the largest and deepest gold mine in North America (see Figure 2.3). The major ore was gold along with minor silver (Smith, 2003). The mine operated from 1877 to 2002. During the first 100 years of operation (1877-1977), between 893 to 1101 megagrams (Mg) of gold was extracted from the mine (Marron, 1992; Caddey et al., 1991; Homestake Gold Mine, 1976). However, approximately 110 million Mg of As enriched mine tailings from the Homestake Gold Mine were discharged into Whitewood Creek and its tributaries: Belle Fourche River and Cheyenne River (Marron, 1992). The floodplains of Whitewood Creek, Cheyenne, and Belle Fourche Rivers still contain a significant portion of the tailings in their storage (Marron, 1992; Goddard, 1987; Cherry et al., 1986).

During early operations, ores were crushed by crude methods and gold was recovered by gravity or mercury amalgamation. By 1880, 60 stamp mills with more than 1000 stamps were set up where ore was crushed to coarse grain size (Cherry et al., 1986). Prior to the turn of the 20th century, most of the ore came from oxide and hydroxide minerals in oxidized zones, and

paleoplacer deposits. The oxidation products are from arsenopyrite, pyrite, and pyrrhotite. By the turn of the century, the mining operation focused below the zone of oxidation (Wuolo, 1986). Large amounts of reduced ores and minerals such as arsenopyrite and pyrrhotite were extracted. The use of cyanide along with mercury in the milling process began during this time. Around 5,000 Mg of tailings were processed each day (Cherry et al., 1986; Wuolo, 1986). Rod and ball milling techniques were used which helped yield finer grains of tailings (Marron, 1992). As the mine became deeper, mine tailings began to accumulate and be discharged to Whitewood Creek. By 1917, the Homestake Gold Mine became the only contributor to filling Whitewood Creek with tailings as other mills in the area ceased operations. By 1955, approximately 50% of mine tailings produced each year were used as backfill in the mine shafts (Waterland, 1973). To comply with early 1970's environmental regulations (such as the EPA's Ore Mining and Dressing Effluent Guidelines), the Grizzly Gulch tailings impoundment dam was created for the tailing storage (see Figure 2.4, located near Lead, 4.8 km south of the mine) (EPA, 2012; Wuolo, 1986). Despite no tailings discharge since December 1977, there are still large concentrations of contaminated sediments, surface water, and groundwater downstream from the mine.

2.3. Past Environmental and Academic Work

Prior to the Clean Water Act of the 1970s, Whitewood Creek did not undergo any environmental regulation. The sanitation districts of Lead and Deadwood released raw sewage that went untreated into the creek. The mix of sewage and mine tailings caused Whitewood Creek to flow black according to local residents (Marron, 1987). This resulted in Whitewood Creek's lack of support for aquatic life (Goddard, 1989; S.D. Dept. of Game, Fish and Parks et al., 2005). In 1978, Stach et al. (1978), found dissolved As concentrations ranging between 2.5-1530 $\mu\text{g/L}$ in well water near large deposits of contaminated sediments. This research provided evidence of possible environmental hazard along Whitewood Creek. Prior to this report, 50

Holstein dairy cattle, part of a dairy operation adjacent to Whitewood Creek, died from an unknown cause during the winter of 1974-75. According to the South Dakota State University Department of Veterinary Science, the cattle died from As poisoning due to consuming corn silage which had been contaminated with mine tailings during silo-filling operations (Bergeland et al., 1976).

Because of the poorly understood spatial extent of the possible environmental hazard and effects on of approximately 85 people and several residences (EPA, 2017), the EPA listed a 30 km length of Whitewood Creek and Belle Fourche River as an Interim Priority Site under the Comprehensive Environmental Response Compensation and Liability Act (CERCLA) in 1981 (see Figure 2.1 and 2.2 for location). By 1983, the EPA added Whitewood Creek to the National Priorities List (NPL), creating the Whitewood Creek Superfund site (EPA, 2017). The Homestake Mining Company made remedial actions in 1984 such as installing a wastewater plant to treat effluent from mining operations discharging into Whitewood Creek (S.D. Dept. of Game, Fish and Parks et al., 2005) and removing 4,500 cubic meters of contaminated sediments from 16 residential yards (EPA, 2017). The Homestake Mining Company also funded several comprehensive environmental studies such as Fox Consultants Inc. (1984a and 1984b) and Cherry et al. (1986).

In the Fall of 1982, the USGS with the cooperation of the South Dakota Department of Water and Natural Resources conducted a 2-year long basin-wide study of the hydrologic effects of the contaminated sediments. This research was used to help accurately evaluate the potential hazards of the Interim Priority Site (Goddard, 1988a). While working simultaneously with the USGS's investigation, Fox Consultants, Inc. (1984a and 1984b) conducted their study on the alluvial aquifers along Whitewood Creek and Belle Fourche River. They issued a series of

unpublished reports in two phases: Phase I discusses field procedures, data, data-analysis control procedures, and a general overview of the study area. Phase II interprets data from Phase I along with a literature review of the topic of concern (Goddard, 1988a). Additional interpretations of the data collected by Fox Consultants, Inc., are presented by Cherry et al., 1986. In 1985, the Whitewood Creek-Belle Fourche River-Cheyenne River-Lake Oahe system was selected by the USGS for its Toxic Substances Hydrology Program--Surface Water Contamination program. The goal of this program is to improve the understanding of how toxic substances enter, are transported, and are removed from surface water systems (Mallard, 1987; Mallard and Ragone, 1988). Basic data collected during the USGS research on tailing contaminations of the Cheyenne River Basin for 1985 and 1986 can be seen in Goddard (1988b) and for 1987 and 1988 can be seen in Goddard (1990). Geochemistry of the floodplain deposits of Whitewood Creek and Belle Fourche River from the USGS studies are summarized by Goddard (1989). On a larger scale, research has been done on how As behaves as a whole in the Whitewood Creek-Belle Fourche-Cheyenne River-Lake Oahe system (Horowitz et al., 1988; Horowitz and Kent, 1990).

Results from the 1980s work shows that the presence of Fe (hydr)oxides as coatings on grain surfaces are the dominant control of dissolved As in the stream water of Whitewood Creek (Cherry et al., 1986; Goddard and Wuolo, 1987; Fuller et al., 1987; Goddard, 1989). Horowitz and Kent (1990) used SEM on the bank and floodplain deposits from Whitewood Creek and Belle Fourche River and found that the major source of As is in Fe oxide coated arsenopyrite. They found that approximately 80% of the As is associated with the sulfide phase while 20% is in the Fe oxides. Fuller et al. (1987) found that the dominant As species is in the form of As (V). The immobilization of As is due to adsorption on Fe oxyhydroxide surfaces on mineral grains (such as arsenopyrite) or precipitation into secondary iron-arsenate minerals (i.e. scorodite)

according to Cherry et al. (1986) and Fuller et al. (1987). Maximum As adsorption occurs at the pH of 6.5 and begins to desorb when the pH goes to 8.5 (Goddard and Wuolo, 1987). Cherry et al. (1986) observed that As release is not dependent on the bacterial oxidization of arsenopyrite. They also found that most of the As is in a solid phase and is not readily soluble, this will result in the contaminated sediments remaining in place for potentially hundreds to thousands of years (Cherry, et al., 1986; Marron, 1989; Goddard, 1989).

One interesting study from the 1987 investigation was conducted by Rees and Ranville (1988) who identified colloid compositions in the waters of Sheeler seeps (Location H, by the Whitewood Creek-Belle Fourche River confluence, see Figure 5.1) and Whitewood Creek. This is an interesting site since the creek downcuts through a historic meander that is filled with tailings and into shale bedrock. Water samples were taken from Whitewood Creek and seeps and analyzed for various chemical components after separation into aliquots that passed 400-, 100-, and 50-nm Nucleopore filters or were unfiltered. Analysis of suspended colloids were determined using photon correlation spectrometry (PCS) and the filtered material was examined through scanning electron microscope (SEM)/X-ray analysis (Rees and Ranville, 1988). Results from the SEM showed that the colloids in the stream water of Whitewood Creek are mostly clay with little Fe. No particles were retained on a 100 nm filter after filtered through 400 nm filters except for calcite and amorphous Fe-oxides. Colloids collected from the seep water comprise amorphous Fe hydr(oxides), crystalline silica with no coating of Fe, and platy Fe coated Ca silicates with a wide range of dimensions from 200-1,000 nm. In addition, a single 700 nm gypsum crystal was found. A third water sample was analyzed from a quiet pool which includes a diversity of minerals such as several non-crystalline calcium-potassium aluminosilicates, well crystallized gypsum, polyframboidal pyrite, magnesium-calcite crystals, and a Ti rich particle

(rutile, brooksite, or anatase). In general, particles with a dimension range 100-400 nm are more abundant at the seep and pool than the creek (Rees and Ranville, 1988).

In the 1990s, Gomez and Marron (1991) investigated how neotectonics affect the sinuosity and channel migration of the Belle Fourche River. Marron (1992) the following year would also publish a sediment budget of the contaminated floodplain deposits in the Belle Fourche River system. Her research estimated that 127×10^6 Mg of tailings were produced from Homestake during its first 100 years of operation (1877-1977). However, only 110×10^6 Mg were discharged into Whitewood Creek while the rest were backfilled in the mine. Of the 110×10^6 Mg discharged tailings, 13% remain in the floodplains of Whitewood Creek (14.5×10^6 Mg), and 29% in the floodplains of Belle Fourche River (31.9×10^6 Mg). The remaining have been transported to the Cheyenne River and settled on its floodplain and/or settled in Lake Oahe. In Whitewood Creek, of the 14.5×10^6 Mg tailings stored, less than 1.0×10^6 Mg are stored between Lead and Whitewood, 5.8×10^6 Mg 20 km downstream of Whitewood, and 8.7×10^6 Mg 6 km before the confluence with the Belle Fourche.

By 1996, the EPA took Whitewood Creek off the NPL (EPA, 2017). The USGS continued to investigate the effect of As contaminated alluvium of Whitewood Creek, Belle Fourche River, and Cheyenne River on benthic flora and processes that control dissolved As (Kuwabara and Fuller 2003). Recent chemical work in the area includes further investigation of metals in the Belle Fourche and Cheyenne Rivers fluvial deposits by Stamm and Hoogstraat (2012), As geochemistry in sediment and pore waters by Pfiefler and Stone (2011) and Pfiefler et al. (2018), bicarbonate and phosphate effects on As release from mine tailings in the Cheyenne River by DeVore et al. (2019), As remediation through plant roots by DeVore et al. (2021), the mobilization of As by microbial reduction by DeVore et al. (2022), and long-term arsenic

behavior in the contaminated sediments of Whitewood Creek and Belle Fourche River by Ji (2021). Other recent work in the area involving geomorphology includes stream erosion and terrace development in the Cheyenne/Missouri River areas (Zaprowski et al., 2001; Stamm et al., 2010; Stamm et al., 2013), modeling and predicting suspended contamination route and storage in the Belle Fourche River (Pizzuto, 2020) and modeling climate change effects on mine tailings of the Cheyenne River system (Shockley, 2021).

The previous work above shows that the As rich sediment behavior is dynamic and unstable due to physical and chemical sediment transportation, active dissolution, and gradual pore water flushing (Pfeifle et al., 2018). Pfeifle et al. (2018) found that As was associated with amorphous, poorly crystalline, and inert highly crystalline iron oxyhydroxides in the sediments. Pore water redox gradients have a major control on As mobilization where reducing conditions dissolve iron oxyhydroxides and release As. DeVore et al. (2019) showed that the introduction of phosphate and bicarbonate to Whitewood Creek tailings causes significant As mobilization due to anion competition. They also found through Mossbauer analyses, that goethite is present in the sediments and may play an important role in As binding. DeVore et al. (2021) found that As-rich sediment along the Cheyenne River can accumulate in plant roots (Little Bluestem) that are amended by endophytic fungi. Arsenic was found to adsorb and/or precipitate with Ca-P minerals on the roots. DeVore et al. (2022) discovered that As release from mine tailings is also strongly controlled by microbial reduction in mine tailings in the Cheyenne River. Ji (2021) concluded that the overall environmental quality of the Whitewood Creek/Belle Fourche area has improved due to environmental regulations and institutional control. She also found that As dissolution into the environment is slow and minimal with the low amount of breakdown products from arsenopyrite dissolution most likely due to coating by Fe oxyhydroxides. Through

sequential extraction, Ji (2021) used deionized water, sodium phosphate, hydroxylamine hydrochloric acid, and hydrochloric acid to determine residence sites of As in the tailings (refer to Figure 2.5 for details of the extraction). She found that 40% of the As in system is labile (0.37% to weakly bounded exchangeable surface sites and water-soluble secondary minerals, 11% to weakly bound organics or exchange sites, 4.8% to weakly bounded amorphous to weakly fine grained oxides/hydroxides, reducible phases, other surface sites, or soluble carbonates, and 24% moderately strong bounds to weakly soluble secondary minerals like clays or crystalline oxides/hydroxides). The remaining 60% are immobile, probably encased in arsenopyrite due to oxyhydroxide coating slowing down dissolution.

She also found that there are no continuous tailings horizons due to variation in thickness, geometry, and lateral extent. For example, a 4 m cutbank at Location G (see Figure 5.1 for location) has only 0.6 m of contaminated sediment on the top followed by 2.4 m of uncontaminated alluvium, and 1 m of shale bedrock. At Location H (see Figure 5.1 for location) however, a 4.5 m cutbanks has 3.5 m of contaminated sediments and 1 m of shale bedrock. Ji (2021) also estimated the annual suspended and dissolved As using a 30 year period (1982-2012) to find the total As transport rate. She used USGS historical databases from the stream gages of Whitewood Creek (Above Whitewood and Above Vale, see Table 5.1) to compile dissolved As concentration, suspended sediment flux, and stream discharge. She also used three different methods such as raw data averaging, rating curves, and As distribution percentage to find average transportation rate. Her findings predict that the total As transportation rate out of the Whitewood Creek drainage basin was estimated to be 34 to 71 Mg per year where total dissolved As ranges from 0.33-3.89 Mg/year and average suspended As ranges from 33-70 Mg per year. At this rate, it would take between 250-1500 years to clear As from Whitewood Creek, however,

this is based on uniform movement of uniformly distributed sediment. Similarly, using models to compute long term timescales across watersheds, Pizzuto (2020) showed that the time to remove As enriched tailings on a 112 km reach on the Belle Fourche River would be approximately 750 years. Overall, the total transportation rate of As in Whitewood Creek has been stable over the last 30 years (Ji and Ridley, 2013). If the regional climate remains the same and As continues to be diluted by uncontaminated sediments, then As will remain stable. However, if the climate changes, changes in pH or Eh or other conditions (such as exposing buried material and change in water table depth), and bank stability failures continue, then As will continue moving downstream (Ji, 2021). Similarly, Shockley (2021) concluded that climate change plays a major role in the mobilization of As in the Cheyenne River Basin. She said that mitigation actions are important to minimize erosion, transportation, dissolution/solubility, and may be adjusted in response to climate change variability. Previous geomorphology work from the area shows that bank stability is a concern for Whitewood Creek and the Belle Fourche River since the regional geomorphology includes active channel adjustments, resulting in unstable channels (Stamm et al., 2013; Stamm et al., 2010; Zaprowski et al., 2001).

CHAPTER 3. GEOLOGICAL SETTING

This chapter will present the geology of the study location and include the following topics: 1) bedrock units, 2) Whitewood Creek's geomorphology and hydrology, 3) Belle Fourche River's geomorphology and hydrology, 4) groundwater hydrology and chemistry, 5) regional geomorphology, and 6) geology of mine tailings.

3.1. Bedrock Units

Whitewood Creek is situated on the northeastern edge of the Black Hills uplift which is composed of Precambrian gneiss, schist, and granitic intrusions. The flanks of the uplift expose steeply dipping sedimentary rocks. Within the Whitewood Creek area, the bedrock consists mostly of shale with lesser amounts of argillaceous sandstone and limestone. These rock units range in age including Permian (Minnekahta Limestone and Minnelusa Formation), Triassic (Spearfish Formation), Jurassic (Morrison Formation, Gypsum Spring, Sundance Formation), and Cretaceous (Lakota Formation, Fall River Formation, Mowry Shale, Belle Fourche Shale, Greenhorn Formation, Carlile Shale, Niobara Formation, and Pierre Shale). Most of the area in this research is underlain by the Pierre Shale. The ages get progressively younger from west to east and south to north. Various shale strata in the area are slightly permeable at shallow depths from vertical joints and horizontal bedrock fractures (Cherry et al., 1986).

3.2. Regional Geomorphology

Zaprowski et al. (2001) recognized and mapped two erosional knickzone fronts in the Cheyenne and Belle Fourche River watersheds. The term "knickzone" is similar to the term "knickpoint", however, a knickzone has a more subtle change in channel slope over kilometers while a knickpoint is an abrupt change in a short distance (e.g., like a waterfall). Identifying knickzones is difficult in the field; it is easier to identify them in a river longitudinal profile. In

the Black Hills area, Zaprowski et al. (2001) correlated the knickzones to the terraces of the Black Hills region (from oldest to youngest: Mountain Meadow, Rapid, Sturgis, Bear Butte, and Farmington). While there were 4 knickzones migrating upstream from the Missouri River, Zaprowski et al. (2001) identified two young knickzone fronts in the Black Hills that are associated with the Sturgis (older) and Farmington (younger) terraces (see Figure 3.1). These knickzones represent erosional fronts upstream from the Cheyenne and Belle Fourche Rivers. At and below a knickzone, the channel can incise through the alluvium and into the bedrock, resulting in floodplain abandonment and terrace formation. Above a knickzone, there is less channel incision, forming a broad valley bottom (Zaprowski et al., 2001).

The causes of the knickzone mechanism and active geomorphology adjustments in the Cheyenne River Basin is complex. In the Black Hills, there are three major regional geomorphological factors and an anthropogenic factor that affect or may affect the fluvial geomorphology of Whitewood Creek and Belle Fourche River. The first is stream piracy. Stream piracy plays an important role in the geomorphology of the Black Hills region, especially in the northern part (Darton, 1909). Stamm et al. (2013) used optically stimulated luminescence (OSL) and radiocarbon to estimate the age of the terraces (as mentioned in the previous paragraph) in the Belle Fourche and Cheyenne Rivers area. Results show that the incision to the level of the Bear Butte terrace was around ~63 ka, Farmington terrace around ~40 ka, and modern levels around ~12-9 ka. They proposed that around 22-21 ka, the ancestral Belle Fourche River pirated the headwaters of the ancestral Little Missouri River. This results in an increase of discharge for the capturing Belle Fourche River, causing an increase in incision and lowering the base level (Zaprowski, 2001).

Another factor is the response of incision in the lower reaches of the Cheyenne River from glacial isostatic rebound. Glaciation plays a major role in flow in the Missouri River Basin. Todd (1914, 1923a, and 1923b) proposed the Missouri River formed along the margins of a blockading continental glacier and by east-west flowing streams that were detouring around the ice pouring into the river. Plumley (1948) found terraces in the eastside of the Black Hills and proposed that their formation might be correlated to the last glaciation stage in eastern South Dakota by downstream blocking of the ice sheets in the Missouri River. Before the appearance of glaciers, streams in the region used to flow from west to east (Hoagstrom, 2006). Once the glaciers receded, the channels and floodplains dynamically coevolved together. These are important components controlling water and sediment (Belmont, 2011). Although the location of the Black Hills region was south of the edge of the continental ice sheet in the north, Zaprowski and Floyd (2005) showed that non-glaciated landscapes on the hinges of glaciated areas can still be affected, even after crustal modification. In the Lower Cheyenne River, incision was as large as 80 m around the time of ~63 ka and ~40 ka (Stamm et al., 2013). According to Stamm et al. (2013), 40 m (out of 80 m) of incision in the lower Cheyenne River might have been associated with glacial isostatic rebound.

The third geomorphic factor is the change of climate from glacial to interglacial. During interglacial periods, there is less sediment influx compared to glacial periods, which results in the increase of incision in the streams (Vandenberghe, 1995). The Northern Plains Region is an area of concern since it can be vulnerable to flooding, drought, and rising temperatures from changing climate (Reidmiller et al., 2018). Knowles et al. (2006) showed that rainfall is occurring more than snowfall and Mote (2003) indicated that the snowpack in the Western United States is decreasing. McCabe and Wolock (2020) found from 1900-2014 runoff data in the United States

that drought events occurred before 1970 followed by pluvial (rain periods) with an increase in precipitation during the Fall (Oct-Dec) in the following years. While flood peak distribution is difficult to determine due to distinctions between man-made and natural variations (Villarini et al., 2009), and having data only going back to about 100 years in the majority of studies.

Shockley, (2021), Kibria et al. (2016), and Norton et al. (2014) observed that there is an upward trend in observed streamflow within the study area from USGS gaging stations from 1960-2011, although Kibria et al. (2016) did not see any significant trends in rainfall. Sando et al. (2008) indicates that South Dakota is progressively becoming semi-arid which helps increase drought conditions. These conditions deplete vegetation cover and help increase peak flow potential. Figure 3.2 shows a hydrograph of the Belle Fourche River near Volunteer (Location K, see Figure 5.1) from 1946 to 2022 where peak discharge has been increasing since the 1980s.

A fourth factor is through anthropogenic activities such as the creation of the Lake Oahe dam are a major factor in establishing new stream base levels. With the establishment of the Lake Oahe dam, suspended sediments are deposited in deltaic and benthic sediments when the river water enters the lake, helping to establish a new base level (Shockley, 2021).

With the presence of the knickzones and incision in the lower Cheyenne River, this indicates that the watershed of the region is still adjusting to these geomorphic factors, resulting in continuing channel instability (Zaprowski et al., 2001; Stamm et al., 2010; Stamm et al., 2013). This may play a major role in the mine tailing storage of Belle Fourche and Cheyenne Rivers (and most likely Whitewood Creek) which could leave them vulnerable to tailing remobilization.

3.2.1. Neotectonics at the Belle Fourche River

Although this may be more local than regional, there is another geomorphic factor that can affect mine tailing storage. On the Belle Fourche River, Gomez and Marron (1991) identified a relationship between sinuosity and floodplain/channel slope within 17 reaches along an 81-kilometer section of the river (starting at the Whitewood Creek confluence and ending near the Elm Creek confluence, see Figure 3.3). Reaches 1-7 are within the Belle Fourche River portion of this project (see Figure 4.3). At the beginning and end (Gomez and Maroon (1991) reaches 1-4 and 11-17, respectively, have relatively stable channels and sinuosity is inverse to channel slope. However, Gomez and Marron (1991) found a discontinuity in the floodplain and channel slopes starting near reach 5 (Reach 4 for this project, see Figure 4.3) through floodplain long profiles. Reaches 5-10 (roughly the middle to the end of the study area; includes Location J and K, see Figure 5.1) have sinuosity that is positively correlated with channel slope. At reaches 5, 6, and 7 (equivalent to Reach 4-9 for this study, see Figure 4.3), sinuosity along with the floodplain slope increases, and the floodplain is anomalously reworked by large channel migration. A positive relationship between sinuosity and floodplain slopes indicates that there may be channel adjustments due to unstable floodplain slope. Near the beginning and end of the Belle Fourche River study area, the slope of the floodplain is constant (mean slope values of 0.000128 and 0.0013, respectively). However, at the reaches 5,6, and 7, the floodplain slope varies (from 0.001-0.0022) (Gomez and Marron, 1991). Interestingly, while these sections of the Belle Fourche River are downstream from the Whitewood Creek and Horse Creek confluences, Gomez and Marron (1991) concluded that the mine tailings and sediment influx is not responsible for the anomalous fluvial behavior due to being more localized in reaches 5, 6, and 7 rather than the entire river. The conclusion of Gomez and Marron (1991) on the cause of these

fluvial behaviors is the response to neotectonic activity. Changes in geodetic survey lines that cross lineaments on the Black Hills uplift's eastern boundary help indicate this. The geodetic survey lines that go through the Belle Fourche River flows show that there is a relative increase in elevation to the west and decrease to the east, indicating neotectonic deformation (Gomez and Marron, 1991). These lineaments are associated with approximately east-west and northwest-southeast trending linear valleys where the Belle Fourche River and its tributaries flow (see Figure 3.3). The lineaments are part of the alignment of major eastward flowing rivers in western South Dakota caused by structural adjustment to tectonically active weak zones in the Precambrian basement (Shurr, 1979; Peter et al., 1988). From a personal communication in Gomez and Marron (1991), there are offsets of Pleistocene age gravels and colluvium about 1300 years old. The offsets are believed to be linked with the Precambrian basement weakness zones. According to Nichols and Collins (1986), these offsets and weak zones could be caused by glacial rebound or erosional changes.

3.3. Whitewood Creek

Whitewood Creek is a small perennial stream that is divided equally between the rolling grass covered hills of the northern Great Plains prairies and the mountainous landscape of the Black Hills (Goddard, 1987). From Lead to Whitewood, Whitewood Creek has a drainage area of 105 km² and from Whitewood to the confluence with the Belle Fourche River, an area of 260 km². Whitewood Creek's water originates from the discharge of groundwater from the Mississippian Madison Limestone and the Cambrian-Ordovician Deadwood Formation in the Black Hill's Precambrian metamorphic and Tertiary intrusive complex as well as from surface runoffs. Downstream from Lead, the basin is underlain by limestone and shale as the creek flows northeast from the Black Hills into the Great Plains (Goddard, 1987). The upstream reach occupies a narrow canyon as a V-shaped channel in the Black Hills incising Paleozoic limestone

and Precambrian bedrock with a minimal floodplain, gradient of 50 m/km, and flowing over channel materials consisting of gravel, cobbles, and bedrock outcrops (Goddard, 1987; Ji, 2021). According to Hortness and Driscoll (1998), Whitewood Creek used to be a losing stream during the 1880s and by the 1980s became a “non-losing” stream. At the town of Whitewood near the base of the Black Hills, the stream changes its morphology as it flows into the Great Plains. The downstream reach has a meandering and locally braided flow with a wider channel and a wide floodplain, a gradient of 20 m/km, and cuts into both alluvium and shale bedrock (mostly Pierre Shale). From Whitewood, the sinuosity index of Whitewood Creek is mostly 1.4 which indicates it is sinuous except for Reach 5, 8 and 9 which is about 1.5 and Reach 10 (Figure 4.2) where it is 2 (meandering) (Figure 6.1). The downstream channel materials consist of gravels, cobbles, and bedrock outcrops. The dominant private land use around Whitewood Creek is livestock grazing, hay cultivation, and rural developments (EPA, 2012). Public lands are also found near the creek where recreational activities such as fishing, boating, and hiking occur (S.D. Dept. of Game, Fish and Parks et al., 2005).

3.3.1 Whitewood Creek Channel and Floodplain Characterization

Whitewood Creek’s channel width of the 20.9 km segment between Lead and Whitewood (mountain section) is between 3 to 5 m. There is relatively low As enrichment of sediment in this reach due to the steep gradient of the creek and lack of alluvial floodplain development. However, Ji (2021) did find As enrichment in some seeps from the alluvium but their volume is small. Downstream in the Great Plains, abandoned meanders can provide localized storage for the mine tailings (Cherry et al., 1986; Goddard, 1989; Marron, 1992). Between the town of Whitewood and the confluence with the Belle Fourche River (41.7 km), Whitewood Creek contains a large volume of contaminated tailings deposited in overbanks and

abandoned meanders. According to the EPA, the upstream portion of this segment has a wide channel with tailings occurring as overbank deposits, some extending up to 100 meters from the channel (EPA, 2012). The downstream portion is dominated by abandoned meanders and channel incisions where the tailings fill the abandoned channels (see Figure 3.9 of a meander being abandoned between 1948 to 2012). The input of mine tailings can be seen in cut banks where the cross sections indicate the channel bed was up to 3 meters higher than the modern channel, indicating that the increased influx of mine derived sediment could be responsible for the rapid channel incision, meander straightening and abandonment, and water input change from water diversion (Marron, 1992).

The average discharge of Whitewood Creek increases downstream; however, low flow discharge decreases downstream in response to surface water tributary inflow, groundwater inflow, and waste effluent discharge (Ji, 2021; Marron, 1992; Goddard, 1987). The large deposits of contaminated sediments completely covering the floodplain in the downstream reach are an important geomorphological characteristic. Before the discharge of the mine tailings, Whitewood Creek was a small meandering stream with inadequate capacity to move large volumes of sediments (Cherry et al., 1986). When large concentrations of tailing sediments were introduced to Whitewood Creek, the result was an increase in floodplain sediments and gradient and straightening of the channel through abandonment of meanders. These abandoned meanders were then filled in by tailings and alluvial sediments. Successive layers of these sediments were deposited in overbanks with the assistance of ice jamming (Cherry et al., 1986). According to Cherry et al. (1986), these meanders were filled before 1900 as evidenced by 75–85-year-old trees growing in the tailings. While the abandoned meanders were being deposited, the stream began downcutting into the shale bedrock. When the discharge of the tailings ended in 1977,

Whitewood Creek incised into the previous channel beds, leaving behind sediments enriched in mine tailings hanging above the level of average river flow at most locations (Marron, 1992) (Figure 3.4 and 3.11 for field photos of hanging tailings). According to Marron (1992), from 1966 to 1986, Whitewood Creek incised about 2 m.

3.3.2 Discharge of Whitewood Creek

Ji (2021) compiled flow data from four river gauges along Whitewood Creek during the 1982-2011 period using USGS databases. On average, spring to early summer (April-June) have high flows with average discharge between 1.56 to 2.83 m³/s (55-100 ft³/s). During mid-summer and through winter (July-March), low flows occur with an average discharge of 0.34 to 0.71 m³/s (12 to 25 ft³/s). Whitewood Creek has mean annual floods of 14.2 m³/s (500 ft³/s) along with 8–10-year floods of 56.6 m³/s (2000 ft³/s) (Mussetter Engineering, Inc. et al., 1996).

3.3.3 Geomorphic and Environmental Changes of Whitewood Creek

Since the 1980s studies of Whitewood Creek showed that the creek itself has evolved. These changes include destabilization of cut banks, incision to bedrock, and straightening of the meanders (see Figure 3.5, 3.6, and 3.9 for aerial photographs and Figure 3.4, 3.7, 3.8, and 3.11 for field photos of Whitewood Creek). The pattern of aggradation of mining sediments, followed by rapid incision has been seen in other river systems, especially those in California below gold mines (Gilbert, 1917; Adler, 1980; Kelsey; 1980, James, 1989; James and Davis, 1994; James, 1999). The cause of this fluvial behavior has been described by Gilbert (1917) where the influx of sediments increases energy of the stream to carry the load. When the sediment influx stops, the stream still has high energy, so it begins to incise through the alluvium/mine tailings and into bedrock. The instability of the cut banks is significant as they can potentially reintroduce contaminated tailings into the creek. According to a property owner from Ji (2021), within one

season, up to 40 feet (~12 m) of cut bank can erode laterally (see Figure 3.8 for field photo of eroded banks). Also, from Ji (2021), through personal conversations, USGS geologist, John Stamm hypothesizes that motion of large ice blocks in the stream during spring can destabilize the cut banks by grinding against them. In 1965, Whitewood Creek did not support aquatic bottom organisms and little to no vegetation occurred in some areas (Wuolo, 1986; EPA, 2012). However, after the 1980s, aquatic invertebrates, insects, algae, and moss began to appear again, trout were reintroduced, and barren areas were covered by riparian vegetation (Mussetter et al., 1996; S.D. Dept. of Game, Fish and Parks et al., 2005).

3.4. Belle Fourche River

Whitewood Creek ends at the confluence with the Belle Fourche River at the southern boundary of Butte County and northwest of Meade County. The Belle Fourche River is the largest tributary of the Cheyenne River. It originates in the Powder River basin in eastern Wyoming and flows southeast around the northern Black Hills. The river then converges with the Cheyenne River and then Lake Oahe (dammed Missouri River). Below the Whitewood Creek confluence, the Belle Fourche River is a meandering stream with an alluvial floodplain and occupies a flat floor valley underlain by Pierre Shale. The mean annual discharge is $10.2 \text{ m}^3/\text{s}$ (Marron, 1992). The floodplains in this valley are confined by terraces and bedrock bluffs. There are active point bars and moderate meanders (see Figure 3.10 for field photo of the Belle Fourche River). Unlike Whitewood Creek, the gradient is much less steep with a slope between 2-5 m/km. The sinuosity index of the Belle Fourche River mostly fluctuates around 1.5 and 2 (meandering) except for Reaches 7 and 8 (see Figure 4.2) which are 2.7 and 3 respectively (see Figure 6.9). The channel material is composed of cobbles and gravel with some sand and silt. (Goddard, 1987; Marron, 1992). Due to its larger channel dimension and wider floodplains than Whitewood Creeks, the Belle Fourche River has a greater capacity for storing mining-derived

sediments (see Figure 4.1 of tailings on the Belle Fourche River). Channel abandonment has been less frequent over time compared to Whitewood Creek, and this results in 60% of tailings stored in overbank deposits, 40% in point bars deposit, and little storage in abandoned channels (Marron, 1992). The Belle Fourche River contaminated sediments can be one meter thick and extend 90 meters laterally from the channel. Arsenic concentrations can be as high as 1,722 mg/kg (Marron, 1992; Ji, 2021).

3.5. Hydrology and Chemistry of Groundwater

Nearly all the aquifers of the Whitewood Creek and Belle Fourche River valleys are made of shallow alluvium in contact with the streams. The alluvium is discontinuous and limited in the deep, narrow canyon of upper Whitewood Creek. Downstream the alluvium generally increases its thickness and lateral extent. The alluvium thickness around the town of Whitewood is about 15 m, further downstream the saturated thickness is about 3 m (Goddard, 1987). The alluvium texture ranges from silty sand to clean gravel (Cherry et al., 1986).

The major ion composition of groundwater in the alluvium is derived from the underlying shale bedrock. The shale provides large concentrations of the dominant anion, SO_4^{2-} , to the groundwater which ranges from 1,000-6,000 mg/l. Dominant cations are Ca and Na (Goddard, 1987).

Groundwater contamination in the Belle Fourche River and Whitewood Creek valleys occurs where alluvial aquifers contact the contaminated sediments. High discharges during the spring can store water as back storage which can flow into the alluvium through seeps (Cherry et al., 1986; Wuolo 1986). The contaminated groundwater has a dissolved oxygen concentration of 0 mg/l and Eh values ranging from 0 to -100 mV (Goddard, 1987; Wuolo, 1986). Dissolved As concentrations in water range between 50 to 500 $\mu\text{g/g}$ in seeps and wells along Whitewood Creek

(Goddard, 1987) and can go up to 1600 $\mu\text{g/g}$ (Ji, 2021). Several factors have been identified that could change groundwater quality and As content. The first factor is that most of the original sulfide minerals have been dissolved due to oxidation or high organic matter. The only sulfides that remain are in fine grained deposits where low permeability creates a reducing environment. The second factor is pH buffering by the occurrence of carbonate minerals and rocks. The carbonates are derived from limestone bedrock upstream of Whitewood Creek, limestone gravel in the alluvium, and carbonate minerals in the shale bedrock. There are carbonate minerals in the ore deposit, as well, and they are present in the mine tailings (explained in next paragraph). Lime was also introduced to milled ore before extracting gold through cyanide. pH levels in the aquifers range from 6.1-7.6 (Goddard, 1987). The third factor is that As is adsorbed to large concentrations of Fe oxides and hydroxides that are present in the aquifer and contaminated sediments. This is to be expected since maximum As adsorption works more efficiently at near neutral pH conditions (Wuolo, 1986). However, Ji's (2021) sequential extraction results showed As adsorption to Fe (hydr)oxides is fairly low.

3.6. Geology of Homestake Mine and Contaminated Tailings

The Homestake Gold Mine contains three formations from youngest to oldest: The Ellison, Homestake, and Poorman Formations. These formations make up the Precambrian core of the northern Black Hills. These rocks were originally sedimentary and volcanic rocks from the early Proterozoic and experienced regional metamorphism ranging to greenschist-upper amphibolite conditions between 2.20 to 1.87 Ga (Redden et al., 1990). Gold mineralization occurred within the Homestake Formation. The Homestake Formation is a sideroplesite (Mg rich Fe-carbonate)-quartz schist containing biotite, chlorite, graphite, magnetite and has been extensively metamorphosed along with replacement of sideroplesite by cummingtonite in and near the ore body (see Figure 3.12 of a rock sample from the Homestake Formation). Parts of the

sideroplesite and cummingtonite in the ore bodies are almost completely chloritized (Slaughter, 1968; Noble and Harder, 1948). The ore bodies contain abundant quartz masses and veins with 7-8% iron sulfide minerals such as pyrrhotite, pyrite, and arsenopyrite (Noble, 1950). Other minor minerals include ankerite, calcite, dolomite, biotite, garnet, graphite, albite, galena, sphalerite, chalcopyrite, specularite (hematite), magnetite, and gold (Noble, 1950; Slaughter, 1968). Arsenopyrite is the most concerning of these minerals as it serves as the main host of arsenic. It is disseminated throughout the Homestake Formation with a volume ranging from more than 15% to trace amounts (Caddey et al., 1991; Noble, 1950). Caddey et al. (1991) stated that gold ore grades greater than 4.7 grams per ton are generally associated with arsenopyrite.

Goddard (1989) analyzed 46 samples by XRD to determine the mineralogy of the contaminated sediments. 75% of these sediments are composed of silicate minerals such as quartz, feldspar, amphibole, pyroxene, and mica which are likely derived from the Homestake Formation. Chlorite and gypsum also make up a portion of the composition (Ji, 2021). 22% consists of clay minerals derived from the weathering of ore body silicates or from the Great Plains shales like the Pierre (Goddard, 1987). Less than 3 % are made up of iron sulfides and carbonates (calcite, ankerite, dolomite, siderite). Pyrite has been found only in 5 out of the 46 samples and never reached a proportion greater than 1%. This was also observed by Cherry et al. (1986), who report 2 of 9 contaminated sediments contain pyrite. Possible reasons why Fe sulfide count is low in the contaminated sediments are that the original sulfides have been weathered to secondary iron minerals, the analytical method destroyed or did not detect sulfides by removing iron hydroxides, or the sulfides were destroyed by cyanide during gold extraction, and hydraulically segregated during downstream transport (Goddard, 1989). In these

calculations, pyrite is the only sulfide mineral that was mentioned. In addition to the Fe removal process from Goddard (1989), other minerals such as gypsum and calcite were also removed.

Water soluble efflorescent salts often form during the dry season in the Cheyenne River Basin on the surface of the tailings. They occur around alluvial seeps by the accumulation of soil-moisture evaporation. The major composition of the salts is hydrated magnesium-sodium sulfate. These salts can encompass heavy metals such as Cu, Ni, Zn, As, and Se. Once they are in the stream water, they dissolve quickly (Roddy et al., 1991; Shockley, 1989).

3.6.1. Lithology of Tailings Contamination

Before the introduction of mine tailings, the non-contaminated floodplain sediment of Whitewood Creek is buff-colored silt, clay, coarse sands, and gravel (Ji, 2021). The thickness is usually less than 10 m, and the composition is clasts of Black Hill's sandstone, limestone, quartzite, and metamorphic rocks. There is also local cementing of the matrix from thin white bands of calcite (Goddard, 1987; Wuolo, 1986).

Almost all the mining waste tailings along Whitewood Creek and the Belle Fourche River include red-brown silt, sand, and gray silty-clay lenses which are derived from various milling processes (Marron, 1992; Goddard, 1989). Pre-1920, the ore was crushed by stamp mills, creating coarse sand size particles. Afterwards, rod and ball mills were installed that grind the ore to finer particles. On the Belle Fourche River and Whitewood Creek, the tailings have intermixed with natural sediments to varying degrees in deposits that can be recognized visually by color, texture, and stratigraphic position. However, these types of deposits cannot be identified further down on the Cheyenne River (Goddard, 1987). These deposits normally comprise sediments that are well sorted, fine sand to silt size particles with laminar and small

angle cross beds. There are three different sediment deposit types: The first is found on the steeply sloping reaches between and near Lead and Deadwood, and is composed of a reddish brown, cemented conglomerate-type sediment. The second is a fine-grained silty sand with brown-red colors. The third is almost identical to the second in terms of texture and grain size and is a medium to dark grey fine-grained silty sand. The second and third sediment types are commonly found alternating in complex patterns. (Goddard, 1989). Color banding is common to the third sediment type, with the color change indicating different degrees of weathering and relative redox state in the contaminated sediment. The gray indicates unoxidized conditions while red implies oxidized conditions resulting in formation of iron oxides and hydroxides. Goddard (1989) identified a possible correlation between particle size and visible characteristics of the sediments. The unoxidized gray sediments contain small grain sizes around less than 0.062 mm while the oxidized red sediments are coarse sand size. It is also possible to have contaminated sediment that has been reworked by the stream which can result in a relatively lighter color, coarser grain size, and a more heterogeneous appearance (Ji, 2021). While there is no defined thickness of contaminated mine tailings from previous studies, some stretches in Whitewood Creek have sharp contacts between pre-mining alluvium and tailings based on color. However, in other areas, the two sediment units can be mixed (Ji, 2021; Marron, 1992).

3.6.2. Chemical Composition of Contaminated Sediments

The contaminated sediments have high levels of Mg, K, Na and lower levels of Ca in comparison to uncontaminated sediments. The Mg and K are most likely derived from the breakdown of feldspars, amphiboles, and micas. While Na is common in silicate minerals, it is more soluble than K or Mg. This helps remove it from the contaminated sediments at a faster rate (Goddard, 1989). The Ca is lower in the contaminated sediments compared to the surrounding

uncontaminated sediments which are naturally enriched in Ca. Naturally high Ca is common in western South Dakota. Sources of Ca include limestone (Paleozoic aged Madison and Minnekahta Formations, and Minnelusa Formation), calcareous shale (Cretaceous aged Belle Fourche Shale, Greenhorn Formation, Carlile Shale, Niobrara Formation and Pierre Shale), and gypsum rich shale (Permian-Triassic Spearfish Formation) (Goddard, 1989).

Arsenic and some other trace elements in the contaminated sediments show several times to several orders of magnitude higher levels when compared to uncontaminated sediments. According to Goddard (1989), these trace elements can be divided into four categories based on their anomalous concentrations compared to the uncontaminated sediment. The first is As, Cd, Cu, and Ag which are linked with the ore and when compared to the uncontaminated sediments, have mean concentrations ranging from 4 (Cu) to 200 (As) times higher. Next are Fe and Mn which are also related to the ore, as well as non-ore, sources and have levels several times higher compared to the uncontaminated sediments. Next are Cr, Pb, Ni, Se, and Zn, which are not related to the ore and do not have a significant difference compared to the uncontaminated sediments. Other chemicals that were used for gold extraction such as cyanide and Hg were found in many contaminated sediments, but barely reached detection limits in the uncontaminated sediments.

Arsenic has the highest anomaly in contaminated sediments. From Goddard (1989), 13 uncontaminated sediment samples have an As mean of 9.2 $\mu\text{g/g}$ compared to 915 contaminated sediment samples with a mean of 1,900 $\mu\text{g/g}$. The As from sites with the larger concentrations are derived from breakdown of the ore mineral, arsenopyrite (Ji, 2021). Noble (1950) found that the arsenopyrite has an As concentration of 0.75 % (3,500 $\mu\text{g/g}$) and South Dakota Department of Health (1960) found an As concentration of 0.25% (1,200 $\mu\text{g/g}$) in whole ore.

CHAPTER 4. GIS METHODS

This chapter will discuss the GIS methodology used to help find the areal distribution of the mine tailings, tailings removal area, and other fluvial parameters to understand the geomorphology of Whitewood Creek and Belle Fourche River.

4.1. Photograph Extraction

The role of the photographs is to provide temporal and spatial data of the contaminated floodplain deposits in Whitewood Creek and Belle Fourche River. The first step is to acquire aerial photographs of the Whitewood Creek and Belle Fourche River areas. Most of these photographs were collected from the USGS's EarthExplorer (<https://earthexplorer.usgs.gov/>), which is a digital database for satellite imagery, aerial photographs, and map products. There are 3 main types of aerial photographs that were gathered in this project: Aerial Photo Single Frames, National Agriculture Imagery Program (NAIP) photos, and aerial photographs of the tailings from an EPA report of the area during 1971 (EPA, 1972). The aerial photo single frames are black and white, natural color, and color infrared aerial photographs taken all over the United States from 1937-2014 (USGS, 2018a). These photographs were taken from the USGS. Single frame Photographs from 1948, 1952, 1958, 1967, 1971, 1977 of the Whitewood Creek and Belle Fourche River valleys were collected. However, only 1948, 1952 (Whitewood Creek only), and 1977 photographs were used because of time constraints for completing this project. It is important to note that the 1948 and 1952 photos have a scale of 1:17,000 compared to the 1977 scale of 1:80,000. While they are grainier, the 1977 photos are larger and cover more area, including most of the study area. However, a downstream stretch of the Belle Fourche River area past Reach 7 is not covered (see Figure 4.3). The 1948 and 1952 photos have a higher resolution but are smaller and do not cover as much. The reason 1952 was used in Whitewood Creek and

not Belle Fourche River is because it helped extend the coverage of the Whitewood Creek area and being temporally close to 1948. The Belle Fourche River area is all covered by 1948 photographs. The second type of photographs that was acquired was from NAIP. These photographs have been administered by the United States the USDA's Farm Service Agency (FSA) since 2003, with the purpose of monitoring the agricultural growing season and "leaf on" conditions. These photographs are orthorectified with a 1-meter resolution and based on a 3.75-minute longitude by 3.75-minute latitude quarter quadrangle, including a 300-meter buffer on all four sides (USGS, 2018b). In this project, the NAIP photographs selected were from 2012 because they cover all the areas of interest and are temporally accurate for geochemical sampling by Ji (2021). The third type of photograph that was used was from the EPA's report (1972) of the mine tailings in the Whitewood Creek and Belle Fourche River valleys. In November of 1971, the EPA used three framing cameras, an infrared line scanner, and side looking radar on aircraft to help identify the tailings. Although not traditional "aerial photographs", these photographs allowed tailings to be identified, and the creation of polygons to overlay on appropriate USGS 7.5-minute quadrangle maps of the area with an error of 50 feet (~15 m) (EPA, 1972). These EPA photographs were accessed by requesting a loan of the EPA (1972) report from the Andrew W. Breidenbach Environmental Research Center Library Services in Cincinnati, Ohio. The photographs from the report were then scanned into a digital format.

4.1.1. Georeferencing of Photographs

After collecting the aerial photographs, the next step was to georeference the aerial photo single frames to the 2012 NAIP photographs. First, using the "Mosaic to New Raster" tool from ArcMap, all the NAIP photographs of the study area were combined as one, generating an important basemap for most of the GIS project. Next was to use the ArcMap's Georeferencing

Toolbar to rectify the single frame photographs over the NAIP basemap using control points. Control points were selected on one feature of the single frame photographs and the same feature on the NAIP photographs to allow overlaying the two photographs. These selected features have not changed over time, for example groves of trees, roads, and bridges. Since the focus of this project is on the streams, all the points were selected around Whitewood Creek and Belle Fourche River. For the 1948 and 1952 photos, about 4 to 6 points were used and in the larger 1977 photographs 8 to 11 points were used. The next step was to georeference the 1972 EPA photographs. This required a different method since they are not true aerial photographs. These photographs have crosses that indicate coordinates that are found in USGS 7.5-minute quad maps of the area. Using the mapping application Avenza, which can access this type of map, these coordinates were identified by hovering the cursor over them. Applying the control points again, the crosses were selected, and a second point was selected on the NAIP basemap by inputting coordinates found from Avenza. Once all the tailing maps were georeferenced, they were then mosaicked together.

4.2. Digitation of Tailings Location and Removal

Once the photographs were georeferenced, the next step was to identify the temporal changes of the contaminated floodplain deposits. To do this, the NAIP is overlaid by one of the aerial photo single frames representing one year (i.e. 1948, 1977). Next, using the Editor Toolbox from ArcMap, the paleochannel of Whitewood Creek and Belle Fourche River was created for each temporal interval by creating polyline shapefiles. This was used to help determine what portion of the floodplain deposit has been eroded and show the temporal behavior of the streams. Next, the EPA (1972) tailings photographs were placed over the single frame photos. Using the Editor Toolbox again, polygon shapefiles of the floodplain deposits were created using the EPA (1972) polygons overlay as a guide. Although the EPA's locations of

the tailings do not perfectly match with the basemap, interpretation of where the contaminated area is was made by seeing the similarity of the shape or seeing floodplains around the suggested location. Once these polygons were created, using the “Calculate by Geometry” tool on the attribute table, the area of the polygons was calculated. The next step was to determine what proportion of the floodplains have been eroded up to when the 2012 photo was taken. Using the 2012 NAIP basemap, along with the paleochannel and tailings polygons of each respective year, a new polygon was created on the portion of the floodplain that had been eroded by the modern 2012 channel. To see a visual example of this process, refer to Figure 4.1.

4.2.1. Areal Calculation of Tailings and Removed Tailings

Once the tailings areal data has been completed, the next step is to understand how these behave spatially. First, digital shapefile lines of the 2012 channel were created for both Whitewood Creek and Belle Fourche River. Next, using the Editor Toolbox, each stream’s line was arbitrary divided into 10 equal segments (see Figure 4.2 for Whitewood Creek and Figure 4.3 for the Belle Fourche River). The result from this division is an individual reach length of 3903.61 m for Whitewood Creek and 7468.19 m for the Belle Fourche River. After dividing the streams, the shapefiles of the contaminated floodplains are added to the map. To find the total sum of tailings area in a reach, an individual segment of a stream is selected. Using the “Select Layer By Location” tool, floodplain deposits within 100 m of the selected reach will also be selected. If a selected floodplain deposit is outside of the reach, it is de-selected. If a floodplain deposit straddles between two reaches, that shapefile is divided into two based on where that reach ends and another begins. The divided end that is outside of the reach will be selected in the subsequent reach. The total area of the selected contaminated deposits is determined by using the “Statistics” popup in the attribute table of the deposits. This is also applied to the removed

sediment shapefiles as well. Finally, the approximate area of contaminated sediment in 2012 was calculated based on difference between the 1948 contaminated sediment area and the removal of the 1948 contaminated sediment area.

4.2.2. Limitations of Digitized Tailings

The following bullet points address some limitations to the digitization of the tailings described above:

- The digitized polygons may not fill in the exact spot of the EPA's (1972) contaminated sites due to different temporal floodplain geometry and georeferencing errors. In this investigation, using the aerial photographs, floodplains that have a lighter colored appearance than the older surrounding deposits are assumed to be the respective contamination areas that EPA (1972) drew.
 - Similarly, due to georeferencing errors, parts of the paleochannel may be off (around 10s of meters), especially in areas where an aerial photograph ends and another one begins.
- It is important to note that not all of EPA's (1972) polygons have been recreated due to being unable to identify any floodplain deposits or the image being too grainy. This is especially a major problem with the 1977 images since they cover larger areas and have a larger scale. This can be seen in the statistics where there are more counts of 1948 polygons than 1977 (see Chapter 6 Appendices).
- The following bullet points compare the surrounded area of tailings calculated in this investigation to EPA's (1972) values. For additional comparisons, refer to Chapter 6 Appendices:

- The 1948 Whitewood Creek tailings polygons have a sum of about 1,100,000 m², 800,000 m² for 1977, and 820,000 m² from EPA (1972). The 1977 and EPA's (1972) polygons have a similar sum value and are the same magnitude. While the 1948 sum is about 30% higher, these tailings underwent more reworking than the 1970s tailings.
- For the Belle Fourche River, the 1948 tailings sum is 3,400,000 m² and 2,900,000 m² for EPA (1972) (up to Reach 10). For the 1977 tailings, the sum is 1,600,000 m² and 1,900,000 m² for the EPA (1972) (up to Reach 7). Similarly, the 1977 tailings sum is similar and the same magnitude with the EPA's (1972) data while the 1948 sum is about 40% higher.

4.3. Creation of Fluvial Parameters

To understand the relationships between the floodplain deposits and dynamic fluvial processes, the following parameters were measured: channel migration, total sediment depositional area, sinuosity, long valley profile, and width of contaminated floodplain.

4.3.1. Channel Migration

The calculation for average channel migration of Whitewood Creek and the Belle Fourche River is based on the document from Legg et al. (2014). To find the average channel migration, the area between the 1948/1952 and 1977 channels to the 2012 channel needs to be determined. To find the channel migration, the "Feature to Polygon" tool was used to make polygons between these two stream lines (i.e. 1948 and 2012 channels). Next, using the "Calculate by Geometry" tool, the area of these polygons was determined. Then a reach was selected and the "Select Layer By Location" tool was used to select polygons that intersect or are within that reach. As described before, if a reach ends in between a polygon, that polygon is

divided up based on where the reach ends. Once the polygons of a certain reach are selected, the sum of their area is determined using the “Statistics” popup from their attribute table. The sum of the area was then divided by the length of the reach (3903.61 m for Whitewood Creek and 7468.19 m for Belle Fourche). This will help determine the average channel migration rate between 1948/1952 and 1977 to 2012.

4.3.2. Total Sediment Deposition Area

To find the total sediment area that was deposited, the polygons from “Feature to Polygon” tool (from channel migration calculation) were used. Areas where these polygons were overlaid by the removed/eroded polygons were then erased using the “Erase” tool since they ideally should be situated around the modern stream location. However, this is not the case for all the polygons since lateral migrations can both erode and deposit sediments. In addition, some polygons occur within the modern channel where channel migration was minimal. To resolve these problems, the polygons are manually checked and were additionally added or removed when necessary. Once the polygons have been edited, like the contaminated and removed polygons, the sum of the area was determined by selecting them within their respective reaches.

4.3.3. Sinuosity

The sinuosity of each reach was determined by dividing the river distance from end to end of the reach to the straight line distance from end to end of the reach. For the river distance, each reach has a consistent length, depending on the stream (Whitewood Creek, each segment is 3903.61 m long while Belle Fourche is 7468.19 m). For the straight line distance was determined by using a straight line ruler from the beginning to the end of the reach.

4.3.4. Contaminated Floodplain Width

The contaminated floodplain width was determined by using tool, “Minimum Bounding Geometry”. The purpose of this tool was to create polygons that enclosed others to help estimate geometric properties such as area, length, and for this parameter, width. There are different shapes that can be used like rectangles and circles, but one option is called “Convex_Hull” which is a good choice for elongated curved shapes like the contaminated floodplains in this project. After running the tool, a few issues arose. The first is that many of the estimated polygons are larger than the actual floodplain polygons, hence overestimating the width. Another potential issue is that the width of these polygons is found by the shortest distance between any two vertices. Ideally, it would be good to have the width perpendicular to the stream, but the results don’t show this. To solve these problems, the floodplains polygons were manually checked and have their widths edited to make sure that they are not too large, and they are approximately perpendicular to the stream. This task can be difficult especially in areas where floodplain widths vary. The length of these floodplains was determined by finding a value between the large and small width in that floodplain. Once all the polygons have been checked, the mean and standard deviation of floodplain width was determined for each reach.

4.3.5. Longitudinal (Long Valley) Profiles

Two longitudinal profiles were made in this project: One for Whitewood Creek from Location E to the Belle Fourche River confluence and one for the Belle Fourche River from the Whitewood Creek confluence to Location K (see Figure 5.1 for location). This task was done by using the tool, “Stack Profile”. This tool creates a table showing the elevation profile of line features over a raster surface. In this case, the line features were the 2012 Whitewood Creek and Belle Fourche River channel lines as mentioned above and the raster surface is a DEM of the

study area. The table was created as an Excel sheet with data including elevation and distance. This information is then represented as a scatter plot with smooth lines. Initially, there is a large amount of data (almost 7000 counts), resulting in the graphs being noisy. To smooth the graphs, the data is manipulated by using Excel's built in "Moving Average" function.

CHAPTER 5. GEOCHEMISTRY METHODS

This chapter describes the geochemical modeling approach to evaluating the following parameters: 1) Mineral saturation indices of Whitewood Creek and Belle Fourche River, 2) Rate of As input into the stream water from arsenopyrite dissolution, and 3) Rate of As input into the stream water as suspended sediment.

5.1. Water Chemistry from Ji (2021)

The chemical data that was used in this project (Appendix 5-2) came from the work of Ji (2021) collected during the summer of 2010. She collected water samples at 13 sites between upstream of Deadwood to Volunteer (see Figure 5.1). In addition, one sample was collected at Whitetail Creek above Lead (Location A) and another about 7.5 kilometers above the Whitewood Creek and Belle Fourche River confluence (Location L). Location L role serves as an uncontaminated control site. Downstream from the confluence, 3 samples were collected along the Belle Fourche River (see Figure 5.1). Overall, 8 samples were taken from Whitewood Creek (Locations A-H), 4 from the Belle Fourche River (Locations I-K), and 3 from seep water locations along Whitewood Creek (Locations B, G, H). The water samples were taken 5 feet (~1.5 m) from the bank. At the same time, dissolved oxygen was measured using a DO-600 ExStik II probe from Extech Instruments along with pH, specific conductivity, and temperature measured with a PCTestr 35 Multi-Parameter probe from Eutech Instruments. An aliquot of the water sample was put inside of a 10 ml plastic syringe through suction and placed in a 15 mL Nalgene screw-top scintillation vial. A second aliquot went through the same procedure but was drawn through a 0.45 μ m syringe-attachment membrane filter (ICMillex-LH filter unit from Millipore). Total metal concentrations were measured in the unfiltered samples while the total dissolved metal concentrations were measured in the filtered samples. To keep the metals in

solution, each scintillation vial was pre-acidified with a small drop of pure nitric acid. The water samples were then placed in a cooler. These samples were analyzed through inductively coupled plasma optical emission spectroscopy ICP-OES and by inductively coupled plasma mass spectroscopy (ICP-MS) at Colorado State University's Center for Environmental Medicine Analytical Laboratory using an ELAN DRC II instrument from Perkin Elmer SCIEX. These two techniques were applied because ICP-MS has lower detection limits for trace to ultra-trace elements while the ICP-OES can detect and quantify major elements, samples with high concentrations, or samples with widely varying elemental concentrations.

5.2. Missing analytes and redox potentials

While most of the water chemistry for this project came from the work of Ji (2021), her data does not contain the following analytes: HCO^- , Cl^- , K^+ , and PO_4^{3-} (except for P at Location E). In addition, another critical chemical parameter that was not included was the redox potential of the stream water (Eh). However, the USGS has three river gauges in this watershed (two on Whitewood Creek and one on the Belle Fourche River) that have obtained data for the missing parameters, going back to at least 1991. The first gauge is called “Whitewood Creek Above Whitewood, South Dakota (# 06436180)” (see Table 5.1), which is located just upstream from the town of Whitewood, near the transition zone for Whitewood Creek from higher to lower gradients. This is also the same site as Ji’s (2021) Location E (see Figure 5.1). The median of the gauge’s missing analyte concentrations from 1991-2021 is assumed the same from Location E to Location G. This applies to the redox potential as well. From Location H-I, the values are from the gauge station called “Whitewood Creek Above Vale, South Dakota (# 06436198)” (see Table 5.1). Similarly, Location K also has different analyte values due to being adjacent to the gauge station “Belle Fourche River Near Sturgis South Dakota (# 06437000)” (see Table 5.1). This station has been in operation since 1946, but for consistency, 1991 was used as the starting year.

However, this station doesn't have redox information, so the redox value from the Whitewood Creek Above Vale station was assumed to be the same as this location. For Location A-D and L, the missing analytes were not included due to not having any USGS gauge stations nearby. Location A-D also flows through different bedrock lithologies such as metamorphic and carbonate material, while most of the other locations have shale bedrock (except for Location E which is underlain by Paleozoic carbonates). The seep water data also do not include these parameters due to little information about their chemistry. However, Wuolo (1986) and Goddard (1987) did calculate the Eh of the alluvial aquifers in Whitewood Creek ranging from 0 to -100 mV. See Table 5.1 for Eh and missing elemental components collected from the USGS.

5.3. Geochemist's Workbench

In this project, the water chemistry reported by Ji (2021) was used to determine what minerals are supersaturated or thermodynamically predicting what mineral could form and be stable in these waters. To perform this task, the chemical data was assembled through the geochemical software, Geochemist's Workbench. This program is a set of software tools that manipulate chemical reactions, calculate equilibrium states of natural waters and mineral stability diagrams, track reaction progress, and plot results of these type of calculations (Bethke et al., 2021).

5.3.1. pH and Eh Input

Important input parameters in all chemical calculations are pH and redox conditions (Eh). Ji's (2021) fieldwork found that the stream water pH ranges from slightly basic to basic (8.1-8.7) (see Figure 5.4.). While Ji (2021) found the concentration of dissolved oxygen to range from 4.56-6.3 mg/l in the stream water, the Eh (oxidation potential) was not measured. The measurement of this parameter is difficult due to redox reactions at low temperature not reaching

equilibrium (Thorstenson et al., 1979; Thorstenson, 1984). For this project, the Eh was determined from three USGS water gauge sites as described above. Redox values from the first station, Whitewood Creek Above Whitewood, had high variability ranging from 781 to -218 mV during 2004 to summer of 2021. These value ranges are generally correlated to discharge, with high discharges showing more oxidized readings and low discharges showing more reduced readings. To simplify this complexity and seeing how Ji's (2021) dissolved oxygen concentration varies little in the stream water (see Figure 5.3), the redox value during the time Ji (2021) conducted her fieldwork (summer of 2010), 155 mV, will be used for Location E to Location G. Below Location G is the next USGS water gauge, Whitewood Creek Above Vale. Like the previous site, the Eh varies greatly, so the value from the summer of 2010, 161 mV, was chosen. This value is also used for Locations H-K (I-K are on the Belle Fourche River). While it would be useful to have redox data for the Belle Fourche, the third USGS gauge station at Location K, Belle Fourche River near Sturgis, does not have that information. Similarly, Location L (above the confluence with Whitewood Creek) does not have any water gauges near it, so the Eh value is assumed to be 161 mV.

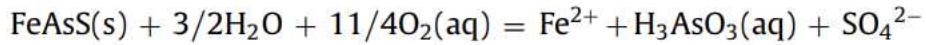
For seep water, Ji (2021) found that pH is lower with a range of 6.9-7.6. Like the stream water, the redox conditions were not evaluated. However, Wuolo (1986) and Goddard (1987) calculated Eh values for contaminated water from the alluvial aquifer along Whitewood Creek, and found a range of 0 to -100 mV with a dissolved oxygen concentration of 0 mg/l. For the seep water redox in this project, the Eh used in calculations is in the middle of this range at -50 mV.

5.3.2. Arsenic Oxidation State Determination

It is important to know the As oxidation state (III or V) and speciation in the stream/seep waters. As mentioned before, Eh and pH have a major control on As species and state. Based on

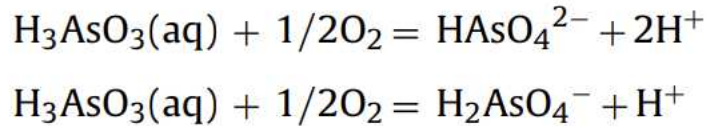
an As Eh-pH diagram (Figure 1.1 and 5.5), at the conditions assumed in this study As will exist in the stream water dominantly in the form of HAsO_4^{2-} . In this form, the As oxidation state is V. This is supported by Fuller et al. (1987) who found that the dominant As oxidation state in Whitewood Creek to be As (V). In addition, this oxidation state was observed in a laboratory setting. While performing an experimental dissolution of arsenopyrite, Wang et al. (2018) studied As (III) oxidation to As(V). This can be seen using the reaction from Yu et al. (2007):

Equation 5.1.



Followed by:

Equation 5.2.



According to the speciation diagram, the dominant species will be HAsO_4^{2-} . The chemical reaction of Yu et al. (2007) also shows that the presence of dissolved oxygen plays an important role for As oxidation although it is kinetically slow at room temperature (Wang et al., 2018). In reality, the As species might be a mixture of As(III) and As(V) with a bias towards As(V). With the presence of dissolved oxygen in the waters, the Eh-pH diagram, and the results from Fuller et al. (1987), it is reasonable to represent all the As in the stream water as As (V) in HAsO_4^{2-} . However, the As species may be different in seep water due to higher acidity (pH 6.9-7.6). According to the Eh-pH diagram (Figure 5.5), As (V) and As (III) speciation ratio will be

approximately 50:50 in the seep water where As (V) will have a speciation of HAsO_4^{2-} and As (III) will be $\text{As}(\text{OH})_3$.

5.3.3. Determination of Mineral Saturation States (SpecE8)

One of the main goals of this project is to observe the conditions of the stream and seep water through mineral saturation states. The initial water is the stream water chemistry with its constituents (i.e., elemental concentration, pH) that was measured by Ji (2021) before being modeled by reactions calculated from Geochemist's Workbench. This task is performed with the Geochemist's Workbench SpecE8 application. SpecE8 models the equilibrium states of geochemical systems in an aqueous fluid (Bethke et al., 2021). It can calculate the aqueous species equilibrium distribution in a fluid, saturation state of the fluid with respect to minerals, the sorption of aqueous species to various surface types, and partial pressure and fugacity of gases dissolved in the fluid (Bethke et al., 2021). Before running the program, two parameters need to be defined. The first is to set the charge balance to zero by adjusting an anion concentration since water analyses are not typically balanced electrically which can lead to an increase in absolute errors depending on how high the anion concentration is. For all locations, the charge balance was set using SO_4^{2-} . This anion is chosen because it is the only anion that Ji (2021) measured and has the highest concentration in Whitewood Creek area (Cherry et al., 1986; Goddard, 1989). The next parameter to set is redox coupling. In the Geochemist's Workbench, there are many different redox pairs and reactions such as Fe (II)-Fe (III) and AsO_4^{3-} - $\text{As}(\text{OH})_4^-$ (equivalent to As (V)-As (III)). If these redox pairs are coupled to each other, this means that the ratio of one pair will be controlled by the ratio of the other. Typically, the pair with the highest concentration of elements is the controlling pair. Geochemist's Workbench also uses the corresponding coupling reaction to eliminate separate redox species from the reactions

in the database. For example, if Fe (III) is coupled with Fe (II), the model will add this coupled reaction to the reaction for hematite which eliminates Fe (III) species independence. This reaction is also dependent on what the redox input is (i.e. Eh) (Bethke, 1996). On the other hand, if they are decoupled, then each species can be independently constrained. However, this requires more analytical data for each element and the fluid redox state. Since there is no information on the different As and Fe species, for simplicity of the project, As (III) with As (V) and Fe (II) with Fe (III) species, respectively, were coupled in this analysis although in reality they are most likely in disequilibrium.

The output of SpecE8 is a Notepad file with a list of minerals that are supersaturated at the conditions set in the program and that might crystallize if equilibrium thermodynamics govern precipitation and if there are no other minerals competing for the same ions. The minerals are listed with their respective Log Q/K where K is the mineral's equilibrium constant, and Q is the ion activity product (IAP). See Appendix 7.1-7.15 for SpecE8 saturation index result for each location (the results are technically from the REACT application described below but it is the same information that SpecE8 produces).

5.3.4. Water-Rock Interaction Application (REACT)

While SpecE8 is good for assessing the equilibrium state of the stream water, there are some limits with predicting mineral precipitation or dissolution from the program results. One limit is that if a mineral shown to be supersaturated precipitates, then it affects the saturation state of other minerals initially listed as supersaturated. Some of the minerals that are supersaturated are not known to form in the geological environment considered here (see Appendix 7-1 to 7-15 for list of indices for each location). For example, the software initially shows antigorite to have the highest saturation index in the stream water, but antigorite is a

metamorphic mineral found in serpentinites while the stream water is at surficial conditions. A second limit is that the numerical value of saturation indices depends on the chemical complexity of the mineral's formula. For example, minerals with large formulas such as clays tend to have the highest indices. A third limit is that the results from SpecE8 are based on equilibrium thermodynamics. At surface conditions, many reactions are kinetically controlled. A fourth limit is SpecE8 does not predict what is the mass of minerals that would precipitate or dissolve to achieve equilibrium with the solution. To evaluate the mass of minerals that would precipitate to achieve equilibrium, another Geochemist's Workbench program called "REACT" is used. REACT is an extensional program of SpecE8 and can use the aqueous species equilibrium distribution in a fluid, and the saturation state of a fluid with respect to minerals calculated by SpecE8 to trace the evolution of an open or closed system as it undergoes reversible or irreversible reactions and can integrate kinetic laws (Bethke et al., 2021). REACT is also useful for programmatically adding minerals to the water to see how the water will interact with the minerals. This is conceptually for minerals from the tailings that eroded into the stream water from the banks, especially for arsenopyrite (see conceptual illustration in Figure 5.7).

In REACT, the basis interface is the same as SpecE8. Similarly, the setup described in SpecE8 will be used in this application. The REACT interface has another parameter called "Reactants"; this is where other elemental species and/or minerals are added to the chemical system and react with the initial fluid in the basis panel. The mass of these reactants for this project are represented as weight percentages (see Appendix 5-3). It is important to note that the weight percentage in Geochemist's Workbench is equal to 100 kilograms of mineral per kilogram of solution. Using the assumption based on Ji's (2021) sequential extraction and Horowitz and Kent's (1990) SEM work where most of the As is stored in arsenopyrite, all of the

As will be sourced from this mineral. Other minerals from the tailings were added in the reactant basis as well (see Appendix 5-3) but their interaction with the water is thermodynamic (reaction is instantaneous) while arsenopyrite will be kinetic. Additional chemical parameters such as Eh and pH are set as well. While there are other complicated factors such as organic matter, agricultural fertilizer, and nutrients that affect chemical parameters in the real world, for simplification, the Eh and pH are fixed at their measured values. This can be reasonable for pH since it has a fairly low variability and remains neutral-basic, according to the Figure 5.4 and USGS river gauges. Eh is more complex as it has more variability, however, its average values are around slightly oxidized (around 155 mV).

5.3.5. Arsenopyrite Kinetic Dissolution

One issue with reacting to the minerals of the tailings is that that they are controlled by thermodynamics. In reality, change of chemistry in the water and mineral dissolution is controlled by both thermodynamic saturation state and kinetics of mineral dissolution. In Geochemist's Workbench, kinetic modelling includes a temporal aspect while thermodynamics are instantaneous. Since this project is interested in changes of As over time, kinetically dissolving its main source, arsenopyrite, is important. This can be simulated in the reactant interface on REACT.

The first step is to estimate the representative amount of arsenopyrite in the tailings. Goddard (1989) says the tailings were originally 7-8% iron sulfides, including arsenopyrite in the ore deposit. However, this includes other iron sulfide minerals such as pyrite and pyrrhotite. In other reports, Noble (1950) reported an average of 0.75% arsenopyrite while South Dakota Department of Health, 1960 says 0.25%. Ji (2021) reported arsenopyrite ranges in the tailings from <3-15% with an average around 5.0%. These values are from field observations, so may

include other sulfides. The reason for the higher percentage in the tailings than in the ore deposit is that some of these sulfides are deposited together in ~cm thick layers, possibly from hydraulic sorting (J. Ridley, personal communication). While future research should include finding a more accurate estimate of arsenopyrite abundance, for this project, a range from the highest to the lowest possible percentage of arsenopyrite will be used based on other research and Geochemist's Workbench. The highest value will be 15% which came from Ji's (2021) field observations. For the lowest percentage, the value will be 0.11%. This was determined by using Geochemist's Workbench by inputting different arsenopyrite concentrations to match Ji's (2021) As level in the stream. This is within the magnitude of Noble (1950)'s report of an average of 0.75% arsenopyrite in the ore deposit and South Dakota Department of Health, (1960) estimate of 0.25%. Although for pyrite, this low value of sulfide minerals in the tailings was estimated from XRD results of Goddard (1989) of the tailings where the mean percentage of As by weight is <1% and Cherry et al. (1986) where it ranges from none to 3% (only 2 counted out of 9 samples). The next step is to estimate the specific surface area of the arsenopyrite in the form of cm²/g. Assuming that the arsenopyrite grains are rounded and the average diameter is 0.3 mm (from Ji's (2021) average of largest arsenopyrite grain observed in the field), the volume of the average grains was determined using the spherical volume equation, $\frac{4}{3}\pi r^3$. Next, the volume is multiplied by the density of arsenopyrite (6.07 g/cm³) to get the average mass. By finding the average surface area using the spherical surface area formula, $4\pi r^2$, and dividing it by the average mass, the surface area per mass of arsenopyrite is 33 cm²/g. The value chosen for the dissolution rate constant, 1.0e-14 mol/cm²/s was from the work of Wang et al. (2018) where arsenopyrite in a lab setting was dissolved at a pH of 8.9, Eh of 36±13 mV, and dissolved oxygen content of about 7.5 mg/l. They also found Fe oxyhydroxide formation on the surface of

arsenopyrite strongly suppresses its dissolution rate. These conditions are similar to those of Whitewood Creek and Belle Fourche River. See Table 5.2 for list of parameters used for modeling arsenopyrite dissolution.

The final component is determining the rate law that governs the dissolution. For this project, the built in rate law in the program for REACT is used. From Bethke et al. (2021), the built in rate law is the following:

Equation 5.3.

$$r_{\vec{r}} = A_S k_+ \prod_j (a_j | m_j)^{p_j} \left(1 - \frac{Q}{K} \right)$$

Where \prod is the product function, A_S is surface area, k_+ is the rate constant, a_j is the activity of promoting and inhibiting species, m_j is the molality of promoting and inhibiting species, a_j/m_j signifies that either molarity or activity is carried, and p_j is the power of that species. As mentioned before, $\text{Log}(Q/K)$ is the saturation index where Q is the activity product and K is the equilibrium constant.

5.4. Determination of Rate of As Dissolution from Tailings into Stream Water

To determine the rate of As dissolution from the contaminated mine tailings into Whitewood Creek and Belle Fourche River, Geochemist’s Workbench was used to create a numerical model to estimate the rate through REACT. It is important to note that this model is being applied only to the Whitewood Creek Great Plains locations (same with suspended As transportation in 5.5). Conceptually, As is entering the stream through tailings erosion where As is dissolving from arsenopyrite, seep water outflow, and stream water covering tailings from

high flow (see Figure 5.7). It is important to note that another independent source of dissolved As may be the hyporheic zone. The hyporheic zone is the water saturated location under a stream where groundwater flows exchange water and chemical components with the stream (Boano et al., 2014). In this zone, both the groundwater and stream water are contaminated since the groundwater flowed through the tailing rich floodplains and the stream bottom sediment is composed of tailings from bank erosion (see Figure 5.7 for visual representation).

The first step is to predict the residence time of water passing through one location. This can be difficult with stream water due to its constant movement and relatively quick exit out of a basin in a short time span. While there are other methods of finding an estimated residence time for stream water, in this project, 2 days was chosen arbitrarily for the estimated time scale of water moving throughout Whitewood Creek. From Reach 1 to 10 (39,036 m), the stream velocity will be about 19,518 m/day or 0.2 m/s. The order of magnitude of this velocity is about the same as for other streams within the Black Hills (Whitetail Creek, Spearfish Creek, Annie Creek, and Squaw Creek) and higher by one or two magnitudes compared to the Great Plains streams (Bear Butte Creek, Hay Creek, and Indian Creek) (Driscoll et al., 2002).

The next step is to determine what is the mass of water flowing through one location at one moment in time. To find the water mass, the first step is to find the average discharge of Whitewood Creek. The unit of discharge, m^3/s , is then converted to m^3/day and multiplied by the density of water ($997 \text{ kg}/\text{m}^3$ at $25 \text{ }^\circ\text{C}$) and 2 days to get a stream water mass of $2.0 \times 10^8 \text{ kg}$ for Whitewood Creek.

For Whitewood Creek:

$$\frac{1.36 \text{ m}^3}{\text{sec}} \times \frac{86400 \text{ sec}}{\text{day}} = \frac{117504 \text{ m}^3}{\text{day}}$$

$$\frac{117504 \text{ m}^3}{\text{day}} \times \frac{997^* \text{ kg}}{\text{m}^3} \times 2 \text{ day} = 2.0 \times 10^8 \text{ kg}$$

* Water density value came from <https://www.usgs.gov/special-topics/water-science-school/science/water-density>

After determining the mass of water, the next step is to input the water mass into the arsenopyrite kinetic dissolution model in REACT. The program runs a numerical model and produces a graph of As concentration (in the form of $\text{As}(\text{OH})_4^-$) in both fluids and as total As in “rock” components (the contaminated sediment) over time. Since this section is interested in dissolved As in the stream water, the graph of $\text{As}(\text{OH})_4^-$ concentration in the fluid is copied into an Excel file and regressed linearly. The slope from the regressed linear equation is the rate of soluble As transportation from tailings per day (see Figure 5.8). Throughout all locations, the rate does not have much variation and is strongly linear (Appendix 7-16 to 7-17 for each location). The rate of As dissolving into the waters of Whitewood Creek with an arsenopyrite content of 15% ranges 0.6132-0.6148 (mg/l)/day and 0.0046-0.0048 (mg/l)/day with a content of 0.11%.

The final step is to find the annual rate of soluble As transportation with respect to each stream’s discharge. The stream’s average discharge value is multiplied by 2 days and converted from m^3 to liter. For Whitewood Creek, the daily volume is 2.4×10^8 l. The volume is then multiplied by the rate of As dissolution (mg/l)/day) to get the soluble As mass rate (mg/day). To compare with Ji’s (2021) values, mg is converted to Mg (megagrams) and day to year. The

results show that if the arsenopyrite percentage is 15%, it will have an annual dissolution rate of 52 Mg/year while 0.11% is 0.39 Mg/year.

Example calculation for soluble As transportation at Whitewood Creek:

$$2 \text{ days} \times 117504 \frac{\text{m}^3}{\text{day}} \times \frac{1000 \text{ l}}{\text{m}^3} = 2.4 \times 10^8 \text{ l}$$

Assuming the arsenopyrite percentage is 15%, the daily soluble As concentration rate will be

$$\text{about } \frac{0.61 \frac{\text{mg}}{\text{l}}}{\text{day}}$$

$$\frac{0.61 \frac{\text{mg}}{\text{l}}}{\text{day}} \times (2.4 \times 10^8 \text{ l}) = 1.5 \times 10^8 \frac{\text{mg}}{\text{day}}$$

$$1.5 \times 10^8 \frac{\text{mg}}{\text{day}} \times \frac{1 \text{ Mg}}{1.0 \times 10^9 \text{ mg}} = 0.14 \frac{\text{Mg}}{\text{day}}$$

$$0.14 \frac{\text{Mg}}{\text{day}} \times \frac{360 \text{ day}}{\text{year}} = 52 \frac{\text{Mg}}{\text{year}}$$

5.5. Determination of Suspended As and Sediment Transportation in Whitewood Creek

To find the suspended contaminated sediment and As concentration in Whitewood Creek the first step is to find the total volume of the creek channel. This was determined by using the creek's length, average width, and thickness of the contaminated sediments. For simplicity, the shape of the sediment will be assumed as a rectangular ribbon. The stream length was defined to be 39036 m, this is length was measured by ArcMap from Location E (2 km south of Whitewood) to the confluence with the Belle Fourche River. The average width of the creek is 6.66 m and was determined using Google Earth (time of season when photos taken was late

summer). The determination of the contaminated height of mobile contaminated sediments requires an “endmember” like approach. These endmember thicknesses were defined by the contaminated sediment’s characteristics in the cutbanks at Locations G and H that were measured by Ji (2021). Location G’s cutbank is 4 m with the upper 0.6 m being composed of contaminated tailings, 2.4 m of pre-mining alluvium in the middle, and 1 m of shale bedrock at the bottom. At Location H, the cutbank is 4.5 m with 3.5 m being contaminated sediment and 1 m being shale bedrock. Hence, the two end members for thickness of contaminated sediment in the overbanks are 0.6 m and 3.5 m. Using a uniform model, the height of each endmember will be assumed the same through Whitewood Creek although actual thickness of the contaminated sediments varies. The total volume of contaminated sediment with a uniform height of 0.6 m is about 160000 m³ while the height of 3.5 m is 910000 m³. After finding the total volume, the next step is to find the density of the suspended contaminated sediments. Geochemist’s Workbench can calculate the mineral mass in the conceptual stream before the reaction by multiplying the mass of the reactants by the mass of the stream water. The results from this calculation can be seen in the initial notepad result (see Figure 5.6). However, this only applies to reactants that are dissolving kinetically. In the case of this model, the only mineral that is kinetically dissolving is arsenopyrite, hence the mineral mass is suspended arsenopyrite only. Since this calculation is only calculating suspended As from one source (arsenopyrite), this is valid. When the tailings height is 0.6 m, arsenopyrite weight percentage is 0.11%, the mineral mass is 1.10x10⁵ kg and 1.10x10⁷ kg when it is 15%. For the 3.5 m height, the mineral mass will be 5x10⁵ kg (for 0.11%) and 5x10⁷ kg (for 15%). The differences in mineral masses for the different thicknesses of the tailings are the results of approximating the difference in tailings amount by half an order of magnitude rather than an exact calculation. The suspended arsenopyrite mass is then divided by

the total volume to get the suspended arsenopyrite density (in the form kg/m³). The next steps are to convert kg to Mg and then multiply the density by the average daily discharge of Whitewood Creek (117504 m³/day) by 2 days (stream residence time). To get the suspended arsenopyrite transportation in 30 years, the mass is divided by 30 to compare to Ji's (2021) values. To get the total suspended As, this value is multiplied by 0.46 (As makes up about 46% of the arsenopyrite molecule weight, see <http://webmineral.com/data/Arsenopyrite.shtml>). The final results shows the average transportation rate of suspended As is 254 Mg/year for 15% arsenopyrite and 2.54 Mg/year for 0.11% if the tailings thickness was 0.6 m. For 3.5 m thickness, the rate will be 59 Mg/year for 15% and 1.98 Mg/year for 0.11%. (see Table 7.7). The suspended As transportation rate range for the 0.6 m tailings is higher than the dissolved As transportation rate range by an order of magnitude. The 3.5 m thickness suspended As transportation rate range is within the same order of magnitude as the dissolved As transportation rate range.

Example calculation for suspended As transportation at Whitewood Creek:

Height = 0.6 m

Stream length = 39036 m

Average Width = 6.66 m

$$\text{Discharge} = \frac{117504 \text{ m}^3}{\text{day}}$$

Arsenopyrite weight percentage = 15%

Suspended arsenopyrite mass = 1.10×10^7 kg

As Percentage in Arsenopyrite = 46%

Total Volume of Suspended Sediment = (0.6 m) x (39036 m) x (6.66 m) = 155988 m³

$$\text{Suspended arsenopyrite density} = \frac{1.10 \times 10^7 \text{ kg}}{155988 \text{ m}^3} = 71 \frac{\text{kg}}{\text{m}^3} \times \frac{1 \text{ Mg}}{1000 \text{ kg}} = 0.071 \frac{\text{Mg}}{\text{m}^3}$$

Total Suspended Arsenopyrite Transportation Rate=

$$2 \text{ day} \times \frac{117504 \text{ m}^3}{\text{day}} \times 0.071 \frac{\text{Mg}}{\text{m}^3} = 16686 \text{ Mg}$$

$$16572 \text{ Mg} \div 30 \text{ years} = 556 \frac{\text{Mg}}{\text{year}}$$

Total Suspended Arsenic =

$$552 \frac{\text{Mg}}{\text{year}} \times 0.46 = 254 \text{ As} \frac{\text{Mg}}{\text{year}}$$

CHAPTER 6: GIS AND FLUVIAL GEOMORPHOLGY RESULTS

This section will describe the results of the evolution of mine tailings within Whitewood Creek and Belle Fourche River from EPA (1972) and the fluvial geomorphology of Whitewood Creek and Belle Fourche River based on aerial photographs 1948, 1977, and 2012.

6.1. Whitewood Creek Results

6.1.1. Whitewood Creek Correlations Significance

Each fluvial and tailings parameter was linearly regressed to the other parameters to find their correlation values (R^2). The significance of the following correlation values was checked using the two-tail t-test which incorporates R^2 values:

Equation 6.1.

$$t = \frac{r\sqrt{n-2}}{\sqrt{1-R^2}}$$

Where t is the t value, n is the sample size, and r is the square root of R^2 . Based on the data, $t=2.228$ (95% confidence interval) and $n=10$ (number of reaches). The test shows that correlation values with a R^2 less than 0.383 are not significant. Refer to Table 8.1 and 8.2 and R^2 values for each correlation pair.

6.1.2. Whitewood Creek Sinuosity and Longitudinal Profile

The sinuosity index of Whitewood Creek was compared in the 3 time periods (1948, 1977, 2012). There were no major changes over time with respect to the 2012 channel, so the following description is from the 2012 channel (see Figure 6.1). The sinuosity index of Whitewood Creek remains fairly consistent with a gradual increase from 1.17 in Reach 1 to 1.53 at Reach 9. These indexes indicate that the stream is sinuous (with minor meandering since some

values are > 1.5). However, at Reach 10, the index increases to 2 which indicates that the stream is more meandering than sinuous. The longitudinal profile shows that Whitewood Creek is mostly smooth but there are some minor irregularities and a gradual decrease in slope (until around 5000 m or Reach 9, see Figure 6.2). Around 13000 m and 23000 m (Reach 7, 5, and 4) from the Belle Fourche River confluence, there are some minor abrupt “bumps” (possible local knickzones?). It is also possible that these may be errors. From 5000 m, the profile’s slope increases and has a minor fluctuation pattern all the way to the confluence.

6.1.3. Whitewood Creek Contaminated Floodplain Width

The contaminated floodplain widths graph behaves in a fluctuating pattern throughout Whitewood Creek (see Figure 6.3). The 1948 floodplain widths range from about 33 to 80 m where they peak at Reach 2, 5, 8, and 10. The variation of floodplain widths (standard deviation measured from ArcMap) goes from 15 to 42 m with an average around 25 m. Similarly, the 1977 pattern fluctuates throughout the stream and has peaks at Reach 2, 5, 8, and 10 but is greater than the 1948 pattern at Reach 2, 4, and 7 (see Figure 6.4). The 1977 contaminated floodplain widths vary from 29 to 91 m. The average standard deviation of the 1977 floodplains is similar to the 1948 floodplain data, with an average value of 26 m (range from 14 m to 65 m). The change in variation between the two years is moderate but Reach 4 has fairly high change of 48% decrease. The 1948 and 1977 floodplain width and standard deviation correlation are positively moderate ($R^2 = 0.5261$ and 0.6077 respectively). The 1977 floodplains width also has a weaker moderate positive correlation with sinuosity ($R^2 = 0.4673$). There are no major differences between 1948 and 1977 contaminated floodplain widths, all values are $< 50\%$ with the largest difference at Reach 1 with 38%. Similarly, there are no major changes for the standard deviation of the contaminated floodplain widths although Reach 4 has the highest change at 48%.

6.1.4. Whitewood Creek Contaminated Sediment Area

The 1948 contaminated sediment area has two major peaks near the town of Whitewood at Reach 2 and at Reach 8 (see Figure 6.5). The area of the 1948 sediments ranges from 44000 to 260000 m². The 1977 graph follows a similar pattern to 1948 but with lower values (varies from 36000 to 201000 m²). The 2012 contaminated sediment area for each reach overall is in between the 1948 and 1977 graphs (33000 to 214000 m²) except for Reach 3, 6, and 7 where the 2012 graph is lower than 1977. From 1948 to 2012, the contaminated sediment in these reaches changed by roughly 45%. Other reaches that underwent major changes were Reach 2 (47%), Reach 4 (66%), and Reach 5 (70%). Both the 1948 and 1977 contaminated sediment areas have a moderate positive correlation with contaminated floodplain width ($R^2 = 0.5793$ and $R^2 = 0.5179$, respectively) along with contaminated floodplain width variations ($R^2 = 0.5793$ and $R^2 = 0.6648$, respectively).

6.1.5. Whitewood Creek Contaminated Sediment Removed Area

From 1948 to 2012, the contaminated removal area peaks from Reach 2-5 and at Reach 8 (see Figure 6.6). Removed area ranges from 5700 to 46000 m² per reach. The 1977 to 2012 removal area period is lower by at the most a magnitude of order with values ranging from 892 to 24000 m². The largest peak occurs at Reach 2 which is followed by a fluctuating decrease to Reach 10. The 1948-2012 period removed sediment area has a moderate correlation with area of contaminated sediment ($R^2 = 0.5320$) and contaminated floodplain width variation ($R^2 = 0.5253$). The 1977-2012 removed area is weakly correlated to these parameters. Major decreases between the 1948-2012 and 1977-2012 occurred where all reaches underwent >50% change except for Reach 2 (43%). The largest decrease is found at Reach 8 with a decrease of 86%.

6.1.6. Whitewood Creek Channel Migration

The 1948-2012 channel migration graph has two peaks at Reach 3,4, 7, and 8 (see Figure 6.7). Channel migration ranges from 18 to 31 m with an average of 19 m. The 1977-2012 pattern is inverse to the 1948 graph where it peaks at Reach 2 and 5. Values are also lower where it varies from 11-23 m. There are 4 reaches that underwent major changes during 1948-2012 and 1977-2012. Reach 3 and 4 had 48% and 54% decrease, respectively and Reach 8 and 9 had a 50% decrease. Reach 2, 5, and 6 are the only reaches where the 1977 migration is greater than the 1948 but they are not significant (5%, 13%, and 2% respectively). Both 1948 and 1977 channel migration have weak correlation with all of the parameters (except for total sediment deposition area).

6.1.7. Whitewood Creek Total Sediment Deposition Area

The overall pattern of sediment deposited from the 1948 to 2012 period is similar to the 1948 to 2012 channel migration (see Figure 6.8). This is the same for the 1977 to 2012 plot. The reason for these similar trends is due to using the same polygons that were used to create the migration of channels. Four reaches underwent major changes: Reach 3 and 4 had a decrease of 66% and 59% respectively and Reach 8 and 9 decreased from 51% and 52% respectively. Reach 5 is the only location where 1977-2012 is greater than 1948-2012 but the difference is small (7%). Both the 1948 and 1977 total sediment deposition area have a strong positive correlation with channel migration ($R^2 = 0.8797$ and 0.8283 respectively). The 1948 area also has a weakly moderate positive correlation with the removed area parameter ($R^2 = 0.5064$).

6.2. Belle Fourche River Results

6.2.1. Belle Fourche River Correlations Significance

Similarly, to Whitewood Creek, a two-tail t test was used to determine the significance of R^2 . While the 1948 data is similar to Whitewood Creek ($R^2 < 0.383$ is insignificant) due to same sample number, 1977 is different ($n=7$ instead of 10), so the t value is different ($t= 2.365$). For the 1977 data, R^2 values that are less than 0.528 are insignificant. Refer to Table 8.3 and 8.4 R^2 values for each correlation pair.

6.2.2. Belle Fourche River Sinuosity and Longitudinal Profile

The sinuosity of the Belle Fourche River from 1948 and 1977 is mostly the same as the 2012 although the 1977 index is lower at 2.3 at Reach 7. The description here is from the 2012 sinuosity (see Figure 6.9). The sinuosity index of the Belle Fourche River is greater than 1.5 at all the reaches. Since these indexes are greater than 1.5, this indicates that all of the reaches in the Belle Fourche River are meandering. The sinuosity progressively gets higher from Reach 1 (1.7) to Reach 8 (3) where it decreases to around 2. The longitudinal profile of the Belle Fourche River is mostly rough between the confluence with Whitewood Creek and the village of Volunteer (see Figure 6.10). However, some of this roughness (especially the area with peaks) could be measurement error results during data extraction such as inaccurate pixels from the DEM. One interesting area is between 30000 m (Reach 4) to about 45000 m (Reach 6) where the profile smooths and levels out briefly (see Figure 6.10). Overall, the slope of the Belle Fourche River is lower than Whitewood Creek's slope.

6.2.3. Belle Fourche River Contaminated Floodplain Width

The 1948 contaminated floodplain width pattern fluctuates where the peaks occur at Reach 2, 6, and 8 (see Figure 6.11). Values range from 57 to 114 m. Standard deviations range from 30 to 229 m (average of 75 m). The 1977 average contaminated floodplain width pattern also fluctuates but has a more sinusoidal nature (especially from Reach 3-6) and has lower values (ranges from 50 to 83 m). Peaks occur at Reaches 2, 4, and 6. The standard deviation in 1977 also has a lower value than 1948 where it ranges from 4 to 59 m with an average of 33 m. There are no major changes in the contaminated floodplain widths from 1948 to 1977 (see Figure 6.12). The largest change is at Reach 6 with a 26% decrease. However, the contaminated floodplain width variation underwent major decreases at all reaches except for Reaches 2, 4, and 7. Reach 1 was 59%, Reaches 3 and 5 were 74%, and Reach 7 was 90%. The correlation between contaminated floodplain width, contaminated floodplain width variation, and sinuosity is weak. The 1977 contaminated floodplain width has the highest R^2 with contaminated floodplain variation (1.989), but this is insignificant according to the t-test.

6.2.4. Belle Fourche River Contaminated Sediment Area

The 1948 graph has two large peaks at Reaches 2 and 5 followed by a gradual constant decrease below Reach 5 (see Figure 6.13). Values range from 210000 to 670000 m² per reach. The 1977 graph follows a similar pattern but with lower values (varies from 140000 to 410000 m²). The 2012 contaminated sediment area follows the same pattern as 1948 but has slightly lower values. There are two reaches that underwent major changes between 1948 and 1977: Reach 5 decreased at 58% and Reach 7 at 53%. Both the 1948 and 1977 contaminated area have low correlation with the parameters mentioned above but the 1948 area has a weakly moderate positive correlation with contaminated floodplain width ($R^2 = 0.4171$).

6.2.5. Belle Fourche River Contaminated Sediment Removed

The pattern of removed contaminated sediments from 1948 to 2012 is sinusoidal where peaks occur at Reaches 2, 5, and 8 (see Figure 6.14). Removed area ranges from 10000 to 52000 m² per reach. The 1977 to 2012 period follows a similar pattern and is greater than the 1948 at Reaches 1-4. Peaks occur at Reaches 2, 4, and 6 with a range of 2500 to 660000 m² per reach. Two reaches have major changes from 1948 to 1977: Reach 5 with a 73% decrease and Reach 7 with a 84% decrease. The 1948-2012 removed contaminated sediment area has a moderate correlation with contaminated sediments ($R^2 = 0.6487$) and the correlation is stronger for 1977-2012 ($R^2 = 0.8962$). The 1948-2012 removed area also has a moderate correlation with floodplain widths ($R^2 = 0.4977$).

6.2.6. Belle Fourche River Migration

The 1948 to 2012 channel migration pattern varies little with peaks at Reaches 2 and 6 and ranges in value from 10 to 34 m (see Figure 6.15). The 1977-2012 period is similar to the 1948-2012 migration pattern but has lower values at Reaches 5 and 6 (ranges from 10 to 27 m). There are no major changes between the two periods; the largest difference is 21% at Reach 5 and 6. The 1948-2012 migration has a weak moderate correlation with contaminated floodplain widths ($R^2 = 0.4143$) while the 1977-2012 has a weak moderate correlation with sinuosity ($R^2 = 0.4201$) and floodplain width ($R^2 = 0.4541$) but these are insignificant.

6.2.7. Belle Fourche River Total Sediment Deposition Area

The 1948 to 2012 total sediment deposition area plot is similar to the 1948-2012 channel migration plot with the exception of Reaches 7 and 8 (see Figure 6.16). Values range from 24000 to 175000 m². The 1977 to 2012 pattern is also similar to the 1977 channel migration plot where

it peaks at Reaches 2 and 6 (values range from 27000 to 130000 m²). Both 1948-2012 and 1977-2012 have strong moderate correlation with channel migration ($R^2 = 0.7729$ and 0.6461 respectively). There are no large changes during the 1948-2012 to 1977-2012 periods with the largest decrease in Reach 7 at 39%.

CHAPTER 7. GEOCHEMISTRY RESULTS

These results are from modeling using SpecE8 and REACT from Geochemist's Workbench (Bethke et al., 2021) as described in the Chapter 5 Geochemistry Method Section for four locations: Whitewood Creek in the mountains (Locations A-E), Whitewood Creek in the Great Plains (Location F-H), Belle Fourche River after confluence (Locations I-K), and Belle Fourche River before the Whitewood Creek confluence (Location L).

7.1. Summary of Water Quality of Whitewood Creek, Belle Fourche River, and Seeps

This is a summary of the water quality from geochemical results in Whitewood Creek, Belle Fourche River, and seeps from Ji (2021). Refer to Appendix 5-2 for analytical results of the waters and their comparison to EPA values.

Ji (2021) compared the following analytes to the EPA's National Primary Drinking Water Regulations maximum contaminant levels (MCLs, highest level of contamination allowed in drinking water): As, Sb, Ba, Be, Cd, Cr, Pb, and Se). Of these elements, As, Sb, Be, Cd, and Pb exceed their respective levels in at least one sample.

Throughout Whitewood Creek and the Belle Fourche River, As is above its MCL (0.01 mg/l) at most locations (see Figure 5.2 for graph of As concentration at each location). Generally, Whitewood Creek mountain locations are below or slightly exceeding the MCL where Location D has the highest level (0.016 mg/l). It is important to note that Location A has a higher value at 0.025 mg/l but it may not be a representative of baseline conditions due to being affected by the nearby Bald Mountain Mine (Ji, 2021). On the plains (Locations E-H), the As levels in Whitewood Creek are higher with Location G being the highest (0.087 mg/l). Downstream in the Belle Fourche River, the levels decrease where the maximum value is at

Location K (0.033 mg/l). Upstream of the Whitewood Creek confluence, Location L's concentration is below the MCL (0.0040 mg/l). While the seep at Location B is similar to the stream water, the As levels at the Location G and H seeps are higher by an order of magnitude (0.4 mg/l). Except for Location L, all of these sites have As levels greater than the average world stream As concentration (0.002 mg/l) (Faure, 1998).

Cadmium exceeding its MCL (0.005 mg/l) was measured at all locations with an average of 0.0206 mg/l. According to USGS (2017), Cd levels in the Black Hills area are generally elevated in the topsoil ranging from 0.3-0.6 mg/kg due to the underlying shale bedrock as well as some influence from the tailings. Other elements exceeded their MCL (Sb, Be, and Pb) are generally in the stream and seep water locations (Location G and H) as well as Location K in the Belle Fourche River.

Ji (2021) also compared the analytes to the EPA's National Secondary Drinking MCLs (non-enforceable guidelines regarding contaminants that may cause aesthetic or cosmetic effects in the drinking water) where Al, Fe, and S exceeded their respective levels. Aluminum exceedance of this MCL (0.2 mg/l) occurred at Locations A and H-L where Location K has the highest value (0.51 mg/l). Iron exceeds its MCL (0.3 mg/l) at all locations (except for Location F). The average Fe level is around 2 mg/l but can be as high at 15 mg/l (Location B seep water). This average also exceeds the average Fe found in stream waters throughout the world (0.04 mg/l) (Faure, 1998). For S, the only locations where it exceeds its MCL (250 mg/l) are Location B and H seeps, and Location K. While the average S concentration is 308 mg/l, Location B seep has the highest value at 1662 mg/l. The S level in the study area is about 2-3 magnitudes higher than the average world stream composition (3.7 mg/l) (Faure, 1998).

In addition, Ji (2021) compared the water composition to the EPA Health Advisory (HA) Life-time Standard (non-enforceable estimates of acceptable drinking water levels for chemical substances) and found Mn, Mo, Ni, and Sr exceed their respective comparison values in at least one sample. These elements are generally found in the seep water locations (Location B, G, and H).

With two exceptions, the water quality of Whitewood Creek and Belle Fourche River is generally good relative to human health standards. The two metals of concern are As and Cd due to their great exceedance of their National Primary Drinking Water Regulations MCLs and widespread distribution. Iron is another interesting analyte due to exceeding its National Secondary Drinking MCL throughout the entire study area. The presence of high Fe in these waters could play a major role in the mobility of As.

7.2. As and Fe Redox Coupling

The geochemistry results given were calculated with the redox of As (V) and As (III), and Fe (II) and Fe (III) are coupled (redox state is defined by the Eh input). If the As species were decoupled, the results of all the minerals are the same, however, no As rich minerals are supersaturated. Different ratios of the As species were modeled and the results remain the same. If the Fe species are decoupled, the results for most of the mineral indices change little, however the nontronite clays are the only minerals to have large saturation index change by at the most a magnitude (i.e., from 17 to 6) depending on the measured concentration of Fe (III). If the Fe (III) concentration decreases, so does the nontronite saturation index. In addition, a few more Fe rich minerals are supersaturated (especially those that take in both Fe (II) and Fe (III)) like greenalite, daphnite, and chamosite). The saturation indices of these minerals will increase as the Fe species ratios increase with respect to Fe (III).

7.3. Minerals Saturation Results

Overall, the mineral saturation indices for stream water overlap and/or are off by 2-3 orders of magnitudes from one location to another in the mountains and Great Plains. In comparison, the seep water has lower indices by at the most 10 orders of magnitude where Fe based minerals see the most change (see Table 7.1 to 7.5 for saturation indices for each general region). The minerals showing the highest indices are clay minerals, Fe (hydr)oxides, phosphate (in the form of hydroxyapatite), and some carbonates and sulfates. One As phase in the form of $Ba_3(AsO_4)_2$ is supersaturated in some locations in Whitewood Creek, but as described in the Discussion section, it is not observed in nature.

One thing to note is that some minerals, especially clays, have more than one value. These are the same minerals but have different exchange cations (i.e., Na-nontronite, Ca-nontronite). These species and their cations can be referred to in Appendix 7-1 to 7-15 for each location. It is also important to note that the comparisons of these different regions of the study are difficult due to different sets of chemical analyses of the water (see Geochemistry Method Section).

7.3.1. Whitewood Creek Mountain Locations (A-E)

In the mountain locations, the mineral with the highest saturation index is the Fe-rich smectite, nontronite, which has a Log Q/K range from 19.3-17.3. Other smectite clays are also supersaturated, with a saponite saturation index range from 7.83-4.38 and beidellite's range from 4.77-0.76. Chlorite minerals are supersaturated in these waters where the saturation index of Mg-rich clinocllore ranges from 8.3-2.22, Fe rich ripidolite from 4.77-0.76, and daphnite at 1.35 (only at Location A). An interesting note is that after nontronite, Locations A and D have saponite as the second highest clay saturation index, while at Locations B and C it is clinocllore.

Two other Mg-rich phyllosilicate minerals, talc and sepiolite, are supersaturated with their saturation index values ranging from 6.81-4.54 and 4.52-1.61 respectively. Kaolinite is also supersaturated with a range of 4.11-2. For the (hydr)oxides, hematite has the highest saturation index for all sites with a value range of 14.9-14.5. With a similar value, the Cu-Fe sulfide delafossite (CuFeO_2) has a range of 14.2-13. Other Fe and Cu rich (hydr)oxides that are supersaturated are goethite (6.98-6.64), a mineral with the formula of $\text{Fe}(\text{OH})_3$ (2.52-2.18) (possibly ferrihydrite), and tenorite (0.6-0.19). The only Al hydr(oxide) that is supersaturated is gibbsite (1.23-0.35). The only sulfate that is supersaturated is barite with a value range of 0.84-0.72. Two silica minerals, quartz and chalcedony, also have low supersaturated values of 0.6-0.43 and 0.32-0.15 respectively.

7.3.2. Whitewood Creek Great Plains Locations (F-H)

For the Great Plains section of Whitewood Creek, nontronite has the highest saturation indices at all sites, ranging from 17.5-15.6. Saponite and beidellite are also supersaturated with values of 8.25-3.38 and 3.06-0.16, respectively. Since these locations are between the USGS gage stations, Whitewood Creek above Whitewood and Whitewood Creek above Vale, additional components are added such as HCO^- , Cl^- , K^+ , and PO_4^{3-} (see Geochemistry Methods). By adding K^+ , two other smectite species are supersaturated under the names of smectite low Fe-Mg and smectite high Fe-Mg. Their indices range from 4.78-2.12 and 4.32-1.77 respectively. Illite is also supersaturated with a value range of 3.95-2.39. For the chlorite, the Mg-rich chlorite, clinochlore is supersaturated with saturation index range of 9.81-2.9, as well as ripidolite with a range from 5.28-1.85 (except at Location F). Al-rich kaolinite has a saturation index range of 2.8-1.13. For other phyllosilicates, Mg-rich talc and sepiolite range from 7.04-3.88 and 4.78-0.57, respectively. Like the mountain location water, hematite has the next highest saturation

indices, ranging from 13.9-12.9, and Cu rich delafossite ranges from 13.9-12.9. The other Fe-rich hydr(oxides), Goethite and $\text{Fe}(\text{OH})_3$, have values ranging from 6.48-6 and 2.11-1.53, respectively. Other metal (hydr)oxides are Cu rich tenorite (0.76-0.09) and Al rich gibbsite (0.81-0.31). Location F, however, is undersaturated with respect to tenorite and gibbsite. The water of Whitewood Creek is also supersaturated with carbonate minerals such as calcite (1.31-0.79) and Mg-rich carbonate minerals like dolomite (3.52-1.21), huntite (1.88-0.82, except at Location F), and magnesite (0.98-0.13). Both Malachite and rhodochrosite are predicted to be supersaturated at 0.009 but only at Location G (for malachite) and Location H (for rhodochrosite). Like the mountains, the only supersaturated sulfate mineral is barite (0.76-0.4). Two phosphate minerals are supersaturated: hydroxyapatite with a high saturation index value ranging from 12.4-9.94 and phosphate mineral with the formula of MnHPO_4 ranging from 1.83-0.26 at Location F and H only. The silica minerals, quartz and chalcedony (not supersaturated at Location H) have values ranging from 0.42-0.19 and 0.14-0.08, respectively.

7.3.3. Belle Fourche River Locations (I-K)

In the Belle Fourche River locations, the saturation indices are similar to Whitewood Creek. Nontronite has the highest saturation indices ranging from 17.4-16.3, with saponite ranging from 5.26-3.63, low Fe-Mg smectite from 3.51-3.2, high Fe-Mg smectite from 3.49-3.13, and beidellite from 2.9-1.07. An interesting note for the Belle Fourche River locations is that they all have clinochlore as the second highest phyllosilicate supersaturation with indices ranging from 5.5-1.62. Other chlorite minerals include ripidolite ranging from 4.04-0.22 and daphnite at 0.75 (for Location I only). For the other clays, illite ranges from 3.61-3.14, and kaolinite from 2.89-2.41. The Mg rich phyllosilicates talc ranges from 4.12-3.8 and sepiolite ranges from 0.69-0.23. For the (hydr)oxide minerals, hematite has the highest index ranging

from 14.4-14 followed by the Cu-Fe delafossite from 13.5-13.1. While goethite and $\text{Fe}(\text{OH})_3$ range from 6.7-6.5 and 2.34-2.13 respectively, tenorite is only supersaturated at Location I at 0.04. Gibbsite is also supersaturated with a low value range of 1-0.73. Like the other sites, the only sulfate mineral that is supersaturated is barite ranging from 0.46-0.41. For the carbonates, dolomite has the highest indices ranging from 3.26-1.58. Other Mg rich carbonates like huntite and magnesite have values from 0.62-0.32 and 0.35-0.27, respectively. Calcite is also supersaturated with saturation indices ranging from 1.29-1.23. The only silica mineral that is supersaturated is quartz with a small index of 0.27-0.18. Finally, the phosphate hydroxyapatite has the third highest indices out of all the saturated minerals, ranging from 13.3-12.3.

7.3.4. Belle Fourche River before Whitewood Creek (L)

Upstream from the confluence of Whitewood Creek, Location L mineral indices are similar to all of the other locations. For the smectites, nontronite has the highest indices ranging from 18-17.5, saponite from 5.19-3.89, smectite at 3.97 (low Fe-Mg) and 3.88 (high Fe-Mg), and beidellite from 3.53-2.22. Clinocllore has the highest chlorite indices ranging from 5.41-2.02 while ripidolite ranges from 4.06-0.67 and daphnite is at 1.3. For the Mg-rich phyllosilicates, talc has an index of 4 while sepiolite is 0.68. Kaolinite has a value of 3.28. Hematite has the highest metal hydr(oxide) index of 14.5 followed by delafossite at 13.6. Other Fe rich (hydr)oxides are goethite (6.79) and $\text{Fe}(\text{OH})_3$ (2.39). Al oxide in the form of gibbsite has an index of 1.04 and Cu oxide in the form of tenorite is at 0.06. The only supersaturated sulfate is barite with a value of 0.62. Finally, two silica minerals, quartz, and chalcedony, are supersaturated with values of 0.36 and 0.08, respectively. Compared to the Belle Fourche River locations downstream (Location I, J, K), the upstream saturation indices overall have similar ranges, although some minerals such

as nontronite, clinocllore, ripidolite, beidellite, daphnite, kaolinite, and gibbsite can have lower indices by around 1-2 orders of magnitude.

7.3.5. Whitewood Creek Seep Locations (B, G, H)

Compared to the stream waters, the saturation indices of the seep water are generally lower, but some of the Al-rich mineral indices are slightly higher. For the smectite clays, nontronite has a value range of 11.1-7.49. It is important to note that Location H has lower values of 8-7.49. Beidellite has the next highest clay index ranging from 5.22-1.36 and saponite has a low range of 0.63-0.1 (with no saponite supersaturation at Location H). Al-rich kaolinite has a value range of 4.92-2.54. There are some chlorite minerals that are superaturated such as daphnite (2.16-1.91, not found at Location H) and chamosite (0.91-0.09, not found at Location H). For the Fe rich (hydr)oxides, hematite ranges from 6.82-6.11 and Cu-Fe rich delafossite ranges from 13.3-11.6, and goethite is supersaturated at 2.95-2.54. Gibbsite has a saturation index range of 1.78-0.62. Another Al hydroxide, boehmite is supersaturated at Location H with saturation index values of 0.18. The silica minerals, quartz and chalcedony, both are supersaturated with the water at 0.78-1.98 and 0.5-0.16 respectively.

7.4. Dissolved As Transportation Rate in Whitewood Creek Stream Water

The Geochemist's Workbench model calculation of dissolved As in Whitewood Creek shows that the annual rate of transportation with an arsenopyrite mass of 15% is $52 \frac{Mg}{year}$ while 0.11% is $0.39 \frac{Mg}{year}$.

7.5. Suspended As Transportation Rate in Whitewood Creek Stream Water

Calculation for average suspended sediment As assuming contaminated sediment has uniform thickness of 0.6 m along Whitewood Creek and 15% arsenopyrite mass shows a

transportation rate would be $\frac{Mg}{year}$. If the arsenopyrite mass was 0.11%, then it would be 2.54

$\frac{Mg}{year}$. If the thickness was 3.5 m with 15% arsenopyrite, then the average transportation rate

would be $59 \frac{Mg}{year}$ while 0.11% arsenopyrite would be $1.98 \frac{Mg}{year}$.

CHAPTER 8. GIS AND FLUVIAL GEOMORPHOLOGY DISCUSSION

This section will present the discussion of Whitewood Creek and Belle Fourche River GIS results. Table 8.1 and 8.2 shows the correlation between each parameter and their significance for Whitewood Creek and Table 8.3 and 8.4 for Belle Fourche River based on Equation 6.1.

8.1. Whitewood Creek Discussion

8.1.1 Whitewood Creek Parameters Correlations

The linear regression results of the different parameters of Whitewood Creek show that there are multiple correlations that are significant over the period 1948-2012. The highest R^2 correlation was between channel migration and total sediment depositional area but as mentioned in the Results section, this may be inherited due to the nature of streams leaving deposits behind as they migrate from their former position. Parameter comparisons with significant moderate positive correlations ($R^2 \sim 0.5$) for both 1948 and 1977 are contaminated sediment area, contaminated floodplain widths, and contaminated floodplain width variations. Additional moderate positive correlations but only for 1948-2012 are contaminated sediment removal area, contaminated sediment area, contaminated floodplain width variations, and total sediment gained area. For 1977, sinuosity and contaminated floodplain width has a significant positive correlation.

8.1.2. Controls on Contaminated Sediment Area in Whitewood Creek

The areal extent of the contaminated mine tailings based on aerial photographs from EPA (1972) in Whitewood Creek is complex and can be explained by multiple factors. The 1948 tailings has a higher area than the 1977 tailings. The decrease in reach area can be as large as 70% (see Figure 6.5). One factor that may cause this is a change in sediment load. From the late

1800s to the mid-1950s, it was acceptable to dispose of all mill tailings into Whitewood Creek. By 1955, 50% of the mine tailings were used as backfill in underground tunnels (Waterland, 1973) and by 1977, all tailing transportation ended. This decrease in sediment load could have affected the fluvial geomorphology of Whitewood Creek. Details of this effect will be explained further below. Another factor that can affect the size of the 1977 tailings is flooding. According to the streamflow graph from the USGS gaging station, Belle Fourche River Sturgis, from 1946 to 2022 (Figure 3.2), there has been an increase in peak flow after 1960 and the magnitude and duration of peak flow have also increased since 1980. Norton et al. (2014), Kibria et al. (2016), and Shockley (2021) also observed upward trends in observed streamflow within the study area from USGS gaging stations. These flooding events can cause major morphologic changes in the stream.

The highest area of tailings occurs mainly around Reach 2 and 8 (see Figure 6.5 and 8.1). Tailings were observed from around Reach 2 to 5 by Marron (1992) who noted that Whitewood Creek in the first 13 km downstream from the town of Whitewood has an anomalously wide channel, channel and meander abandonment, and channel incision. Using aerial photos and channel position of a surveyed map from Darton (1919), Marron (1992) indicated that extensive meander abandonment occurred between 1910 and 1939. However, Cherry et al. (1986) says that the abandoned meanders may have filled with tailings before 1900 as seen by 75–85-year-old trees growing in the tailings (seen in Location G and one site in Reach 8). These meander abandonments, along with channel incisions, strongly influence the deposition of the mine tailings. Figure 8.1 shows that these reaches have high channel migration, sediment deposition, and tailings removal. The tailings also occur as overbank deposits, and some locations of these deposits can extend 100 m from the channel (see Figure 3.5 for aerial photograph). While the

aerial maps from EPA (1972) do not display these abandoned meanders filled with tailings clearly, the overbank deposits are observable.

There are multiple possibilities why Reach 2 (as well as Reaches 3-5) might have a high storage area compare with the tailings. One control could be lithological. Above Reach 2, Reach 1 begins near the contact of the Permian Minnekahta Limestone and the Triassic Spearfish Formation, which is composed of red mudstone, siltstone, fine-grained sandstone and gypsum beds (Fagan and Lisenbee, 2017). Below the town of Whitewood and beginning of Reach 2, the lithology changes to the Jurassic Gypsum Springs Formation (gypsum beds), Sundance Formation (sandstone, siltstone, shale), and Morrison Formation (bentonitic claystone, siltstone, sandstone with minor limestone). Towards the downstream end of Reach 2, the Cretaceous Lakota Formation and Fall River Formation (fine grained quartz arenite and mudstone) form low hills. This is followed by the beginning of the Great Plains shale units with the Skull Creek and Mowry Shales at Reach 3 (Fagan and Lisenbee, 2017). Areas with mudstones, shale, gypsum, and siltstone, are more vulnerable to fluvial erosion and expansion of floodplains. This can be seen in the maps of Lisenbee et al. (2015) and Fagan and Lisenbee (2017), where the alluvium and terrace complex of Whitewood Creek is wide (can be around 2500 feet (~762 m)). Even the floodplain where the creek cuts into the hills composed of the sandstone Lakota Formation and Fall River Formation can be up to 2000 feet wide (~610 m) (see Figure 3.5 for aerial photograph of this area). However, despite Reach 1 flowing over the mudstone/siltstone Spearfish Formation, its contaminated sediment area is not as wide as Reach 2. Reach 2 may also have high storage area compare with tailings because it is roughly at the transition zone from a steep narrow mountain channel to the flat, meandering Great Plains channel. Following the continuity formula:

$$Q = vA$$

Equation 8.1.

where Q is discharge, v is velocity, A is cross sectional area, as the velocity decreases due to the flatter topography, this will increase the cross-sectional area, hence increasing channel and floodplain area. This could also explain why the floodplain size is wide within the more resistant sandstone Lakota Formation and Fall River Formation.

Another area with a high area of tailings is at Reach 8, which is about 6 km above the Belle Fourche River confluence (see Figure 6.5 for aerial photograph). Part of this reach was also studied by Marron (1992) who says that the 6 km stretch to the confluence stores more than half of the 14.5×10^6 Mg tailings found through Whitewood Creek. According to Cherry et al. (1986), the tailings around this reach are greatly augmented by an artificial tailing structure that was built in the early 1900s around Location H. At the beginning of the reach is a wide stretch of floodplain about 1.5 km long, with tailings areas of 238,000 m² for 1948, 201,000 m² for 1977, and around 100-200 m wide. The high storage in this reach could possibly be controlled geomorphologically. Reach 8 may be on top of a knickzone as described by Zaprowski et al. (2001). They mapped two erosion fronts (knickzones) in the eastern Black Hills (see Figure 3.1). The lower front (labeled Farmington front) is found near the confluence with the Belle Fourche River. As seen in the longitudinal profile overlayed with the tailings area of Whitewood Creek (Figure 8.2), there is a minor increase in gradient just below Reach 8 is located. Topographically, above these knickzones are broad valley bottoms; at and below them are channel incisions into bedrock, floodplain abandonment, and terrace development (Zaprowski et al., 2001). The broad valley bottoms could explain why sediment storage as well as channel migration is high at Reach 8 followed by a decrease due to channel incision in Reach 9 (see Figure 8.1). Belmont (2011)

found in a study in southern Minnesota that above knickzones, floodplains are relatively wide and unconfined compared to within the knickzone, where floodplains progressively narrow and lose 25-60% of their width. While this can be seen in the tailings area graph, it is not observable on the contaminated floodplain width graph (see Figure 8.1). In the field, a deep channel incision into bedrock as high as 15 feet (~4.6 m, by eye) was observed in the field at the Vale Cut Off Road (Reach 9), which may be below the Farmington front (see Figure 3.7 and 8.2).

The other erosional front (the Sturgis front) appears to be around the town of Whitewood near Reach 2. While it seems that this knickzone may control Reach 2's large storage, the longitudinal profile doesn't show any sharp changes in that general area unlike Reach 8 (see Figure 3.1). Zaprowski et al. (2001) has the front southwest of Whitewood in Paleozoic units whereas Reaches 2-3 are located northeast of Whitewood in Mesozoic units. The Sturgis front crosses Whitewood Creek within the Black Hills roughly between the Homestake Mine and the town of Whitewood. Hazelwood and Stetler (2019) mapped knickzones found in the transitional landscape between the crystalline Black Hills and the shaley Great Plains outside of Rapid City (about 64 km southwest of Whitewood). While the town of Whitewood appears to be on the margins of the Black Hills, Hazelwood and Stetler (2019) put the upper limit of the knickzones in Precambrian metamorphic rocks and the lower limit in both Precambrian metamorphic rocks and Paleozoic sedimentary rocks.

8.1.3. Controls on Contaminated Sediment Removed Area in Whitewood Creek

Except for Reach 2, all the reaches underwent major erosional changes by at the most around 70-80%. The highest area of erosion occurs at Reaches 2-3 for both 1948-2012 and 1977-2012, 3-5 and 8 for 1948-2012 (see Figure 6.6). A decrease in erosion over time is a pattern that has been observed in mining affected streams, especially streams near the gold mines of

California. The general pattern is high aggradation from high input of mining sediment followed by high incision once mining has ceased. This pattern may be explained by Gilbert (1917), who said that streams with high loads of sediment during times of mining adjust their morphology to maximize sediment transport. One of the responses from this adjust is aggradation which can make the stream more braided. The braided nature of Whitewood Creek can be seen in the 1948 aerial photographs (see Figures 3.5, 3.6, and 3.9). Once mining ceases and sediment supply declines, energy employed in carrying the sediment responds by downward incision through mining/natural alluvium and into the bedrock. In contrast, however, Cherry et al. (1986) suggests that downcutting began during the filling of abandoned meanders in Whitewood Creek which would have been before 1900 (about 50 years before mine sediment input was reduced). An increase in incision at Whitewood Creek can be seen from the decrease of tailings erosion area over time as well as channel migration (Figure 8.1). The correlation tables show that the R^2 values decreased in the 1977-2012 period when the tailings erosion area was compared to total sediment gained area, contaminated floodplain width, and contaminated sediment area. Stream incision was observed in the field at the Vale Cutoff Road (Reach 9) and 194th Street (Reach 7) (see Figure 3.4, 3.7, and 3.11). Ji (2021) also observed incisions at Location G (Reach 5) and Location H (Reach 10) which have cutbank heights of 4 m and 4.5 m, respectively.

Based on the correlations from Table 8.1 and 8.2, high tailings erosion from 1948-2012 occurs in areas with high contaminated sediment area, contaminated floodplain widths, and width variations. Areas with high floodplain storage such as Reaches 2 and 8 will have a higher likelihood of eroding tailings into Whitewood Creek. They may serve as important sources of tailings transportation. While channel migration is high in Whitewood Creek, it has a weak correlation with removal of contaminated sediments ($R^2 \sim 0.3$) and may not be a major control in

tailings transportation. Generally, bank erosion processes play a major role and are influenced heavily by multiple processes that are dependent on local geomorphology (Miller and Miller, 2007). For example, as mentioned before, local USGS geologist John Stamm suggested that large ice blocks during the spring can grate against the bank and cause large blocks of bank sediments to erode into the stream (Ji, 2021). Zabilansky et al. (2002) indicated that river ice can affect prevailing stream conditions and can have an influence on alluvial channel morphology and vertical and lateral distribution of stream flow. In addition, Cherry et al. (1986) say that periods of ice jamming can lead to deposition in overbank areas. The change in contaminated floodplain width variation is interesting as it shows how the floodplains are being reworked over time. Compared to the Belle Fourche River floodplain variations (Figure 6.12), Whitewood Creek has small changes. Despite the large blocks of banks eroding into the stream, seeing this lower change could be significant because it shows that tailings in the floodplains is being reworked is slow and will have a longer residency in Whitewood Creek.

8.2. Belle Fourche River Discussion

8.2.1. Belle Fourche River Parameters Correlations

The parameters with significant moderate positive R^2 values when compared to each other are contaminated sediment area, contaminated sediment removed area, contaminated floodplain, and channel migration. However, by 1977-2012, contaminated sediment area, contaminated sediment removed area, and channel migration are significant. Like Whitewood Creek, channel migration and total sediment deposition area also have a high R^2 value but as mentioned before, it may be inherently correlated.

One interesting difference is how the contaminated sediment area and removed contaminated sediment area has a higher correlation that increases over time (0.6487 for 1948-

2012 and 0.8962 for 1977-2012). The high R^2 values for these correlations may support the idea discussed regarding Whitewood Creek that areas of high removal of contaminated material are controlled by the location of areas with high contaminated sediment area. The higher the areal extent of mine tailings, the higher the chance of removal. Since the Belle Fourche River has a larger area and extent of contaminated sediments than Whitewood Creek, this could explain why the correlation of these two parameters is stronger than for Whitewood Creek (see Figure 6.5 and 6.13).

8.2.2. Controls on Contaminated Sediment Area and Removal in Belle Fourche River

The temporal patterns of the 1948 and 1977 contaminated sediment areas are similar to each other (see Figure 6.13). Reach 2 has the largest area with a value of 670,000 m² for 1948 and 412,000 m² for 1977 (see aerial photos of this Reach from Figure 4.1). The cause for this maximum may be its proximity to the confluence of Whitewood Creek (about 7 km downstream) as well as local high floodplain storage for the tailings to deposit on. During times of large mine tailings influx, the sediments could have accumulated a short distance downstream from the confluence in the location of Reach 2.

At Reach 4 and downstream, the area of the 1977 tailings begins to decrease. Reaches 4-8 are within the channel discontinuities described by Gomez and Marron (1991) due to neotectonics (see Figure 6.13). Reaches upstream from Reach 4, are interpreted by Gomez and Marron (1991) to have stable floodplains with a constant slope, as seen by an inverse relationship of channel slope and sinuosity due to meander cutoffs. Within the discontinuities, however, the reaches show a positive relationship between sinuosity and floodplain slope, which suggests that channel adjustment and floodplain instability are occurring. According to Gomez and Marron (1991), from 1939 to 1981 about two thirds of floodplain reworking in Reaches 5, 6, and 7 is

caused by eastward channel migration. Above Reach 5, all the reaches have minor to moderate changes in tailings area from 1948 to 2012. Reaches 5 and 7, however, have major changes: Reach 5 decreased by 58% and Reach 7 by 53% (see Figure 6.13) (Note that for 1977, Reach 7 is shorter than the other reaches than the other reaches). Seeing major changes in tailings area in these reaches is most likely controlled by neotectonic effects on the fluvial system from Precambrian lineaments caused by reactivation of Precambrian faults (Figure 3.3 and Figure 8.4). The result of this effect is a relative elevation increase to the west and decrease to the east (Gomez and Marron, 1991). High channel migration at Reaches 4-8 and high erosion in Reach 5 and 8 (see Figure 8.3) suggest that unstable and adjusting floodplains may explain the relative decrease in the area of contaminated sediments over time from 1948 to 2012. However, there may be other complex factors such as flooding events that have influenced storage and areal distribution of mine tailings.

One interesting pattern to see is how the 1977 period contaminated sediment removed area is greater than the 1948 period from Reach 2-4 (see Figure 6.14). One reason for this is the difference is the large size of the floodplains relative to Whitewood Creek. As in the Belle Fourche River contaminated sediment area graph, the 1948 floodplains are wider than the 1977 floodplains (see Figure 8.3). It is possible that due to the larger size, the 1948 floodplains extend sufficiently far and are more elevated. This requires a large magnitude flood to rework them, unlike the 1977 floodplains, which are lower and closer to the modern channel (Marron, 1987). While the 1948 floodplains obviously saw more flooding events than 1977, the 1977 floodplains are situated where more frequent and smaller magnitude floods can reach and rework them.

As in all streams, flooding events are a major influence on the fluvial geomorphology of the Belle Fourche River. However, the contaminated floodplain variation in the Belle Fourche

River is different from Whitewood Creek floodplain variation. The Belle Fourche River underwent major changes in variation from 1948 to 2012 while the Whitewood Creek changes are minor in comparison. As seen in Figure 6.12, the Belle Fourche River underwent changes in Reaches 1, 3, and 5 where differences between the 1948 and 1977 periods range from 59 to 74%. Reach 2 and 6 are around 40% while Reach 4 is 8%. Reach 7 is shown to have a change of 98%, but as mentioned above, Reach 7's length is shorter (see Figure 6.12). In comparison to Whitewood Creek, Figure 6.4 shows that the largest change occurs at Reach 4 with a change of 48%. Other reaches have lower percentages with a range of 3 to 35%. Seeing these differences show how vulnerable the floodplains of the Belle Fourche River are to reworking, which is most likely due to an increase in high discharge flow in the region since the end of the 20th century (see Figure 3.2), larger stream discharge, and a longer course where other streams merge with it upriver. Whitewood Creek, on the other hand, has slower floodplain reworking due to deep stream incision (floodplains elevated above the active channel), having a lower discharge, fewer confluences with other streams, and a shorter course. This is important because the contaminated sediments in the Belle Fourche River are being reworked more than Whitewood Creek but, at the same time, are getting diluted by uncontaminated sediments from other streams and being carried out of the study area sooner. While Whitewood Creek's contaminated sediments are being reworked more slowly, it will likely remain on the floodplains longer and slowly continue to contaminate the stream over time.

CHAPTER 9. GEOCHEMISTRY DISCUSSION

This section will present the discussion of geochemical modeling of mineral saturation in the waters of Whitewood Creek and Belle Fourche, and calculation of annual dissolved and suspended As transportation in Whitewood Creek.

9.1. Comments About Mineral Saturation Indices:

Before discussing the mineral saturation indices of Whitewood Creek and the Belle Fourche River waters, it is important to mention the meaning and significance of mineral saturation indices. As Bethke (1996) stated, interpreting saturation indices for natural waters can be tricky due to data errors that can strongly affect calculated values. One problem with mineral saturation indices is that they are dependent on the mineral formula unit. For example, if quartz's unit was in the form Si_2O_4 , then its indices will double. This is why large formula units such as clays appear frequently at the top of a list of most highly supersaturated minerals (Bethke, 1996). A second problem is some minerals that are supersaturated thermodynamically do not exist in surface conditions (i.e. andradite is shown to be supersaturated in these waters). A third problem is that the calculations are only based on equilibrium thermodynamics. In reality, mineral precipitation/dissolution in surface conditions are not in equilibrium and are based on complex combination of thermodynamic and kinetic processes. Overall, it is important to remember that high saturation index values do not necessarily mean there will be more of that mineral or any of that mineral at all; the saturation index values only indicate whether a mineral is supersaturated, saturated, or undersaturated with respect to a particular water composition. The saturation indices indicate that there is a sufficient abundance of constituents of a mineral to allow it to form, however it does not mean that it will form.

9.2. Mineral Saturations in Stream Water:

9.2.1 Clay and Phyllosilicate Minerals

Overall, the stream waters have similar saturation indices of clay and phyllosilicate species in Whitewood Creek and the Belle Fourche River and have saturation indices that vary by around 2-3 (see Table 7.1 to 7.3). The presence of clay rich colloids in the stream water may explain why the clay and phyllosilicates saturation indices are high. Rees and Ranville (1988) used a SEM on the colloids from the stream water of Whitewood Creek and found that the colloids are composed of mostly clay minerals with little Fe. According to the Geochemist's Workbench model, the majority of phyllosilicate species that are supersaturated in these waters are smectite in the form of saponite (Mg rich) and nontronite (Fe rich), and Mg rich chlorite (clinochlore). In addition, other Mg-rich phyllosilicates such as talc and sepiolite are also supersaturated as well as Mg- and Fe-rich chlorites like ripidolite and daphnite (chamosite as well if the Fe species are not coupled). This is reasonable due to the high Mg, Ca, and Fe of the different materials that the stream water interacts with. The Homestake Formation is dominantly Mg and Fe rich due to minerals such as sideroplesite (Mg rich siderite), cummingtonite, chlorite, biotite, and Fe sulfides. In the mine tailings downstream, about 30% of the mineralogy is clays (includes kaolinite, smectite, chlorite, illite, mixed-layer clay minerals) (Goddard, 1989). The Pierre Shale forms most of the bedrock and has an average composition of 53% clay content (70% illite-smectite mixed layer (specifically beidellite for the smectite) 16% illite, 3% chlorite, and 9% kaolinite) (Schultz et al., 1980). Additional silicates like biotite, albite, amphiboles, and pyroxene in the tailings can create more clay minerals by breakdown during chemical weathering and transportation. Because of their high specific surface area, clay minerals may be important for adsorbing As, although there has been limited research on it. Ji (2021) found that 40% of As

in the tailings is labile and that 24% of the labile As has moderate bonding in weakly soluble secondary minerals such as adsorbed onto clays or fine grained crystalline metal (hydr)oxides. Since these minerals have moderate bond strength with As, As will have a slower desorption time (Wang and Mulligan, 2006). The adsorption of As(V) in clay minerals (specifically kaolinite, montmorillonite, illite, halloysite, and chlorite) can occur around slightly acidic to neutral pH and begins to decrease as conditions become more basic (Lin and Puls, 2000). Clays with impure Fe species may also be essential for As adsorption by forming Fe (hydr)oxides minerals in their structures which can increase sorption capacity. The chlorite mineral group is an important group for sorption due to Fe in the structure (i.e., clinocllore, ripidolite and chamosite) (Lin and Puls, 2000). However, the clays with the highest saturation indices are nontronites (Fe rich smectite) along with smectite with high Fe-Mg. DeVore et al. (2019) found Fe in clay minerals and silicates through the use Mossbauer spectroscopy (Fe speciation was mostly Fe (III)) and XRD in the mine tailings of Whitewood Creek's floodplains. According to Violante and Pigna (2002), phyllosilicates that are enriched in Fe such as nontronite can be effective in adsorption of As(V), even in the presence of PO₄. Arsenic is more likely to be adsorbed in these types of minerals when the environment is neutral-acidic. However, PO₄ can inhibit As(V) adsorption if the environment is neutral-alkaline. While DeVore et al. (2019) worked on the contaminated floodplain sediment, the stream water colloidal work from Rees and Ranville (1988) shows that most of the clay minerals in the stream water have little Fe. Ideally, the Pierre Shale bedrock underlying the stream could also be an important natural site of adsorbing As due to its clay rich nature. In the Zimapán Valley mining district in Mexico, the Soyatal Formation (calcareous shale with abundant kaolinite and illite) was known to be an effective As adsorbent in the groundwater (Ongley et al., 2001). It would be interesting to see in

future research how As concentration behaves in shale bedrock streambeds of Whitewood Creek and the Belle Fourche River. However, due to the different degrees of charge imbalance and surface charge distributions in clay mineralogy, As adsorption in a clay rich environment is most likely very complex.

9.2.2. Oxides/Hydroxides

The (hydr)oxide minerals are similar through Whitewood Creek and Belle Fourche River where the variation of saturation index is at the most around 2. The (hydr)oxide minerals with the highest saturation indices are Fe based with hematite having the highest index at 13. As mentioned in the beginning, total Fe average in these waters is about 2 mg/l. The main source of Fe in these waters comes from the mine tailings which are composed of Fe-rich oxides, (hydr)oxides, carbonates, and sulfides. Although it is not clearly shown in these results, the dissolved Fe content is higher in Whitewood Creek than the Belle Fourche due to seep water delivering dissolved loads into Whitewood Creek (Ji, 2021). The highest Fe (hydr)oxide saturation index is hematite and goethite as the third highest. While goethite has more surface area than hematite, it is less stable. Goethite can transform to the more stable hematite. During this transformation, it can desorb some As, but can also create a more stable solid where As can be retained (Appelo et al., 2002; Fendorf et al., 2010). Although this is in the mine tailings, DeVore et al.'s (2019) Mossbauer analyses show that goethite is present in the tailings and may play an important role as an As binder. Pfeifle et al. (2018) found through sequential extractions, that most of the As in the sediments banks of the Belle Fourche and Cheyenne Rivers is primarily associated with amorphous and poorly crystalline Fe oxyhydroxides. In contrast, Ji (2021) found through sequential extraction of the mine tailings that As does not have a strong correlation to Fe bearing oxyhydroxides, amorphous and fine grained secondary minerals. A

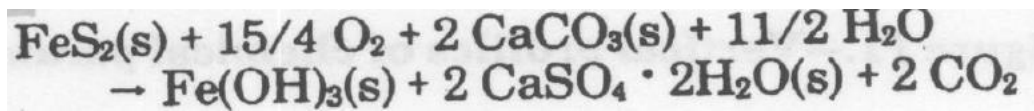
possible explanation of this is that there is low concentration of amorphous to poorly crystalline Fe oxyhydroxide or As is bound in non Fe bearing secondary minerals. In the stream water, analysis of colloids by Rees and Ranville (1988) found amorphous Fe oxides that are <100 nm and little Fe in larger particles.

Two other metal oxides, those of Cu and Al, are predicted to be supersaturated. The Cu-Fe oxide in the form of CuFeO_2 is supersaturated and has the second highest (hydr)oxide SI after hematite, except it is slightly higher than hematite at the Whitewood Creek plain sites (specifically Location G). At the same location, another the Cu hydroxide-carbonate species malachite is calculated to be oversaturated. The average Cu concentration in these waters (0.005 mg/l) is the same magnitude as the world average in stream water (0.007 mg/l) (Faure, 1998). While Cu and other base metals are rare and minor in orogenic gold deposits (Ridley, 2013), seeing this saturation index could indicate that other metals from the mine tailings are likely binding with (hydr)oxide minerals. In addition, tenorite (CuO) is predicted to be supersaturated throughout Whitewood Creek and parts of the Belle Fourche River. The Al (hydr)oxide species that is predicted to form is gibbsite. While gibbsite can be an important adsorbent for As, Al (hydr)oxides are commonly found in more acidic environments rather than basic (Wang and Mulligan, 2006). According to sequential extraction from Ji (2021), mobile Al was found to be predominantly associated with fine grained clay minerals.

9.2.3. Sulfates

The only sulfate mineral that is supersaturated is barite. While the saturation index is lower than other minerals (around 0.6), if barite is present, it could potentially immobilize As(V) by incorporating it into the barite structure (Ma et al., 2017). Although gypsum is shown not to be supersaturated in the stream water, it may play a major role in the floodplains of the

Whitewood Creek and Belle Fourche River valleys. These stream valleys are naturally enriched in gypsum and other soluble sulfate minerals within the bedrock and alluvium (Cherry et al., 1986; Fagan and Lisenbee, 2017; Ji, 2021). In addition to natural gypsum, this mineral could also form in the tailings as a result of sulfide oxidation with calcite crystals and sulfate rich water from probable shale origin flowing through into the tailings from the alluvium (Cherry et al., 1986):



Equation 9.1.

Gypsum was identified by Pfeifle et al. (2018) through SEM and XRD in the mine tailings along the Belle Fourche River at Volunteer (Location K) and by Rees and Ranvilles using SEM (1988). Arsenic (V) has been seen to be incorporated into the structure of gypsum by isomorphic substitution of SO_4^{2-} (Fernández-Martínez et al., 2006; Fernández-Martínez et al., 2008; Lin et al., 2013). If gypsum from the contaminated bank is eroded into the water of Whitewood Creek and Belle Fourche River, it could be dissolved and release As. Sulfate could be a competitor for adsorption sites, however, according to Jain and Loeppart (2000), SO_4 does not have any effect on As(V) mobilization.

9.2.4. Carbonates

Carbonate minerals throughout Whitewood Creek and Belle Fourche River have similar saturation indices and little variation (except for huntite which at the most has at the most a change of one). Calcium and magnesium carbonate minerals such as calcite and dolomite are calculated to be oversaturated in the stream water of Whitewood Creek and Belle Fourche River.

This is to be expected since the mine tailings are composed of carbonate minerals such as sideroplesite (Mg rich siderite), ankerite, calcite, and dolomite (Noble, 1950; Slaughter, 1968). Other carbonate minerals that are predicted to be supersaturated in the stream water are malachite and rhodochrosite. Both are supersaturated at locations with seeps (Location G for malachite and Location H for rhodochrosite). The possible occurrence of these minerals could reflect the metal and carbonate rich seep water mixing with the stream water. However, no Fe-rich carbonates are supersaturated in the stream water. Other sources of carbonates include bedrock units such as the Pahaspa Limestone, Englewood Limestone, Whitewood Dolomite, Winnipeg Formation (massive dolomite), and calcareous shales such as Belle Fourche Shale, Greenhorn Formation, Carlile Shale, Niobrara Formation and Pierre Shale (Ji, 2021; Goddard, 1989). The dissolution of carbonate minerals into the stream water can be explain from the pH through the study area (see Figure 5.4) where the pH remains constant above 8. This is most likely due to carbonate buffering of the water. Carbonates were also confirmed by Rees and Ranville (1988) where calcite crystals were found to be < 100 nm in the seep water. Calcite may be an important mineral to immobilize As since it can buffer high pH and reduce desorption (Wang and Mulligan, 2006). It can also immobilize As (V) through adsorption and coprecipitation at basic conditions such as pH of 8.3 (Alexandratos et al., 2007).

9.2.5. Phosphates

Phosphate is a chemical constituent of interest due to the similarity of its properties to those of As (V) and resulting competition in occupying adsorption sites. Due to extensive farming activities around Whitewood Creek and Belle Fourche River, runoff enriched in P from fertilizer could have an impact on As mobilization. DeVore et al. (2019) conducted a batch experiment where they mixed mine tailing sediments from Whitewood Creek (0.49 km

downstream from Homestake Mine) and Deal Ranch (on the Cheyenne River) with HCO_3^- and PO_4^{3-} . They found that the As release from mixing with PO_4^{3-} is at least 10 times greater than from mixing with HCO_3^- . According to Geochemist's Workbench, the phosphate mineral apatite ($\text{Ca}_5(\text{PO}_4)_3\text{OH}$) is supersaturated in these waters with a high saturation index around 12. Compared to Whitewood Creek, the Belle Fourche has a higher apatite saturation index by one. This mineral could be important for As control since it can incorporate As (V) into its structure by replacing the PO_4^{3-} in alkaline conditions, as seen in As-rich waste where lime was introduced (Bothe and Brown, 1999). In addition, other Ca- AsO_4 minerals such as pharmacolite ($\text{Ca}(\text{HAsO}_4) \cdot 2\text{H}_2\text{O}$), Weillite (CaHAsO_4), and micropharmacolite ($\text{Ca}_4\text{Mg}(\text{AsO}_4)(\text{HAsO}_3\text{OH})_2 \cdot 11\text{H}_2\text{O}$) could be present since they can be stable in alkaline conditions (Chukhlantsev, 1956). Due to the basic pH and Ca-rich nature of sediments around Whitewood Creek and Belle Fourche River, it is possible that As is incorporated into apatite or another Ca-rich secondary mineral in the mine tailings and water. Geochemist's Workbench also calculated supersaturation for another phosphate mineral, MnHPO_4 . This mineral has been reported in fertilized, neutral to alkaline soil of Northwestern India where the soil is neutral to alkaline and is enriched in P from fertilized soil although the climate is subtropical (the southwest corner is semi-arid however) (Hundal et al., 2019). However, comparing northwest India to western South Dakota is speculative.

9.3. Mineral Saturation States in Seep Water

The mineral saturation indices from the seep water show similar species to be supersaturated as the stream water. However, some of the Fe rich minerals such as nontronite, saponite, hematite, goethite, and $\text{Fe}(\text{OH})_3$ have lower indices by around 4 to 10 log units. Ferrihydrite, $\text{Fe}(\text{OH})_3$, is calculated to be undersaturated in these waters. In addition, the chlorite mineral, clinocllore, is undersaturated, while chamosite and daphnite have higher indices than

the stream water by an order of magnitude. Some of the Al-rich minerals such as beidellite and kaolinite have higher indices by 2. Another type of Al-oxide in the form of boehmite ($\text{AlO}(\text{OH})$) is supersaturated (Location H only). The large decrease of Fe (hydr)oxides saturation in the seep water is interpreted to be related to its acidic-neutral and reducing condition where these types of minerals are unstable relative in the weakly oxidizing alkaline stream water. This may be an issue for retaining As since Fe (hydr)oxides are one of the principle sorbents. In these conditions, the As speciation will more likely be a more “even” mixture of As (III) and As (V) than the As (V) dominated stream water as seen in Figure 5.5. Arsenic (III) in this condition is in the net zero charge form, $\text{As}(\text{OH})_3$ compared to the As(V)’s HAsO_4^- . By having a neutral charge, $\text{As}(\text{OH})_3$ does not have the potential to adsorb or adsorbs weakly to any surfaces and will be mobile. This results in the seep water of Whitewood Creek being a major source releasing As and other dissolved metals into the creek since it comes from groundwater flowing through contaminated sediments. Ji (2021) found that in general, dissolved As concentrations in seep water are about 1 order of magnitude greater than stream water. However, Fuller and Davies (2003) described rapid precipitation/coprecipitation of As and ferrihydrite in Whitewood Creek’s bed sediment where As rich groundwater seeped into the oxidizing creek water. Pfeifle et al. (2018) found that the pore water redox gradient in the tailings appears to be the dominant mechanism of As mobility. Areas of alluvium with low permeability (such layers with high silt and clay) have limited recharge from seasonal flushing (high discharge during spring runoffs) and are more reduced, which can dissolve (hydr)oxide minerals and release As. Biological factors are also important in the release of As where the presence of microbes can change the redox environment. Downstream in the Cheyenne River, DeVore et al. (2022) found that As was released from the mine tailings due to changing the redox conditions from aerobic to anaerobic.

According to Cherry et al. (1986), the chemical conditions of the seep water, along with the stream water, will remain about the same due to minimal acid production from carbonate mineral buffering around neutral pH and slow oxidation of sulfide minerals. This could change however from physical changes such as reworking action from floods, climatic changes, and/or anthropogenic processes such as removing the tailings.

9.4. Belle Fourche River Before Whitewood Creek Mineral Saturation Indices (L)

The saturation indices at the control site (Location L) have similar supersaturated species to the Whitewood Creek and Belle Fourche River streams. The saturation indices are generally around 1-3 orders of magnitude lower at Location L, especially for the clay and other phyllosilicate species. When compared to Whitewood Creek's locations, species such as clinocllore, saponite, talc, and sepiolite have higher indices by at the most around 3. This indicates that there are higher concentrations of elements such as Mg, Al, and Fe. When compared to the downstream Belle Fourche River locations, the indices are similar to each other and have differences around one. The supersaturated minerals are generally clays such as nontronite, daphnite, and clinocllore. The similarities of the Belle Fourche River locations may be due to the river flowing over shale bedrocks at all locations. In contrast, Whitewood Creek flows over a range of rock types such as igneous, metamorphic, sandstones, shales, carbonates, and gypsum. The similarities also may indicate that the tailings do not have a strong influence on the stream chemistry unlike in Whitewood Creek's stream water which mixes with the metal rich seep water. The supersaturation of $Ba_3(AsO_4)$ in the Whitewood Creek locations and undersaturation in Location L reflects this. One possible reason why the tailings influence decreases at the downstream Belle Fourche River might be dilution by sediment and water from other streams.

9.5. Similarity of Saturated Species Throughout Study Area

While there are some significant differences in saturation indices, nearly all the locations have similar supersaturated species. There are multiple reasons why the species may be similar throughout the study area. One is that Geochemist's Workbench uses thermodynamic equilibrium calculations for calculations of saturation indices which depend on temperature. The water temperature range varies little and stays within the range of 17.9-28 C° throughout the study area (see Appendix 5-5) at the time of sampling. Other factors that can influence saturation indices calculation is pH and redox. As seen in Figure 5.4 there is little variation in pH throughout the stream water of Whitewood Creek and Belle Fourche River (8.1-8.7). For the redox, Figure 5.3 shows the dissolved oxygen concentration in the stream water has minor variation ranging from 4.56 to 6.1 mg/l. The relative consistency of these parameters and fixing their input in Geochemist's Workbench (see Geochemistry Methods) may contribute to similar species for each general stream location. Although this is only for Whitewood Creek, another example of saturation index dependency on pH and redox can be seen when the stream water is compared to the seep water. In the seeps, the pH is more acidic and the redox is more reducing, which can lead to differences of indices as large as 10 orders of magnitude.

Despite having similar mineral saturation indices, there are some elements that are significantly different between Whitewood Creek, and the Belle Fourche River. When compared to uncontaminated Location L, Whitewood Creek has high levels of As and S. This is due to the presence and dissolution of arsenopyrite (as well as pyrite and pyrrhotite) in the tailings along Whitewood Creek. Compared to the Belle Fourche River locations downstream from the confluence, Whitewood Creek has lower Ca and S levels around the mountain locations and steadily increases downstream. The increasing levels of both Ca and S are likely due to the

dissolution of gypsum and other soluble sulfate minerals found in the bedrock and alluvial sediments (Ji, 2021; Cherry et al., 1986).

9.6. Arsenic Adsorption Capacity in Stream Water through Eh and pH

A concern about introducing As rich sediment into the waters of Whitewood Creek and Belle Fourche is how stream water pH and Eh conditions are different compared to the overbank's pore water conditions. As seen in Figure 1.1 and 5.5, Jacks (2017) shows that maximum As adsorption occurs at a pH range from about 3-8 and Eh range from about 0 to 1.1 volts in the presence of Fe. While the overall Eh is within the range of efficient adsorption in Whitewood Creek and Belle Fourche River, the pH may be a concern since it is around the pH of 8. Fuller et al. (1993) found that significant As (V) adsorption begins to decrease from Fe hydroxides around pH approximately 8 and greater due to repulsion as the sorbent surface becomes more negative. However, since the stream water is enriched in cations such as Ca and Mg, As adsorption may increase since these elements can form positive surfaces on oxide solids. For example, As (V) adsorption on Al oxides can be enhanced by the presence of Ca at a pH level above 8 (Ghosh and Teoh, 1985) as well as ferrihydrite at pH 9 (Wilkie and Hering, 1996).

9.7. Arsenic Phases in Stream and Seeps Waters

At most locations, the only As solid phase that is supersaturated is $Ba_3(AsO_4)_2$. However, this phase may not be found in nature and is an unlikely source for As control. According to Zhu et al. (2005), this mineral is unstable under natural conditions in drinking water sources and is only stable at $pH > 10.3$. Lu and Zhu (2011) showed that the $Ba_3(AsO_4)_2$ stability field disappears at a Ba molarity less than 10^{-4} (or approximately 13 ppm). This is higher than the average Ba concentration throughout the study area (0.056 ppm) and average worldwide stream water concentration (0.02 ppm) (Faure, 1998).

One of the most common weathering products of arsenopyrite is scorodite ($\text{FeAsO}_4 \cdot 2\text{H}_2\text{O}$). However, this mineral does not appear to be saturated according to SpecE8. A reason scorodite may not form in the stream water is the pH. Scorodite is known to persist in acidic environments (Moldovan and Hendry, 2005; Frau and Arda, 2004). However, the waters of Whitewood Creek and the Belle Fourche River are basic, so they may make precipitation unlikely. While scorodite may not form in the water, it may form in the tailings and be incorporated into the water from erosion. According to Bluteau and Demopoulos (2007) from a laboratory investigation, scorodite dissolves incongruently at a decreasing exponential rate at a wide pH range (5-9). However, Demopoulos (2005) found that scorodite can be stable at higher pH (>6.75) in lower temperatures and gypsum saturated solutions. Similar consideration applied to another common secondary As mineral and weathering product of arsenopyrite, jarosite ($\text{KFe}_4(\text{SO}_4)_3(\text{OH})_4 \cdot 6-7\text{H}_2\text{O}$), where AsO_4 can substitute for SO_4 . This mineral is especially interesting since the Whitewood Creek and Belle Fourche valleys are enriched in SO_4 . Like scorodite, jarosite is thermodynamically unstable at circumneutral pH and can release As if it is eroded into the stream water (Rodriguez-Freire et al., 2016; Saup et al., 2017). While the SEM work from Pfeifle et al. (2018) did not detect any secondary As minerals or crystalline forms of As along with Fe, further research must be done on the details of the mine tailings mineralogy and particulates in the stream.

According to Ji (2021), 60% of As in the tailings are interpreted to be immobile in arsenopyrite due to slow kinetic dissolution which is controlled by oxyhydroxide coating. The other 24% is bonded moderately in weakly soluble secondary minerals (clay, crystalline metal (hydr)oxides), 4.8 % weakly bonded on amorphous and poorly crystalline metal hydr(oxides), 11% on organics and exchange sites, and 0.37% on readily exchangeable sites and water-soluble

secondary minerals. This conclusion was also made by Horowitz and Kent (1990) who observed through SEM work that most of the As was stored in arsenopyrite. However, previous work on the tailings concluded that Fe (hydr)oxide minerals and solids play a larger role. Recent work by DeVore et al. (2019) shows that Mossbauer analysis of the tailings indicates a presence of goethite (higher proportion of Fe (III) than Fe (II)). This may play an important role in bonding As in the tailings. Pfeifle et al. (2018) also performed sequential extraction on the tailings sediment along the Belle Fourche and Cheyenne Rivers. They found 40 to 60% of total As was strongly adsorbed or associated with amorphous/poorly crystalline Fe solids. They also found As in Fe bearing phases of the tailings at the Volunteer location of the Belle Fourche River (Location K) through SEM. Using energy dispersive spectroscopy (EDS) of a 200 μm area of the sediment, they found that 1.12% of As in elemental form or 1.72% in the form of arsenic pentoxide (As_2O_5). Arsenic and Fe were undetectable in crystalline form, which lead to the assumption they were finely disseminated and within amorphous and nanocrystalline phases. While the contaminated sediment at the Volunteer site had the highest concentration of As, there was little detection of it being soluble. This was due to a combination of oxidized pore water, microbial inhibition and being incorporated in arsenopyrite and/or Fe hydr(oxide) phases. However, in other locations where the pore water is more reduced, there is a higher concentration of mobile As (Pfeifle et al., 2018).

According to Ji (2021), there are multiple interpretations of why her sequential extraction did not show a strong correlation between Fe-bearing minerals and As: 1) The As released may be bound to other non-Fe-bearing secondary minerals and is not affected by the dissolution of Fe bearing minerals through reduction; 2) There may be more crystalline Fe (hydr)oxides than amorphous/poorly crystalline or the amorphous/poorly crystalline (hydr)oxides are low and the

concentration of hydroxylamine HCl was not strong enough to remove As (amorphous to poorly crystalline (hydr)oxides, see Figure 2.5).

9.8. Transportation Rate of Dissolved As in Whitewood Creek

Two days were assumed as the residence time of water in Whitewood Creek. While this is arbitrary, the numerical model shows that there is little difference in the soluble As transport rate if the residence time was 7 days. The Geochemist's Workbench model calculation shows that the rate of As dissolving into the waters of Whitewood Creek with an arsenopyrite concentration of 15% ranges from 0.6132-0.6148 (mg/l)/day while 0.11% ranges from 0.0046-0.0048 (mg/l)/day. The minor fluctuation is caused by the different As concentration for each location's initial input water chemistry. The calculation predicts that with a tailings composition of 15% arsenopyrite in the stream water, 52 Mg per year will be the annual transportation rate of dissolved As while the rate for 0.11% arsenopyrite is 0.39 Mg per year (see Table 7.6).

Ji's (2021) average 30 year dissolved As transportation rate from Whitewood Creek ranges from 3.89-0.33 Mg per year. Her range fits between the two arsenopyrite endmembers of this project with a bias towards the lower end. Using Ji's (2021) transportation rate, the average rate of dissolved As will be about 0.014 (mg/l)/day and average arsenopyrite percentage of 0.34% in the tailings (which is about 0.16% As). While the 15% endmember is most likely an overestimate, the lower 0.11% matches closely to Ji's (2021) prediction. In addition, it also matches closely to South Dakota Department of Health's (1960) 0.12% and Noble's (1950) 0.35% As concentration in the tailings. Since the only source of As was from arsenopyrite in this model, seeing the similar values from a statistical approach (Ji, 2021) and geochemical approach (this investigation) may indicate that arsenopyrite dissolution into the stream water is a significant source of dissolved As despite having low breakdown rates. However, it is important

to note that most of the arsenopyrite grains in the tailings to some degree have Fe (hydr)oxide coatings where As can be also be stored (Horowitz and Kent, 1990).

It is important to layout other potential sources of dissolved As. If Rees and Ranville (1988) are correct about the stream water colloids being mostly clays, these could be potential sites to host As. Another possible source of As may be secondary As bearing phases occurring in the tailings. Due to the alkaline and Ca rich nature of the soils of the Great Plains, there could possibly be secondary minerals composed of Ca-AsO₄ such as pharmacolite (Ca(HAsO₄)·2H₂O), weilite (CaHAsO₄), and picropharmacolite (Ca₄Mg(AsO₄) (HAsO₃OH)₂·11H₂O). In addition, As(V) can substitute into common minerals such as calcite and gypsum, which are ubiquitous in the Whitewood Creek and Belle Fourche valleys and in the tailings. In addition to chemical factors, biological factors such as microbes and organics have been observed in the stream waters and tailings of the Cheyenne River Basin and can play an important role in controlling As (Goddard, 1989; Fuller and Davis, 2003; Pfeifle et al., 2018; DeVore et al., 2019).

9.9. Transportation Rate of Suspended As in Whitewood Creek

The calculation of As in the suspended sediment shows that with an arsenopyrite composition of 15% and a tailings thickness of 0.6 m, the As suspended sediment transportation rate in Whitewood Creek would be 254 Mg per year and 2.54 Mg per year if the composition is 0.11%. If the tailings thickness was 3.5 m, then 15% arsenopyrite will have a rate of 59 Mg per year while 0.11% will have a rate of 1.98 Mg per year. Arsenic value range from a tailing thickness of 0.6 m is within the range Ji (2021) estimated for the 30 year annual total suspended As range (33 to 70 Mg/yr) (see Table 7.8). For the 3.5 m thickness, the upper range is within Ji's (2021) range but the lower end differs by a couple of orders of magnitude. Using Ji's (2021) estimated 30 year annual total suspended As range, if the thickness of the tailings was 0.6 m, the

arsenopyrite composition in the tailings will have a range between 3-1.9%. For a thickness of 3.5 m, the range will be between 3.9-2.5% (see Table 9.1). Overall, the range of values for suspended As transportation based on different tailing thicknesses and arsenopyrite percentages ranges from 254 to 1.98 Mg/year. While Ji's (2021) values are within this range (33 to 70 Mg/year) the range found in this investigation varies greatly. Using the same calculation with Ji's (2021) range and the same two tailing thicknesses, the arsenopyrite percentage will range from 3.9-1.9%. These percentages are within the range used in this research (15-0.11%). The values of South Dakota Department of Health (1960) and Noble (1950) who calculated As concentration in the tailings (0.12% and 0.35% respectively) are within the As concentration range in this research, 6.9-0.05% (multiplying the arsenopyrite concentration by 46%, which is the As proportion in arsenopyrite). Since the values calculated in this investigation match closely to Ji's (2021), South Dakota Department's (1960), and Noble's (1950) calculations, this suggests that there may be some appreciable suspended sediment As transportation in the form of arsenopyrite.

9.10. Difference Between Dissolved and Suspended As Transportation

The difference between the calculated dissolved and suspended As transportation is to be expected. There are two ways As can move out of Whitewood Creek and Belle Fourche River: 1. In a dissolved phase where it can come from seep discharge into the stream from shallow alluvial aquifers where it is released from sediments. In addition, some of the dissolved As can come from tailings in the creek bed. 2. In a suspended phase from sediment input due to bank erosion. Ji (2021) observed that during times of high discharge or flooding, total and suspended As concentration increases while dissolved values decrease. The reason for this pattern is due to high water levels reworking the alluvial sediments on the banks and floodplains and introducing As enriched solids into the water. The increased load of particulates and solids in the stream

water dilutes the soluble As. In addition, the increase in flow velocity decreases the stream water residence time which lowers the dissolution rate of arsenopyrite. However, this trend occurs during rapid precipitation/runoff events such as floods. Although somewhat contradictory, on the Belle Fourche River, Marron (1987) observed that As concentration was greater in vertically accreted overbank deposits adjacent to the river than the more distant and higher topographic overbank deposits. The cause of this spatial difference is dilution of As-rich suspended load from erosion and incorporation of clean alluvium during major flooding events where high flood water and sediment can reach the higher topographic deposits. Seeing these trends indicates that physical movements through fluvial actions like flooding and dilution of sediments are significant controls on adding and reducing suspended As into the stream water. While physical factors such as clean sediment dilution can control dissolved As concentration, it is also controlled chemically. Low dissolved As concentration in the environment shows arsenopyrite is in a relatively stable state and its breakdown products are low. However, Whitewood Creek will still slowly continue to transport dissolved and suspended As from the contaminated sediment due to breakdown of arsenopyrite, seasonal flushing of the tailings, and fluvial flooding and erosion (Pfeifle et al., 2018, Fuller and Davis, 2003; and Goddard, 1989). It will remain within Whitewood Creek for a long time and continue to gradually pollute As rich sediments downstream for future generations.

CHAPTER 10. CONCLUSION AND RECOMMENDATION

The following is the summarization of the main conclusions of the investigation goals that were listed in Chapter 1.

1. Identify and monitor floodplains with contaminated sediment and their erosion on Whitewood Creek and the Belle Fourche River to identify future movement of contaminated sediments and where bank stability can be developed.

The location and evolution of contaminated floodplains in Whitewood Creek and the Belle Fourche River is very complex. In Whitewood Creek, areas with thick tailings are located above the confluence of the Belle Fourche River (Reach 8) and below the town of Whitewood (Reach 2). One possible control on the thick tailings at Reach 8 is knickzone geomorphology where there is a broad valley and storage for floodplain sediments. At Reach 2, multiple processes could have resulted in the thick tailings storage such as transition from hard resistant sedimentary rocks to softer erosional shale and changes in stream energy from a steep narrow mountain channel to a broad low gradient channel. Based on the GIS from this study, erosion of contaminated sediments has been decreasing over time in Whitewood Creek with progressive removal of mining sediments, allowing the fluvial system to incise through the alluvium into shale bedrock. While erosion of contaminated sediments has been lower, they are still in place and will slowly contaminate Whitewood Creek and downstream for multiple generations.

On the Belle Fourche River, areas with high tailings are about 7 km below the confluence with Whitewood Creek (Reach 2) due to its close proximity and influx of tailings from Whitewood Creek and high floodplain storage area. Reach 4-9 is in an area affected by rapid floodplain

reworking from neotectonism from lineaments caused by weak zones in the underlying Precambrian basement. As seen by changes in variation of contaminated floodplain widths, Belle Fourche River undergoes more floodplain reworking than Whitewood Creek due to higher frequency of floods, sediments from other streams, and local neotectonism. While contaminated sediments from Whitewood Creek will continue to pollute the Belle Fourche River, fluvial reworking will prevent the contaminated sediments from being static and will decrease the concentration of As due to mixing with uncontaminated sediments from upstream sources.

2. Model mineral saturation indices in the waters of Whitewood Creek and Belle Fourche River to see what minerals and As bearing minerals are thermodynamically predicted to precipitate.

The calculated mineral saturation indices of Whitewood Creek and Belle Fourche River waters show that the only As mineral that is supersaturated is $Ba_3(AsO_4)_2$. However, this mineral has not been detected in nature before. Despite inconsistency of the water chemistry analytes, the mineral saturation indices of Whitewood Creek and Belle Fourche River stream water have similar saturation indices to each other (including the uncontaminated Location L) and differ by only around 2-3 orders of magnitude. Minerals that are supersaturated are phyllosilicates (mostly clays), Fe, Cu, and Al (hydr)oxides, and carbonates with minor sulfates and phosphates.

Compared to the seep water, the mineral saturation indices are lower by at the most around 10 orders of magnitude with the Fe based minerals showing the most change. This is reflective of the different chemical conditions where the stream water is oxidizing and has a basic pH (~8) and the seep water is reducing and has a neutral to slight acidic pH (~7).

3. Model the daily release of dissolved and suspended As as a result of contaminated sediment being added to the waters of Whitewood Creek.

The calculation for daily release of dissolved As from contaminated sediment added to the waters of Whitewood Creek ranges from 52 to 0.39 Mg per year based on the range of possible arsenopyrite concentrations in the contaminated sediment (15 to 0.11%). Ji's (2021) estimated daily release of dissolved As ranges from 3.89-0.33 Mg/year (based on statistical analysis of 30 years of USGS datasets) is within the lower end of this range. Using Ji's (2021) value, the average dissolving arsenopyrite concentration will be about 0.34%. For the daily release of suspended As in the form of arsenopyrite based on tailings thickness in the range of 0.6-3.5 m and arsenopyrite concentration (15 to 0.11%), the range is from 1.98 to 254 Mg per year. Despite having a large range, Ji's (2021) suspended As value range of 33 to 70 Mg per year fits within this research's calculations. Seeing the similarities between Ji's (2021) value (based on statistical analysis) and this investigation (based on the arsenopyrite geochemistry modeling) indicates that arsenopyrite is to some degree significant in controlling As transportation in Whitewood Creek.

Recommendation for additional research

- Investigating As phases as well as chemistry and mineralogy within the suspended sediments and colloids in the stream water.
- Detailed analysis of the tailings mineralogy, especially for the different types of sulfides.
- The potential effect of river management on reaches where there are large areas of tailings such as structures to stabilize the banks.

- Set up surface water and groundwater quality stations or assessments to monitor the transportation of As, especially after anthropogenic impacts and shifts (such as reworking contaminated floodplains) in the region.

TABLES

Chapter 5. – Tables

Table 5.1. Redox potential and average additional species concentration added to Ji (2021) water chemistry.

Locations	Redox Potential (Eh, mV)	USGS Gaging Station	HCO ₃ ⁻ (mg/l)	HPO ₄ ²⁻ (mg/l)	Cl ⁻ (mg/l)	K ⁺ (mg/l)
Locations E, F, G (Stream)	155	Whitewood Creek Above Whitewood	154	0.4337	27	10
Locations H (Stream), I, J	161	Whitewood Creek Above Vale	218	0.0418	28	10 (no values in Vale)
Location K	161 (none in Sturgis)	Belle Fourche River near Sturgis	197	0.061	24.15	9.1
Location L	161	-	-	-	-	-

Table 5.2. Parameters for modeling the kinetic dissolution of arsenopyrite in REACT.

Parameters	Value
Surface Area (cm ² /g)	33 ^a
Dissolution Rate Constant (mol/cm ² /s)	1.0e-14 ^b
Amount of Arsenopyrite	0.11% and 15%
Rate Law Equation	Built in (see Equation 5.3)

a. From Ji (2021)

b. From Wang et al. (2018)

Chapter 7.- Tables

Table 7.1. Mineral Saturation Indices for Whitewood Creek Mountain Locations (A-D).

Category	Mineral	Formula	Log Q/K (Supersaturated Only)
Clays	Nontronite	$(\text{CaO}_{0.5}, \text{Na})_{0.3} \text{Fe}^{3+}_2 (\text{Si}, \text{Al})_4 \text{O}_{10} (\text{OH})_2 \cdot n\text{H}_2\text{O}$	19.3-17.3
	Clinochlore	$\text{Mg}_5 \text{Al} (\text{AlSi}_3 \text{O}_{10}) (\text{OH})_8$	8.3-2.22
	Saponite	$\text{Ca}_{0.25} (\text{Mg}, \text{Fe})_3 ((\text{Si}, \text{Al})_4 \text{O}_{10}) (\text{OH})_2 \cdot n(\text{H}_2\text{O})$	7.83-4.38
	Talc	$\text{Mg}_3 \text{Si}_4 \text{O}_{10} (\text{OH})_2$	6.81-4.54
	Beidellite	$(\text{CaO}_{0.5}, \text{Na})_{0.3} \text{Al}_2 (\text{Si}, \text{Al})_4 \text{O}_{10} (\text{OH})_2 \cdot n\text{H}_2\text{O}$	4.77-0.76
	Ripidolite	$(\text{Mg}, \text{Fe}, \text{Al})_6 (\text{Si}, \text{Al})_4 \text{O}_{10} (\text{OH})_8$	4.63-0.02
	Sepiolite	$\text{Mg}_4 \text{Si}_6 \text{O}_{15} (\text{OH})_2 \cdot 6\text{H}_2\text{O}$	4.52-1.61
	Kaolinite	$\text{Al}_2 (\text{Si}_2 \text{O}_5) (\text{OH})_4$	4.11-2
	Daphnite ^a	$(\text{Mg}, \text{Fe})_3, (\text{Fe}, \text{Al})_3 (\text{Si}, \text{Al})_4 \text{O}_{10} (\text{OH})_8$	1.35
Oxides and Hydroxides	Hematite	Fe_2O_3	14.9-14.2
	Delafossite	CuFeO_2	14.2-13
	Goethite	$\alpha\text{-Fe}^{3+} \text{O} (\text{OH})$	6.98-6.64
		$\text{Fe} (\text{OH})_3$	2.52-2.18
	Gibbsite	$\text{Al} (\text{OH})_3$	1.23-0.35
	Tenorite	CuO	0.6-0.19
Sulfates	Barite	BaSO_4	0.84-0.72
Silica	Quarz	SiO_2	0.6-0.43
	Chalcedony	SiO_2	0.32-0.15
Arsenate		$\text{Ba}_3 (\text{AsO}_4)_2$	10.9-9.56

a: found only at Location A

Table 7.2. Mineral Saturation Indices for Whitewood Creek Great Plains Locations (E-H).

Category	Mineral	Formula	Log Q/K (Supersaturated Only)
Clays	Nontronite	$(\text{CaO}_{0.5}, \text{Na})_{0.3} \text{Fe}^{3+}_2 (\text{Si}, \text{Al})_4 \text{O}_{10} (\text{OH})_2 \cdot n\text{H}_2\text{O}$	17.5-15.6
	Saponite	$\text{Ca}_{0.25} (\text{Mg}, \text{Fe})_3 ((\text{Si}, \text{Al})_4 \text{O}_{10}) (\text{OH})_2 \cdot n(\text{H}_2\text{O})$	7.06-3.38
	Clinochlore	$\text{Mg}_5 \text{Al} (\text{AlSi}_3 \text{O}_{10}) (\text{OH})_8$	7-2.59
	Talc	$\text{Mg}_3 \text{Si}_4 \text{O}_{10} (\text{OH})_2$	6.09-3.88
	Illite	$\text{K}_{0.65} \text{Al}_{2.0} (\text{Al}_{0.65} \text{Si}_{3.35} \text{O}_{10}) (\text{OH})_2$	3.9-1.72
	Smectite-low-Fe- Mg	$\text{Na}_{0.15} \text{Ca}_{0.02} \text{K}_{0.2} \text{Mg}_{0.9} \text{Fe}_{0.45} \text{Al}_{1.25} \text{Si}_{3.75} \text{O}_{10} (\text{OH})_2$	3.75-2.12
	Smectite-high-Fe-Mg	$\text{Na}_{0.1} \text{Ca}_{0.025} \text{K}_{0.2} \text{Mg}_{1.15} \text{Fe}_{0.7} \text{Al}_{1.25} \text{Si}_{3.5} \text{O}_{10} (\text{OH})_2$	3.58-1.77
	Sepiolite	$\text{Mg}_4 \text{Si}_6 \text{O}_{15} (\text{OH})_2 \cdot 6\text{H}_2\text{O}$	3.57-0.57
	Ripidolite ^a	$(\text{Mg}, \text{Fe}, \text{Al})_6 (\text{Si}, \text{Al})_4 \text{O}_{10} (\text{OH})_8$	3.32-2.89
	Beidellite	$(\text{CaO}_{0.5}, \text{Na})_{0.3} \text{Al}_2 (\text{Si}, \text{Al})_4 \text{O}_{10} (\text{OH})_2 \cdot n\text{H}_2\text{O}$	3.03-0.16
	Kaolinite	$\text{Al}_2 (\text{Si}_2 \text{O}_5) (\text{OH})_4$	2.89-1.13
Oxides and Hydroxides	Delafossite	CuFeO_2	14.1-12.9
	Hematite	Fe_2O_3	13.9-12.9
	Goethite	$\alpha\text{-Fe}^{3+} \text{O} (\text{OH})$	6.48-6
		$\text{Fe} (\text{OH})_3$	2.11-1.53
	Gibbsite ^a	$\text{Al} (\text{OH})_3$	0.85-0.31
	Tenorite	CuO	0.76-0.09
Carbonates	Dolomite	$\text{CaMg} (\text{CO}_3)_2$	3.52-1.21
	Huntite ^f	$\text{CaMg}_3 (\text{CO}_3)_4$	1.35-0.82
	Calcite	$\text{Ca} (\text{CO}_3)$	1.31-1.01
	Magnesite ^b	$\text{Mg} (\text{CO}_3)$	0.58-0.13

Table 7.2. Mineral Saturation Indices for Whitewood Creek Great Plains Locations (E-H).

Category	Mineral	Formula	Log Q/K (Supersaturated Only)
Carbonates	Malachite ^d	Cu ₂ (CO ₃)(OH) ₂	0.009
	Rhodocrosite ^e	Mn(CO ₃)	0.009
Sulfates	Barite	BaSO ₄	0.76-0.4
Phosphates	Hydroxyapatite	Ca ₅ (PO ₄) ₃ OH	12.6-12.1
		MnHPO ₄ ^g	0.53-0.26
Silica	Quartz	SiO ₂	0.42-0.19
	Chalcedony ^c	SiO ₂	0.14-0.08
Arsenate		Ba ₃ (AsO ₄) ₂ ^c	10.5-9.1

a: not found at Location F

b: not found at Location E

c: not found at Location H

d: Location G only

e: Location H only

f: Location E and H only

g: Location F and H only

Table 7.3. Mineral Saturation Indices for Belle Fourche River Locations (Location I-K).

Category	Mineral	Formula	Log Q/K (Supersaturated Only)
Clays	Nontronite	$(\text{CaO}_{0.5}, \text{Na})_{0.3}\text{Fe}^{3+}_2(\text{Si}, \text{Al})_4\text{O}_{10}(\text{OH})_2 \cdot n\text{H}_2\text{O}$	17.4-16.3
	Clinochlore	$\text{Mg}_5\text{Al}(\text{AlSi}_3\text{O}_{10})(\text{OH})_8$	6.19-1.62
	Saponite	$\text{Ca}_{0.25}(\text{Mg}, \text{Fe})_3((\text{Si}, \text{Al})_4\text{O}_{10})(\text{OH})_2 \cdot n(\text{H}_2\text{O})$	5.34-3.63
	Talc	$\text{Mg}_3\text{Si}_4\text{O}_{10}(\text{OH})_2$	4.11-3.8
	Ripidolite	$(\text{Mg}, \text{Fe}, \text{Al})_6(\text{Si}, \text{Al})_4\text{O}_{10}(\text{OH})_8$	4.04-0.22
	Illite	$\text{K}_{0.65}\text{Al}_{2.0}[\text{Al}_{0.65}\text{Si}_{3.35}\text{O}_{10}](\text{OH})_2$	3.61-3.11
	Smectite-low-Fe- Mg	$\text{Na}_{0.15}\text{Ca}_{0.02}\text{K}_{0.2}\text{Mg}_{0.9}\text{Fe}_{0.45}\text{Al}_{1.25}\text{Si}_{3.75}\text{O}_{10}(\text{OH})_2$	3.51-3.2
	Smectite-high-Fe- Mg	$\text{Na}_{0.15}\text{Ca}_{0.02}\text{K}_{0.2}\text{Mg}_{0.9}\text{Fe}_{0.45}\text{Al}_{1.25}\text{Si}_{3.75}\text{O}_{10}(\text{OH})_2$	3.49-3.11
	Beidellite	$(\text{CaO}_{0.5}, \text{Na})_{0.3}\text{Al}_2(\text{Si}, \text{Al})_4\text{O}_{10}(\text{OH})_2 \cdot n\text{H}_2\text{O}$	2.9-1.07
	Kaolinite	$\text{Al}_2(\text{Si}_2\text{O}_5)(\text{OH})_4$	2.89-2.41
	Sepiolite	$\text{Mg}_4\text{Si}_6\text{O}_{15}(\text{OH})_2 \cdot 6\text{H}_2\text{O}$	0.68-0.29
Daphnite ^b	$(\text{Mg}, \text{Fe})_3, (\text{Fe}, \text{Al})_3(\text{Si}, \text{Al})_4\text{O}_{10}(\text{OH})_8$	0.29-0.09	
Oxides and Hydroxides	Hematite	Fe_2O_3	14.4-14
	Delafossite	CuFeO_2	13.5-13.1
	Goethite	$\alpha\text{-Fe}^{3+}\text{O}(\text{OH})$	6.7-6.5
		$\text{Fe}(\text{OH})_3$	2.34-2.13
	Gibbsite	$\text{Al}(\text{OH})_3$	1-0.73
	Tenorite ^a	CuO	0.04

Table 7.3. Mineral Saturation Indices for Belle Fourche River Locations (Location I-K).

Category	Mineral	Formula	Log Q/K (Supersaturated Only)
Carbonates	Dolomite	$\text{CaMg}(\text{CO}_3)_2$	3.17-1.58
	Calcite	$\text{Ca}(\text{CO}_3)$	1.24-1.23
	Huntite	$\text{CaMg}_3(\text{CO}_3)_4$	0.51-0.32
	Magnesite	$\text{Mg}(\text{CO}_3)$	0.33-0.27
Sulfates	Barite	BaSO_4	0.47-0.27
Phosphates	Hydroxyapatite	$\text{Ca}_5(\text{PO}_4)_3\text{OH}$	13.3-10.9
Silica	Quarz	SiO_2	0.27-0.18

a: Location I only

b: not found at Location J

Table 7.4. Mineral Saturation for Location L (Belle Fourche River above Whitewood Creek confluence).

Category	Mineral	Formula	Log Q/K (Supersaturated Only)
Clays	Nontronite	$(\text{CaO}_{0.5}, \text{Na})_{0.3} \text{Fe}^{3+}_2 (\text{Si}, \text{Al})_4 \text{O}_{10} (\text{OH})_2 \cdot n \text{H}_2\text{O}$	18-17.5
	Clinochlore	$\text{Mg}_5 \text{Al} (\text{AlSi}_3 \text{O}_{10}) (\text{OH})_8$	5.41-2.02
	Saponite	$\text{Ca}_{0.25} (\text{Mg}, \text{Fe})_3 ((\text{Si}, \text{Al})_4 \text{O}_{10}) (\text{OH})_2 \cdot n (\text{H}_2\text{O})$	5.19-3.89
	Ripidolite	$(\text{Mg}, \text{Fe}, \text{Al})_6 (\text{Si}, \text{Al})_4 \text{O}_{10} (\text{OH})_8$	4.06-0.67
	Talc	$\text{Mg}_3 \text{Si}_4 \text{O}_{10} (\text{OH})_2$	4
	Beidellite	$(\text{CaO}_{0.5}, \text{Na})_{0.3} \text{Al}_2 (\text{Si}, \text{Al})_4 \text{O}_{10} (\text{OH})_2 \cdot n \text{H}_2\text{O}$	3.53-2.22
	Kaolinite	$\text{Al}_2 (\text{Si}_2 \text{O}_5) (\text{OH})_4$	3.28
	Daphnite	$(\text{Mg}, \text{Fe})_3, (\text{Fe}, \text{Al})_3 (\text{Si}, \text{Al})_4 \text{O}_{10} (\text{OH})_8$	1.3
	Sepiolite	$\text{Mg}_4 \text{Si}_6 \text{O}_{15} (\text{OH})_2 \cdot 6 \text{H}_2\text{O}$	0.68
Oxides and Hydroxides	Hematite	$\text{Fe}_2 \text{O}_3$	14.5
	Delafossite	CuFeO_2	13.6
	Goethite	$\alpha\text{-Fe}^{3+} \text{O} (\text{OH})$	6.79
		$\text{Fe} (\text{OH})_3$	2.39
	Gibbsite	$\text{Al} (\text{OH})_3$	1.04
	Tenorite	CuO	0.06
Sulfates	Barite	BaSO_4	0.62
Silica	Quarz	SiO_2	0.36
	Chalcedony	SiO_2	0.08

Table 7.5. Mineral Saturation Indices for Seep Locations (Locations B, G, H).

Category	Mineral	Formula	Log Q/K (Supersaturated Only)
Clays	Nontronite	$(\text{CaO}_{0.5}, \text{Na})_{0.3} \text{Fe}^{3+}_2 (\text{Si}, \text{Al})_4 \text{O}_{10} (\text{OH})_2 \cdot n \text{H}_2\text{O}$	11.1-7.49
	Beidellite	$(\text{CaO}_{0.5}, \text{Na})_{0.3} \text{Al}_2 (\text{Si}, \text{Al})_4 \text{O}_{10} (\text{OH})_2 \cdot n \text{H}_2\text{O}$	5.22-1.36
	Kaolinite	$\text{Al}_2 (\text{Si}_2 \text{O}_5) (\text{OH})_4$	4.92-2.54
	Daphnite ^c	$(\text{Mg}, \text{Fe})_3, (\text{Fe}, \text{Al})_3 (\text{Si}, \text{Al})_4 \text{O}_{10} (\text{OH})_8$	2.16-1.91
	Chamosite ^c	$(\text{Fe}^{2+}, \text{Mg}, \text{Al}, \text{Fe}^{3+})_6 (\text{Si}, \text{Al})_4 \text{O}_{10} (\text{OH}, \text{O})_8$	0.91-0.09
	Sepiolite	$\text{Mg}_4 \text{Si}_6 \text{O}_{15} (\text{OH})_2 \cdot 6 \text{H}_2\text{O}$	0.68
	Saponite	$\text{Ca}_{0.25} (\text{Mg}, \text{Fe})_3 ((\text{Si}, \text{Al})_4 \text{O}_{10}) (\text{OH})_2 \cdot n (\text{H}_2\text{O})$	0.63-0.1
Oxides and Hydroxides	Delafossite	CuFeO_2	13.3-11.6
	Hematite	Fe_2O_3	6.82-6.11
	Goethite	$\alpha\text{-Fe}^{3+}\text{O}(\text{OH})$	2.95-2.69
	Gibbsite	$\text{Al}(\text{OH})_3$	1.78-0.62
	Boehmite ^a	$\text{AlO}(\text{OH})$	0.18
Sulfates	Barite	BaSO_4	0.69-0.25
Silica	Quarz	SiO_2	0.78-0.42
	Chalcedony	SiO_2	0.5-0.16
Arsenates		$\text{Ba}_3(\text{AsO}_4)_2^{\text{b}}$	5.01

a: Location H only

b: Location G only

c: not at Location G

Table 7.6. Results from average transportation rate of dissolved As calculation in Whitewood Creek.

Weight Percentage of arsenopyrite	15%	0.11%
Annual dissolved As transportation rate	$52 \frac{Mg}{year}$	$0.39 \frac{Mg}{year}$

Table 7.7. Results from average transportation rate of As in suspended sediment in Whitewood Creek.

Weight Percentage of arsenopyrite	15%	0.11%
Tailing thickness = 0.6 m	$254 \frac{Mg}{year}$	$2.54 \frac{Mg}{year}$
Tailing thickness= 3.5 m	$198 \frac{Mg}{year}$	$1.98 \frac{Mg}{year}$

Chapter 8. - Tables

Table 8.1. Whitewood Creek R² correlation of changes in fluvial parameters in the period 1948-2012. Yellow highlights are significant based on Equation 6.1.

	Sinuosity	Contaminated Floodplain Widths	Contaminated Floodplain Widths Variation	Contaminated Sediment Area	Contaminated Removed Area	Channel Migration	Total Sediment Depositional Area
Sinuosity							
Contaminated Floodplain Widths	0.2013						
Contaminated Floodplain Widths Variation	0.027	0.5261					
Contaminated Sediment Area	0.0084*	0.5793	0.6648				
Contaminated Removed Area	0.0861*	0.1104	0.5253	0.532			
Channel Migration	0.1954*	0.0247*	0.1182	0.0358	0.3508		
Total Sediment Depositional Area	0.2522*	0.0316*	0.1817	0.0717	0.5064	0.8797	

* Pairs are negatively correlated

Table 8.2. Whitewood Creek R² correlation of changes in fluvial parameters in the period 1977-2012. Yellow highlights are significant based on Equation 6.1.

	Sinuosity	Contaminated Floodplain Widths	Contaminated Floodplain Widths Variation	Contaminated Sediment Area	Contaminated Removed Area	Channel Migration	Total Sediment Depositional Area
Sinuosity							
Contaminated Floodplain Widths	0.4673						
Contaminated Floodplain Widths Variation	0.0992	0.6077					
Contaminated Sediment Area	0.0025	0.5179	0.5408				
Contaminated Removed Area	0.1533*	0.0107	0.0091*	0.1721			
Channel Migration	0.092*	0.0093*	0.0053*	0.0003	0.2848		
Total Sediment Depositional Area	0.1973*	0.0216*	8E-05*	0.0275*	0.0214	0.8283	

* Pairs are negatively correlated

Table 8.3. Belle Fourche River R² correlation of changes in fluvial parameters in the period 1948-2012. Yellow highlights are significant based on Equation 6.1.

	Sinuosity	Contaminated Floodplain Widths	Contaminated Floodplain Widths Variation	Contaminated Sediment Area	Contaminated Removed Area	Channel Migration	Total Sediment Depositional Area
Sinuosity							
Contaminated Floodplain Widths	0.0005						
Contaminated Floodplain Widths Variation	0.2187	0.2638					
Contaminated Sediment Area	0.0537	0.4171	0.0023				
Contaminated Removed Area	0.0049	0.4977	0.2705	0.6487			
Channel Migration	0.1139	0.4143	0.16	0.0849	0.1889		
Total Sediment Depositional Area	0.0296	0.0361	0.0361	0.009	0.031	0.7729	

* Pairs are negatively correlated

Table 8.4. Belle Fourche River R² correlation of changes in fluvial parameters in the period 1977-2012. Yellow highlights are significant based on Equation 6.1.

	Sinuosity	Contaminated Floodplain Widths	Contaminated Floodplain Widths Variation	Contaminated Sediment Area	Contaminated Removed Area	Channel Migration	Total Sediment Depositional Area
Sinuosity							
Contaminated Floodplain Widths	0.2915						
Contaminated Floodplain Widths Variation	0.0227	0.4489					
Contaminated Sediment Area	0.0326	0.2725	0.2549				
Contaminated Removed Area	0.0379	0.1661	0.1056	0.8962			
Channel Migration	0.4201	0.4541	0.0683	0.0087	0.0102		
Total Sediment Depositional Area	0.0116	0.3677	0.3677	0.0202	0.0186	0.6461	

* Pairs are negatively correlated

Chapter 9. - Tables

Table 9.1. Arsenopyrite weight percentage using Ji's (2021) 30 year As suspended sediment transportation rate based on calculations from Chapter 5.5 in Geochemistry Methods.

Suspended As Transportation rate	$33 \frac{Mg}{year}$	$70 \frac{Mg}{year}$
Tailing height = 0.6 m	1.9%	3%
Tailing height = 3.5 m	2.5%	3.9%

FIGURES

Chapter 1. - Figures

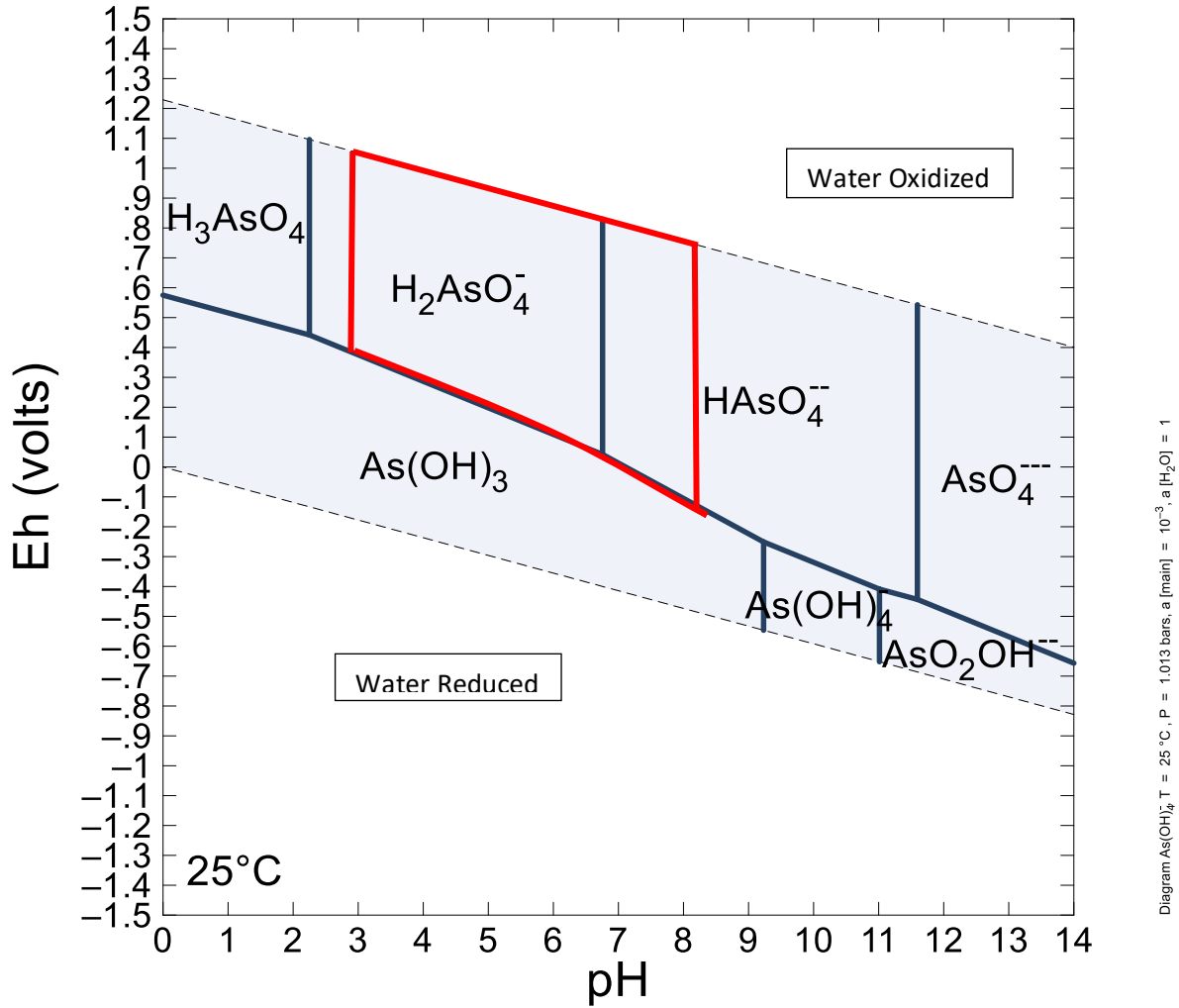


Figure 1.1. As Eh-pH diagram. Red square represents zone of effective As removal with the presence of Fe from Jacks (2017). Around the right edge of the square is the point of zero charge for Fe (hydr)oxides where adsorbing decreases. Most Fe oxyhydroxides have a point of zero charge in the pH range from 7.5 to 8.5 (Stumm, 1992).

Chapter 2. - Figures

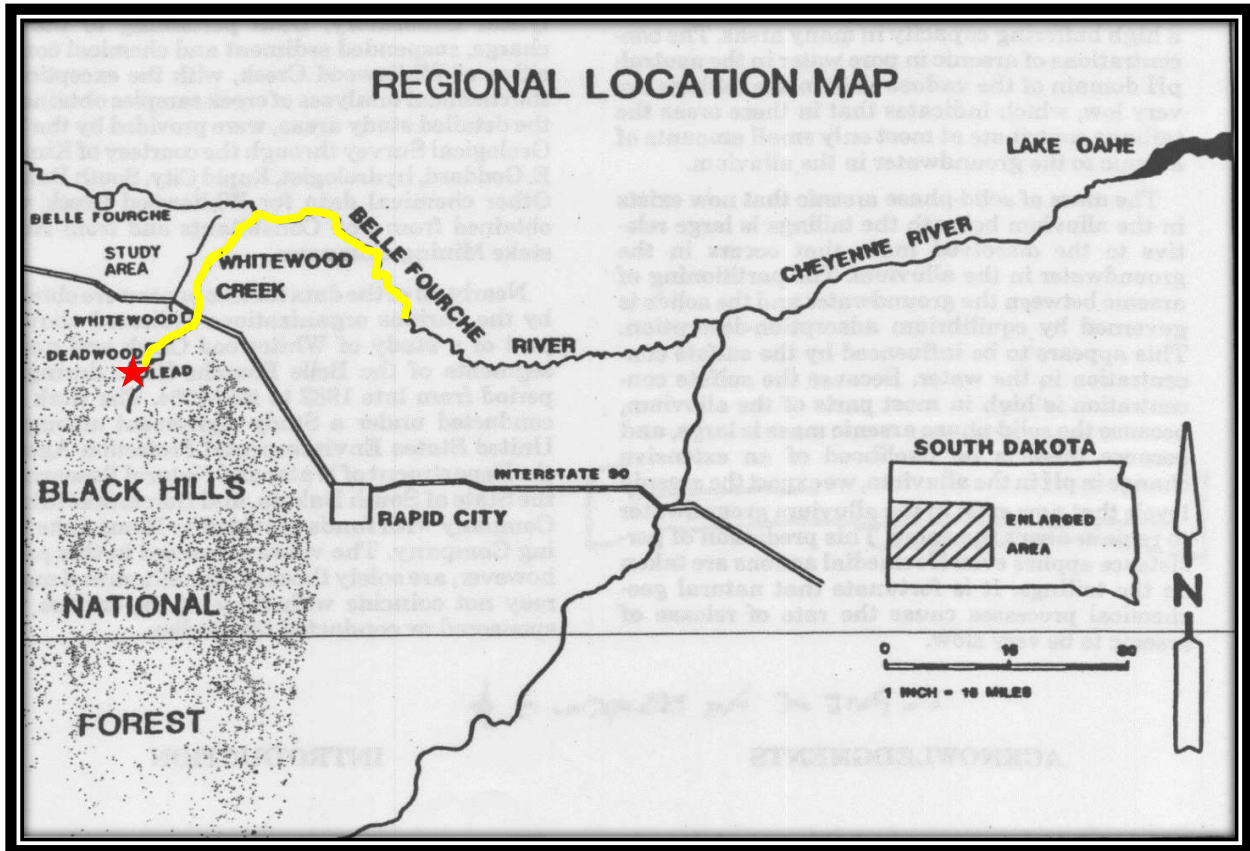


Figure 2.1. Regional location of the study area. Red Star is the location of the Homestake Gold Mine, yellow lines are reaches that are described in this project. Modified from Cherry et al. (1986).



Figure 2.2. Detailed view of the Whitewood Creek valley and the Whitewood Creek Superfund site. Yellow highlight is the superfund site area, green highlight is Whitewood Creek, dashed lines around Whitewood Creek is its delineated drainage basin. Modified from Cherry et al. (1986) and Ji (2021).



Figure 2.3. Aerial photo of the Homestake Gold Mine circa 2020. From <https://www.lonelyplanet.com/news/smithsonian-channel-aerial-america-free-episodes-online>

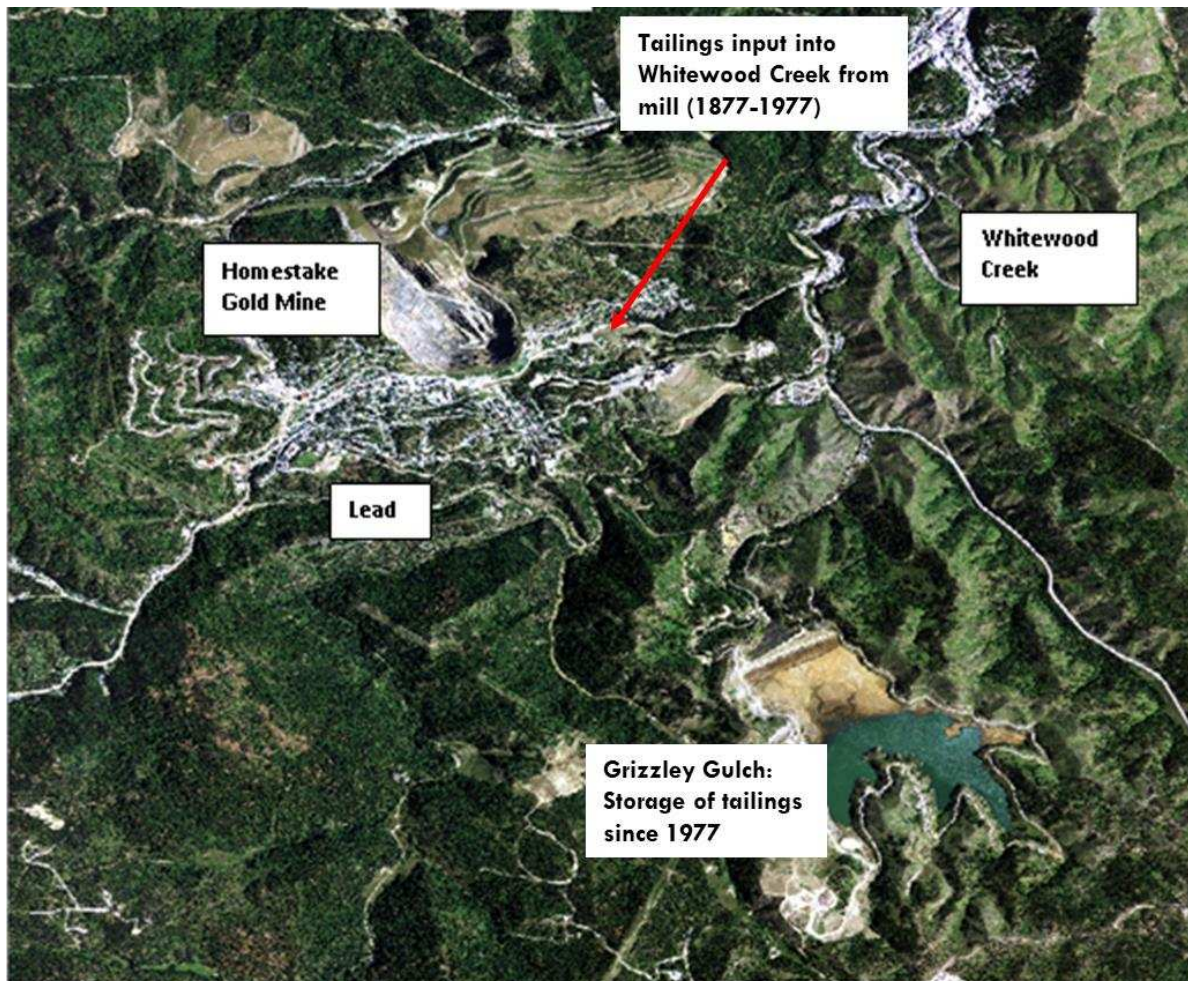


Figure 2.4. Aerial photograph of the town of Lead, Homestake Gold Mine, Grizzly Gulch tailings impoundment, and Whitewood Creek flowing to the northeast (from Google Earth).

Extractant used:	De-ionized Water	1M Sodium Phosphate (NaH ₂ PO ₄)	0.2M Hydroxylamine HCL (NH ₂ OH·HCl)	1M Hydrochloric Acid (HCl)	
	<i>pH= 6.0-6.5</i>	<i>pH= 4.5</i>	<i>pH= 2.0</i>	<i>pH= 0</i>	
As Residence Site Targeted:	Surface Electrostatic Bonds	Ion Exchange Sites	Fine-grained: Fe, Mn, Al Oxides	Secondary Minerals	Arsenopyrite / Residual
As Bond Strength:	Weakly Bound			Strongly Bound	
As Mobilization Rate:	Rapid			Very Slow	
	0.37%	11%	4.8%	24%	60%

Figure 2.5. Sequential extraction system performed by Ji (2021) with extractant, As residency, bond strength, and rate of As mobility. Percentages are results from the extraction. Modified from Ji and Ridley (2013).

Chapter 3. - Figures

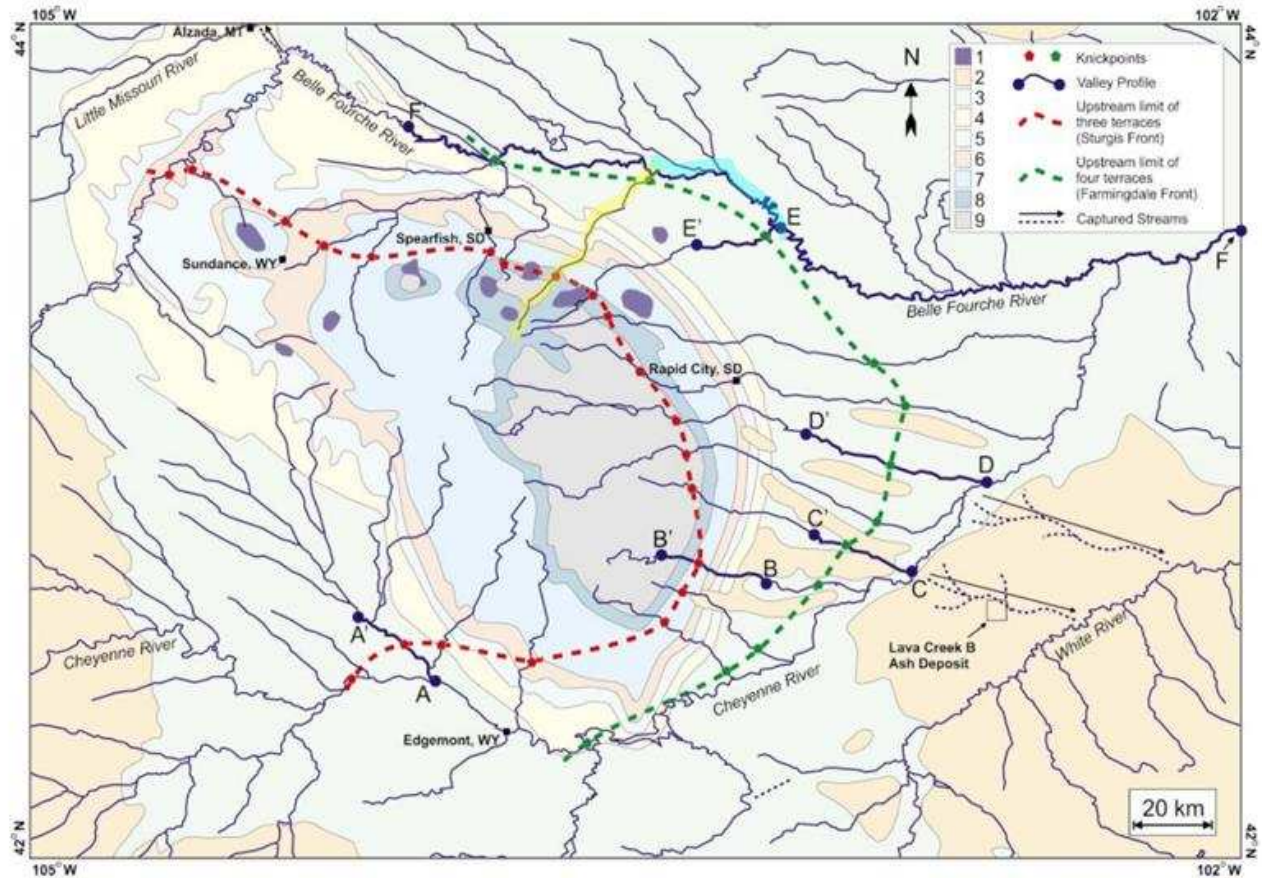


Figure 3.1. Overview of the erosional/knickzone fronts in the Black Hills Region that were described by Zaprowski et al. (2001). The red dashed line represents the upper Sturgis front and the green represents the lower Farmingdale front. Yellow highlight is Whitewood Creek and cyan highlight is Belle Fourche River approximately within the project area. Modified from Zaprowski et al. (2001).

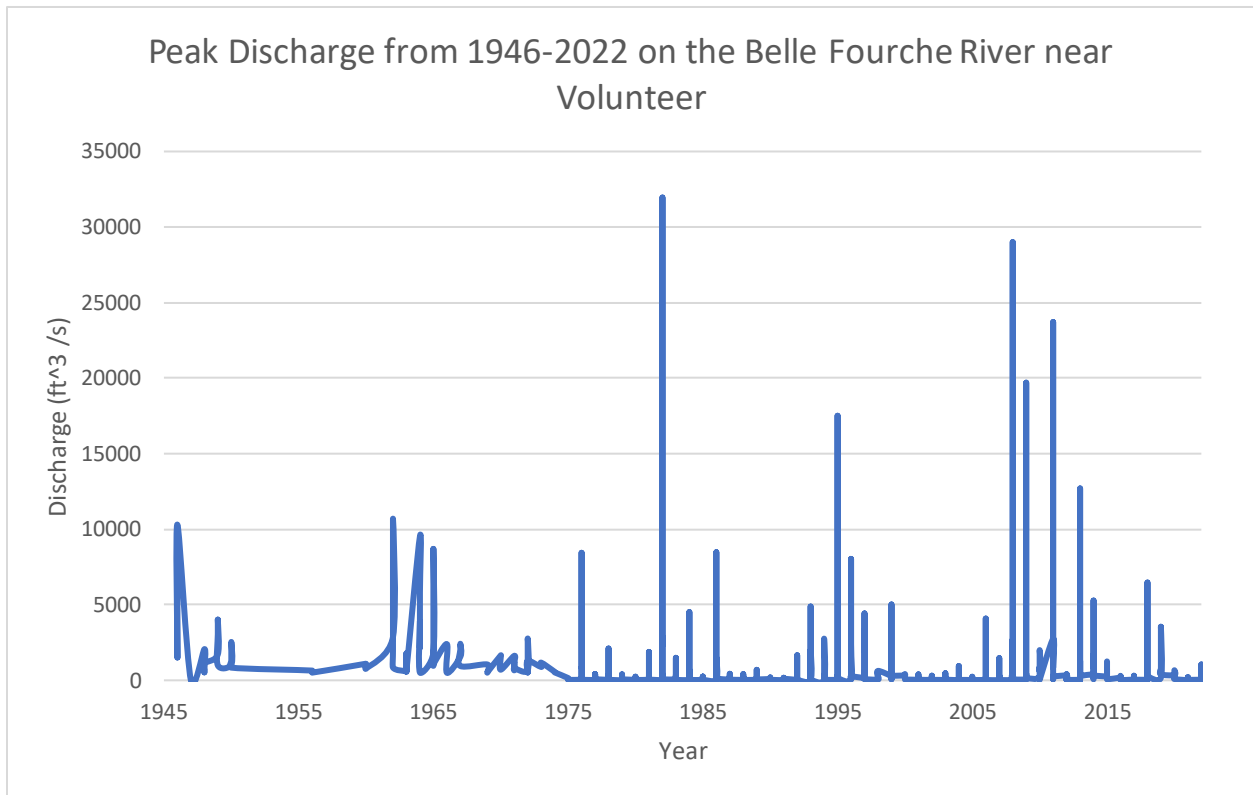


Figure 3.2. Hydrograph showing peak discharge from 1946 to 2022 on the Belle Fourche River near the village of Volunteer. Data came from USGS gaging station, Belle Fourche River near Sturgis, SD (https://waterdata.usgs.gov/nwis/uv/?site_no=06437000).

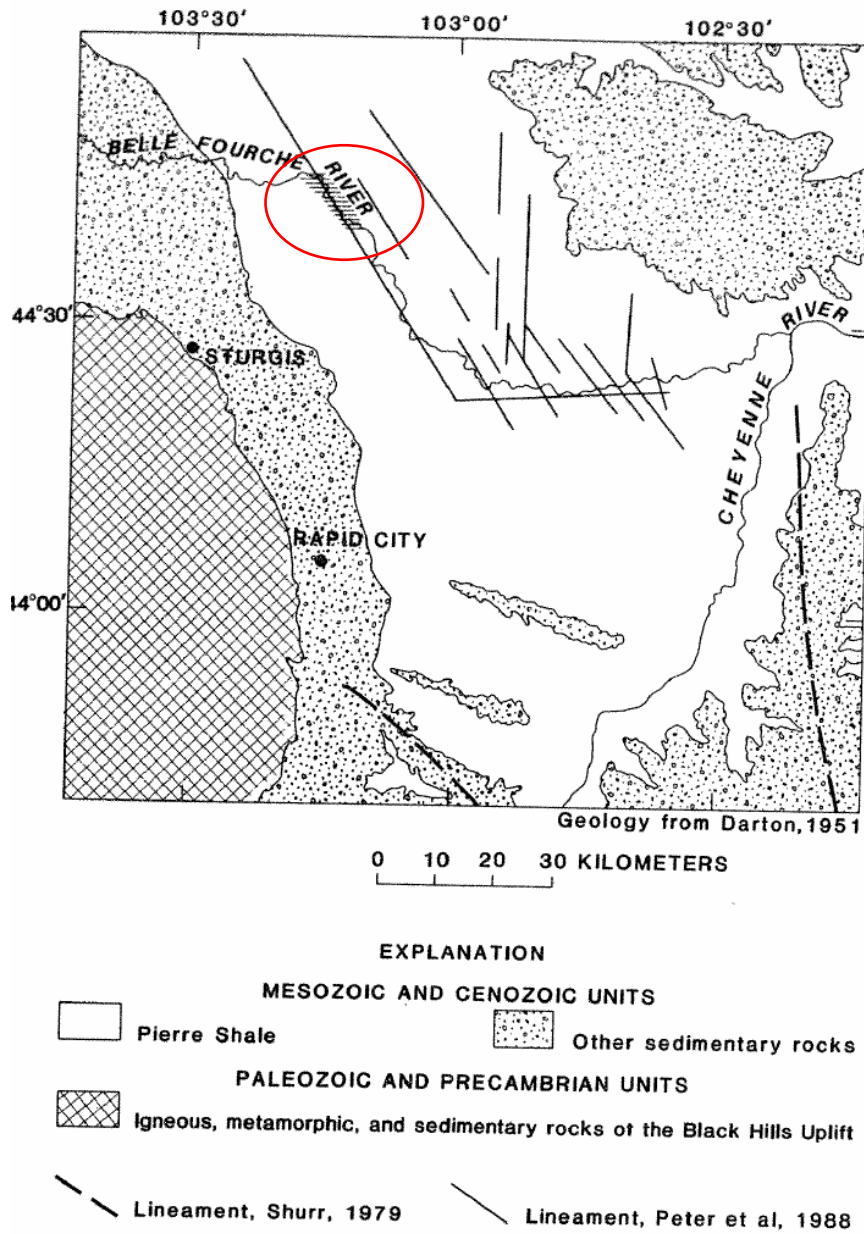


Figure 3.3. Map of the Belle Fourche and Cheyenne River basins east of the Black Hills showing where basement rock lineaments occur from Shurr (1979) and Peter et al. (1988) with respect to bedrock geology (Darton, 1951). Notice how the study area portion of the Belle Fourche (red circle) goes through one of Peter et al. (1988) lineaments. Shaded area within the circle is the discontinuity described by Gomez and Marron (1991). Modified from Gomez and Marron (1991).



Figure 3.4. View of Whitewood Creek at 194th Street bridge (on Reach 7, see Figure 4.2) looking to the north (Photograph by Charles Marr).

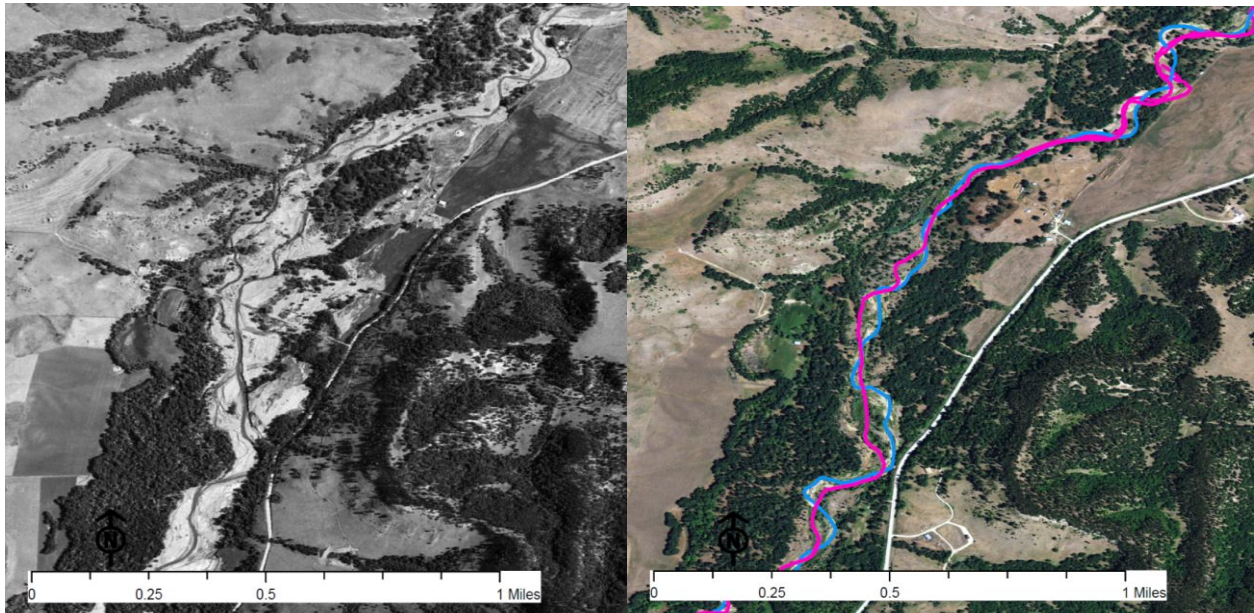


Figure 3.5. View of Whitewood Creek 3 km north of Whitewood at Reach 2 (see Figure 4.2). Left photo is the creek from 1952 and the right is from 2012. Magenta line is the 1952 main channel from the top photo and blue line is the 2012 channel. Notice the high sediment accumulation around Whitewood Creek during 1952. Most of the sediment is covered by vegetation by 2012.

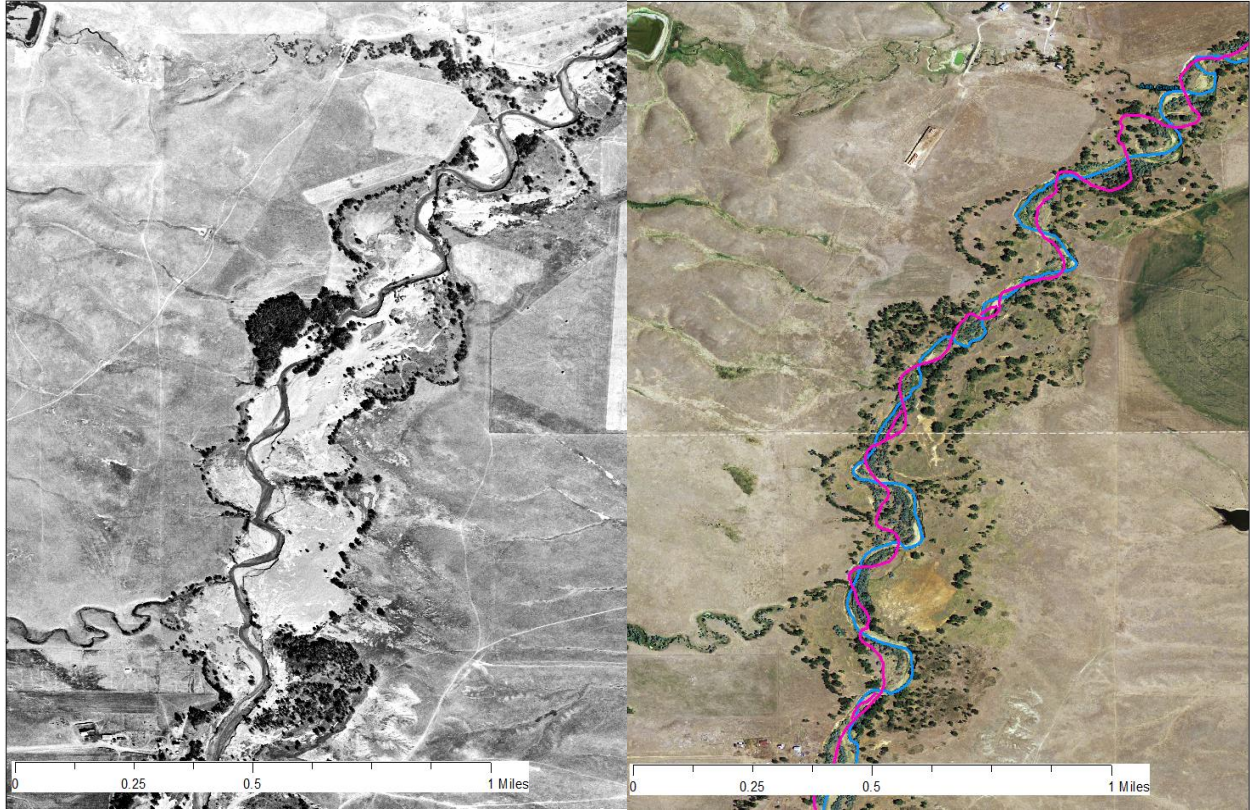


Figure 3.6. View of Whitewood Creek about 5 km upstream from the Belle Fourche River confluence at Reach 8 (see map from Figure 4.2). Left photo is the creek from 1948 and the right is from 2012. Magenta line is the 1948 main channel from the top photo and blue line is the 2012 channel.



Figure 3.7. View of Whitewood Creek from the Vale Cutoff Road (Reach 9, see Figure 4.2) looking to the northeast. Note the high incision into the shale bedrock (gray sediment at the bottom of the cutbank). Height is approximately 15 feet (~4 m) (by eye) (Photograph by Charles Marr).



Figure 3.8. Whitewood Creek at around the Location G (see Figure 5.1) where high bank instability and lateral erosion occurs in the cutbanks. From Ji (2021).

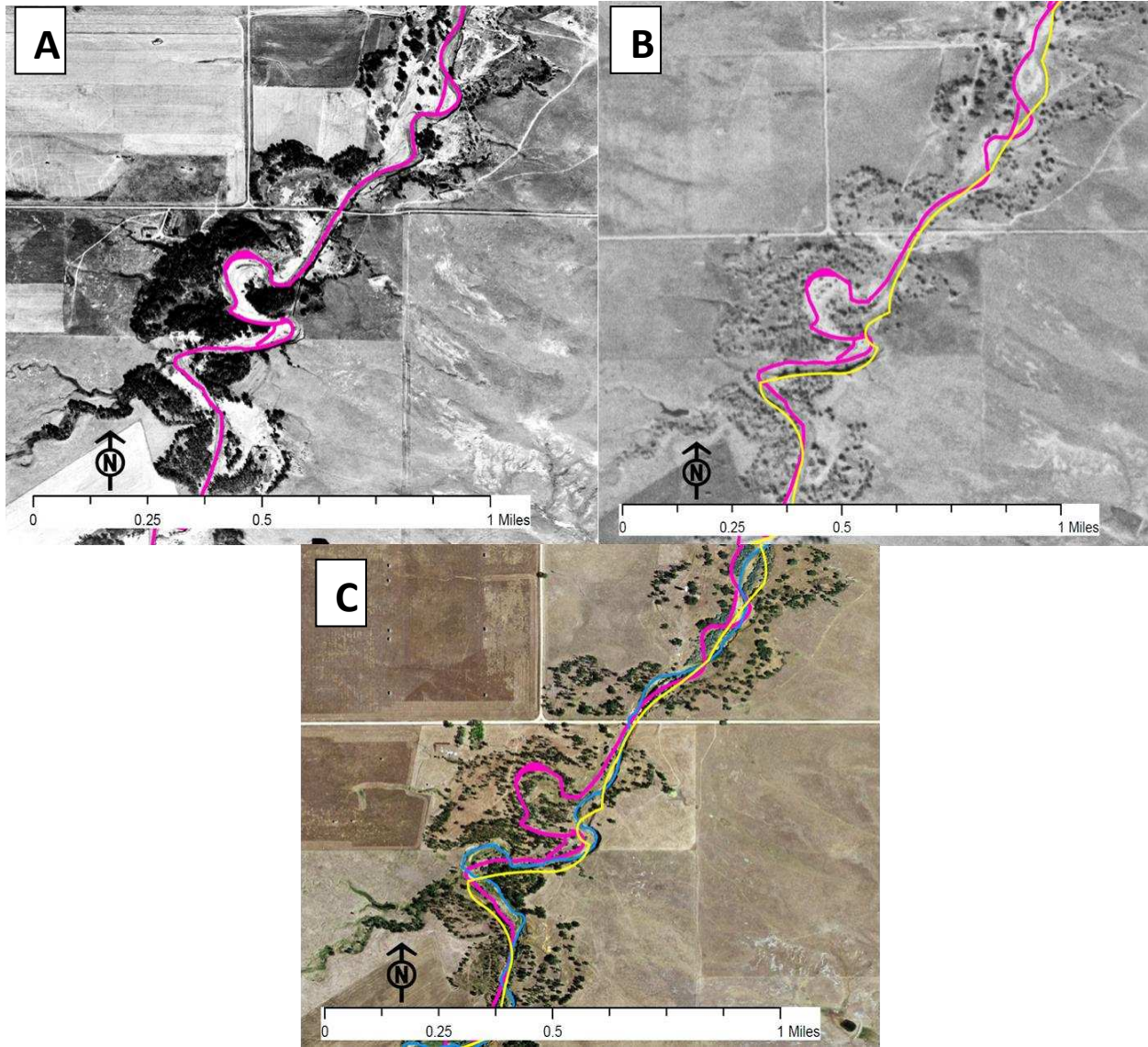


Figure 3.9. Aerial photographs of Whitewood Creek showing the abandonment of a meander between 1948 to 2012. The road that crosses the creek is 194th Street (Reach 7, see Figure 4.2). A is from 1948, B is from 1977, and C is from 2012. Magenta line is the 1948 channel, yellow line is 1977 channel, and blue line is 2012 channel.



Figure 3.10. View of the Belle Fourche River near Highway 34 and the village of Volunteer looking to the northwest (Reach 10, see Figure 4.3) (Photograph by Charles Marr).



Figure 3.11. View of the possible uncontaminated (lower buff colored sediment) overlaid by possible contaminated sediment (darker red colored sediment) looking north from 194th Street bridge (Reach 7, see Figure 4.2). (Photograph by Charles Marr).



Figure 3.12. Auriferous sulfidic chlorite schist from the Homestake Formation. Dark green material is composed of chamosite chlorite. Metallic lustered areas are composed of pyrrhotite and arsenopyrite. From James St John's Flickr account.

Chapter 4. - Figures

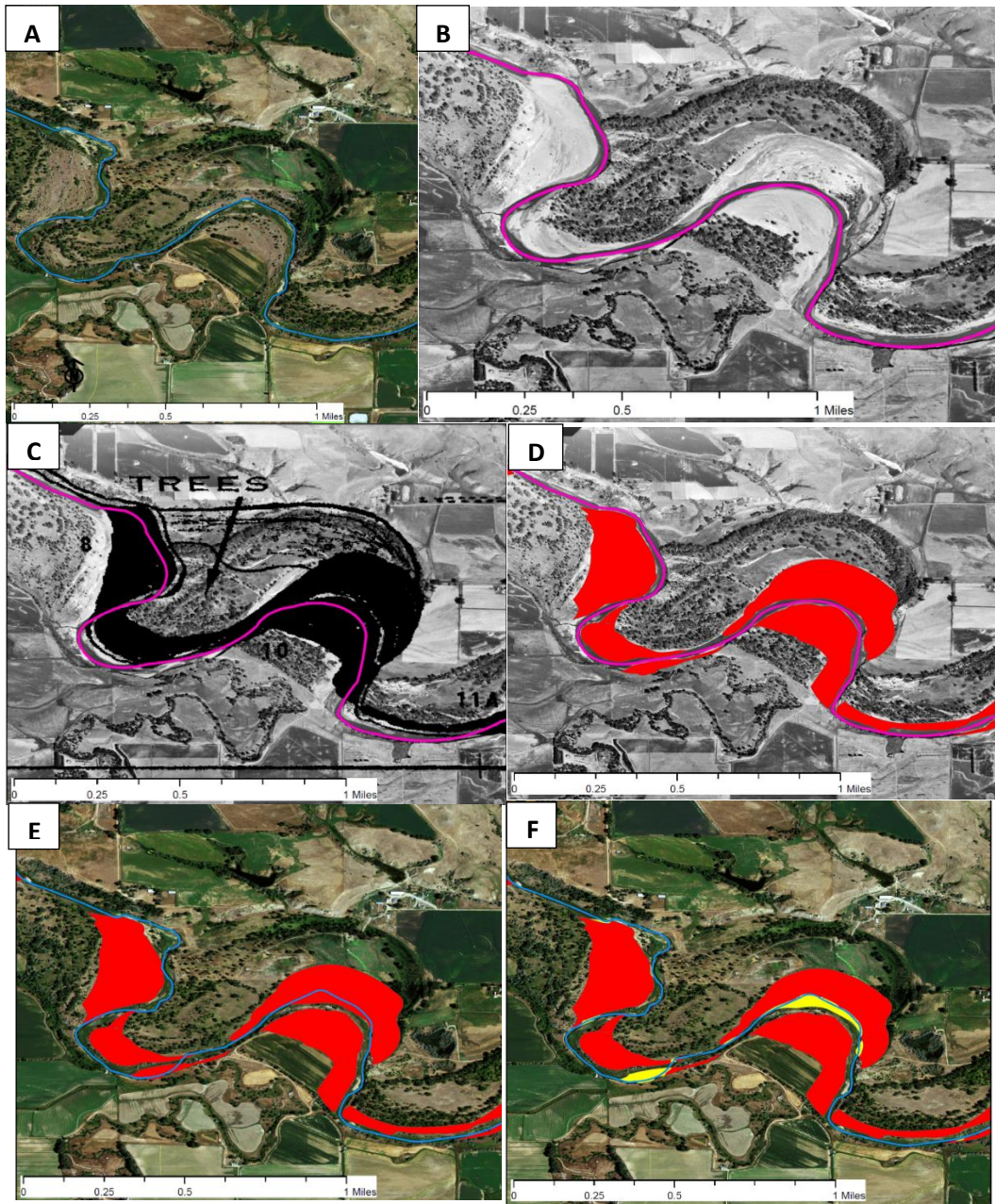


Figure 4.1. Workflow process of digitizing contaminated floodplains and their removal using a section of the Belle Fourche River (Reach 2, see Figure 4.3) for example. A is the 2012 NAIP aerial photo (blue line is 2012 channel). B is from the 1948 aerial photograph (magenta line is 1948 channel). C is the 1948 aerial photograph overlaid by EPA's (1972) tailings (black polygon). D is the digitized tailings (red polygons). E is the digitized tailings overlaying the 2012 aerial photo with the 2012 channel (blue line). F shows the portions of the tailings that have been eroded away (yellow polygons) from the 2012 channel migration.

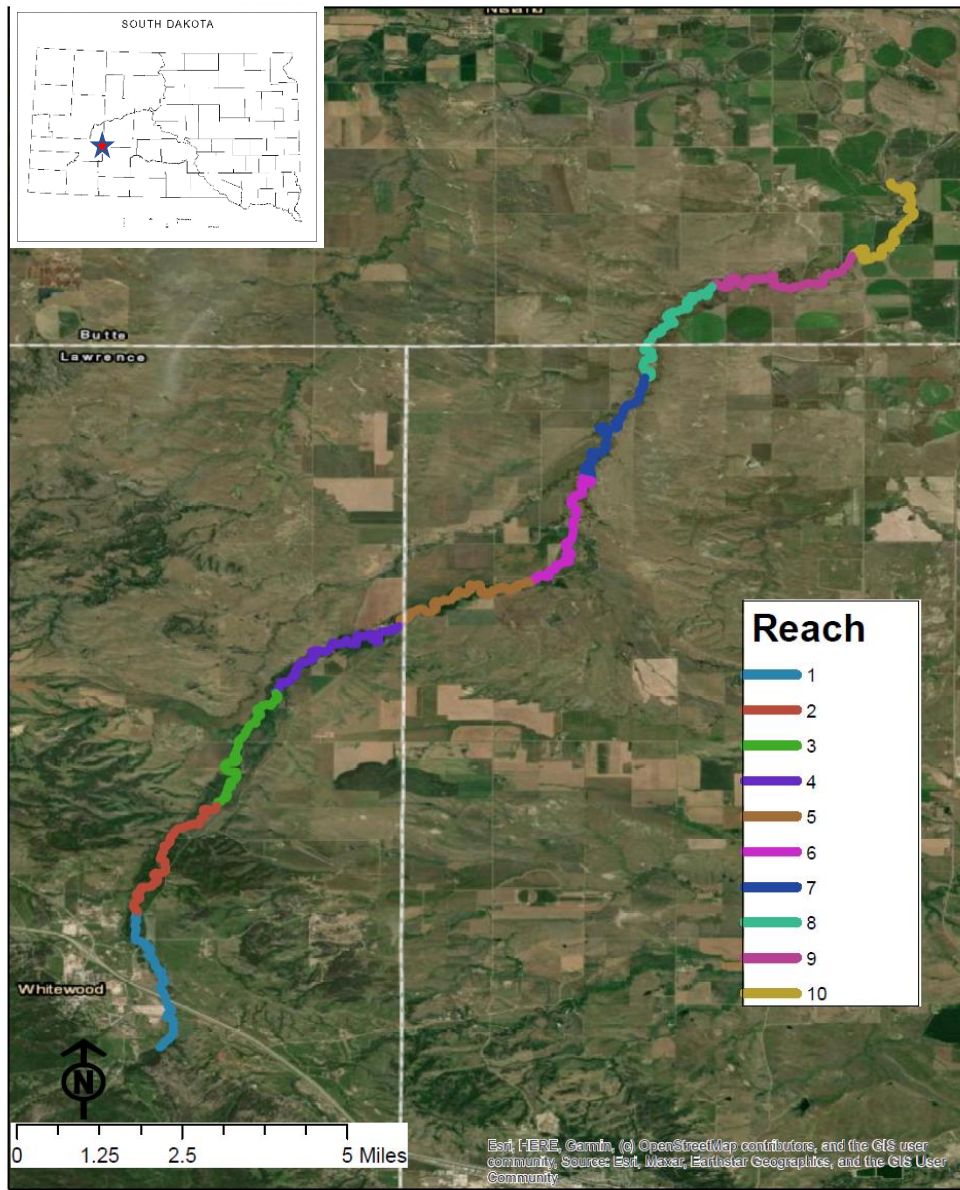


Figure 4.2. The location of Whitewood Creek reaches that were created for this study.

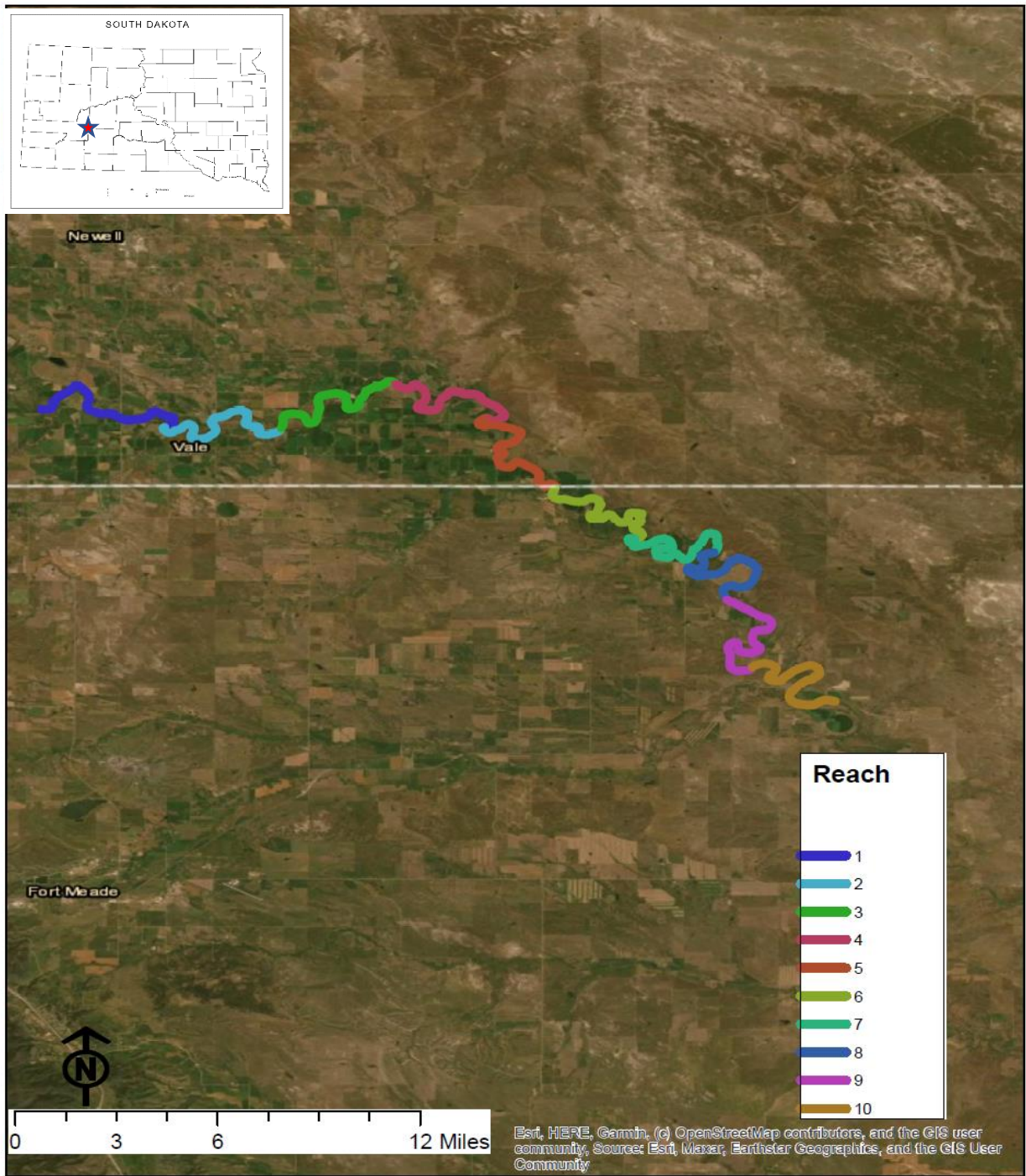


Figure 4.3. The location of Belle Fourche River reaches that were created for this study.

Chapter 5. – Figures

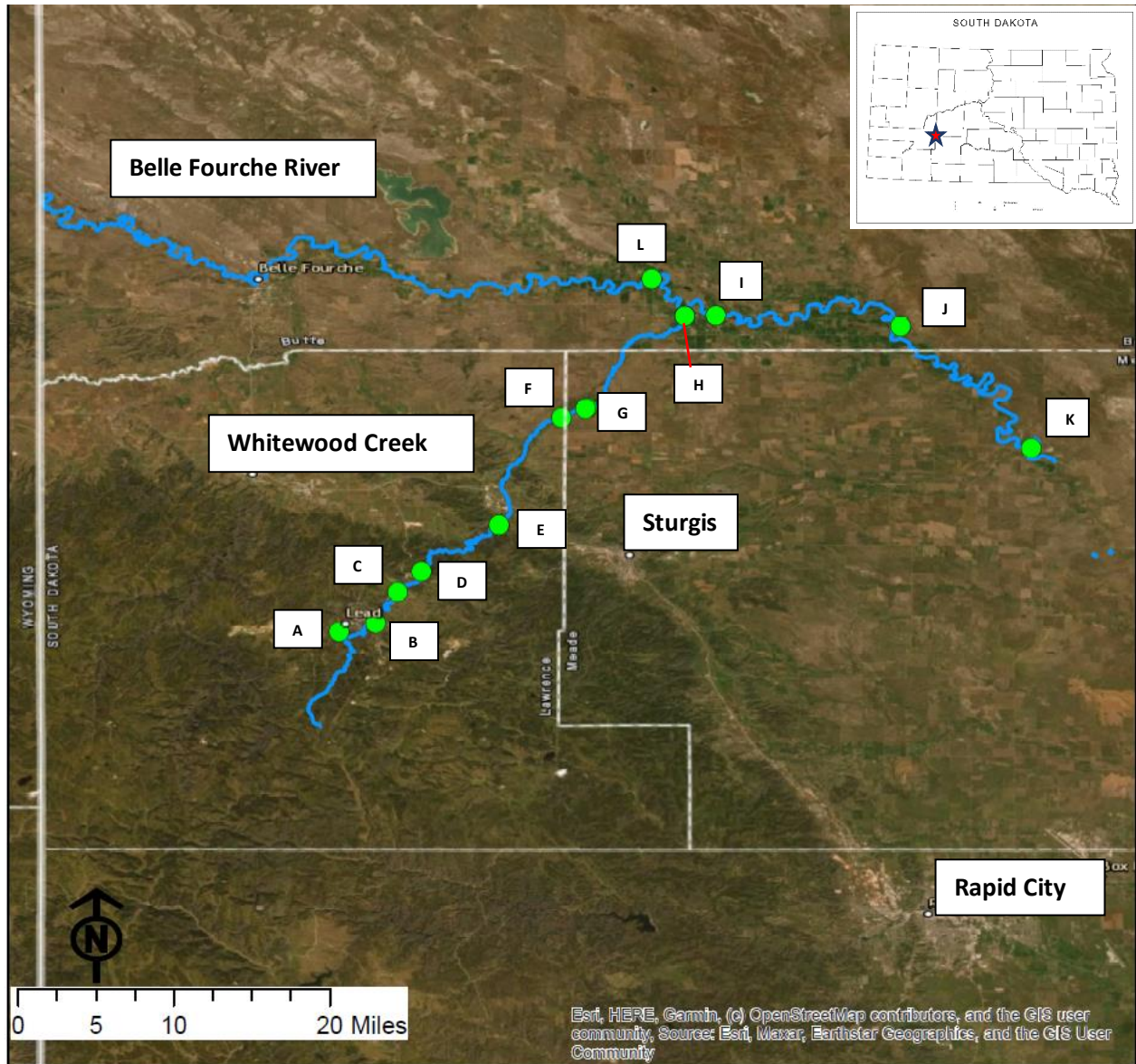


Figure 5.1. Regional map of Whitewood Creek and Belle Fourche River with the location of Ji (2021) sample sites.

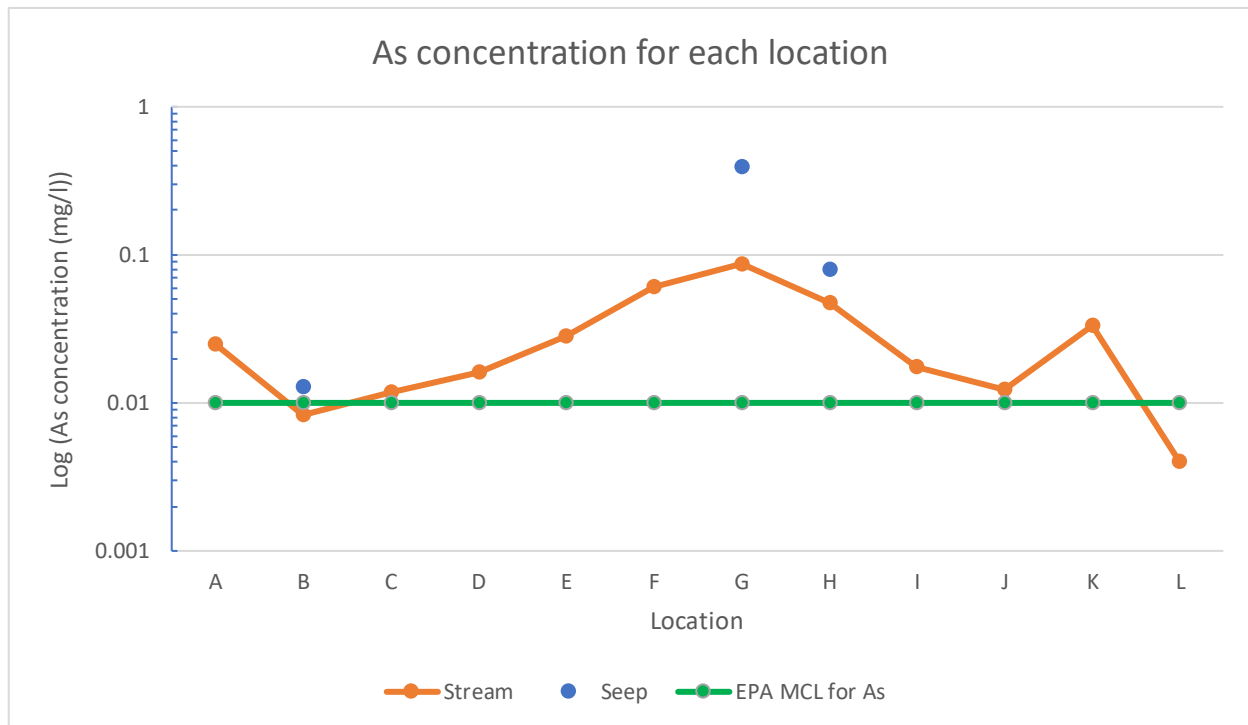


Figure 5.2. Arsenic concentration for stream (orange line) and seep water (blue points) for each location from Ji (2021) fieldwork. Green line is the EPA maximum contaminated level (MCL) for As in drinking water (0.01 ppm).

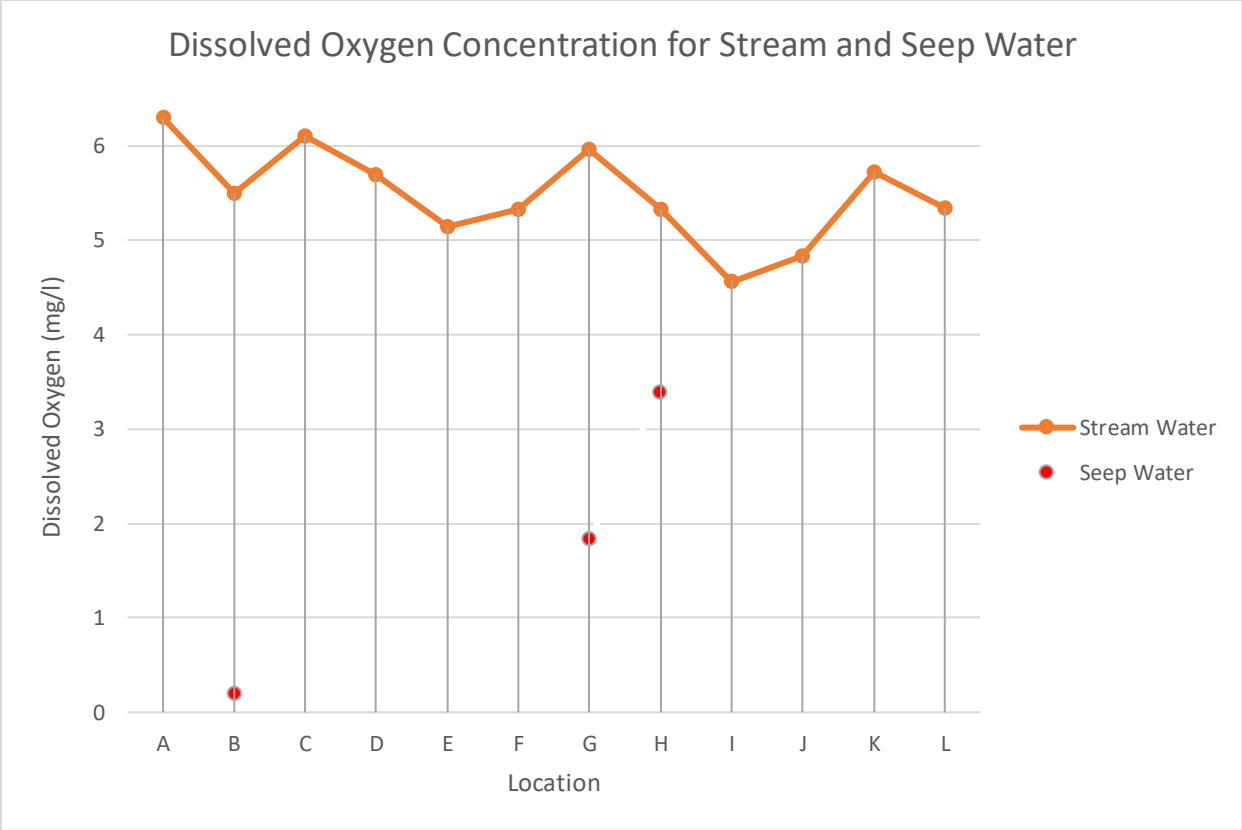


Figure 5.3. Dissolved oxygen concentration levels of stream and seep water for each location from Ji (2021).

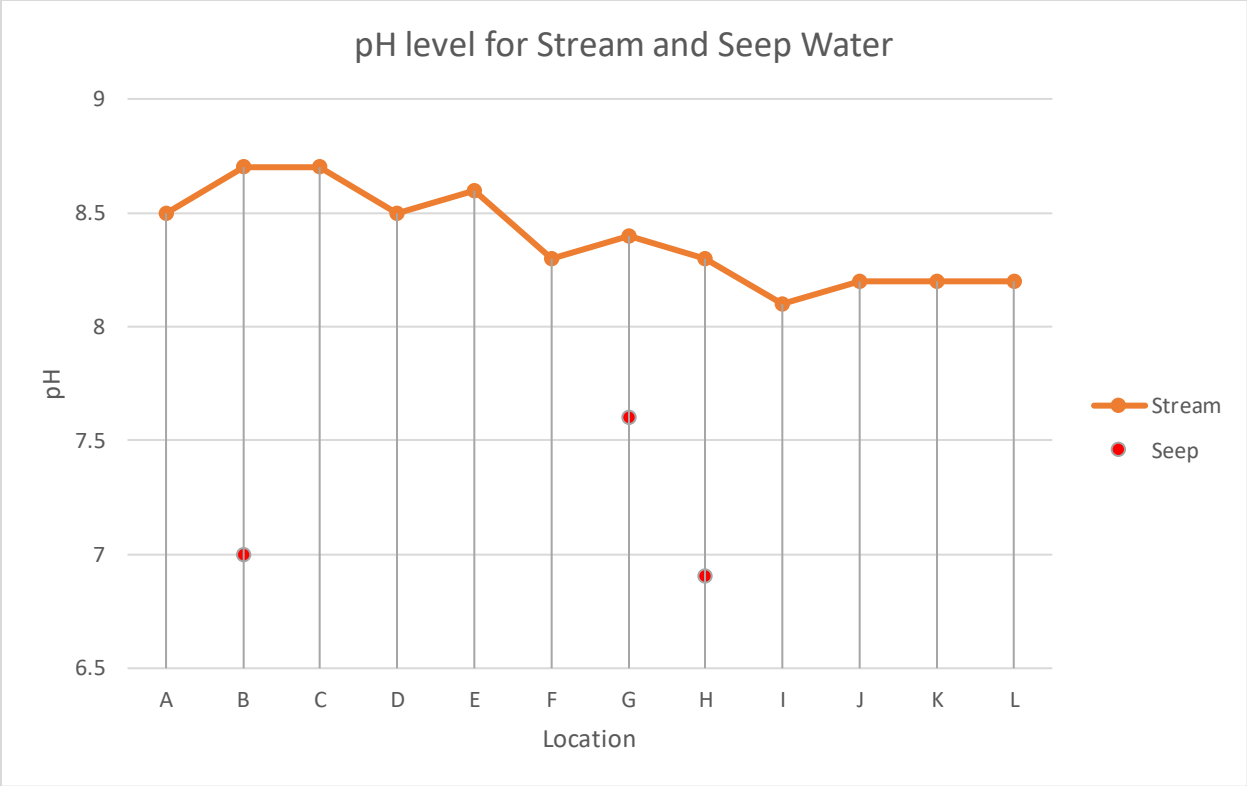


Figure 5.4. pH levels of stream and seep water for each location from Ji (2021).

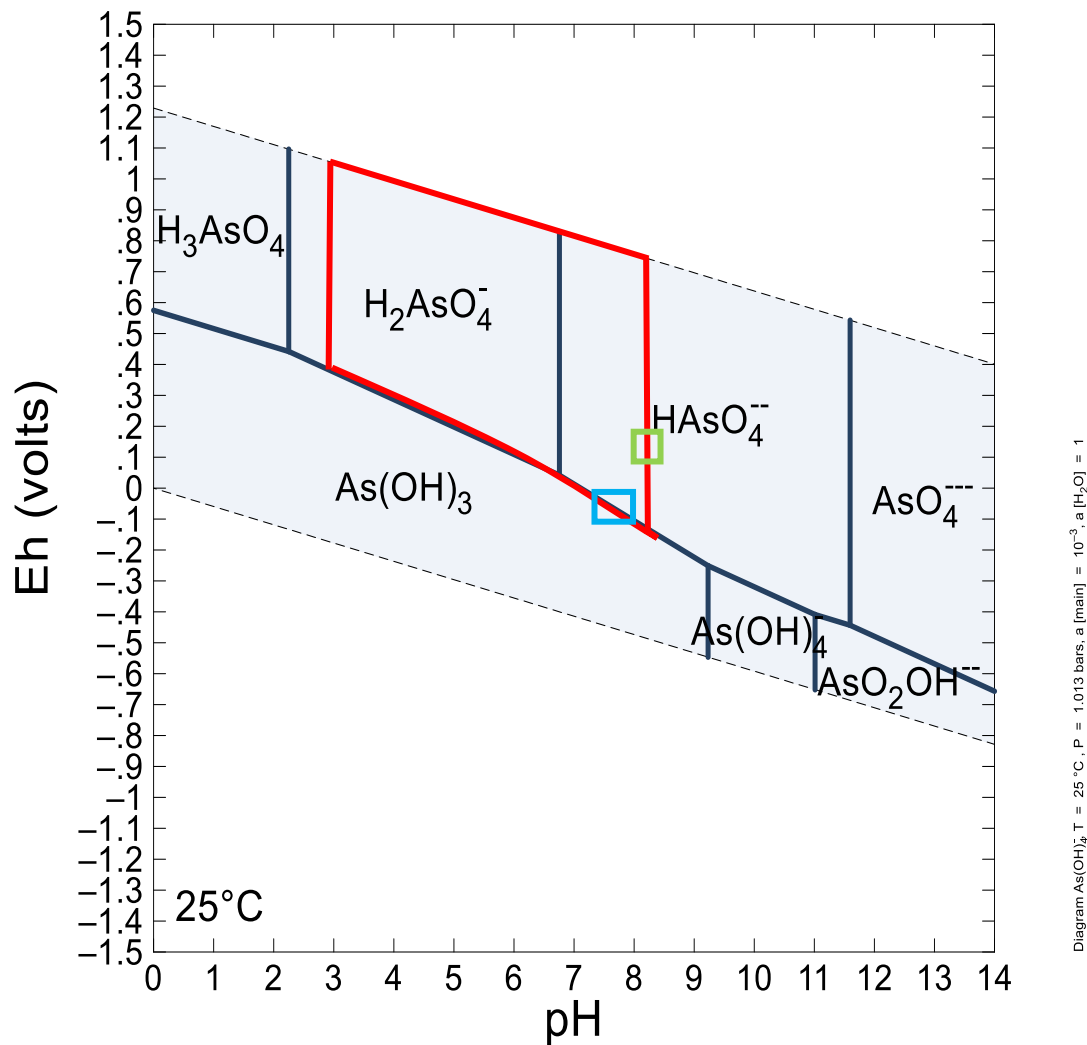


Figure 5.5. Arsenic Eh-pH diagram. Red square represents zone of effective As removal (i.e. adsorption) with the presence of Fe from Jacks (2017). Green square is the general area where Whitewood Creek (Location F-H) and Belle Fourche River (Location I-K) stream waters are. Blue square is the general area where the waters from the seeps of Whitewood Creek values are (Location B, G, H). The pH values of the boxes came from Ji's (2021) fieldwork. The Eh values of the stream water box is from USGS gage stations (see Table 5.1) and the seep water box is from Goddard (1987) and Wuolo (1986). As mentioned in Figure 1.1, around the right edge of the red square is the point of zero charge for Fe (hydr)oxides where adsorbing decreases (Stumm, 1992).

```

Step #      0                Xi = 0.0000
Time = 0 secs (0 days)

Temperature = 17.5 C      Pressure = 1.013 bar
pH = 8.300                log fO2 = -41.420
Eh = 0.1550 volts        pe = 2.6878
Ionic strength = 0.021944 molal
Activity of water = 0.999974
Solvent mass = 1.0000e+08 kg
Solution mass = 1.0010e+08 kg
Mineral mass = 1.1011e+05 kg
Fluid density = 0.998 g/cm3
  compressibility = 4.536e-05 /bar
  expansivity = 0.0001942 /C
  viscosity = 0.011 poise
Chlorinity = 0.000749 molal
Dissolved solids = 1037 mg/kg sol'n
Elect. conductivity = 1266.02 uS/cm (or umho/cm)
Hardness = 677.90 mg/kg sol'n as CaCO3
  carbonate = 126.52 mg/kg sol'n as CaCO3
  non-carbonate = 551.38 mg/kg sol'n as CaCO3
Carbonate alkalinity = 126.52 mg/kg sol'n as CaCO3
Water type = Ca-S04
Bulk volume = 1.00e+11 cm3
Fluid volume = 1.00e+11 cm3
Mineral volume = 1.79e+07 cm3
Inert volume = 0.00 cm3
Porosity = 100. %
Permeability = 98.1 cm2
Mass reacted = 0 g

```

Figure 5.6. Parameters calculated from initial condition from REACT calculation at Location F. The mineral mass (red underline) is used to calculate the density of suspended arsenopyrite in the stream bottom assuming that there is 0.11% arsenopyrite in the tailings.

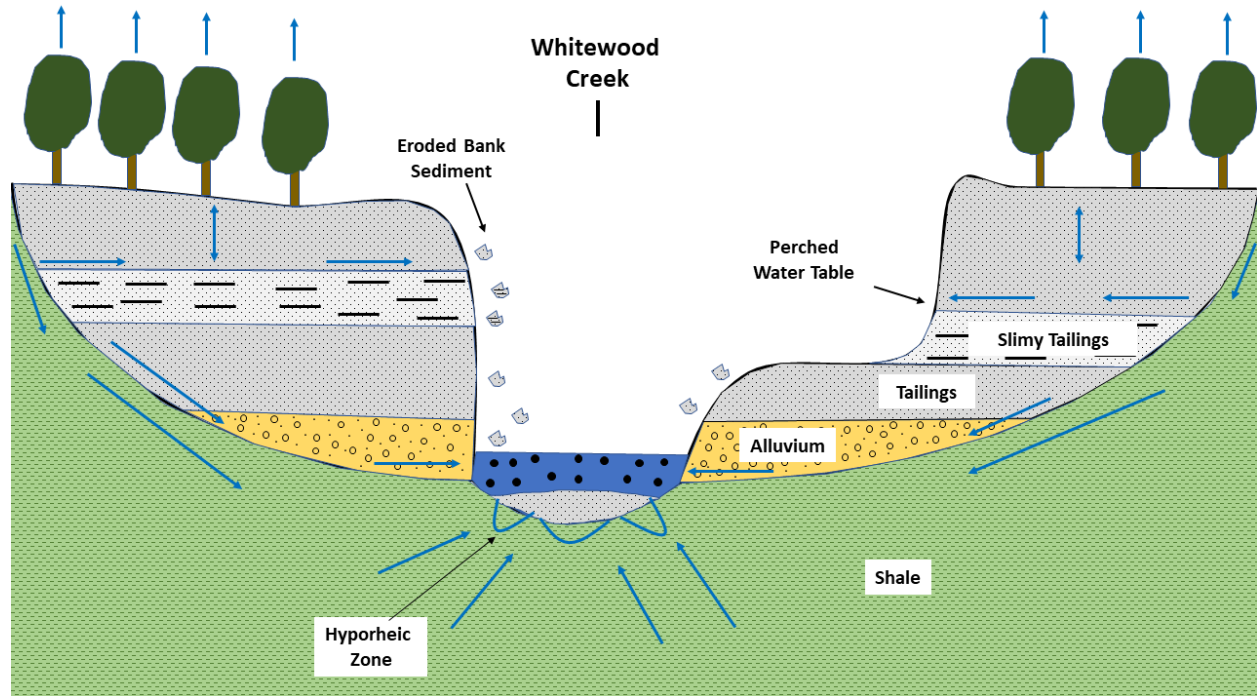


Figure 5.7. Conceptual illustration of the mine tailings interacting with the hydrology and geology of Whitewood Creek. Arrows are pathways of water circulation. Black dots in the stream represent suspended sediments. Parabolic flow underneath the stream bottom represents hyporheic flow (Boana et al., 2014). Modified from Cherry et al. (1986).

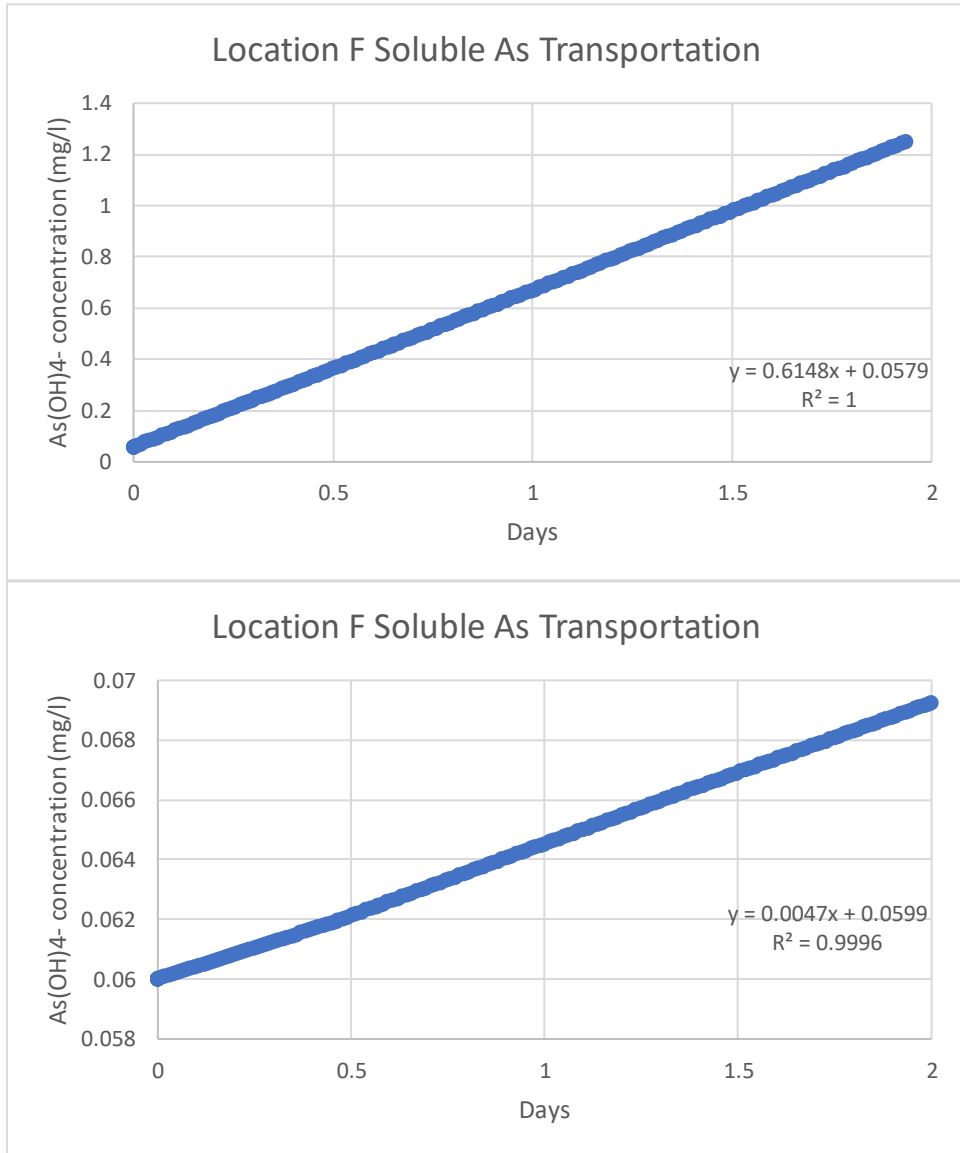


Figure 5.8. Example of As concentration dissolving into the stream water from arsenopyrite dissolution in two days from REACT calculation at Location F. The initial concentrations are the measured levels from Ji (2021). The slope of the best fit line is the concentration of soluble As (mg/L) per day. Top graph is assuming an arsenopyrite concentration of 15% and the bottom graph assumes 0.11% (see Appendix 7-16 and 7-17 for plots for Location G and H).

Chapter 6. - Figures

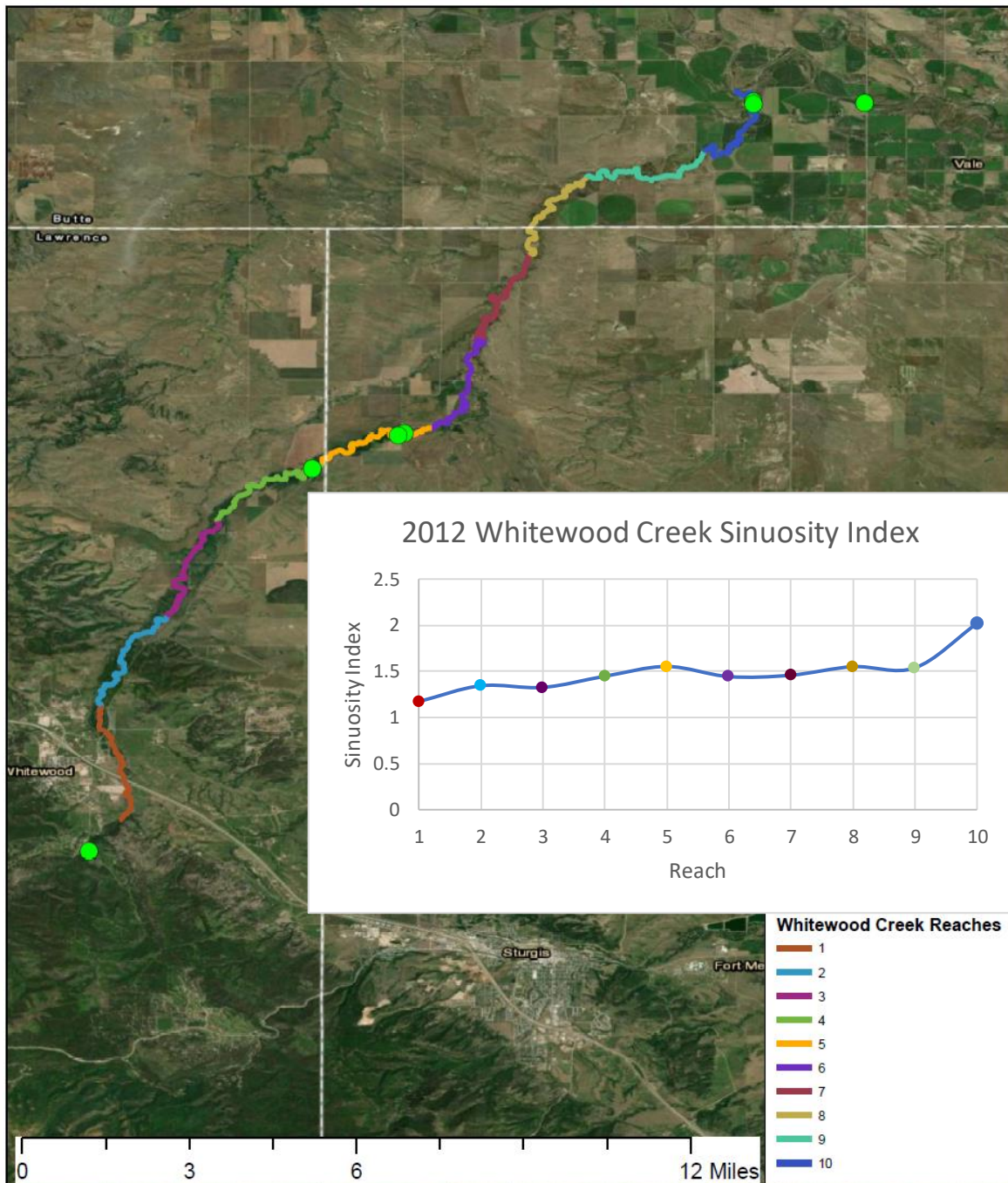


Figure 6.1. Sinuosity index for each reach at Whitewood Creek using the 2012 channel.

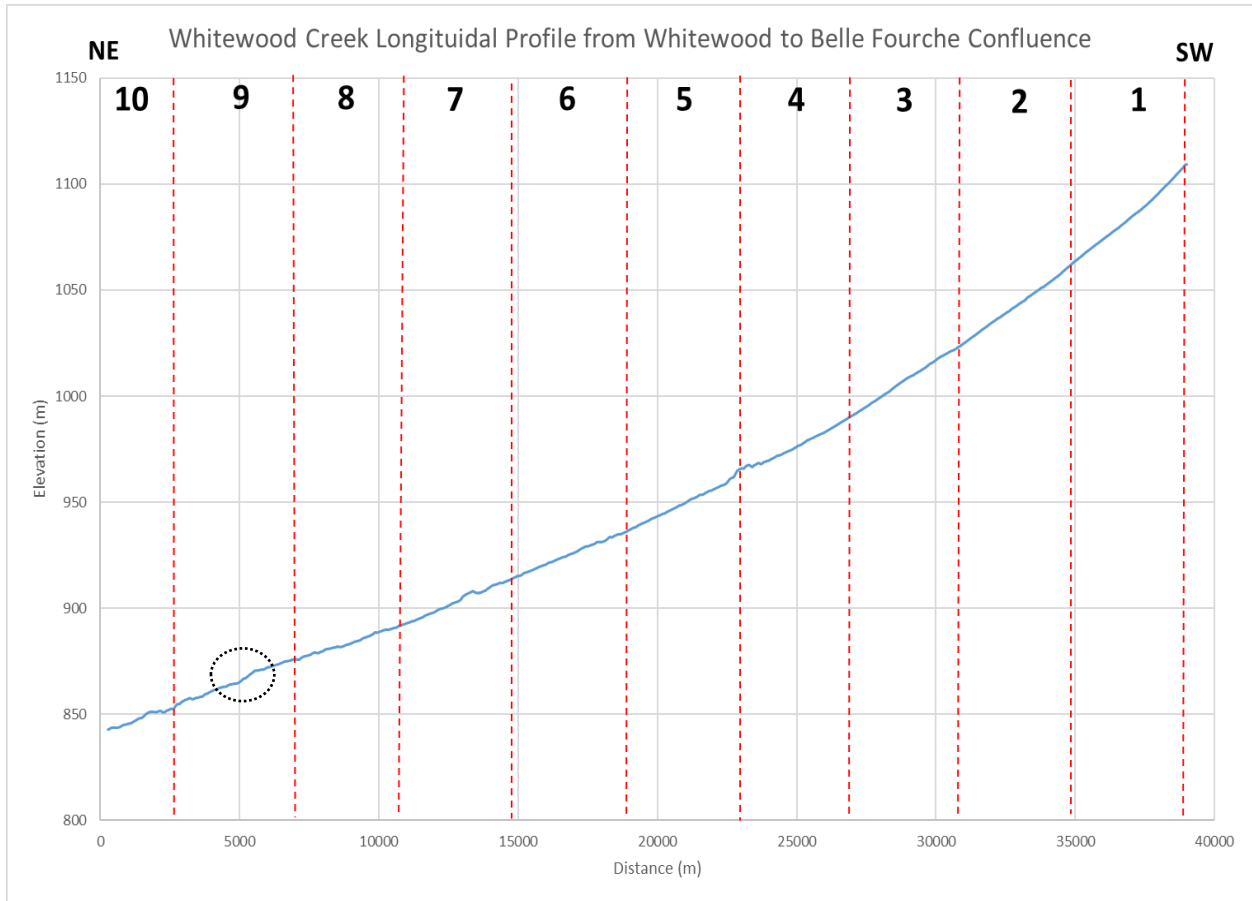


Figure 6.2. Longitudinal profile of Whitewood Creek’s reaches from Whitewood to Belle Fourche River confluence. Moving average was used to smooth graph. About 6926 points were averaged in the moving average. Black circle portion is approximately location of Zaprowski et al. (2001) Farmington Front knickzone (see Figure 3.1).

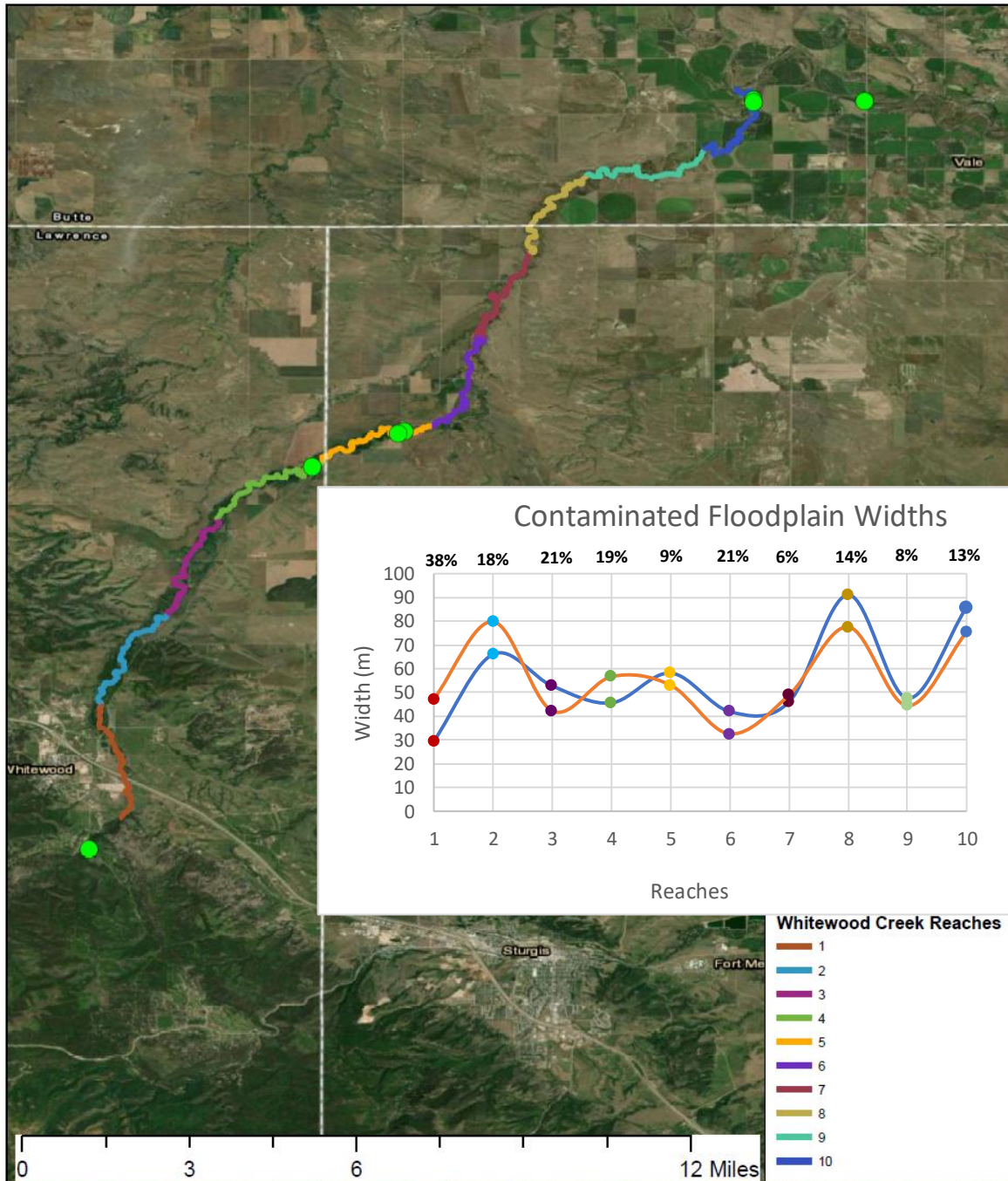


Figure 6.3. Contaminated floodplain widths at Whitewood Creek reaches. Blue line represents the 1948 contaminated sediment and orange line is for 1977. Percentages are the difference between the larger and smaller value divided by the larger value for each respective reach.

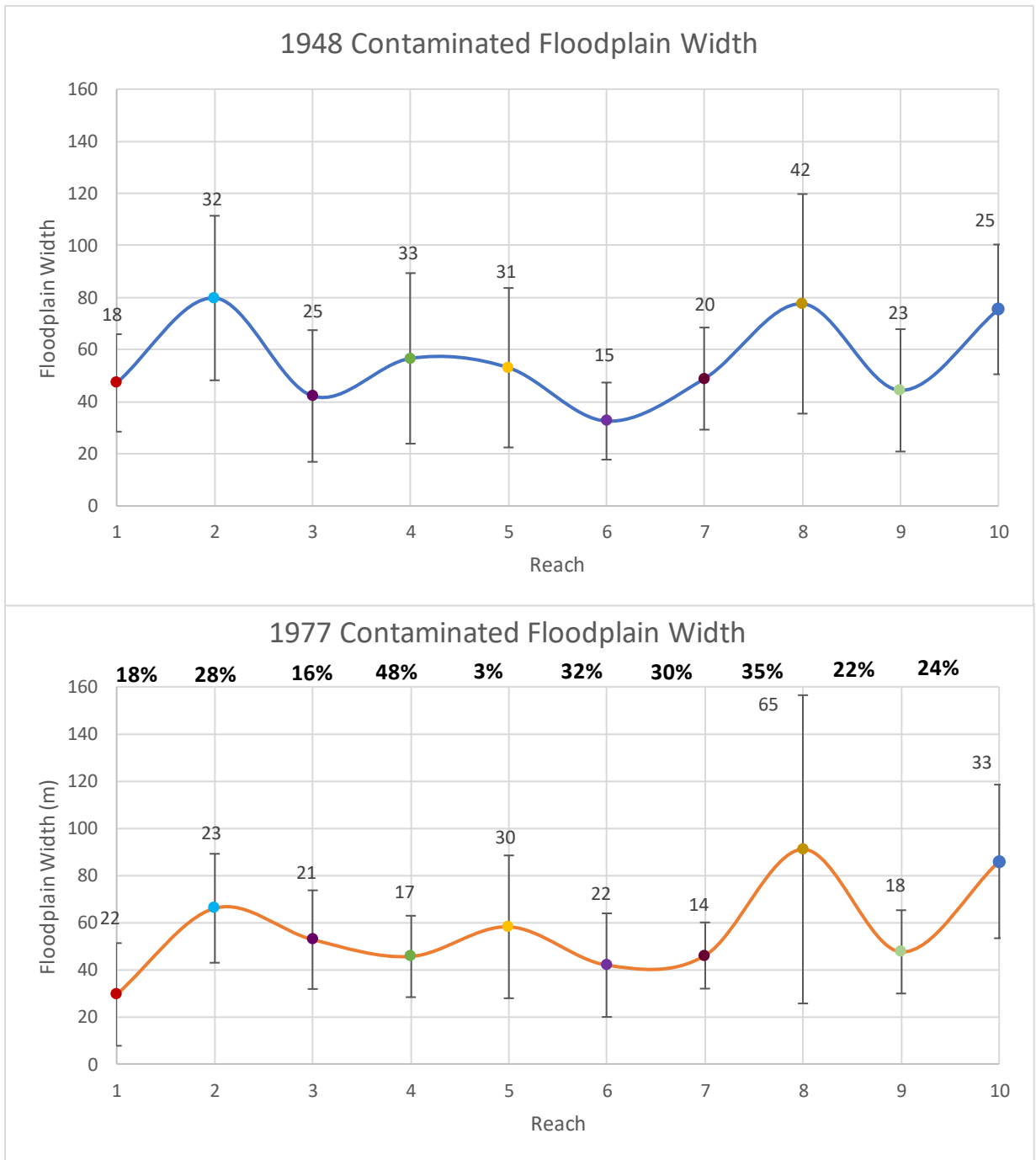


Figure 6.4. Contaminated floodplain widths and their variation (standard deviation) at Whitewood Creek reaches. Percentages are the difference between the larger value and smaller value of the standard deviation divided by the larger value for each respective reach. Standard deviation was calculated through ArcMap.

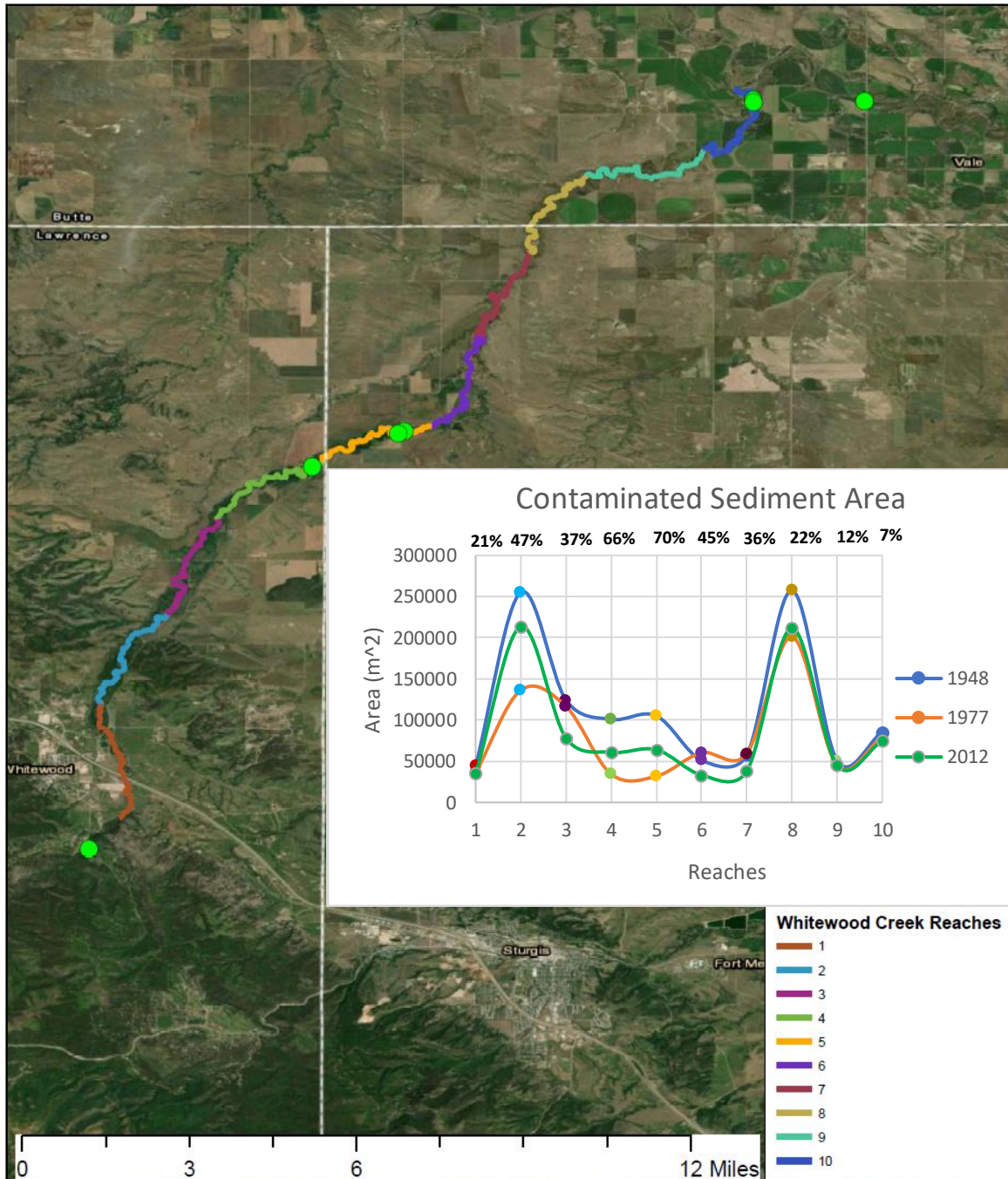


Figure 6.5. Distribution of contaminated sediment area and Whitewood Creek reaches. Blue line represents the 1948 contaminated sediment and orange line is for 1977. Percentages are the difference between the larger value and smaller value divided by the larger value for each respective reach.

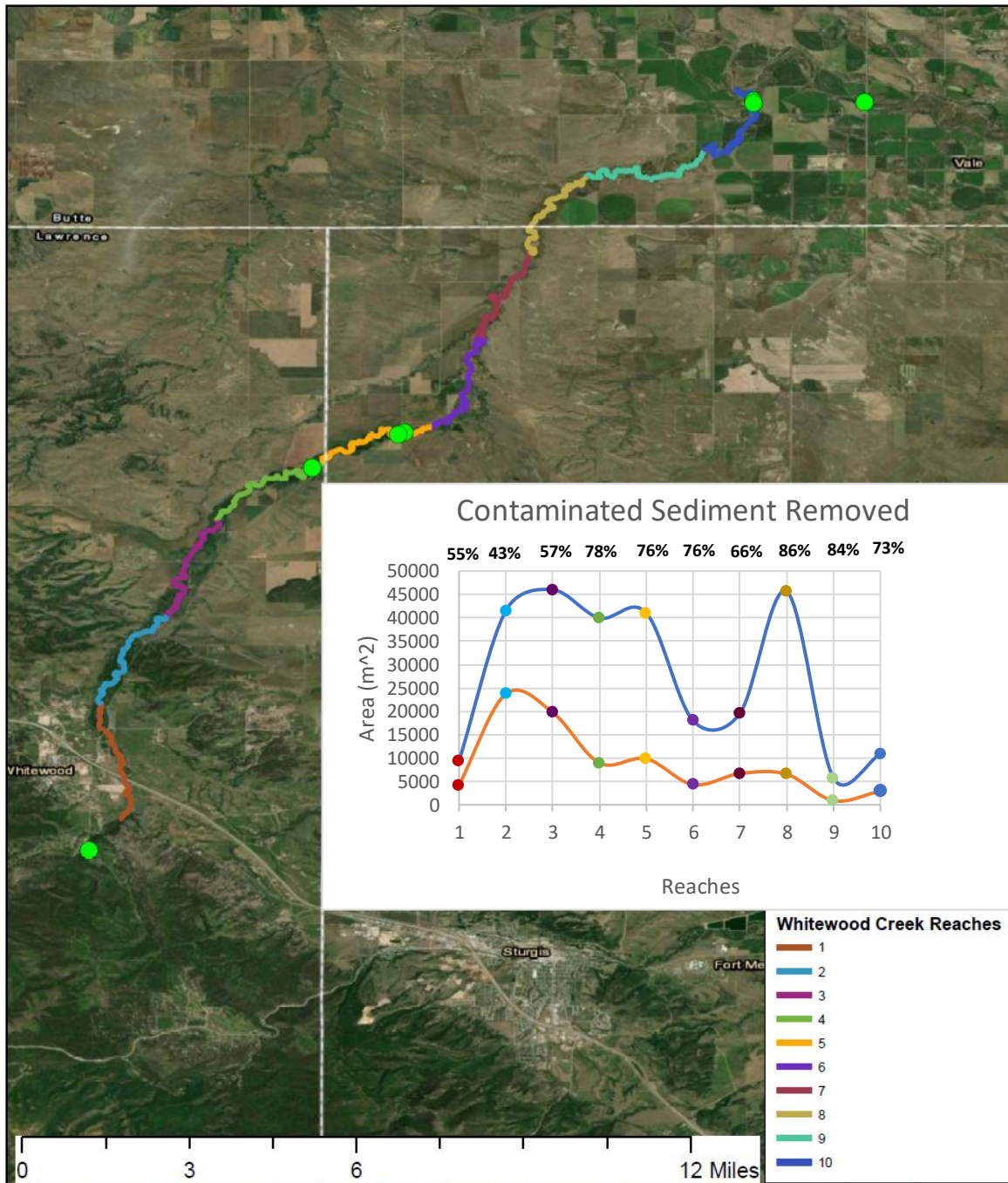


Figure 6.6. Contaminated sediment removed area at Whitewood Creek reaches. Blue line represents the 1948 to 2012 contaminated sediment removal period and orange line is for 1977 to 2012 contaminated sediment removal period. Percentages are the difference between the larger value and smaller value divided by the larger value for each respective reach.

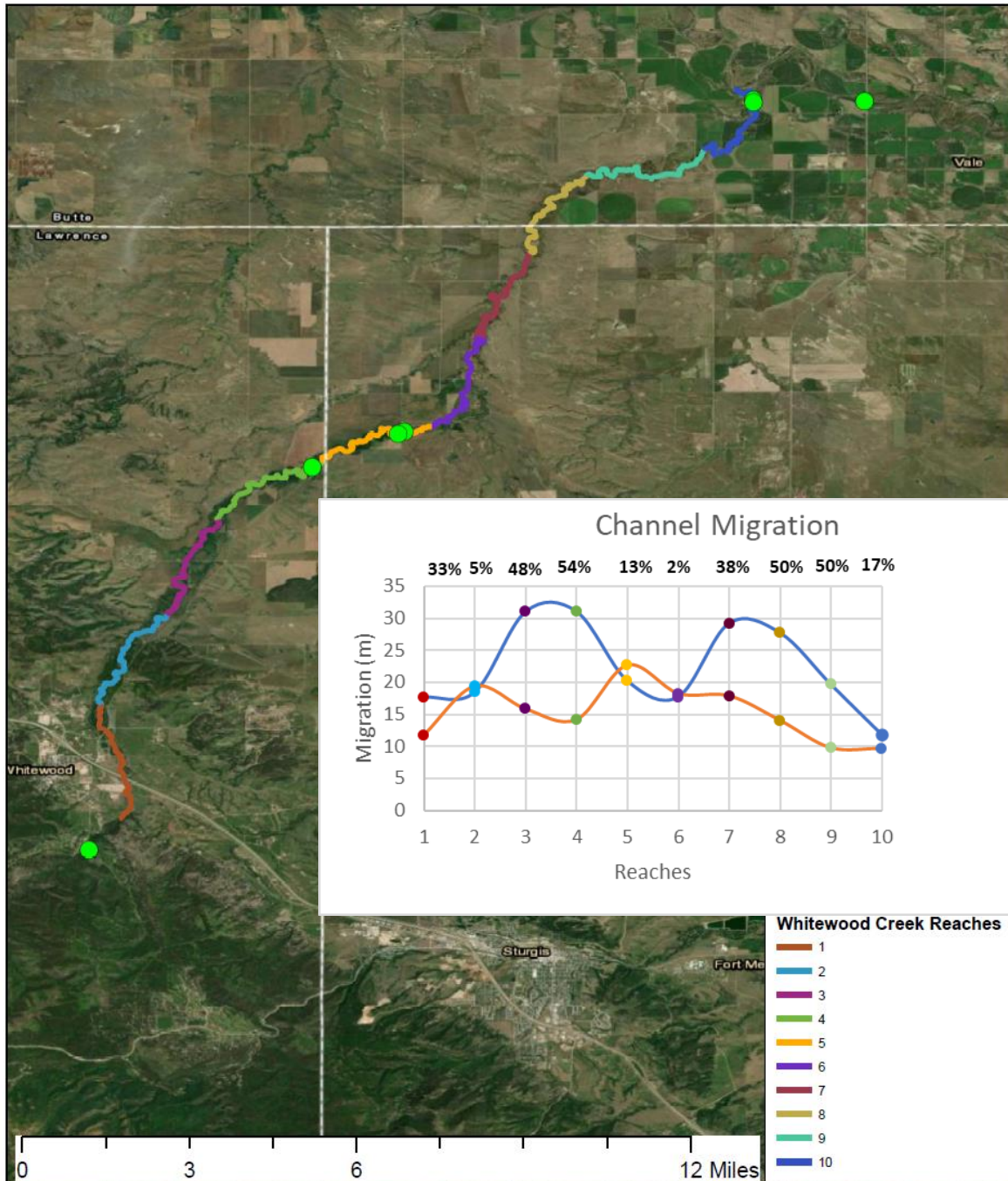


Figure 6.7. Result plot from GIS method of the channel migration at Whitewood Creek reaches. Blue line represents the 1948 to 2012 channel migration and orange line is for 1977 to 2012. Percentages are the difference between the larger value and smaller value divided by the larger value for each respective reach.

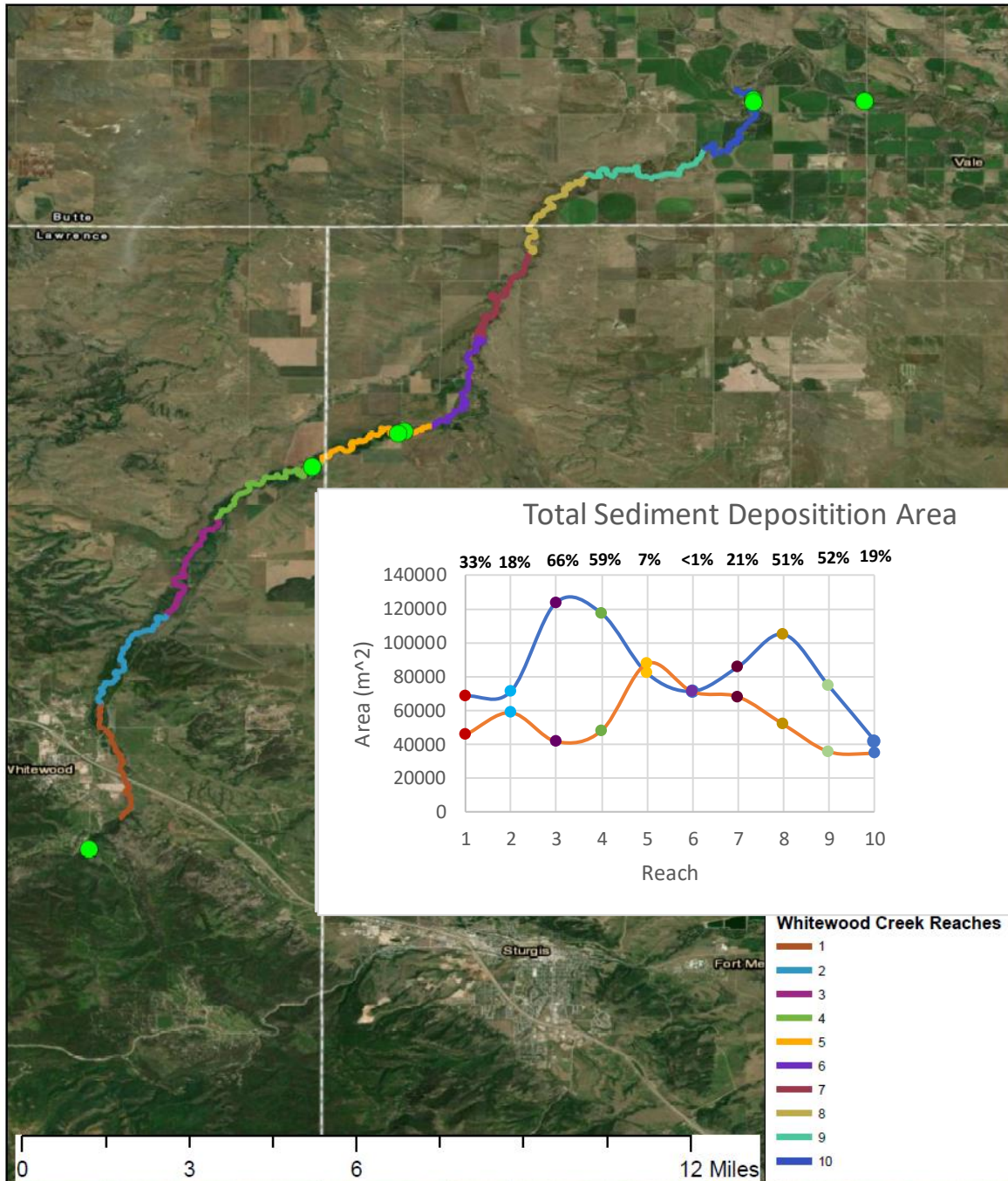


Figure 6.8. Result plot from GIS method of total sediment deposition area at Whitewood Creek reaches. Blue line represents the 1948 to 2012 total sediment gained area and orange line is for 1977 to 2012. Percentages are the difference between the larger value and smaller value divided by the larger value for each respective reach.

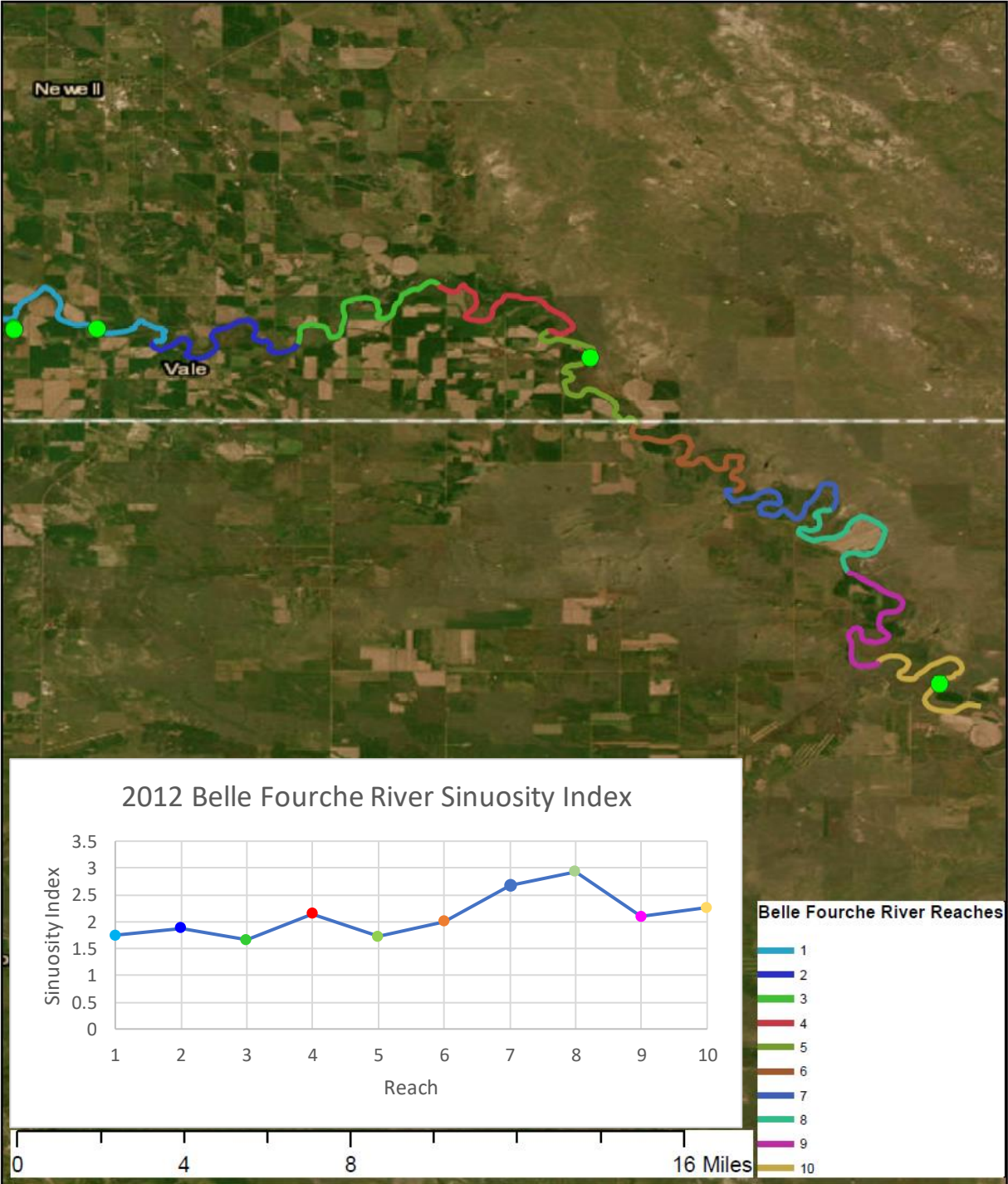


Figure 6.9. Sinuosity index for each reach at Belle Fourche River using the 2012 channel.

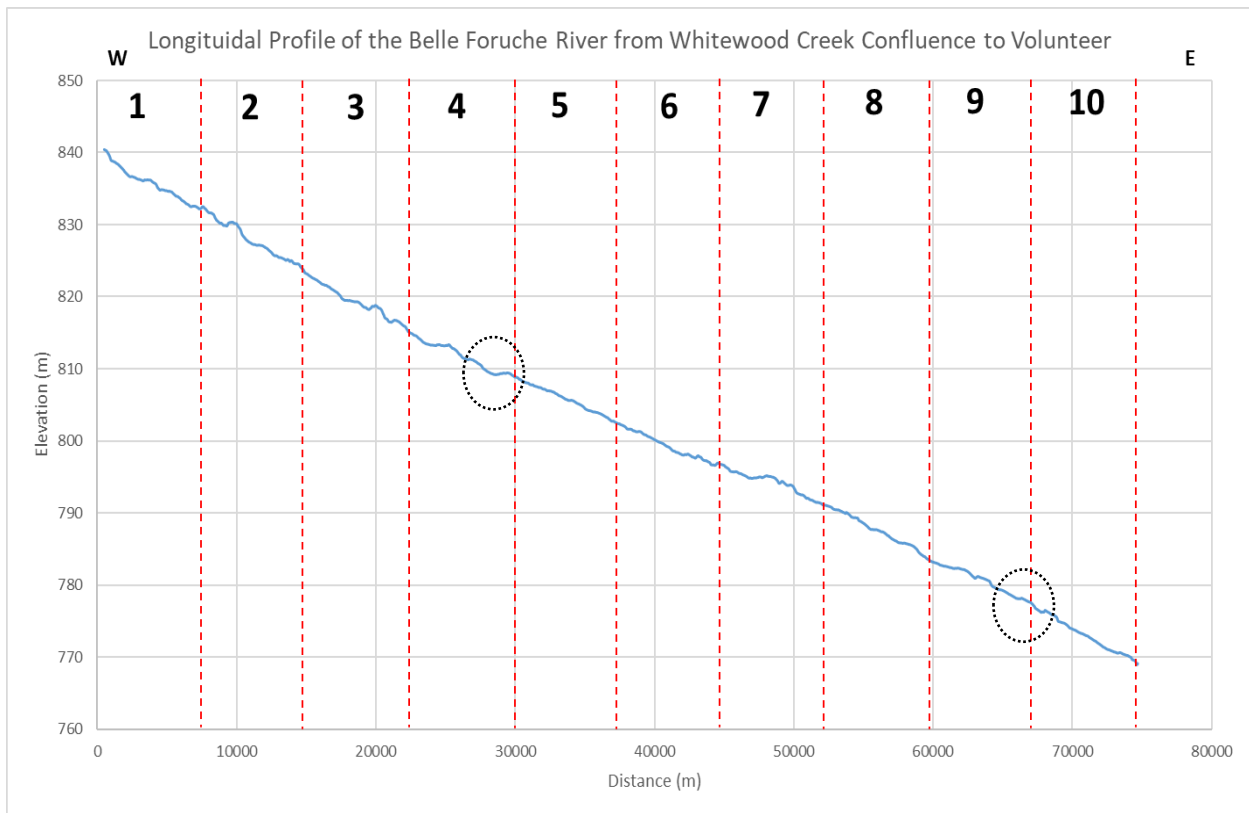


Figure 6.10. Longitudinal Profile of Belle Fourche River from the Whitewood Creek confluence to the village of Volunteer. Moving average was used to smooth graph. About 11222 points were averaged in the moving average. Between the two black circles is the approximate location of the discontinuity from neotectonics discussed by Gomez and Marron (1991).

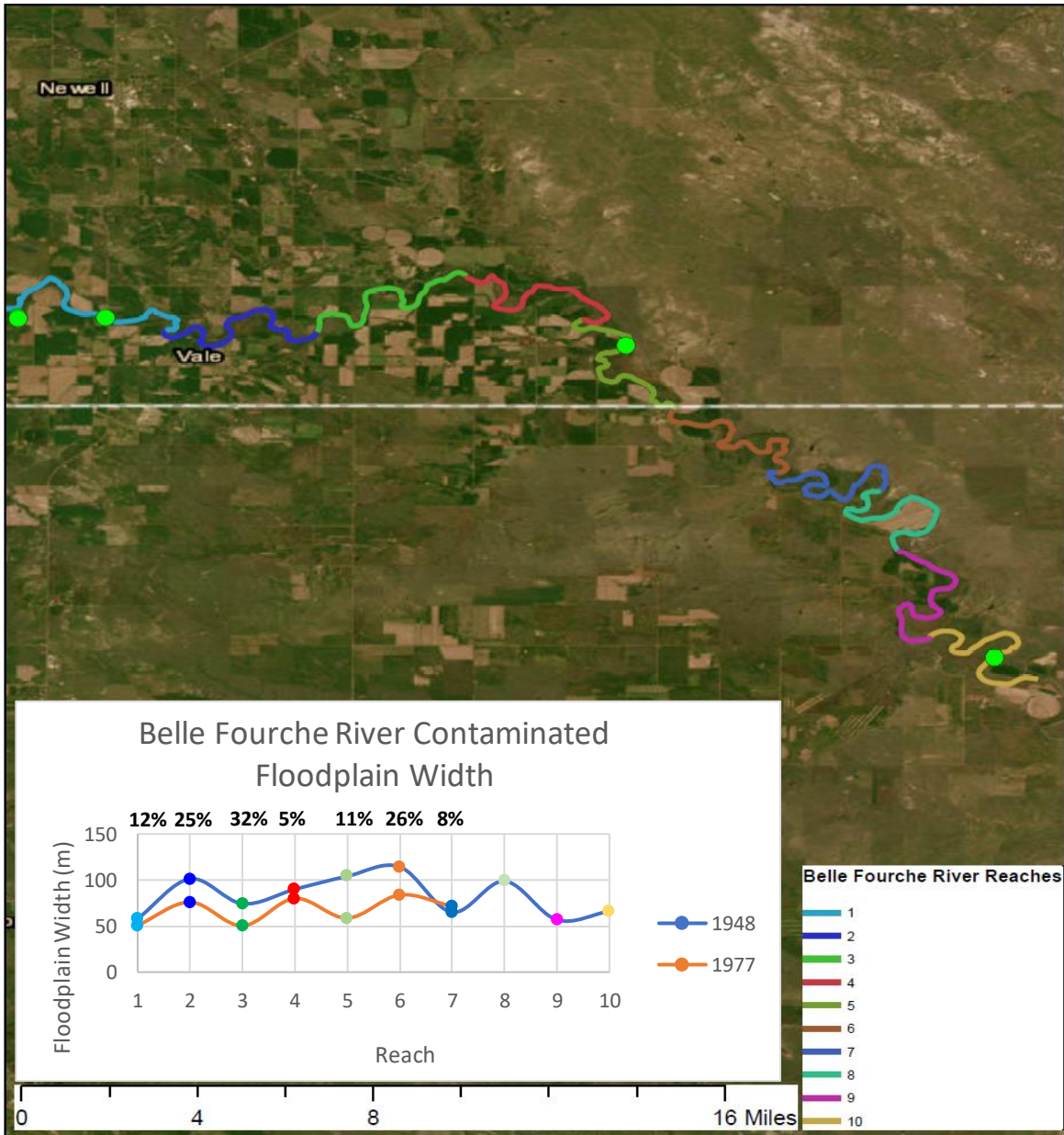


Figure 6.11. Contaminated floodplain widths at Belle Fourche River reaches. Blue line represents the 1948 contaminated sediment and orange line is for 1977. Percentages are the difference between the larger value and smaller value divided by the larger value for each respective reach.

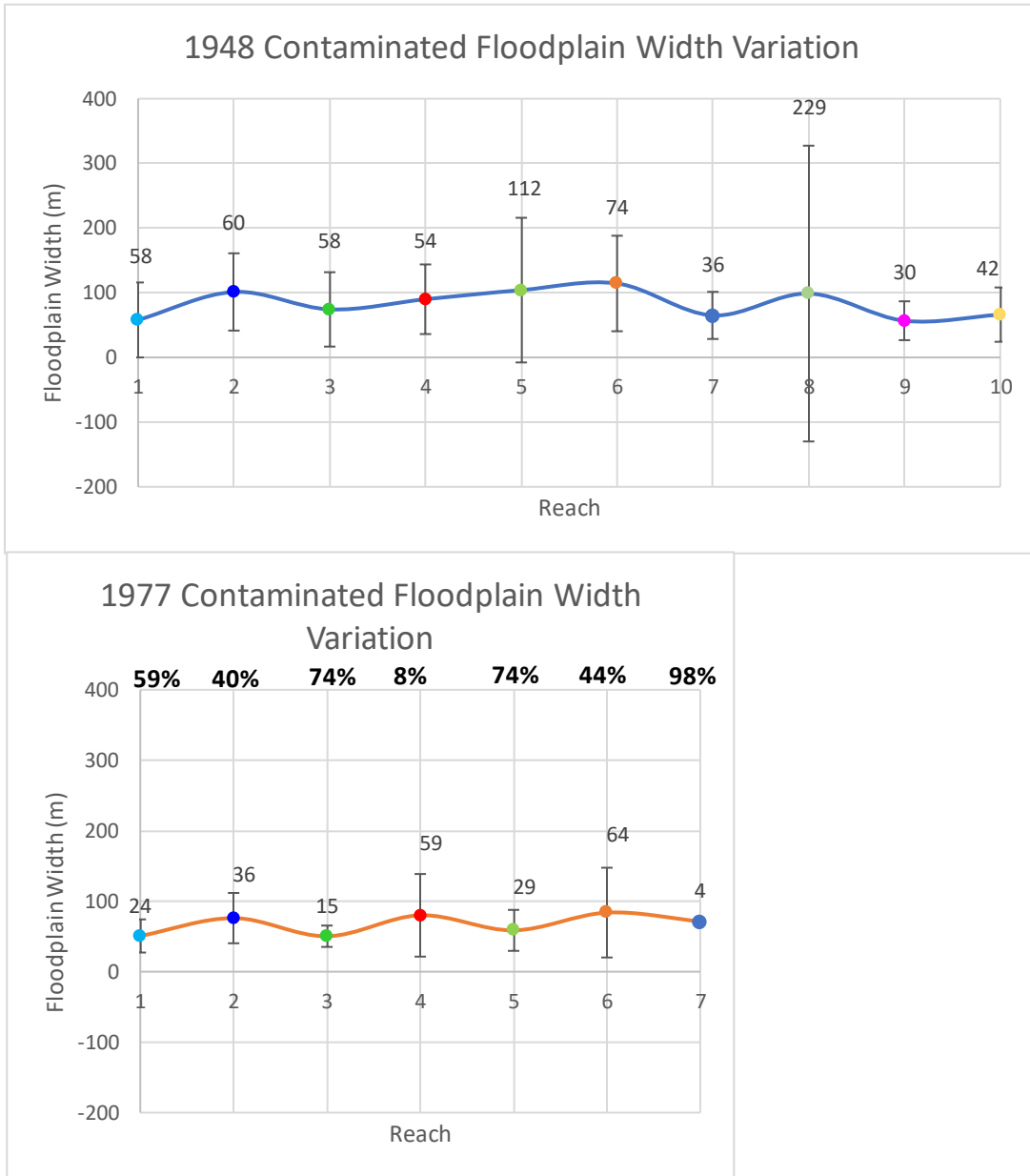


Figure 6.12. Contaminated floodplain widths and their variation (standard deviation) at Belle Fourche River reaches. Percentages are the difference between the larger value and smaller value of the standard deviation divided by the larger value for each respective reach.

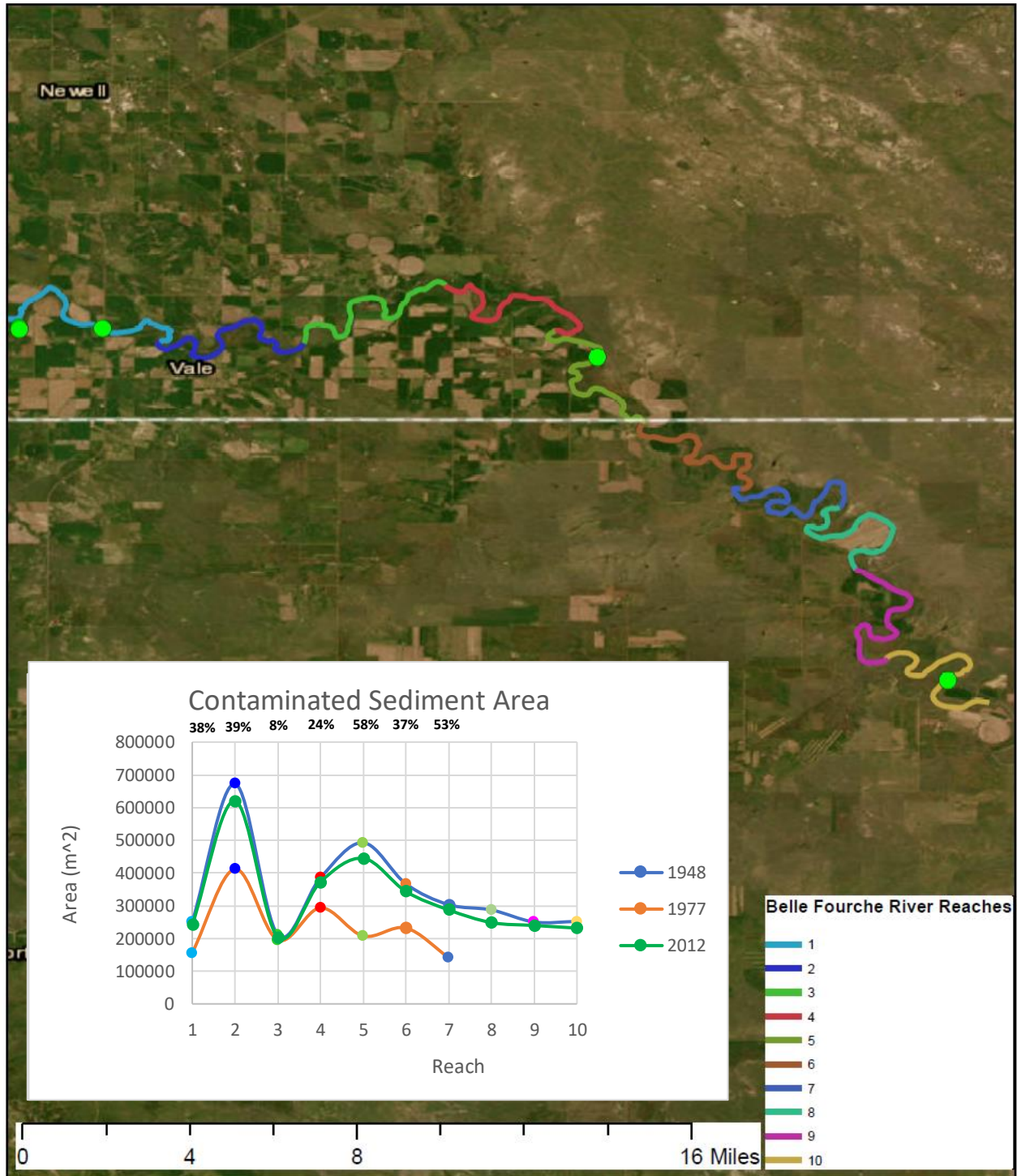


Figure 6.13. Result plot from GIS method of the distribution of contaminated sediment area and Belle Fourche reaches. Blue line represents the 1948 contaminated sediment and orange line is for 1977. Percentages are the difference between the larger value and smaller value divided by the larger value for each respective reach.

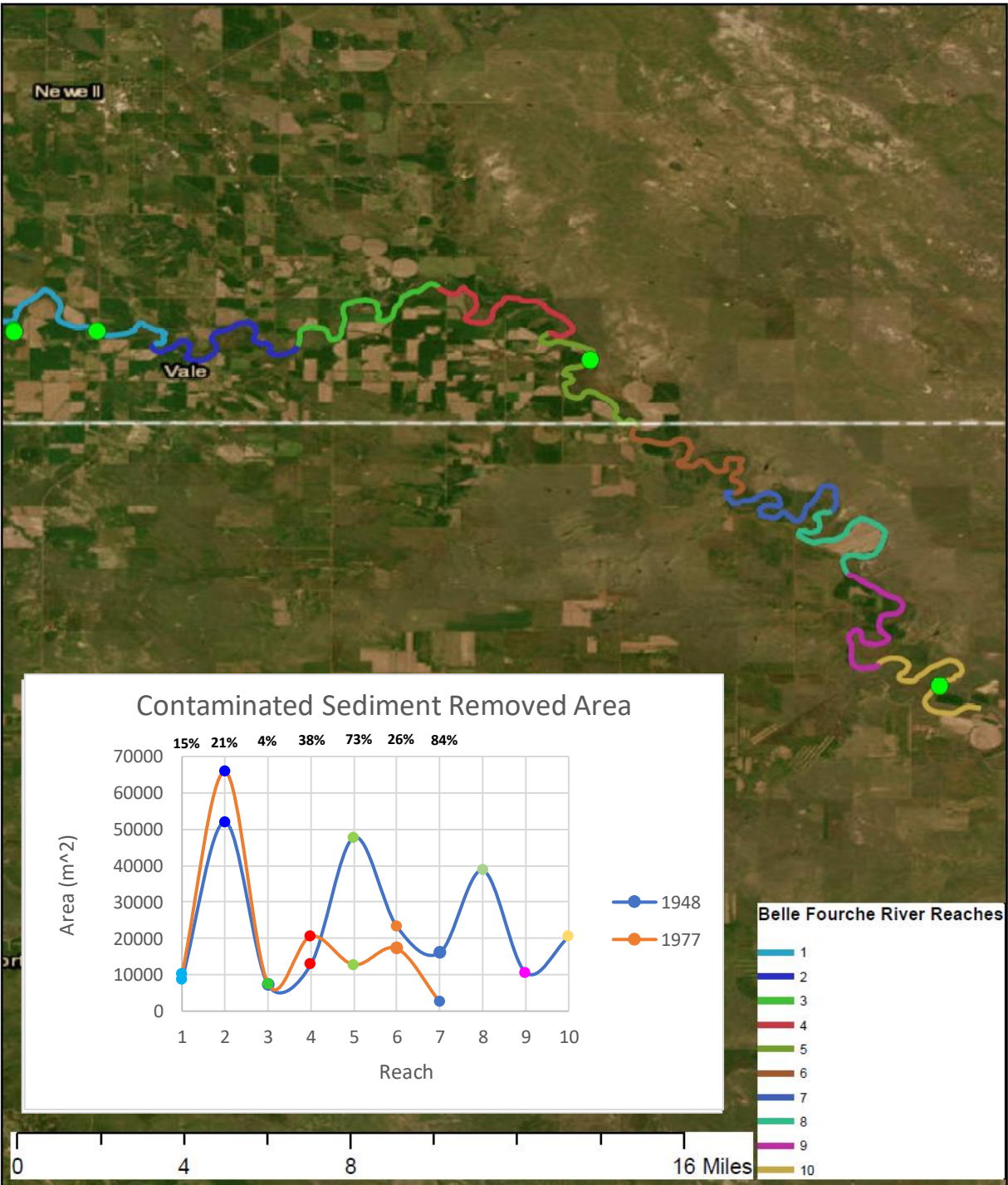


Figure 6.14. Result plot from GIS method of the contaminated sediment removed area at Belle Fourche River reaches. Blue line represents the 1948 to 2012 contaminated sediment and orange line is for 1977 to 2012. Percentages are the difference between the larger value and smaller value divided by the larger value for each respective reach.

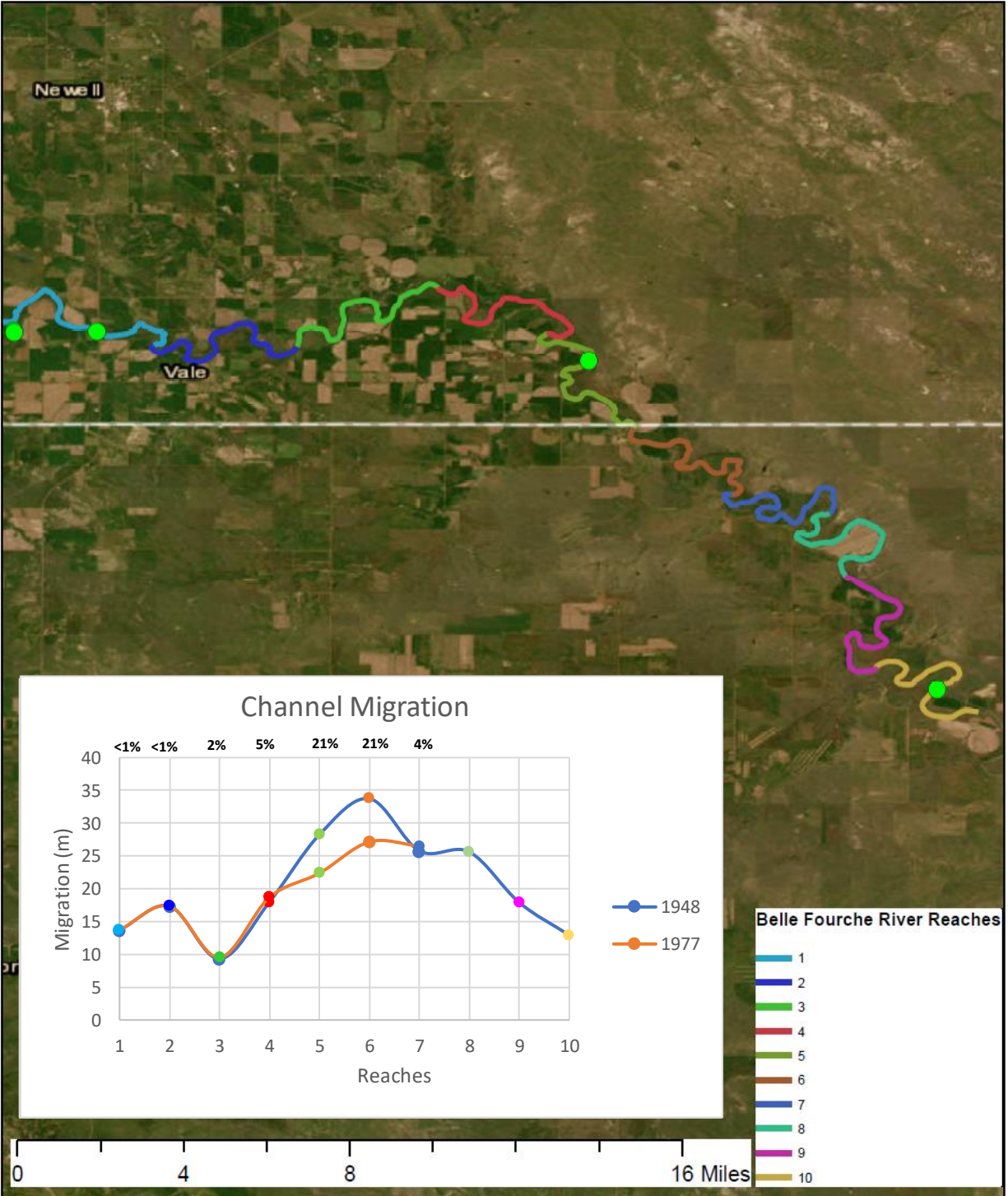


Figure 6.15. Result plot from GIS method of channel migration at Belle Fourche River reaches. Blue line represents the 1948 to 2012 contaminated sediment and orange line is for 1977 to 2012. Percentages are the difference between the larger value and smaller value divided by the larger value for each respective reach.

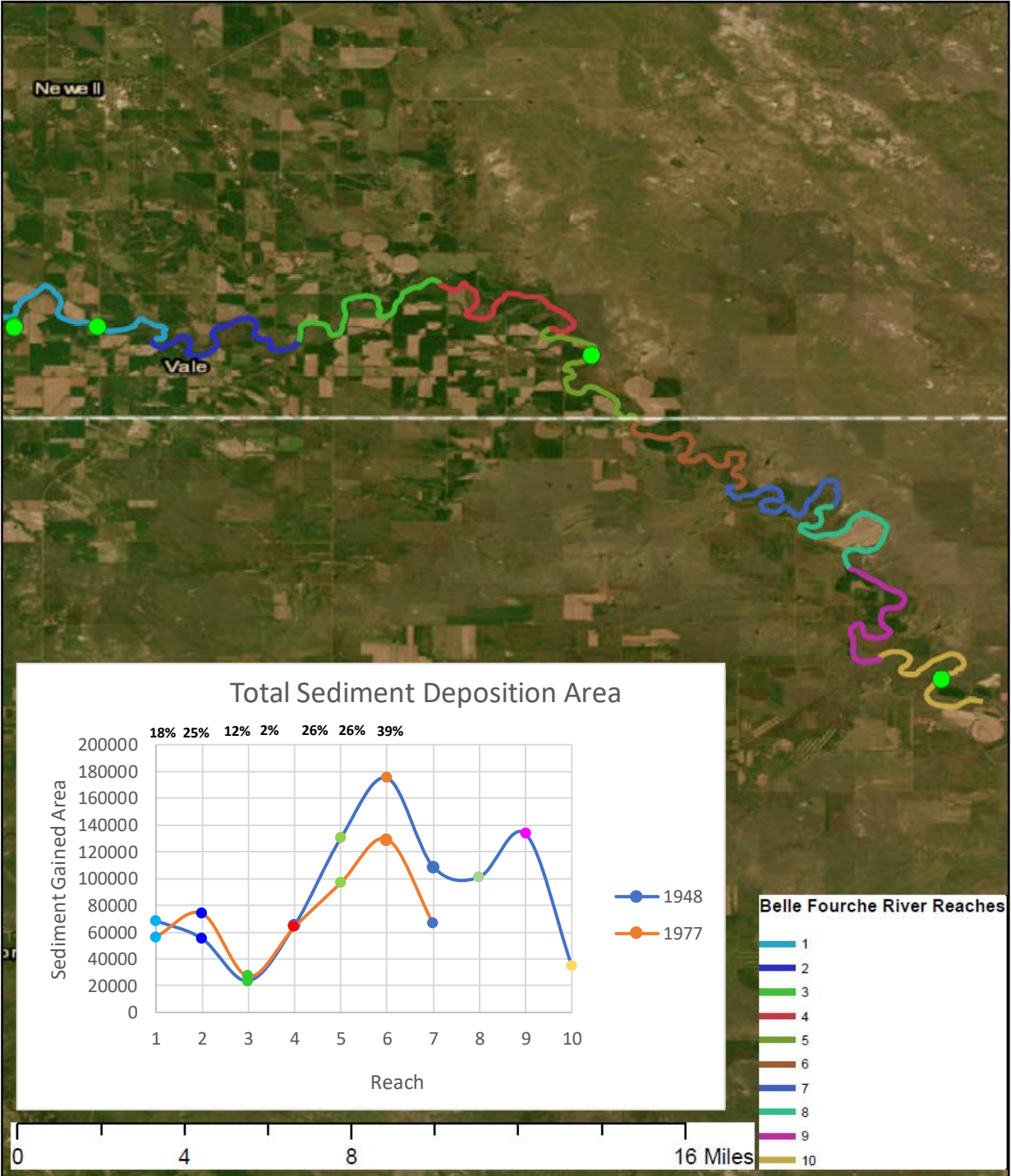


Figure 6.16. Total sediment deposition area at Belle Fourche River reaches. Blue line represents the 1948 to 2012 contaminated sediment and orange line is for 1977 to 2012. Percentages are the difference between the larger value and smaller value divided by the larger value between the two years for each respective reach.

Chapter 8. – Figures

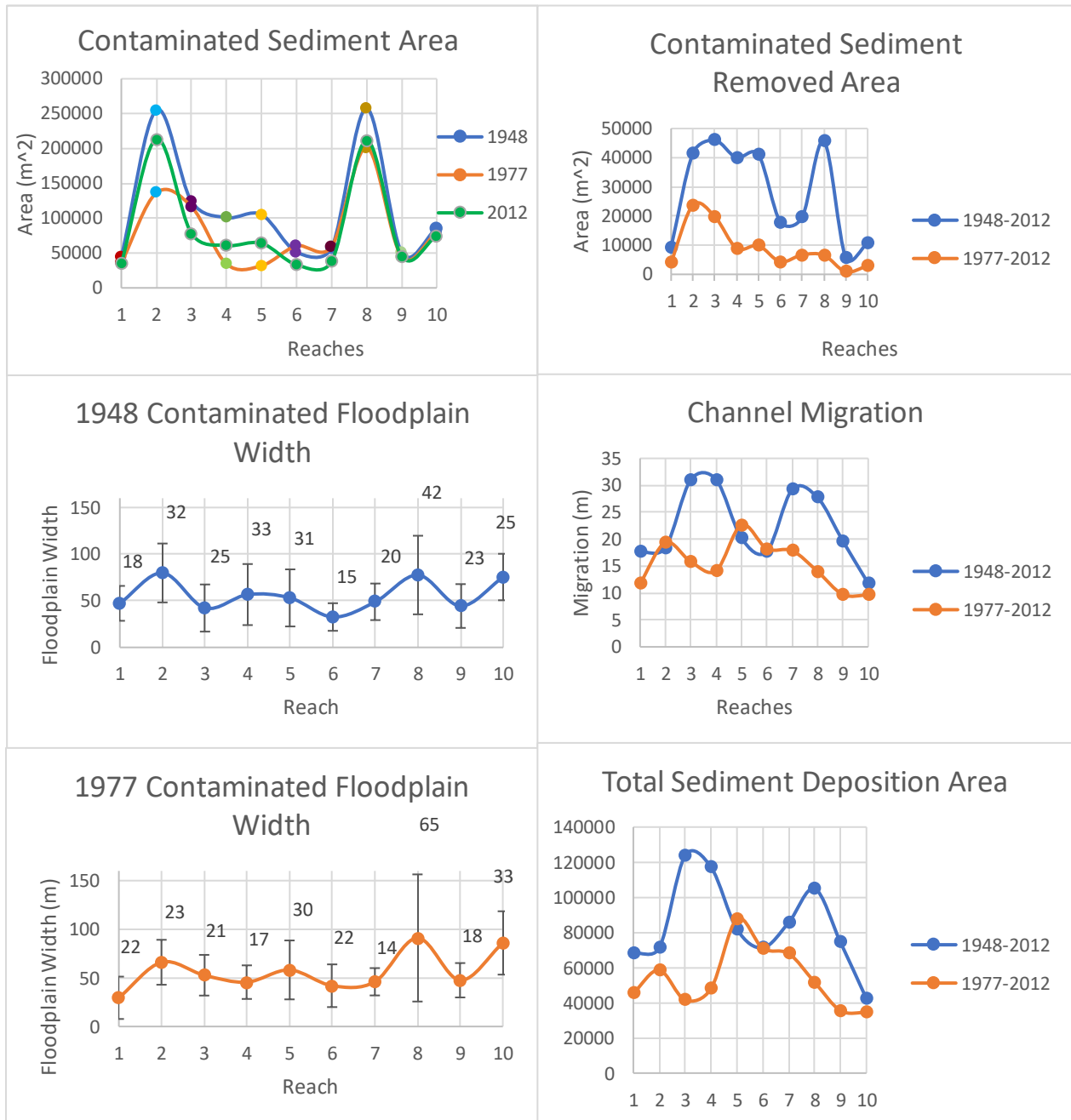


Figure 8.1. Comparison of different parameters plots in Whitewood Creek. Note, on the contaminated floodplain width plots, the error bars with overlaying numbers are standard deviations (variation) of the floodplain widths. See Figure 4.2 for location of each reach in Whitewood Creek.

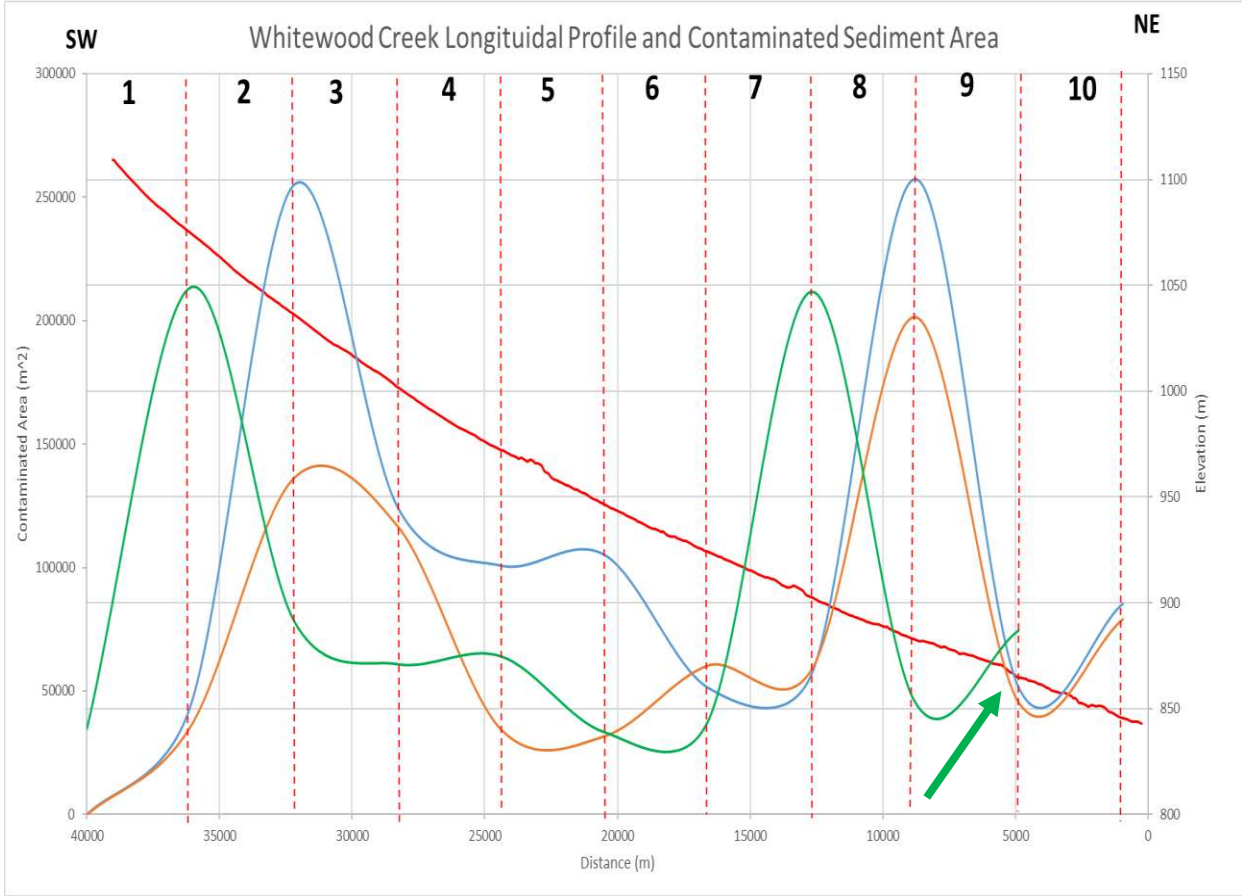


Figure 8.2. Comparison of Whitewood Creek’s contaminated sediment area and longitudinal profile. The blue line is the 1948 contaminated sediment area, orange line is 1977 contaminated sediment area, green line is 2012 contaminated area, red line is Whitewood Creek’s stream profile, and the green arrow is pointing towards a potential knickzone (Farmington front) described by Zaprowski et al. (2001).

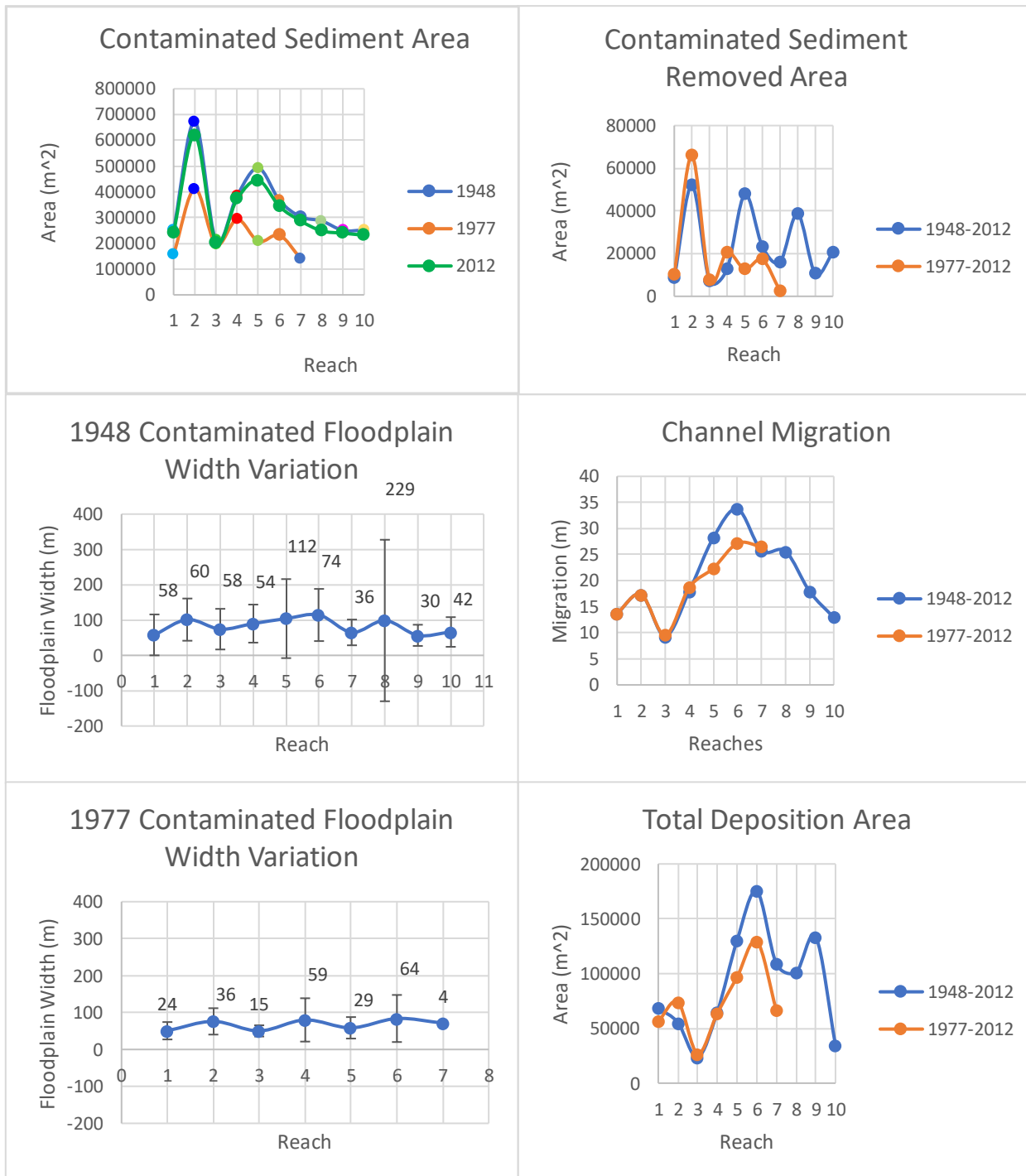


Figure 8.3. Comparison of different parameters plots in Belle Fourche River. Note, on the contaminated floodplain width plots, the error bars with overlaying numbers are standard deviations (variation) of the floodplain widths. See Figure 4.3 for location of each reach in Belle Fourche River.

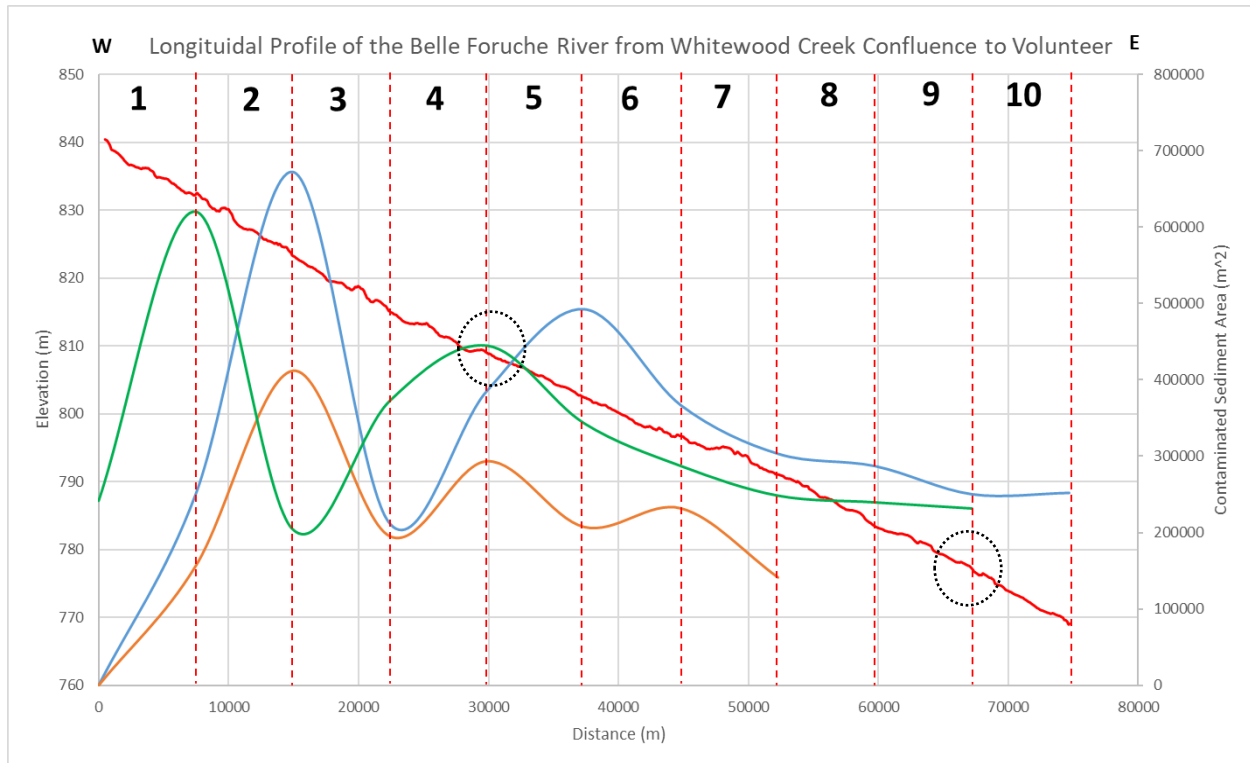


Figure 8.4. Comparison of Belle Fourche River’s contaminated sediment area and longitudinal profile. Blue line is 1948 contaminated sediment area, orange line is 1977 contaminated sediment area, green line is 2012 contaminated sediment area and red line is Belle Fourche River’s longitudinal profile. Between the two black circles is the approximate location of the channel discontinuity caused by neotectonics discussed by Gomez and Marron (1991).

REFERENCES

- Adler, L. L., 1980, Adjustment of the Yuba River, California, to the influx of hydraulic mining debris, 1849-1979: M. A. thesis, Department of Geography, University of California, Los Angeles, CA, p. 180.
- Alexandratos, V.G., Elzinga, E.J., and Reeder, R.J., 2007, Arsenate uptake by calcite: Macroscopic and spectroscopic characterization of adsorption and incorporation mechanisms: *Geochimica et Cosmochimica Acta*, v. 71 (17), p. 4172-4187.
- Antelo, J., Arce, F., and Fiol, S., 2015, Arsenate and phosphate adsorption on ferrihydrite nanoparticles. Synergetic interaction with calcium ions: *Chemical Geology*, v. 410, p. 53-62.
- Appelo, C.A.J., Van der Weiden, M.J.J., Tournassat, C., and Charlet, L., 2002, Surface complexation of ferrous iron and carbonate on ferrihydrite and the mobilization of arsenic: *Environmental Science and Technology*, v. 36: p. 3096-3103.
- Belmont, Patrick, 2011, Floodplain width adjustments in response to rapid base level fall and knickpoint migration: *Geomorphology*, v. 128, p. 92-102.
- Benito, G., Benito-Calvo, A., Gallart, F., Martín-Vide, J.P., Regüs, and D., Bladé E., 2001, Hydrological and geomorphological criteria to evaluate the dispersion risk of waste sludge generated by the Aznalcóllar mine spill (SW Spain): *Environmental Geology*, v. 40, p. 417-428.
- Bethke, C.M., Farrell, B., and Yeakel, S., 2021, *GWB essentials guide: Illinois*, Champaign Aqueous Solutions, LLC, 238 p.

- Bethke, C.M., 1996, *Geochemical reaction modeling: Concepts and applications*: New York, Oxford, Oxford University Press, 397 p.
- Bergeland, M.E., Ruth, G.R., Stack, R.L., and Emerick, R.J., 1976, Arsenic toxicosis in cattle associated with soil and water contamination from mining operations: South Dakota State University: *Agricultural Experiment Station Journal*, v. 1461, p. 6.
- Boano, F., Harvey, J. W., Marion, A., Packman, A. I., Revelli, R., Ridolfi, L., and Wörman, A., 2014, Hyporheic flow and transport processes: Mechanisms, models, and biogeochemical implications: *Rev. Geophys.*, v. 52, p. 603–679.
- Borch, T., Masue, Y., Kukkadapu, R.K., Fendorf, S., 2007, Phosphate imposed limitations on biological reduction and alteration of Ferrihydrite: *Environmental Science and Technology*, v. 41, p. 166-172.
- Bothe, J.V., and Brown, P.W., 1999, Arsenic immobilization by calcium arsenate formation: *Environ. Sci. Technol*, v. 33, p. 3806-3811.
- Bowell R.J., and Parshley J., 2001, Arsenic cycling in the mining environment. Characterization of waste, chemistry, and treatment and disposal, proceedings and summary report on U.S. EPA workshop on managing arsenic risks to the environment, May 1–3, Denver, Colorado, USA.
- Cherry, J.A., Morel, F.M.M, Rouse, J.V., Schnoor, J.L., and Wolman, M.G., 1986, Hydrochemistry of sulfide and arsenic-rich tailings and alluvium along Whitewood Creek, South Dakota: Colorado School of Mines, *Mineral and Energy Resources*, v. 29; no. 4, 5, 6.

- Chukhlantsev, V.G., 1956, The solubility products of a number of arsenates: *J Inorg Chem Russian*, v. 1, p. 1975–1982 in Russian.
- Cox, C.D., and Ghosh, M.M., 1994, Surface complexation of methylated arsenates by hydrous oxides: *Water Res.* v. 28, p. 1181–1188.
- Darton, N.H., 1951, Geologic Map of South Dakota: U.S. Geological Survey, scale: 1:500,000.
- Darton, N.H., 1919, Description of the Newell Quadrangle, South Dakota: *Geological Atlas*, Newell folio, v. 209, 7 p.
- Darton, N.H., 1909, Geology and Water Resources of the Northern Portion of the Black Hills and Adjoining Regions in South Dakota and Wyoming: U.S. Geological Survey Professional Paper 65, Reston, VA, 105 p.
- DeVore, C.L., Rodriguez-Freire, L., Villa, N., Soleimanifar, M., Gonzalez-Estrella, J., Ali, A.M.S., Lezama-Pacheco, J., Ducheneaux, C., and Cerrato, J.M., 2022, Mobilization of As, Fe, and Mn from contaminated sediment in aerobic and anaerobic conditions: chemical and microbial triggers?: *ACS Earth and Space Chemistry*, v. 6, p. 1644-1654.
- DeVore, C.L., Hayek, E.E., Busch, T., Long, B., Mann, M., Rudgers, J.A., Ali, A-S, S., Howard, T., Spilde, M.N., Brearly, A., Ducheneaux, C., and Cerrato, J.M., 2021, Arsenic accumulation in hydroponically grown *Schizachyrium scoparium* (Little Bluestem) amended with root-colonizing endophytes: *ACS Earth and Space Chemistry*, v. 5 (6), p. 1278-1287.

- DeVore, C.L., Rodriguez-Freire, L., Mehdi-Ali, A., Ducheneaux, C., Artyushkova, K., Zhou, Z., Latta, D.E., Lueth, V.W., Gonzales, M., Lewis, J., and Cerrato, J.M., 2019, Effect of bicarbonate and phosphate on arsenic release from mining-impacted sediments in the Cheyenne River watershed, South Dakota, USA: *Environ. Sci.: Processes Impacts*, v. 21, p. 456-468.
- Drahota, P., and Filippi, M., 2009, Secondary arsenic minerals in the environment: A review: *Environment International*, v. 35, p. 1243-1255.
- Driscoll, D.G., Carter, J.M., Williamson, J.E., and Putnam, L.D., Hydrology of the Black Hills area, South Dakota: U.S. Geological Survey Water Resources Investigation Report 02-4094.
- Dzombak, D.A. and Morel, F.M.M. 1990. Surface Complexation Modeling – Hydrous 17 Ferric Oxide: John Wiley & Sons, New York.
- Environmental Protection Agency (EPA), 2017, Fourth five year review report for Whitewood Creek Superfund Site Lawrence, Meade and Butte Counties, South Dakota: (<https://semspub.epa.gov/work/08/100001404.pdf>)
- Environmental Protection Agency (EPA), 2012, Third five year review report for Whitewood Creek Superfund Site Lawrence, Meade and Butte Counties, South Dakota: (<https://semspub.epa.gov/work/08/1239648.pdf>)
- Environmental Protection Agency (EPA), 1972, Remote Sensing Study, Whitewood Creek/ Belle Fourche River, South Dakota: Division of Field Investigations-Denver Center.

- Fagan, B.A., and Lisenbee, A.L., 2017, Geologic map of the Sturgis quadrangle, South Dakota: South Dakota Department of Environment and Natural Resources, scale 1:24,000 (http://www.sdgs.usd.edu/pubs/pdf/GQ24K-27_2017.pdf).
- Faure, G., 1998, Principles and applications of geochemistry, 2nd edition: Pearson, Upper Saddle River, New Jersey, 600 p.
- Fendorf, S., Nico, P.S., Kocar, B.D., Masue, Y., Tufano, K.J., 2010, Chapter 12 – Arsenic Chemistry in Soils and Sediments, v. 34, p. 357-378.
- Fernández-Martínez, A., Román-Ross, G., Guello, G.J., Turrillas, X., Charlet, L., Johnson, M.R., and Bardelli, F., 2006, Arsenic uptake by gypsum and calcite: Modelling and probing by neutron and X-ray scattering: *Phys. B Condens. Matter*, v. 385–386, p. 935-937.
- Fernández-Martínez, A., Guello, G.J., Johnson, M.R., Bardelli, F., Román-Ross, G., Charlet, L., and Turrillas, X., 2008, Arsenate incorporation in gypsum probed by neutron, X-ray scattering and density functional theory modeling: *J. Phys. Chem. A*, v. 112, p. 5159-5166.
- Fox Consultants, Inc. 1984a, Whitewood Creek Study, Phase I. Prepared for the South Dakota Department of Water and Natural Resources Office of Air Quality and Solid Waste. April 16, 1984.
- Fox Consultants, Inc. 1984b, Whitewood Creek Study, Phase II. Prepared for the South Dakota Department of Water and Natural Resources Office of Air Quality and Solid Waste, Homestake Mining Company and the United States Environmental Protection Agency. November 1984.

- Frau, F., and Ardaù, C., 2004, Mineralogical controls on arsenic mobility in the Baccu Locci stream catchment Sardinia, Italy affected by past mining: *Mineral Mag*, v. 68 p. 15–30.
- Fuller, C.C., and Davis, J.A., 2003, Section II: Evaluation of the processes controlling dissolved arsenic in Whitewood Creek, South Dakota: In “Toxic substances in surface waters and sediments—a study to assess the effects of arsenic-contaminated alluvial sediment in Whitewood Creek, South Dakota.” U.S. Geological Survey Professional Paper 1681
- Fuller, C.C., Davis, J.A., Waychunas, G.A., 1993, Surface chemistry of ferrihydrite: Part 2. Kinetics of arsenate adsorption and coprecipitation: *Geochimica et Cosmochimica Acta*, v. 57, p. 2271-2282.
- Fuller C.C., Davis, J.A., and Claypool-Frey, R.G., 1987, Partitioning of arsenic by iron oxides in Whitewood Creek, South Dakota: in Mallard, G.E., ed., U.S. Geological Survey Toxic Substances Hydrology Program: Surface-Water Contamination: Proceedings of the technical meeting, Denver, Colorado, February 2-4, 1987: U.S. Geological Survey Open File Report 87-764, p. 19-21.
- Gao, X., Wang, T., Hu, Q., and Su, C., 2011, Effects of anion competitive adsorption on arsenic enrichment in groundwater: *Journal of Environmental Science and Health Part*, v. 46, p. 1-9.
- Gilbert, G. K., 1917, Hydraulic-mining debris in the Sierra Nevada, U.S. Geological Survey Professional Paper, v. 105, 154 p.

- Ghosh, M.M., and Teoh, R.S., 1985, Adsorption of arsenic on hydrous aluminum oxide: Proceedings of Seventh Mid-Atlantic Industrial Waste Conference, p. 139-155.
- Goddard, K.E., 1990, U.S. Geological Survey applied research studies of the Cheyenne River system, South Dakota: Description and collation of data, Water years 1987-88: U.S. Geological Survey Open-File Report 89-580.
- Goddard, K.E., 1989, Composition, distribution, and hydrologic effects of contaminated sediments resulting from the discharge of gold milling wastes to Whitewood Creek at Lead and Deadwood, South Dakota: U.S. Geological Survey Water-Resources Investigations Report 87-4051.
- Goddard, K.E., 1988a, Gold-Mill-Tailings contamination of the Cheyenne River System, western South Dakota: U.S. Geological Society Toxic Substance Hydrology Program-Surface Water Contamination Report 87-764.
- Goddard, K.E., 1988b, U.S. Geological Survey applied research studies of the Cheyenne River system, South Dakota: Description and collation of data, Water years 1985-86: U.S. Geological Survey Open-File Report 88-484.
- Goddard, K.E. and Wuolo, R.W., 1987. Processes controlling the concentration of dissolved arsenic in Whitewood Creek, South Dakota: in Mallard, G.E., ed., U.S. Geological Survey Toxic Substances Hydrology Program: Surface-Water Contamination: Proceedings of the technical meeting, Denver, Colorado, February 2-4, 1987: U.S. Geological Survey Open File Report 87-764, p. 23-25.
- Goddard, K.E., 1987, Chapter A: Gold-mill-tailings contamination of the Cheyenne River System, Western South Dakota: in Mallard, G.E., ed., U.S. Geological Survey Toxic

Substances Hydrology Program Program-- Surface-Water Contamination:

Proceedings of the Technical Meeting, Denver, Colorado, February 2-4, 1987, Open-File Report 87-764.

Goldberg, S., 2002, Competitive adsorption of arsenate and arsenite on oxides and clay minerals:

Soil Sci. Soc. Am. J., v. 66, p. 413–421.

Goldberg, S., and Glaubig, R.A., 1988, Anion sorption on a calcareous, montmorillonitic soil –

arsenic: *Soil Sci. Soc. Am. J.*, v. 52, p. 1297-1300.

Gomez, B., and Marron, D.C., 1991, Neotectonic effects on sinuosity and channel migration,

Belle Fourche River, Western South Dakota: *Earth Surface Processes and*

Landforms, v. 16, p. 227-235.

Goudie, A.S., 2006, Global warming and fluvial geomorphology: L.A James, W.A. Marcus

(Eds.), *The Human Role in Changing Fluvial Systems*, v. 79, Elsevier (2006), p. 384-394.

Haffert L., and Craw D., 2008, Mineralogical controls on environmental mobility of arsenic from

historic mine processing residues, New Zealand: *Appl Geochem*, v. 23, p. 467-1483.

Hazelwood, K.T., and Stetler, L.D., 2019, New insights into the fluvial geomorphology and its

effects on paleofloods in the Black Hills, South Dakota: *Geomorphology*, v. 327, p.

80-92.

Hoagstrom, C.W., 2006, Fish Community Assembly in the Missouri River Basin: Ph.D.

Dissertation, South Dakota State University, Brookings, SD, 364 p.

Homestake Gold Mine, 1976, 1876 Homestake Centennial 1976, Homestake Mining Company, Lead, South Dakota.

Horowitz, A.J., and Elrick, K.A., 1988, Interpretation of bed sediment trace metal data: Methods of dealing with grain size effect: In: Lichtenberg J.J., Winter, J.A., Weber, C.C., Fradkin L., (eds) O Chemical and biological characterization of sludges, sediments, dredge spoils, and drilling mids. American Society for Testing and Materials, p. 114-128.

Horowitz, A.J., Kent, A.E., and Callender, E., 1988, The effect of mining on the sediment-trace element geochemistry of cores from the Cheyenne River arm of Lake Oahe, South Dakota, U.S.A.: *Chemical Geology*, v. 67, p.17-33.

Horowitz, and A.J., Kent, A.E., 1990, Arsenopyrite in the bank deposits of Whitewood Creek-Belle Fourche-Cheyenne River-Lake Oahe system, South Dakota, U.S.A.: *The Science of the Total Environment*, v. 97/98, p. 219-233.

Hortness, J.E., and Driscoll, D.G., 1998, Streamflow losses in the Black Hills of western South Dakota: U.S. Geological Survey Water-Resources Investigations Report 98-4116.

House, W.A., and Donaldson, L., 1986, Adsorption and coprecipitation of phosphate on calcite: *J. Colloid Interface Sci.*, v. 112, p. 309-324.

Hudson-Edwards, K.A., 2003, Sources, mineralogy, chemistry and fate of heavy metal-bearing particles in mining-affected river systems: *Mineralogical Magazine*, v. 67 (2), p. 205-217.

- Hundal, H.S., Singh, K., and Singh, D., 2019, Geochemistry of manganese in neutral to alkaline of Punjab Northwest India and its availability to wheat and rice plants: *Communications in Soil Science and Plant Analysis*, v. 50, n. 5, p. 627–638.
- Jacks, G., 2017, Redox reaction in groundwater with health implications: IntechOpen, Redox (<http://dx.doi.org/10.5772/intechopen.68751>).
- Jain, A., and Loeppart, R.H., 2000, Effect of competing anions on the adsorption of arsenate and arsenite by ferrihydrite: *J. Environ. Qual*, v. 29, p. 1422-1430.
- James, A., 1999, Time and the persistence of alluvium: River engineering, fluvial geomorphology, and mining sediment in California: *Geomorphology*, v. 31, p. 265-290.
- James, L.A., and Davis, J.D., 1994, Glaciation and hydraulic gold-mining sediment in the Bear and South Yuba Rivers, Sierra Nevada Trip Guide: Assn. Amer. Geographers, S.F. Meeting. 113 p.
- James, L.A., 1989, Sustained storage and transport of hydraulic gold mining sediment in the Bear River, California: *Ann Assoc Am Geogr* v. 79 (4), p. 570–592.
- Ji, M., 2021, Characterization and prediction of long term arsenic mobility, dissolution, and kinetic behavior in arsenic contaminated floodplain deposits of Whitewood Creek and the Belle Fourche River, South Dakota: M.S. thesis, Department of Geosciences, Colorado State University, Fort Collins, CO, 303 p.

- Ji, A., and Ridley, J., 2013, Long-term arsenic mobility and behavior in a contaminated floodplain: Seventh International Conference on Remediation of Contaminated Sediments, Dallas, Texas, February 2013.
- Jeane, E., 1976, Trace element sorption by sediments and soils- site and processes: In. Chappell, W., Peterson, K., (eds) Symposium on molybdenum, v. 2, Marcel-Dekker, New York, p. 425-553.
- Kelsey, H. M., 1980, A sediment budget and an analysis of geomorphic process in the Van Duzen River basin, north coastal California 1941-1975: *Geological Society of America Bulletin*, v. 91-11, p. 119-1216.
- Kibria, K.N., Ahiablame, L., Hay, C., and Djira, G., 2016, Streamflow trends and responses to climate variability and land cover change in South Dakota: *Hydrology*, v. 3 (1), 20 p.
- Knighton, A.D., 1991, Channel bed adjustment along mine-affected rivers of northeast Tasmania: *Geomorphology*, v. 4, p. 205-219.
- Knowles, N., Dettinger, M.D., and Cayan, D.R., 2006, Trends in snowfall versus rainfall in the western United States: *Journal of Climate*, v. 19, p. 4545–4559.
- Kocar, B. D., Herbel, M. J., Tufano, K. J., Fendorf, S., 2006, Contrasting effects of dissimilatory iron(III) and arsenic(V) reduction on arsenic retention and transport: *Environmental Science and Technology*, v. 40, p. 6715-6721.
- Kuwabara, J.S., and Fuller, C.C., 2003, Toxic substances in surface waters and sediments-a study to assess the effects of arsenic-contaminated alluvial sediment in Whitewood Creek, South Dakota: U.S. Geological Survey Professional Paper 1681.

- Larios, R., Martinez, R.F., Alvarez, and Rucandio, R.I., 2012, Arsenic pollution and fractionation in sediments and mine waste samples from different mine sites: *Science of the Total Environment*, v. 431, p. 426-435.
- Legg, N.T., Heimburg, C., Collins, B.D., and Olson, P.L., 2014, The channel migration toolbox: ArcGIS® tools for measuring stream channel migration: State of Washington Department of Ecology Publication no. 14-06-032.
- Lewin, J., and Macklin, M.G., 1987 Metal mining and floodplain sedimentation in Britain: V. Gardiner (Ed.), *International Geomorphology 1986 Part 1*, Wiley, Chichester, p. 1009-1027.
- Lin, J., Chen, N., Nilges, M.J., and Pan, Y., 2013, Arsenic speciation in synthetic gypsum (CaSO₄·2H₂O): a synchrotron XAS, single-crystal EPR, and pulsed ENDOR study: *Geochim. Cosmochim. Acta*, v. 106, p. 524-540.
- Lin, Z., and Puls, R.W., 2000, Potential indicators for the assessment of arsenic attenuation in the subsurface: *Adv. Environ. Res.*, v.7, p. 825-834.
- Lisenbee, A.L., Redden, J. A., and Fahrenback, M.D., 2017, Geologic map of the Deadwood North quadrangle, South Dakota: South Dakota Department of Environment and Natural Resources, scale 1:24,000 (http://www.sdgs.usd.edu/pubs/pdf/GQ24K-24_2015.pdf).
- Lu, P., and Zhu, C., 2011, Arsenic Eh–pH diagrams at 25 °C and 1 bar: *Environ Earth Sci*, v. 62, p. 1673–1683.

- Ma, X., Yuan, Z., Gomez, M.A., Wang, X., Wang, S., Yao, S., and Jia, Y., 2017, A qualitative and quantitative investigation of partitioning and local structure of arsenate in barite lattice during coprecipitation of barium, sulfate, and arsenate: *American Mineralogist*, v. 102 (12), p. 2512–2520.
- Macklin, M.G., Brewer, P.A., Hudson-Edwards, K.A., Bird, G., Coulthard, T.J., Dennis, I.A., Lechler, P.J., Miller, J.R., and Turner, J.N., 2006, A geomorphological approach to the management of rivers contaminated by metal mining: *Geomorphology*, v. 79, p. 423-447.
- Macklin, M.G., Hudson-Edwards, K.A., Jamieson, H.E., Brewer, P., Coulthard, T.J., Howard, A.J., and Renenda, V.H., 1999, Physical stability and rehabilitation of sustainable aquatic and riparian ecosystems in the Río Guadiamar, Spain, following the Aznalcóllar mine tailings dam failure: Mine, Water and Environment, International Mine Water Association Congress, Seville, Spain, p. 271-278.
- Mallard, G.E., and Ragone, S.E., 1988, US Geological Survey Toxic Substances Hydrology Program—Proceedings of the technical meeting, Phoenix, Arizona, September 26-30: Water Resource Investigation Report 88-4220.
- Mallard, G.E., 1987, US Geological Survey Toxic Substances Hydrology Program--Surface Water Contamination: Proceedings of the technical meeting, Denver, Colorado, February 2-4, 1987: Open File Report 87-764.
- Manning, B.A., Fendorf, S., Bostick, B.C., and Suarez, D.L., 2002, Arsenic (III) oxidation and arsenic (V) adsorption reactions on synthetic birnessite: *Environmental Science and Technology*, v. 36, p. 976-981.

- Manning, B.A., and Goldberg, S., 1997, Adsorption and stability of arsenic(III) at the clay mineral-water interface: *Environ Sci Technol*, v. 31, p. 2005–2011.
- Matera, V., Le Hecho, I., Laboudigue, A., Thomas, P., Tellier, and S. Astruc, M., 2003, A methodological approach for the identification of arsenic bearing phases in polluted soils: *Environmental Pollution*, v. 126, p. 51-64.
- Marron, D. C., 1992, Floodplain storage of mine tailings in the Belle Fourche river system: A sediment budget approach: *Earth Surface Processes and Landforms*, v. 17 (7), p. 675–685.
- Marron, D.C., 1989, Physical and chemical characteristics of a metal-contaminated overbank deposit, west-central South Dakota, U.S.A: *Earth Surface Processes and Landforms*, v. 14, p. 419-432.
- Marron, D.C., 1987, Floodplain storage of metal-contaminated sediments downstream of a gold mine at Lead, South Dakota: In: Averett RC, McKnight DM (eds) Chemical quality of water and the hydrological cycle, Lewin Publishers, Chelesea, p. 193-209.
- Martin, J.M., and Meybeck, M., 1979, Elemental mass balance of material carried by world major rivers: *Marine Chemistry*, v 7, p. 173-206.
- McCabe, G. and Wolock, D., 2020, Multi-year hydroclimatic droughts and pluvials across the conterminous United States: *International Journal of Climatology*, v. 41, p. 1731–1746.
- Meng, X., Bang, S., and Korfiatas, G.P., 2000, Effects of silicate, sulfate, and carbonate on arsenic removal by ferric chlorite: *Water Res.*, v.34, p. 1255-1261.

- Miller, J.R., and Miller, S.M., 2007, Contaminated rivers: A geomorphological-geochemical approach to site assessment and remediation: Dordrecht, Springer, 417 p.
- Miller, J.R., 1997, The role of fluvial geomorphic processes in the dispersal of heavy metals from mine sites: *Journal of Geochemical Exploration*, v. 58, p. 101-118.
- Moldovan, B.J., and Hendry, M.J., 2005, Characterizing and quantifying controls on arsenic solubility over a pH range of 1–11 in a uranium mill-scale experiment: *Environ Sci Technol*, v. 37, p. 873–9.
- Mote, P.W., 2003, Trends in snow water equivalent in the Pacific Northwest and their climatic causes: *Geophysical Research Letters*, v. 30 (12).
- Mussetter Engineering, Inc., Owen Ayres and Associates, Inc., Harner and Associates, Inc., Chadwick Ecological Consultants, Inc., 1996, Reclamation Plan for the Redex Mine Reach of Whitewood Creek, South Dakota: Prepared for Homestake Mining Company, Inc.
- Nichols, T.C., and Collins, D.S., 1986, In situ and laboratory geotechnical tests of the Pierre Shale near Hayes, South Dakota- a characterization of engineering behavior: *Canadian Geotechnical Journal*, v. 23, p. 181-194.
- Noble, A., 1950, Ore mineralization in the Homestake Gold Mine, Lead, South Dakota: *Geological Society of America Bulletin*, v. 61, no. 3, p. 221-251.
- Noble, A., and Harder, O., 1948, Stratigraphy and metamorphism in a part of the northern Black Hills and the Homestake Mine, Lead, South Dakota: *Geological Society of American Bulletin*, v. 59(9), p. 941-975.

- Noll Jr, P.D., Newsom, H.E., Leeman, W.P., Ryan, J.G., 1996, The role of hydrothermal fluids in the production of subduction zone magmas: Evidence from siderophile and chalcophile trace elements and boron: *Geochimica et Cosmochimica Acta*, v. 60, Issue 4, p. 587-611.
- Nordstrom D.K., and Archer D.G., 2003, Arsenic thermodynamic data and environmental geochemistry. In: Welch AH, Stollenwerk KG, editors. Arsenic in ground water. Boston, Massachusetts, USA: Kluwer Academic Publishers.
- Norton, P.A., Anderson, M.T., and Stamm, J.F., 2014, Trends in Annual, Seasonal, and Monthly Streamflow Characteristics at 227 Streamgages in the Missouri River Watershed, Water Years 1960–2011: USGS Scientific Investigations Report 2014-5053, p. 128.
- O’Day, P.A., 2006, Chemistry and mineralogy of arsenic: *Elements*, v. 2, p. 77-83.
- Ongley, L.K., Armienta, M.A., Heggeman, K., Lathrop, A.S., Mango, H., Miller, W., and Pickelner, S., 2001, Arsenic removal from contaminated water by the Soyatal Formation, Zimapán Mining District, Mexico – a potential low-cost low-tech remediation system: *Geochemistry: Exploration, Environment, Analysis*, v. 1, v. 1, p. 23-31.
- Oscarson, D.W., Huang, P.M., Liaw, W.K., 1981, Role of manganese in the oxidation of arsenite by freshwater lake sediments: *Clays and Clay Minerals*, v. 29, p. 219-225.
- Peter, K.D., Kolm, K.E., Downsey, J.S., and Nichols, T.C., 1988, Lineaments: significance, criteria for determination, and varied effects on ground-water systems- a case history in the use of remote sensing: *American Society of Testing and Materials Special Publications*, v. 967, p. 46-68.

Peryea, F.J., and Kammerack, R., 1997, Phosphate-enhanced movement of arsenic out of a lead arsenate contaminated topsoil and through uncontaminated subsoil: *Water Air Soil Pollution*, v. 93, p. 243-254.

Pierce, M.L., and Moore, C.M., 1982, Adsorption of arsenite and arsenate on amorphous iron hydroxide: *Water Res*, v. 16, p. 1247-1253.

Pizzuto, J., Suspended sediment and contaminant routing with alluvial storage: New theory and applications: *Geomorphology*, v. 352.

Pfiefle, B.D., Stamm, J.F., and Stone, J.J., 2018, Arsenic geochemistry of alluvial sediments and pore waters affected by mine tailings along the Belle Fourche and Cheyenne River floodplains: *Water, Air, and Soil Pollution*, v.229, p. 183.

Pfiefle, B.D., and Stone, J.J., 2011, Arsenic speciation in sediment and pore waters of the historical mining-impacted Belle Fourche and Cheyenne River floodplains: National Meeting of the American Society of Mining and Reclamation, Bismarck, ND
Reclamation: Sciences Leading to Success June 11 - 16, 2011

Plumley, W.J., 1948, Black Hills terrace gravels: a study in sediment transport: *Journal of Geology*, v. 56, p. 526-577.

Pokrovski G.S., Gout R., Schott J., Zotov A., Harrichoury J.C., 1996, Thermodynamic properties and stoichiometry of As(III) hydroxide complexes at hydrothermal conditions: *Geochim Cosmochim Acta*, v. 60, p. 737-49.

- Rahman, M.M., Ng, J.C., and Naidu, R., 2009, Chronic exposure of arsenic via drinking water and its adverse health impacts on humans: *Environmental Geochemistry and Health*, v. 31, p. 189-200.
- Rancourt, D.G., Fortin, D., Pichler, T., Thibault, P., Laflamme, G., Morris, R.V., Mercier, P.H.J., 2001, Mineralogy of a natural As-rich hydrous ferric oxide coprecipitate formed by mixing of hydrothermal fluid and seawater: Implications regarding surface complexation and color banding in ferrihydrite deposits: *American Mineralogist*, v. 86, p. 834–851.
- Redden, J.A., Peterman, Z.E., Zartman, R.E., and DeWitt, Ed, 1990, Early Proterozoic Trans-Hudson orogen of North America: in Geological Survey of Canada Special Paper 37: p. 229-251.
- Reidmiller, D.R., Avery, C.W., Easterling, D.R., Kunkel, K.E., Lewis, K.L.M., Maycock, T.K., and Stewart, B.C., eds., 2018, Impacts, Risks, and Adaptation in the United States: Fourth National Climate Assessment, V.II: USGCRP publication, 1515 p.
- Ridley, J., 2013, Ore deposit geology: Cambridge University Press, v. 1, 398 p.
- Roddy, W.R., Green, E.A., and Sowards, C.L., 1991, Reconnaissance investigation of water quality, bottom sediment, and biota associated with irrigation drainage in the Belle Fourche Reclamation Project, Western South Dakota, 1988-1989: U.S. Water-Resources Investigations Report 90-4192, 113 p.
- Rodriguez-Freire, L., Avasarala, S., Ali, A., Agnew, D., Hoover, J., Artyushkova, K., Latta, D., Peterson, E., Lewis, J., Crossey, L., Brearley, A., and Cerrato, J., 2016, Post Gold

King Mine Spill Investigation of Metal Stability in Water and Sediments of the Animas River Watershed: *Environ. Sci. Technol.*, v. 50, p. 11539–11548.

Rees, T.F., and Ranville, J.F., 1988, Colloids in Seeps and Springs along Whitewood Creek. In: (Goddard, 1988b), U.S. Geological Survey Applied Research Studies of the Cheyenne River System, South Dakota: Description and Collation of Data, Water Years 1985-86 U.S. Geological Survey. Open-File Report 88-484, p. 125-139.

Sando, S.K., Driscoll, D.G., Parrett, C., 2008, Peak-flow frequency estimates based on data through water year 2001 for selected streamflow-gaging stations in South Dakota: U.S. Scientific Investigations Report 2008–5104, 367 p.

Savage, K.S., Tingle, T.N., O'Day, P.A., Waychunas, G.A., and Bird, D.K., 2000, Arsenic speciation in pyrite and secondary weathering phases, Mother Lode Gold District, Tuolumne County, California: *Applied Geochemistry*, v. 15, p. 1219–1244.

Saup, C., Williams, K., Rodriguez-Freire, L., Cerrato, J., Johnston, M., and Wilkins, M., 2017, Anoxia stimulates microbially catalyzed metal release from Animas River sediments: *Environ. Sci.: Processes Impacts*, v. 19, p. 578–585.

Shockley, J.C., 2021, Modeling watershed sensitivity to climate change in systems affected by discharge of mine tailings: Ph.D. dissertation, University of Nebraska, Lincoln, NB, 437 p.

Shockley, J.C., 1989, The occurrence and spatial distribution of trace elements in bottom sediments of the Whitewood Creek, Belle Fourche River, and Cheyenne River system, Western South Dakota: Unpublished M.S. Thesis, South Dakota School of Mines and Technology, Rapid City, SD.

Shurr, G.W., 1979, Upper Cretaceous tectonic activity on lineaments in Western South Dakota: U.S. Geological Survey Open File Report, 25 p.

Slaughter, A.L., 1968, Homestake Mine, jri Guidebook, Black Hills area, South Dakota, Montana, Wyoming: Wyoming Geological Association, 20th Field Conference, 1968, p. 157-171.

Smedley, P.L., and Kinniburgh, D.G., 2002, A review of the source, behaviour and distribution of arsenic in natural waters: *Applied Geochemistry*, v. 17 (5), p. 517-568.

Smith, D.A., 2003, Here's to low-grade ore and plenty of it, the Hearsts and the Homestake Mine: *Mining Engineering*, v. 55, p. 10-14.

South Dakota Department (S.D. Dept.) of Game, Fish and Parks, S.D. Dept. of Environment and Natural Resources, U.S. Dept. of Interior Fish and Wildlife Service, U.S. Dept. of Interior Bureau of Land Management, U.S. Dept. of Interior Bureau of Reclamation, 2005, Final conceptual restoration and compensation plan for Whitewood Creek and the Belle Fourche and Cheyenne River watersheds, South Dakota.

South Dakota Department of Health, 1960, Report on gold recovery wastes, Homestake Mining Company, Lead, South Dakota: Pierre, 35 p.

Sø, H.U., Postma, D., Jakobsen, R., and Larsen, F., 2008, Sorption and desorption of arsenate and arsenite on calcite: *Geochimica et Cosmochimica Acta*, v. 72, p. 5871-5884.

Stach, R.L., Helgerson, R.N., Bretz, R.F., Tipton, M.J., Beisse, D.R., and Harksen, J.C., 1978, Arsenic levels in the surface and ground waters along Whitewood Creek, Belle

Fourche River, and a portion of the Cheyenne River, South Dakota: South Dakota Geological Survey Completion Report, Project Number A-054-SDAK, 42 p.

Stamm, J. F., Hendricks, R. R., Sawyer, J. F., Mahan, S. A., Zaprowski, B. J., Geibel, N. M., & Azzolini, D. C., 2013, Late Quaternary stream piracy and strath terrace formation along the Belle Fourche and lower Cheyenne Rivers, South Dakota and Wyoming: *Geomorphology*, v. 197, p. 10–20.

Stamm, J. F., and Hoogestraat, G. K., 2012, Concentrations of selected metals in Quaternary-age fluvial deposits along the lower Cheyenne and middle Belle Fourche Rivers, western South Dakota, 2009–2010: U.S. Geological Survey Data Series 695.

Stamm, J.F., Hendricks, R.R., Mahan, S.A., Zaprowski, B.J., and Geibel, N.M., 2010, Late Pleistocene to early Holocene terrace deposits of the lower Cheyenne River, South Dakota: *Geological Society of America Abstracts with Program*, v. 42, p. 181.

Stumm, W., 1992, Chemistry of the solid-water interface: processes at the mineral-water and particle-water interface in natural systems: Wiley-Interscience, New York, 428 p.

Thorstenson, D.C., 1984, The concept of electron activity and its relation to redox potential in aqueous geochemical systems: U.S. Geological Survey Open File Report 84-072, 45 p.

Thorstenson, D.C., Fisher, D.W., and Croft, M.G., 1979, The geochemistry of the Fox Hills-Basal Hell Creek aquifer in southwest North Dakota and northwest South Dakota: *Water Resources Research*, v. 15, p. 1479-1498.

Todd, J.E., 1914, The Pleistocene history of the Missouri River: *Science* v. 39 (39), p. 263-74.

- Todd, J.E., 1923a, Glacial diversion of the Missouri River: *Pan-American Geologist*, v. 39 (3), p. 169-184.
- Todd, J.E., 1923b, Is the channel of the Missouri River through North Dakota of Tertiary origin?: *Geol. Soc. America Bull.*, v. 34, p. 469-494.
- Tufano, K.T., Reyes C.W., Saltikov, C., Fendorf, S., 2008, Reductive processes controlling arsenic retention: Revealing the relative importance of iron and arsenic reduction: *Environmental Science and Technology*, v. 42, p. 8283-8289.
- Vance, F.W., and Greenberg, A., 2010, Water chemistry effects on arsenic removal: *Water Technology*, <https://www.watertechonline.com/wastewater/article/15529494/water-chemistry-effects-on-arsenic-removal>
- Vandenbergh, J., 1995, Timescales, climate and river development: *Quaternary Science Reviews* v. 14, p. 631–638.
- Vaughan, D.J., 2006, Arsenic: *Elements*, v. 2, p. 71-75.
- Villarini, G., Serinaldi, F., Smith, J.A., and Krajewski, W.F., 2009, On the stationarity of annual flood peaks in the continental United States during the 20th century: *Water Resour. Res.*, v. 45.
- Violante, A., and Pigna, M., 2002, Competitive sorption of arsenate and phosphate on different clay minerals and soils: *Soil Sci. Soc. Am. J.*, v. 66, p. 1788-1796.
- United States Geological Survey (USGS), 2018a, USGS EROS archive - Aerial photography - Aerial photo single frames: ([https://www.usgs.gov/centers/eros/science/usgs-eros-](https://www.usgs.gov/centers/eros/science/usgs-eros)

archive-aerial-photography-aerial-photo-single-frames?qt-science_center_objects=0#qt-science_center_objects).

United States Geological Survey (USGS), 2018b, USGS EROS archive - Aerial photography – National agriculture imagery program (NAIP):
(<https://www.usgs.gov/centers/eros/science/usgs-eros-archive-aerial-photography-national-agriculture-imagery-program-naip>).

United States Geological Survey (USGS), 2017, Geochemical and Mineralogical Maps, with Interpretation, for Soils of the Conterminous United States: USGS Scientific Investigations Report 2017-5118.

Waterland, J. K., 1973, Hydraulic backfilling at Homestake: Jubilee Symposium on Mine Filling, Mount Isa, August 1973, North West Queensland Branch, I.M.M., 161-170.

Wang, S., Jiao, B., Zhang, M., Zhang, G., Wang, X., and Jia, Y., 2018, Arsenic release and speciation during the oxidative dissolution of arsenopyrite by O₂ in the absence and presence of EDTA: *Journal of Hazardous Materials*, v. 36, p. 194-190.

Wang, S., and Mulligan, C.N., 2006, Natural attenuation processes for remediation of arsenic contaminated soils and groundwater: *Journal of Hazardous Materials*, v. B138, p. 459–470.

Wilkie, J.A., and Hering, J.G., 1996, Adsorption of arsenic onto hydrous ferric oxide: effects of adsorbate/adsorbent ratios and co-occurring solutes: *Colloid Surf. A*, v.107, p. 97-110.

- Wuolo, R.W., 1986, Laboratory studies of arsenic adsorption in alluvium contaminated with gold-mine tailing along Whitewood Creek, Black Hills, South Dakota: M.S. thesis. South Dakota School of Mines and Technology, Rapid City, SD, 166 p.
- Yu, Y., Zhu, Y., Gao, Z., Gammons, C.H., and Li, D., 2007, Rates of arsenopyrite oxidation by oxygen and Fe(III) at pH 1.8–12.6 and 15–45°C: *Environ. Sci. Technol.*, v. 41, p. 6460–6464.
- Zabilansky, L.J., Ettema, R., Wuebben, J., Yankielun, N., 2002, Survey of river ice influences on channel bathymetry along the Fort Peck reach of the Missouri River, winter 1998-1999: USACE ERDC/CRREL TR-02-14.
- Zaprowski, B.J., and Floyd, J., 2005, Modeling the effects of glacial isostasy on stream terrace formation: *The Pennsylvania Geographer* v. 43, p. 3–20.
- Zaprowski, B.J., 2001, The Geomorphic Evolution of the Black Hills of South Dakota and Adjacent High Plains during the Late Cenozoic: Knickpoint Propagation: Ph.D Thesis. Lehigh University, Bethlehem, PA, 93 p.
- Zaprowski, B.J., Evenson, E.B., Pazzaglia, F.J., and Epstein, J.B., 2001, Knickzone propagation in the Black Hills and northern High Plains: a different perspective on the late Cenozoic exhumation of the Laramide Rocky Mountains: *Geology* v. 29, p. 547–550.
- Zhu, Y., Zhang, X., Xie, Q., Chen, Y., Wang, D., Liang, Y., and Lu, J., 2005, Solubility and stability of barium arsenate and barium hydrogen arsenate at 25 °C: *Journal of Hazardous Materials*, v. 120, p. 37-44.

APPENDICES

Appendix 5-1. Field parameters collected of in-stream and seep water samples in Whitewood Creek and Belle Fourche River from Ji (2021).

Location	pH		Dissolved Oxygen (mg/L)		Specific Conductance (μS/cm)		Water Temperature (°C)		
	Stream	Seep	Stream	Seep	Stream	Seep	Stream	Seep	
A	8.5		6.3		568		17.9		
WWC	B	8.7	7	5.5	0.2	514	8,010	18.4	13.8
	C	8.7		6.1		1,145		18.4	
	D	8.5		5.7		1,288		17.2	
	E	8.6		5.14		1,171		17.5	
	F	8.3		5.33		1,276		17.5	
	G	8.4	7.6	5.96	1.84	1,270	1,373	18.6	14.5
	H	8.3	6.9	5.33	3.38	1,459	3,580	26.8	27.6
BFR	I	8.1		4.56		1,472		27.7	
	J	8.2		4.83		1,535		27	
	K	8.2		5.73		1,574		28	
	L	8.2		5.34		1,465		24.1	

Appendix 5-2. Analytical results from Ji's (2021) water samples. From Ji (2021).

Location	Sample Type	Total or Dissolved	As		Al		B		Ba	Be		Ca	Cd		Co		
			MS	OES	MS	OES	MS	OES	OES	MS	OES	OES	MS	OES	MS	OES	
MDL:			2.6E-05	0.02	1.0E-05	0.005	1.0E-05	0.01	0.0005	5.0E-06	0.0002	0.05	2.0E-06	0.001	1E-06	0.005	
Calculated PQL:			7.8E-05	0.06	0.00003	0.015	0.00003	0.03	0.0015	0.000015	0.0006	0.15	6E-06	0.003	3E-06	0.015	
1/2 MDL:			1.3E-05	0.01	5E-06	0.0025	5E-06	0.005	0.00025	2.5E-06	0.0001	0.025	1E-06	0.0005	5E-07	0.0025	
Comparison Values:			0.01		0.2		6.0		2.0	0.004		n/a	0.005		0.0022 - 0.0029		
Whitewood Creek	A	In Stream	Dissolved	0.0129		0.0061		0.0228		0.086	1.1E-05		79.38	0.0156		0.0010	
			Total	0.0250		0.4450		0.0250		0.102	1.4E-04		83.47	0.0168		0.0020	
	B	In Stream	Dissolved	0.0048		0.0311		0.0279		0.081	1.5E-05		64.36	0.0227		0.0009	
			Total	0.0082		0.1974		0.0284		0.083	4.1E-05		63.92	0.0253		0.0011	
	C	Seep	Total	0.0127		0.0120		0.0902		0.032	2.3E-04		506.15	0.0104		0.0298	
			Dissolved	0.0077		0.0212		0.0741		0.069	1.6E-05		98.67	0.0114		0.0007	
	D	In Stream	Total	0.0117		0.1014		0.0704		0.067	6.5E-05		101.31	0.0046		0.0008	
			Dissolved	0.0139		0.0337		0.0787		0.071	4.6E-05		108.12	0.0147		0.0006	
	E	In Stream	Total	0.0160		0.0666		0.0746		0.074	2.0E-05		106.32	0.0245		0.0005	
			Dissolved	0.0236		0.0112		0.0714		0.075	3.6E-05		104.14	0.0176		0.0003	
	F	In Stream	Total	0.0280		0.0645		0.0715		0.076	6.6E-05		103.82	0.0326		0.0003	
			Dissolved	0.0554		0.0098		0.0799		0.053	4.5E-05		150.86	0.0204		0.0003	
	G	In Stream *	Total	0.0608		0.0154		0.0862		0.052	3.0E-05		150.25	0.0100		0.0003	
			Dissolved	--	0.018	--	0.065	--	0.016	0.050	--	0.002	149.58	--	0.024	--	-0.014
	H	Seep	Total	--	0.087	--	0.167	--	-0.006	0.053	--	0.002	152.01	--	0.034	--	-0.008
			Dissolved	0.4506		0.0062		0.0808		0.024	5.6E-05		190.86	0.0123		0.0009	
	I	In Stream	Total	0.3953		0.0089		0.0691		0.026	3.6E-05		191.38	0.0167		0.0008	
			Dissolved	0.0629		0.0105		0.1484		0.043	4.5E-05		182.66	0.0109		0.0009	
J	In Stream	Total	0.0472		0.1380		0.1119		0.045	4.5E-05		177.19	0.0273		0.0004		
		Dissolved	--	1.650	--	0.210	--	0.172	0.020	--	0.004	526.48	--	0.070	--	0.032	
K	Seep *	Total	--	0.080	--	0.176	--	0.150	0.024	--	0.006	512.75	--	0.045	--	0.015	
		Dissolved	0.0467		0.1008		0.2366		0.054	6.5E-05		224.42	0.0183		0.0032		
L	In Stream	Total	0.0176		0.2478		0.1952		0.053	8.1E-05		226.42	0.0100		0.0012		
		Dissolved	0.0089		0.0024		0.2112		0.049	3.1E-05		210.33	0.0232		0.0002		
M	In Stream *	Total	0.0124		0.2410		0.2145		0.050	9.3E-05		214.18	0.0165		0.0003		
		Dissolved	--	BDL	--	0.02	--	0.17	0.043	--	BDL	185.48	--	0.02	--	BDL	
N	In Stream	Total	--	0.033	--	0.511	--	0.129	0.046	--	0.001	202.47	--	0.036	--	-0.018	
		Dissolved	0.0090		0.0185		0.1945		0.054	1.0E-05		217.18	0.0235		0.0005		
O	In Stream	Total	0.0040		0.3472		0.1761		0.058	1.2E-04		223.23	0.0352		0.0005		

Appendix 5-2. Analytical results from Ji's (2021) water samples. From Ji (2021).

Location	Sample Type	Total or Dissolved	Cr		Cu		Fe	Li		Mg	Mn	Mo		Na	Ni		Pb		
			MS	OES	MS	OES	OES	MS	OES	OES	OES	MS	OES	OES	MS	OES	MS	OES	
MDL:			1.3E-05	0.005	6E-06	0.005	0.01	1.0E-05	0.01	0.01	0.002	2E-06	0.005	0.01	4E-06	0.002	1E-06	0.02	
Calculated PQL:			3.9E-05	0.015	1.8E-05	0.015	0.03	0.00003	0.03	0.03	0.006	6E-06	0.015	0.03	1.2E-05	0.006	3E-06	0.06	
1/2 MDL:			6.5E-06	0.0025	3E-06	0.0025	0.005	5E-06	0.005	0.005	0.001	1E-06	0.0025	0.005	2E-06	0.001	5E-07	0.01	
Comparison Values:			0.1		1.0		0.3	0.001 - 0.003		n/a	0.3	0.04		n/a	0.1		0.015		
Whitewood Creek	A	In Stream	Dissolved	0.0007		0.0012		0.016	0.0055		16.57	0.018	0.0005		10.78	0.0024		0.0000	
		Total	0.0037		0.0082		0.961	0.0074		18.22	0.133	0.0002		10.96	0.0066		0.0106		
	B	In Stream	Dissolved	0.0006		0.0020		0.042	0.0072		25.81	0.095	0.0004		6.40	0.0042		0.0001	
		Total	0.0011		0.0028		0.535	0.0077		25.60	0.107	0.0004		6.36	0.0048		0.0006		
	C	Seep	Dissolved	0.0009		0.0118		15.488	0.0518		1250.09	15.440	0.0020		96.96	0.0834		0.0003	
		Total	0.0009		0.0026		0.053	0.0284		74.19	0.057	0.0010		34.58	0.0074		0.0000		
	D	In Stream	Dissolved	0.0011		0.0045		1.175	0.0276		79.86	0.143	0.0011		35.14	0.0084		0.0087	
		Total	0.0010		0.0053		0.135	0.0267		88.19	0.097	0.0014		37.99	0.0083		0.0034		
	E	In Stream	Dissolved	0.0009		0.0033		0.655	0.0251		84.21	0.062	0.0014		38.79	0.0077		0.0005	
		Total	0.0008		0.0036		0.028	0.0245		80.94	0.006	0.0017		36.36	0.0062		0.0002		
	F	In Stream	Dissolved	0.0010		0.0038		0.340	0.0244		80.60	0.014	0.0015		36.06	0.0072		0.0007	
		Total	0.0006		0.0043		0.074	0.0241		73.60	0.026	0.0015		34.56	0.0058		0.0055		
	G	In Stream *	Dissolved	0.0005	0.010	--	-0.003	0.144	--	0.260	72.73	0.039	--	0.031	35.04	--	0.018	--	0.095
		Total	0.0005	0.013	--	0.016	0.458	--	0.219	73.95	0.052	--	0.038	35.13	--	0.018	--	0.077	
	H	Seep	Dissolved	0.0005		0.0018		1.447	0.0216		74.01	0.872	0.0020		39.79	0.0087		0.0025	
		Total	0.0006		0.0053		0.684	0.0458		94.82	0.236	0.0026		51.09	0.0083		0.0004		
	I	In Stream	Dissolved	0.0013		0.0046		0.628	0.0368		91.53	0.131	0.0022		50.48	0.0068		0.0004	
		Seep *	Dissolved	--	0.072	--	-0.028	46.386	--	0.533	283.04	9.565	--	0.210	98.53	--	0.102	--	0.464
	J	Total	0.0005	0.072	--	-0.074	3.389	--	0.328	286.61	9.316	--	0.110	96.83	--	0.080	--	0.292	
		Total	0.0022		0.0154		1.661	0.0657		68.99	0.296	0.0082		56.57	0.0133		0.0038		
K	In Stream	Dissolved	0.0015		0.0067		1.108	0.0578		66.97	0.175	0.0065		57.03	0.0097		0.0018		
	Total	0.0005		0.0040		0.014	0.0668		66.00	0.021	0.0081		70.53	0.0069		0.0000			
L	In Stream	Dissolved	0.0012		0.0045		0.658	0.0697		67.68	0.080	0.0067		72.22	0.0080		0.0008		
	Total	--	BDL	--	BDL	0.0116	--	0.06	66.16	0.0118	--	0.01	79.22	--	0.003	--	BDL		
M	In Stream *	Dissolved	--	0.010	--	-0.011	0.971	--	0.064	67.09	0.070	--	0.006	81.57	--	0.003	--	0.072	
	Total	0.0007		0.0050		0.143	0.0587		58.52	0.044	0.0094		51.75	0.0084		0.0016			
N	In Stream	Dissolved	0.0016		0.0054		1.069	0.0540		58.87	0.158	0.0074		57.23	0.0101		0.0014		
	Total	0.0016		0.0054		1.069	0.0540		58.87	0.158	0.0074		57.23	0.0101		0.0014			

Appendix 5-2. Analytical results from Ji's (2021) water samples. From Ji (2021).

Location	Sample Type	Total or Dissolved	Pb		S	Sb		Se		Si	Sn		Sr	V		Zn	
			MS	OES	OES	MS	OES	MS	OES	OES	MS	OES	OES	MS	OES	MS	OES
MDL:			1E-06	0.02	0.05	2E-06	0.02	0.00007	0.02	0.01	1E-06	0.02	0.005	5E-06	0.005	1.0E-05	0.001
Calculated PQL:			3E-06	0.06	0.15	6E-06	0.06	0.00021	0.06	0.03	3E-06	0.06	0.015	1.5E-05	0.015	0.00003	0.003
1/2 MDL:			5E-07	0.01	0.025	1E-06	0.01	3.5E-05	0.01	0.005	5E-07	0.01	0.0025	2.5E-06	0.0025	5E-06	0.0005
Comparison Values:			0.015		250	0.006		0.05		n/a	n/a		4.0	0.00004 - 0.22		5.0	
Whitewood Creek	A	In Stream	Dissolved	0.0000	37.85	0.0004		0.0018		7.68	0.0000		0.292	0.0005			0.0367
		Total	0.0106		39.57	0.0005		0.0017		8.47	0.0000		0.311	0.0045			0.0888
	B	In Stream	Dissolved	0.0001	27.39	0.0003		0.0009		6.34	0.0000		0.168	0.0008			0.0323
		Total	0.0006		26.87	0.0003		0.0009		6.42	0.0000		0.168	0.0015			0.0413
	C	Seep	Total	0.0003	1661.79	0.0001		0.0008		10.02	0.0000		2.260	-0.0015			0.0901
		In Stream	Dissolved	0.0000	147.80	0.0002		0.0010		5.79	-0.0001		0.405	0.0005			0.0143
	D	In Stream	Total	0.0087	157.78	0.0002		0.0011		6.04	0.0000		0.414	0.0014			0.0225
		Dissolved	0.0034		169.61	0.0003		0.0012		6.03	0.0001		0.413	0.0006			0.0494
	E	In Stream	Total	0.0005	167.58	0.0003		0.0012		6.18	0.0000		0.416	0.0012			0.0474
		Dissolved	0.0002		155.34	0.0003		0.0012		5.51	0.0000		0.404	0.0005			0.0247
	F	In Stream	Total	0.0007	155.48	0.0003		0.0010		5.63	0.0000		0.400	0.0010			0.0329
		Dissolved	0.0055		169.47	0.0003		0.0016		4.73	0.0000		0.770	0.0002			0.0279
	G	In Stream *	Total	0.0003	169.26	0.0003		0.0017		4.73	0.0000		0.771	0.0003			0.0127
		Dissolved	--	0.095	166.79	--	0.081	--	0.001	4.87	--	0.006	0.789	--	-0.014	--	-0.102
	H	Seep	Total	0.0077	169.64	0.0001		0.100	-0.010	5.11	--	-0.048	0.769	--	0.053	--	-0.078
		Dissolved	0.0025		201.08	0.0001		0.0001		4.92	0.0000		0.762	-0.0001			0.0163
	I	In Stream	Total	0.0004	200.88	0.0001		0.0001		4.92	0.0000		0.757	-0.0001			0.0153
		Dissolved	0.0004		237.67	0.0004		0.0020		4.54	0.0001		1.033	0.0002			0.0251
	J	Seep *	Total	0.0004	224.38	0.0003		0.0017		4.66	0.0001		0.980	0.0027			0.0255
		Dissolved	--	0.464	745.44	--	0.472	--	-0.102	11.97	--	-0.273	4.127	--	-0.021	--	-0.579
K	In Stream	Total	--	712.89	--	0.602	--	-0.081	7.92	--	0.045	3.880	--	-0.338	--	-0.681	
	Dissolved	0.0038		233.21	0.0004		0.0022		5.57	0.0005		2.580	0.0019			0.1563	
L	In Stream	Total	0.0018	217.50	0.0003		0.0019		5.71	0.0001		2.658	0.0032			0.0576	
	Dissolved	0.0000		231.86	0.0003		0.0022		4.45	0.0000		2.430	0.0010			0.0178	
M	In Stream	Total	0.0008	232.70	0.0003		0.0021		5.08	0.0000		2.476	0.0032			0.0231	
	Dissolved	--	BDL	262.24	--	BDL	--	BDL	4.21	--	BDL	2.6164	--	0.00	--	0.02	
N	In Stream *	Total	--	271.93	--	0.134	--	-0.024	4.79	--	-0.045	2.706	--	0.003	--	0.030	
	Dissolved	0.0016		206.90	0.0002		0.0021		5.20	0.0000		2.634	0.0016			0.1191	
O	In Stream	Total	0.0014	210.75	0.0002		0.0019		6.13	0.0000		2.689	0.0056			0.2926	

Appendix 5-2. Analytical results from Ji's (2021) water samples. From Ji (2021).

Notes:

Analytes of Concern (AOCs) are highlighted in light yellow and are discussed in depth in the text.

Concentrations are reported in milligram per liter (mg/L)

Total samples were collected directly into the container; dissolved samples were filtered through a 0.45µm syringe-attachment membrane filter.

In-stream * or Seep * = Only ICP-OES results are reported (i.e., not enough sample was left to be analyzed by ICP-MS).

Negative results = concentration is below the method detection limit

ICP-MS = inductively coupled plasma mass spectroscopy

ICP-OES = inductively coupled plasma optical emissions spectroscopy

BDL = below detection limit; concentration is below the method detection limit.

MDL = method detection limit

PQL = practical quantitation limit (set to 3x the MDL)

Comparison Values:

U.S. Environmental Protection Agency's (USEPA) National Primary Drinking Water Regulations maximum contaminant level (MCL) = the highest level of a contaminant that is allowed drinking water; these analytes include: arsenic, antimony, barium, beryllium, cadmium, chromium, lead, and selenium.

Results exceeding the EPA Primary MCL are highlighted in light green.

The EPA National Secondary Drinking MCLs = non-enforceable guidelines regarding contaminants that may cause cosmetic or aesthetic effects in drinking water; these analytes include: aluminum, copper, iron, sulfate (as sulfur), and zinc. Results exceeding the comparison value are highlighted in grey.

Results exceeding the EPA Secondary MCL are highlighted in grey.

EPA Health Advisory (HA) Life-time Standard = non-enforceable estimates of acceptable drinking water levels for a chemical substance based on health effects information; these analyt include: boron, manganese, molybdenum, nickel, and strontium. Results exceeding the comparison value are highlighted in light green.

Results exceeding the EPA HA standard are highlighted in light blue.

0.001 - 0.003 (concentration ranges) = Average concentrations found in surface water. Human health based drinking water ingestion comparison values not established by EPA. Average surface water concentration ranges reported in the literature are presented; these analytes include: cobalt, lithium, and vanadium. See References below for source documentation.

Exceedances of these concentration ranges are not highlighted.

n/a = comparison value is not available due to the analyte's low toxicity; these analytes include: calcium, magnesium, silicon, tin, and sodium.

References:

EPA MCL and HA standards:

U.S. Environmental Protection Agency (USEPA) 2018. *Drinking Water Standards and Health Advisories*. Office of Water USEPA. EPA 822-F-18-001. Washington, DC. March 2018.

Cobalt:

Cobalt and inorganic cobalt compounds. James H. Kim, Herman J. Gibb, Paul D. Howe. *Concise international chemical assessment document* ; 69. World Health Organization. 2006.

Lithium:

Oram, Brian, P.G. Date Unknown. *Lithium in Groundwater, Drinking Water Marcellus Shale Water Testing*. Water Research Center. Pennsylvania. Accessed online 12/21/2019.

Vanadium:

Agency for Toxic Substances and Disease Registry (ATSDR). Date Unknown. *Public Health Statement - Vanadium*.

Appendix 5-3. Mineralogy of mine tailing and their respective mineral mass in weight percentage. Formulas are from the database of Geochemist's Workbench.

Mineral	Formula	Wt % (100 times kilogram kilogram solution)
Kaolinite	$\text{Al}_2\text{Si}_2\text{O}_5(\text{OH})_4$	3 ^b
Quartz	SiO_2	83 ^a
Hematite	Fe_2O_3	2.9 ^a
Dolomite	$\text{CaMg}(\text{CO}_3)_2$	1 ^{b*}
Siderite	FeCO_3	1 ^{b*}
Calcite	CaCO_3	1 ^{b*}
Smectite-high-Fe-Mg	$\text{Na}_{0.1}\text{Ca}_{0.25}\text{K}_{.2}\text{Mg}_{1.15}\text{Fe}_{0.7}\text{Al}_{1.25}\text{Si}_{3.5}\text{O}_{10}(\text{OH})_2$	12 ^b
Clinochlore (Clinochl-14A)	$\text{Mg}_5\text{Al}_2\text{Si}_3\text{O}_{10}(\text{OH})_8$	5 ^{b%}
Illite	$\text{K}_{0.6}\text{Mg}_{0.25}\text{Al}_{2.3}\text{Si}_{3.5}\text{O}_{10}(\text{OH})_2$	5 ^b
Albite	$\text{NaAlSi}_3\text{O}_8$	9 ^{b\$}
Anthophyllite	$\text{Mg}_7\text{Si}_8\text{O}_{22}(\text{OH})_2$	8 ^{b\$}
Diopside	$\text{CaMgSi}_2\text{O}_6$	1 ^{b*}
Gypsum	$\text{CaSO}_4 \cdot 2\text{H}_2\text{O}$	5.25 ^c

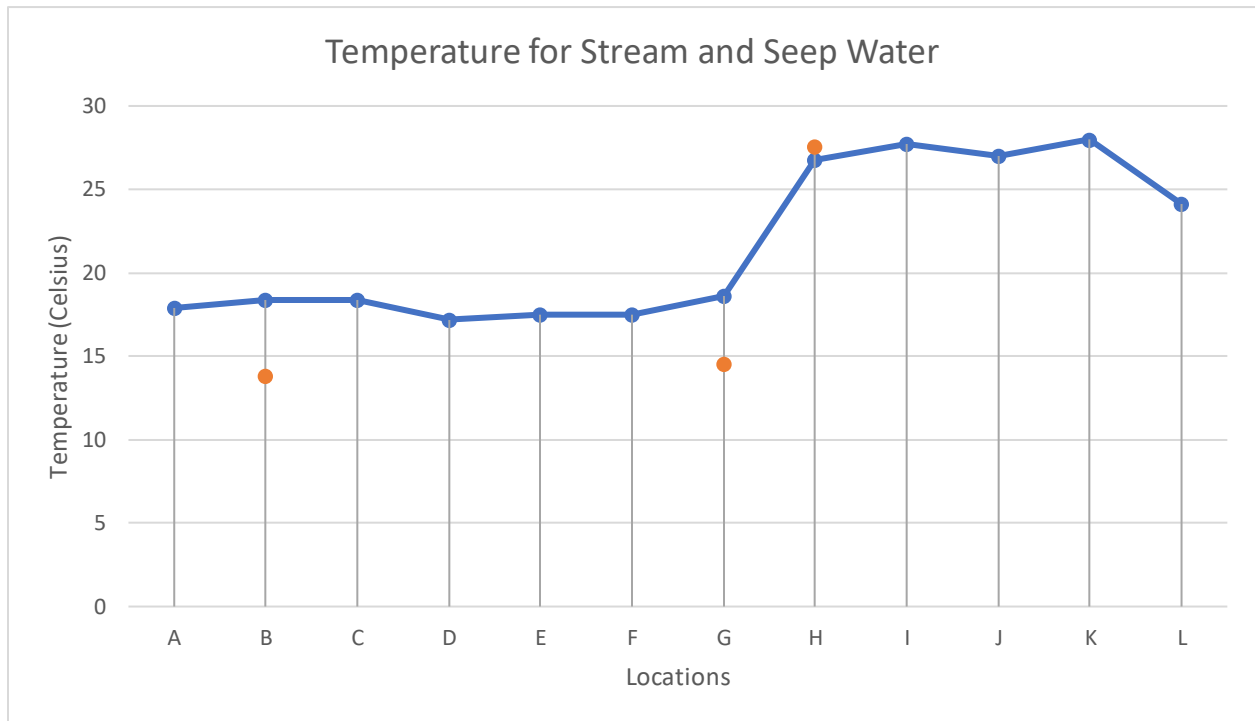
- a. Average % from mineralogy observation by Ji (2021)
- b. Mean wt% from Goddard (1989)
 - *: Actual value is < 1%, may be overestimate
 - \$: Albite represents all feldspars and anthophyllite represents all amphiboles.
 - % clinochlore represents all chlorite minerals
- c. Approximate wt % from Cherry et al. (1984)

Appendix 5-4. Mean mineral composition for the Pierre Shale. From Schultz et al. (1980) found through X-ray methods. The top table is the general composition of the shale and the bottom table is the composition of the clay mineral fraction.

Mineral	Composition (%)
Clay minerals	53
Quartz	24
Cristobalite	1
Potassium feldspar	1
Plagioclase	6
Calcite	5
Dolomite	4
Organic matter	1
Gypsum, jarosite, pyrite, zeolites, augite, siderite, Fe-Mn oxides	Trace

Clay mineral fraction	Composition (%)
Mixed layered illite-smectite	70
Illite	16
Chlorite	3
Kaolinite	1

Appendix 5-5. Temperature of stream and seep water for each location measured by Ji (2021).



Appendix 6-1. 1948 Whitewood Creek statistics of fluvial parameters for Reach 1-10 based on statistical analysis from ArcMap. Statistical parameters include number of polygons (count), sum, mean, and standard deviation.

Parameter	Count	Sum	Mean	Standard Deviation
Contaminated Area (m ²)	155	1132024	7303	11361
Contaminated Area Removed (m ²)	141	277740	1970	2484
Channel Migration (m)	351	1078093	28	6.75
Floodplain Width (m)	154	8555	56	32
Total Sediment Deposition Area (m ²)	393	844643	2149	3131

Appendix 6-2. 1977 Whitewood Creek statistics of fluvial parameters for Reach 1-10 based on statistical analysis from ArcMap. Statistical parameters include number of polygons (count), sum, mean, and standard deviation.

Parameter	Count	Sum	Mean	Standard Deviation
Contaminated Area (m ²)	100	801157	8012	11077
Contaminated Area Removed (m ²)	67	85744	1280	1747
Channel Migration (m)	288	571312	15	4.28
Floodplain Width (m)	96	5478	57	35
Total Sediment Deposition Area (m ²)	318	542202	1705	3094

Appendix 6-3. EPA's (1972) Whitewood Creek statistics of contaminated sediment area for Reach 1-10 based on statistical analysis from ArcMap. Statistical parameters include number of polygons (count), sum, mean, and standard deviation.

Parameter	Count	Sum	Mean	Standard Deviation
Contaminated Area (ft ²)	43	8810496	204895	179585
(m ²)	43	818522	19035	16684

Appendix 6-4. 1948 Belle Fourche River statistics of fluvial parameters for Reach 1-10 based on statistical analysis from ArcMap. Statistical parameters include number of polygons (count), sum, mean, and standard deviation.

Parameter	Count	Sum	Mean	Standard Deviation
Contaminated Area (m ²)	141	3368349	23889	29374
Contaminated Area Removed (m ²)	115	237556	2066	3340
Channel Migration (m)	212	1471623	20	7.75
Floodplain Width (m)	136	11345	83	110
Total Sediment Deposition Area (m ²)	224	2576607	11503	12615

Appendix 6-5. 1977 Belle Fourche River statistics of fluvial parameters for Reach 1-7 based on statistical analysis from ArcMap. Statistical parameters include number of polygons (count), sum, mean, and standard deviation.

Parameter	Count	Sum	Mean	Standard Deviation
Contaminated Area (m ²)	69	1637194	23727	18041
Contaminated Area Removed (m ²)	84	136692	1627	2785
Channel Migration (m)	141	917590	12	6.50
Floodplain Width (m)	68	4625	68	44
Total Sediment Deposition Area (m ²)	224	2576607	11503	12615

Appendix 6-6. EPA's (1972) Belle Fourche River statistics of contaminated sediment area for Reach 1-7 based on statistical analysis from ArcMap. Statistical parameters include number of polygons (count), sum, mean, and standard deviation.

Parameter	Count	Sum	Mean	Standard Deviation
Contaminated Area (ft ²)	81	20626370	254647	269997
(m ²)	-	1916300	23657	25084

Appendix 6-7. EPA's (1972) Belle Fourche River statistics of contaminated sediment area for Reach 1-10 based on statistical analysis from ArcMap. Statistical parameters include number of polygons (count), sum, mean, and standard deviation.

Parameter	Count	Sum	Mean	Standard Deviation
Contaminated Area (ft ²)	116	29966970	258336	264745
(m ²)	-	2784000	24000	24596

Appendix 7-1. Mineral saturation indices of stream water calculated by Geochemist's Workbench at Location A (Whitetail Creek).

Mineral saturation states			
	log Q/K		log Q/K
Nontronit-Ca	19.2607s/sat	Daphnite-14A	1.3543s/sat
Nontronit-Mg	19.1962s/sat	Chrysotile	1.3437s/sat
Nontronit-Na	18.6026s/sat	Gibbsite	1.2385s/sat
Antigorite	17.8813s/sat	Margarite	1.1298s/sat
Hematite	14.7836s/sat	Mordenite-Na	1.0291s/sat
CuFeO2(c)	14.2479s/sat	Barite	0.8352s/sat
Cronstedt-7A	13.7267s/sat	Albite low	0.8233s/sat
Magnetite	13.6936s/sat	Albite	0.8232s/sat
Ferrite-Zn	13.6290s/sat	Ripidolit-7A	0.7985s/sat
Andradite	12.7993s/sat	Tenorite	0.5989s/sat
Ferrite-Cu	12.7563s/sat	Quartz	0.5983s/sat
Ba3(AsO4)2(c)	10.9396s/sat	Clinozoisite	0.5450s/sat
Epidote-ord	9.5742s/sat	Zoisite	0.4987s/sat
Epidote	9.5736s/sat	Tridymite	0.4258s/sat
Clinoptil-Ca	7.1065s/sat	Diaspore	0.3837s/sat
Goethite	6.9244s/sat	Chalcedony	0.3203s/sat
Ferrite-Ca	6.7537s/sat	Minnesotaite	0.0924s/sat
Ferrite-Mg	6.7022s/sat	Analcime	0.0383s/sat
Saponite-Ca	5.7018s/sat	Cristobalite	0.0312s/sat
Clinochl-14A	5.6497s/sat	Chamosite-7A	-0.1574
Saponite-Mg	5.6381s/sat	Wairakite	-0.4049
Amesite-14A	5.3428s/sat	Boehmite	-0.4986
Heulandite	5.3084s/sat	Albite high	-0.5432
Saponite-Na	5.0436s/sat	Amrph^silica	-0.7469
Beidellit-Ca	4.7660s/sat	Diopside	-0.9257
Beidellit-Mg	4.7014s/sat	Gypsum	-1.2575
Tremolite	4.5661s/sat	Jadeite	-1.3985
Talc	4.5443s/sat	Anhydrite	-1.5051
Saponite-H	4.3769s/sat	Kyanite	-1.5484
Laumontite	4.2357s/sat	Ferrosilite	-1.6731
Ripidolit-14A	4.2326s/sat	Enstatite	-1.7288
Kaolinite	4.1144s/sat	Greenalite	-1.7705
Beidellit-Na	4.1077s/sat	Andalusite	-1.8420
Paragonite	3.7676s/sat	Celestite	-2.0316
Pyrophyllite	3.6129s/sat	Daphnite-7A	-2.0838
Beidellit-H	3.4375s/sat	Anorthite	-2.1026
Petalite	2.7798s/sat	Hercynite	-2.1086
Lawsonite	2.5158s/sat	Bassanite	-2.1359
Fe(OH)3(ppd)	2.4560s/sat	Sillimanite	-2.2150
Clinochl-7A	2.2174s/sat	FeO(c)	-2.2290
Clinoptil-Mg	2.2072s/sat	CaSO4^1/2H2O(bet	-2.3135
Prehnite	2.1690s/sat	Rhodonite	-2.4099
Clinoptil-Na	2.0642s/sat	Spodumene-a	-2.6598
Sepiolite	1.6150s/sat	Anthophyllite	-2.7380

(only minerals with log Q/K > -3 listed)

Appendix 7-2. Mineral saturation indices of stream water calculated by Geochemist's Workbench at Location B.

Mineral saturation states			
	log Q/K		log Q/K
Antigorite	29.5295s/sat	Prehnite	1.2322s/sat
Nontronit-Ca	18.0365s/sat	Petalite	0.9500s/sat
Nontronit-Mg	18.0162s/sat	Barite	0.7184s/sat
Nontronit-Na	17.3164s/sat	Gibbsite	0.6567s/sat
Hematite	14.2223s/sat	Quartz	0.4571s/sat
CuFeO2(c)	13.4847s/sat	Tenorite	0.3384s/sat
Ferrite-Zn	13.1746s/sat	Tridymite	0.2851s/sat
Andradite	12.7792s/sat	Anthophyllite	0.2582s/sat
Magnetite	12.6560s/sat	Clinoptil-Mg	0.2385s/sat
Cronstedt-7A	12.0638s/sat	Chalcedony	0.1796s/sat
Ferrite-Cu	11.9398s/sat	Ripidolit-7A	0.0225s/sat
Ba3(AsO4)2(c)	10.1747s/sat	Cristobalite	-0.1089
Epidote-ord	8.3598s/sat	Diaspore	-0.1936
Epidote	8.3592s/sat	Albite low	-0.2020
Tremolite	7.0131s/sat	Albite	-0.2021
Clinochl-14A	7.0008s/sat	Mordenite-Na	-0.2779
Saponite-Ca	6.8006s/sat	Diopside	-0.2963
Saponite-Mg	6.7811s/sat	Clinoptil-Na	-0.5497
Ferrite-Mg	6.7437s/sat	Analcime	-0.8456
Goethite	6.6430s/sat	Amrph^silica	-0.8840
Ferrite-Ca	6.5283s/sat	Clinozoisite	-0.9605
Saponite-Na	6.0805s/sat	Zoisite	-1.0067
Talc	5.7356s/sat	Boehmite	-1.0733
Saponite-H	5.4249s/sat	Margarite	-1.1321
Amesite-14A	5.0981s/sat	Enstatite	-1.2779
Clinoptil-Ca	4.8610s/sat	Gypsum	-1.3961
Clinochl-7A	3.5726s/sat	Albite high	-1.5651
Heulandite	3.4866s/sat	Anhydrite	-1.6388
Ripidolit-14A	3.4524s/sat	Wairakite	-1.7893
Sepiolite	3.1037s/sat	Minnesotaite	-1.9084
Beidellit-Ca	2.9539s/sat	Rhodonite	-2.2073
Beidellit-Mg	2.9336s/sat	Bassanite	-2.2694
Laumontite	2.8350s/sat	Jadeite	-2.2827
Chrysotile	2.8185s/sat	Ferrosilite	-2.2894
Kaolinite	2.6719s/sat	Celestite	-2.3221
Beidellit-Na	2.2337s/sat	Chamosite-7A	-2.4094
Fe(OH)3(ppd)	2.1801s/sat	CaSO4^1/2H2O(bet	-2.4463
Pyrophyllite	1.8929s/sat	Daphnite-14A	-2.6215
Paragonite	1.5839s/sat	Brucite	-2.6891
Beidellit-H	1.5745s/sat	FeO(c)	-2.7032
Lawsonite	1.3958s/sat	Kyanite	-2.8356

(only minerals with log Q/K > -3 listed)

Appendix 7-3. Mineral saturation indices of seep water calculated by Geochemist's Workbench at Location B.

Mineral saturation states			
	log Q/K		log Q/K
CuFeO ₂ (c)	12.4977s/sat	Cristobalite	0.2071s/sat
Nontronit-Mg	11.1412s/sat	Saponite-Na	0.1024s/sat
Nontronit-Ca	11.0317s/sat	Chamosite-7A	0.0882s/sat
Nontronit-Na	10.6138s/sat	Epidote-ord	0.0689s/sat
Hematite	6.2952s/sat	Epidote	0.0681s/sat
Clinoptil-Ca	6.0432s/sat	Lawsonite	0.0068s/sat
Cronstedt-7A	5.5485s/sat	Gypsum	-0.0709
Magnetite	5.2350s/sat	Talc	-0.1074
Beidellit-Mg	5.0595s/sat	Analcime	-0.3443
Beidellit-Ca	4.9501s/sat	Saponite-H	-0.3467
Beidellit-Na	4.5321s/sat	Anhydrite	-0.3597
Kaolinite	4.5005s/sat	Ripidolit-14A	-0.5290
Pyrophyllite	4.3292s/sat	Boehmite	-0.5356
Beidellit-H	4.0804s/sat	Amorph [^] silica	-0.5958
Heulandite	3.6888s/sat	Albite high	-0.7663
Paragonite	3.5738s/sat	Celestite	-0.7687
Goethite	2.6866s/sat	Bassanite	-0.9916
Petalite	2.6044s/sat	CaSO ₄ [^] 1/2H ₂ O(bet	-1.1744
Clinoptil-Na	2.4050s/sat	Greenalite	-1.2367
Ferrite-Cu	2.2236s/sat	Daphnite-7A	-1.3114
Daphnite-14A	2.1648s/sat	Tenorite	-1.4000
Clinoptil-Mg	2.1289s/sat	Kyanite	-1.4642
Laumontite	2.0821s/sat	Ferrosilite	-1.4675
Ba ₃ (AsO ₄) ₂ (c)	2.0294s/sat	Margarite	-1.5145
Ferrite-Zn	1.4662s/sat	Amesite-14A	-1.5835
Gibbsite	1.2612s/sat	Andalusite	-1.7687
Mordenite-Na	1.1999s/sat	Jadeite	-1.7781
Minnesotaite	0.9832s/sat	Fe(OH) ₃ (ppd)	-1.8286
Quartz	0.7837s/sat	Epsomite	-1.9649
Barite	0.6919s/sat	Sillimanite	-2.1500
Saponite-Mg	0.6312s/sat	Hercynite	-2.1679
Albite low	0.6283s/sat	FeO(c)	-2.2169
Albite	0.6282s/sat	Hexahydrite	-2.2841
Tridymite	0.6072s/sat	Pentahydrite	-2.6098
Saponite-Ca	0.5204s/sat	Wairakite	-2.6931
Chalcedony	0.5018s/sat	Clinochl-14A	-2.8341
Diaspore	0.3691s/sat		
(only minerals with log Q/K > -3 listed)			

Appendix 7-4. Mineral saturation indices of stream water calculated by Geochemist's Workbench at Location C.

Mineral saturation states			
	log Q/K		log Q/K
Antigorite	38.6171s/sat	Prehnite	0.7193s/sat
CuFeO ₂ (c)	17.0321s/sat	FeO(c)	0.6558s/sat
Daphnite-14A	13.4742s/sat	Tenorite	0.5268s/sat
Ripidolit-14A	10.6692s/sat	Quartz	0.4279s/sat
Daphnite-7A	10.0407s/sat	Gibbsite	0.3509s/sat
Ba ₃ (AsO ₄) ₂ (c)	9.6332s/sat	Tridymite	0.2559s/sat
Tremolite	8.9624s/sat	Chalcedony	0.1504s/sat
Clinochl-14A	8.2984s/sat	Diopside	0.1377s/sat
Minnesotaite	8.0518s/sat	Albite low	0.1277s/sat
Saponite-Mg	7.8370s/sat	Albite	0.1276s/sat
Saponite-Ca	7.8060s/sat	Hematite	0.0000 sat
Saponite-Na	7.3091s/sat	Mordenite-Na	-0.0065
Ripidolit-7A	7.2394s/sat	Clinoptil-Na	-0.0070
Talc	6.8169s/sat	Cristobalite	-0.1380
Greenalite	6.5279s/sat	Clinoptil-Mg	-0.2653
Saponite-H	6.4150s/sat	Goethite	-0.4681
Amesite-14A	5.4141s/sat	Analcime	-0.4867
Clinochl-7A	4.8702s/sat	Hedenbergite	-0.4987
Cronstedt-7A	4.5303s/sat	Diaspore	-0.4993
Sepiolite	4.5259s/sat	Fe(OH) ₂ (ppd)	-0.8167
Clinoptil-Ca	4.0510s/sat	Enstatite	-0.9077
Chrysotile	3.9581s/sat	Amrph [^] silica	-0.9132
Chamosite-7A	3.6678s/sat	Hercynite	-0.9849
Nontronit-Mg	3.6519s/sat	Gypsum	-1.0267
Nontronit-Ca	3.6216s/sat	Albite high	-1.2354
Nontronit-Na	3.1248s/sat	Andradite	-1.2515
Anthophyllite	2.8201s/sat	Anhydrite	-1.2694
Heulandite	2.7640s/sat	Boehmite	-1.3790
Laumontite	2.2000s/sat	Ferrite-Zn	-1.4185
Beidellit-Mg	2.1801s/sat	Celestite	-1.7606
Beidellit-Ca	2.1499s/sat	Clinozoisite	-1.7791
Kaolinite	2.0021s/sat	Zoisite	-1.8253
Magnetite	1.7927s/sat	Bassanite	-1.9000
Beidellit-Na	1.6529s/sat	Jadeite	-1.9238
Fayalite	1.4195s/sat	CaSO ₄ [^] 1/2H ₂ O(bet	-2.0769
Paragonite	1.3022s/sat	Ferrite-Cu	-2.0940
Petalite	1.1783s/sat	Rhodonite	-2.2115
Pyrophyllite	1.1648s/sat	Brucite	-2.2898
Ferrosilite	1.0404s/sat	Margarite	-2.3203
Lawsonite	0.8190s/sat	Wustite	-2.3378
Beidellit-H	0.7551s/sat	Wairakite	-2.4244
Barite	0.7546s/sat	CaSi ₂ O ₅ [^] 2H ₂ O	-2.9899
Epidote-ord	0.7357s/sat	Manganite	-2.9958
Epidote	0.7352s/sat		

(only minerals with log Q/K > -3 listed)

Appendix 7-5. Mineral saturation indices of stream water calculated by Geochemist's Workbench at Location D.

Mineral saturation states			
	log Q/K		log Q/K
Antigorite	28.5297s/sat	Barite	0.8288s/sat
Nontronit-Mg	18.2710s/sat	Lawsonite	0.6290s/sat
Nontronit-Ca	18.2426s/sat	Quartz	0.4728s/sat
Nontronit-Na	17.7617s/sat	Gibbsite	0.4422s/sat
Hematite	14.4868s/sat	Tridymite	0.2996s/sat
CuFeO2(c)	13.7191s/sat	Clinoptil-Na	0.2327s/sat
Magnetite	13.2424s/sat	Chalcedony	0.1942s/sat
Cronstedt-7A	13.0065s/sat	Tenorite	0.1877s/sat
Ferrite-Zn	12.9155s/sat	Albite low	0.1595s/sat
Ferrite-Cu	12.0406s/sat	Albite	0.1594s/sat
Andradite	12.0157s/sat	Prehnite	0.1157s/sat
Ba3(AsO4)2(c)	9.5614s/sat	Mordenite-Na	0.1134s/sat
Epidote-ord	7.3684s/sat	Ripidolit-7A	0.1069s/sat
Epidote	7.3678s/sat	Anthophyllite	-0.0538
Ferrite-Mg	6.9135s/sat	Cristobalite	-0.0959
Goethite	6.7772s/sat	Clinoptil-Mg	-0.1386
Saponite-Mg	6.5995s/sat	Diaspore	-0.4189
Saponite-Ca	6.5701s/sat	Analcime	-0.5003
Ferrite-Ca	6.4001s/sat	Diopside	-0.6878
Clinochl-14A	6.3271s/sat	Minnesotaite	-0.8631
Tremolite	6.1419s/sat	Amrph [^] silica	-0.8782
Saponite-Na	6.0893s/sat	Gypsum	-0.9940
Talc	5.6401s/sat	Albite high	-1.2117
Saponite-H	5.2482s/sat	Anhydrite	-1.2487
Clinoptil-Ca	4.2095s/sat	Boehmite	-1.3051
Amesite-14A	4.0034s/sat	Enstatite	-1.3313
Ripidolit-14A	3.5471s/sat	Daphnite-14A	-1.3774
Sepiolite	2.9999s/sat	Celestite	-1.7463
Clinochl-7A	2.8890s/sat	Bassanite	-1.8797
Heulandite	2.7879s/sat	Jadeite	-1.9366
Chrysotile	2.6889s/sat	Ferrosilite	-1.9547
Beidellit-Mg	2.4598s/sat	CaSO4 [^] 1/2H2O(bet	-2.0581
Beidellit-Ca	2.4314s/sat	Chamosite-7A	-2.1922
Fe(OH)3(ppd)	2.3008s/sat	Clinzoisite	-2.3229
Kaolinite	2.2655s/sat	Zoisite	-2.3695
Laumontite	2.0953s/sat	Margarite	-2.3802
Beidellit-Na	1.9505s/sat	FeO(c)	-2.3865
Pyrophyllite	1.5061s/sat	Greenalite	-2.4726
Paragonite	1.5036s/sat	Wairakite	-2.5680
Petalite	1.1716s/sat	Brucite	-2.7552
Beidellit-H	1.1060s/sat		

(only minerals with log Q/K > -3 listed)

Appendix 7-6. Mineral saturation indices of stream water calculated by Geochemist's Workbench at Location E.

Mineral saturation states			
	log Q/K		log Q/K
Antigorite	32.9231s/sat	Sanidine high	1.0566s/sat
Nontronit-Mg	17.4778s/sat	Pyrophyllite	1.0455s/sat
Nontronit-Ca	17.4498s/sat	Paragonite	1.0403s/sat
Nontronit-K	17.0514s/sat	Aragonite	0.9901s/sat
Nontronit-Na	16.9567s/sat	Huntite	0.8169s/sat
Hematite	13.8908s/sat	Barite	0.7617s/sat
CuFeO2(c)	13.4576s/sat	Petalite	0.6999s/sat
Hydroxyapatite	12.5576s/sat	Beidellit-H	0.6205s/sat
Ferrite-Zn	12.4129s/sat	Lawsonite	0.4925s/sat
Magnetite	12.3377s/sat	Magnesite	0.4841s/sat
Andradite	11.9406s/sat	Quartz	0.4218s/sat
Cronstedt-7A	11.7374s/sat	Gibbsite	0.3112s/sat
Ferrite-Cu	11.5109s/sat	Tenorite	0.2507s/sat
Ba3(AsO4)2(c)	10.4778s/sat	Tridymite	0.2489s/sat
Smectite-Reykjan	9.8645s/sat	Monohydrocalcite	0.1770s/sat
Tremolite	7.2832s/sat	Prehnite	0.1546s/sat
Epidote-ord	7.1111s/sat	Chalcedony	0.1435s/sat
Epidote	7.1105s/sat	MnHPO4(c)	-0.0302
Saponite-Mg	7.0632s/sat	Albite low	-0.0451
Saponite-Ca	7.0344s/sat	Albite	-0.0452
Clinochl-14A	7.0151s/sat	Cristobalite	-0.1462
Saponite-K	6.6333s/sat	Mordenite-Na	-0.1928
Ferrite-Mg	6.5472s/sat	Ripidolit-7A	-0.2630
Saponite-Na	6.5412s/sat	Diopside	-0.3431
Goethite	6.4787s/sat	Clinoptil-Na	-0.3797
Phlogopite	6.1057s/sat	Diaspore	-0.5472
Talc	6.0937s/sat	Alstonite	-0.5865
Ferrite-Ca	6.0373s/sat	Analcime	-0.6538
Whitlockite	5.8855s/sat	Clinoptil-Mg	-0.6780
Saponite-H	5.6767s/sat	Barytoalcite	-0.7478
Clinoptil-K	5.3327s/sat	Rhodochrosite	-0.8818
Phengite	4.8870s/sat	Amrph [^] silica	-0.9267
Muscovite	4.3080s/sat	Gypsum	-1.1177
Amesite-14A	4.2687s/sat	Annite	-1.1388
Clinoptil-Ca	3.6677s/sat	Enstatite	-1.1590
Smectite-low-Fe-	3.6382s/sat	Malachite	-1.1788
Clinochl-7A	3.5795s/sat	Smithsonite	-1.3047
Sepiolite	3.5674s/sat	Anhydrite	-1.3693
Smectite-high-Fe	3.5017s/sat	Albite high	-1.4143
Dolomite	3.3157s/sat	Boehmite	-1.4317
Dolomite-ord	3.3157s/sat	Kalsilite	-1.7976
Chrysotile	3.2451s/sat	Dawsonite	-1.8430
Ripidolit-14A	3.1747s/sat	Celestite	-1.8705
Illite	3.0383s/sat	Strengite	-1.9372
Mordenite-K	2.6663s/sat	Minnesotaitite	-1.9973
Heulandite	2.3991s/sat	Bassanite	-2.0002
Maximum Microcli	2.3067s/sat	Jadeite	-2.0903
K-feldspar	2.3054s/sat	Siderite	-2.1241
Witherite	2.2892s/sat	CaSO4 [^] 1/2H2O(bet	-2.1783
Beidellit-Mg	2.0095s/sat	Ferrosilite	-2.3136
Fe(OH)3(ppd)	2.0057s/sat	Clinozoisite	-2.4071
Beidellit-Ca	1.9816s/sat	CaHPO4 [^] 2H2O	-2.4085
Kaolinite	1.9039s/sat	Zoisite	-2.4535
Laumontite	1.8579s/sat	Brucite	-2.5327
Dolomite-dis	1.7151s/sat	Nesquehonite	-2.5495
Beidellit-K	1.5805s/sat	FeO(c)	-2.6939
Beidellit-Na	1.4884s/sat	Margarite	-2.7655
Strontianite	1.3095s/sat	Wairakite	-2.7956
Calcite	1.1557s/sat	Artinite	-2.9952
Anthophyllite	1.0897s/sat		

(only minerals with log Q/K > -3 listed)

Appendix 7-7. Mineral saturation indices of stream water calculated by Geochemist's Workbench at Location F.

Mineral saturation states			
	log Q/K		log Q/K
Antigorite	16.1414s/sat	Beidellit-K	0.4930s/sat
Nontronit-Ca	16.0817s/sat	Beidellit-Na	0.3924s/sat
Nontronit-Mg	16.0763s/sat	Quartz	0.3596s/sat
Nontronit-K	15.6603s/sat	MnHPO4(c)	0.2964s/sat
Nontronit-Na	15.5572s/sat	Sanidine high	0.2472s/sat
CuFeO2(c)	13.0020s/sat	Amesite-14A	0.2161s/sat
Hematite	12.9336s/sat	Tridymite	0.1867s/sat
Hydroxyapatite	12.1820s/sat	Pyrophyllite	0.1429s/sat
Magnetite	11.2018s/sat	Magnesite	0.1326s/sat
Ferrite-Zn	10.4241s/sat	Chalcedony	0.0813s/sat
Cronstedt-7A	10.3607s/sat	Monohydrocalcite	0.0279s/sat
Ferrite-Cu	10.2766s/sat	Ripidolit-14A	0.0115s/sat
Andradite	9.4382s/sat	Gibbsite	-0.0156
Ba3(AsO4)2(c)	9.3519s/sat	Tenorite	-0.0263
Smectite-Reykjan	7.8160s/sat	Cristobalite	-0.2084
Goethite	6.0000s/sat	Beidellit-H	-0.3694
Whitlockite	5.7861s/sat	Huntite	-0.3869
Ferrite-Mg	4.9347s/sat	Paragonite	-0.4483
Epidote-ord	4.8864s/sat	Clinochl-7A	-0.5367
Epidote	4.8858s/sat	Lawsonite	-0.7385
Saponite-Ca	4.6580s/sat	Diaspore	-0.8740
Saponite-Mg	4.6534s/sat	Albite low	-0.8800
Ferrite-Ca	4.6272s/sat	Albite	-0.8801
Saponite-K	4.2339s/sat	Rhodochrosite	-0.8811
Saponite-Na	4.1334s/sat	Gypsum	-0.9221
Talc	3.8793s/sat	Amrph^silica	-0.9889
Clinoptil-K	3.4650s/sat	Petalite	-1.0124
Saponite-H	3.3750s/sat	Mordenite-Na	-1.1522
Phengite	3.3602s/sat	Anhydrite	-1.1738
Phlogopite	3.3307s/sat	Alstonite	-1.2223
Clinochl-14A	2.8989s/sat	Barytocalcite	-1.3836
Muscovite	2.8449s/sat	Analcime	-1.4266
Dolomite	2.8150s/sat	Malachite	-1.4292
Dolomite-ord	2.8150s/sat	Celestite	-1.5534
Tremolite	2.6040s/sat	Diopside	-1.5755
Smectite-low-Fe-	2.1619s/sat	Prehnite	-1.5914
Clinoptil-Ca	1.9391s/sat	Boehmite	-1.7585
Smectite-high-Fe	1.8343s/sat	Strengite	-1.7863
Witherite	1.8026s/sat	Bassanite	-1.8047
Mordenite-K	1.7324s/sat	Enstatite	-1.8764
Illite	1.7275s/sat	CaSO4^1/2H2O(bet	-1.9827
Fe(OH)3(ppd)	1.5271s/sat	Siderite	-1.9991
Maximum Microcli	1.4972s/sat	Smithsonite	-2.0326
K-feldspar	1.4959s/sat	Dawsonite	-2.1877
Strontianite	1.2819s/sat	CaHPO4^2H2O	-2.2318
Dolomite-dis	1.2144s/sat	Albite high	-2.2492
Chrysotile	1.1552s/sat	Clinoptil-Na	-2.2984
Kaolinite	1.1258s/sat	Kalsilite	-2.4827
Calcite	1.0065s/sat	Annite	-2.4841
Beidellit-Ca	0.9170s/sat	Ferrosilite	-2.5545
Beidellit-Mg	0.9116s/sat	Clinoptil-Mg	-2.6090
Heulandite	0.8571s/sat	Minnesotaite	-2.7820
Aragonite	0.8409s/sat	Jadeite	-2.8630
Barite	0.6199s/sat	FeO(c)	-2.8725
Sepiolite	0.5734s/sat	Nesquehonite	-2.9010
Laumontite	0.5025s/sat		

(only minerals with log Q/K > -3 listed)

Appendix 7-8. Mineral saturation indices of stream water calculated by Geochemist's Workbench at Location G.

Mineral saturation states			
	log Q/K		log Q/K
Antigorite	22.6711s/sat	Lawsonite	1.2854s/sat
Nontronit-Ca	17.3564s/sat	Sanidine high	1.2630s/sat
Nontronit-Mg	17.3532s/sat	Calcite	1.1202s/sat
Nontronit-K	16.9267s/sat	Aragonite	0.9547s/sat
Nontronit-Na	16.8292s/sat	Gibbsite	0.8510s/sat
CuFeO2(c)	14.1040s/sat	Tenorite	0.7627s/sat
Hematite	13.8568s/sat	Prehnite	0.7101s/sat
Hydroxyapatite	12.6051s/sat	Barite	0.6080s/sat
Magnetite	12.4960s/sat	MnHP04(c)	0.5339s/sat
Cronstedt-7A	12.0180s/sat	Quartz	0.3691s/sat
Ferrite-Cu	12.0009s/sat	Magnesite	0.2604s/sat
Andradite	11.1749s/sat	Tridymite	0.1973s/sat
Ba3(AsO4)2(c)	9.9639s/sat	Albite low	0.1532s/sat
Smectite-Reykjan	9.6457s/sat	Albite	0.1531s/sat
Epidote-ord	7.6561s/sat	Monohydrocalcite	0.1395s/sat
Epidote	7.6556s/sat	Huntite	0.1189s/sat
Goethite	6.4599s/sat	Chalcedony	0.0918s/sat
Ferrite-Mg	6.1618s/sat	Malachite	0.0090s/sat
Clinochl-14A	6.0130s/sat	Diaspore	0.0026s/sat
Whitlockite	5.9930s/sat	Mordenite-Na	-0.0984
Ferrite-Ca	5.8435s/sat	Ripidolit-7A	-0.1091
Saponite-Ca	5.8179s/sat	Clinoptil-Na	-0.1907
Saponite-Mg	5.8155s/sat	Cristobalite	-0.1964
Muscovite	5.5954s/sat	Annite	-0.3796
Clinoptil-K	5.5262s/sat	Analcime	-0.4023
Saponite-K	5.3858s/sat	Clinoptil-Mg	-0.4672
Saponite-Na	5.2907s/sat	Rhodochrosite	-0.5089
Phlogopite	5.1390s/sat	Margarite	-0.8450
Amesite-14A	4.8153s/sat	Boehmite	-0.8760
Talc	4.7134s/sat	Gypsum	-0.9178
Phengite	4.6371s/sat	Amrph^silica	-0.9704
Tremolite	4.5449s/sat	Alstonite	-0.9996
Saponite-H	4.4968s/sat	Diopside	-1.0187
Clinoptil-Ca	4.0486s/sat	Anhydrite	-1.1584
Illite	3.8985s/sat	Barytocalcite	-1.1609
Smectite-low-Fe-	3.7545s/sat	Albite high	-1.2085
Smectite-high-Fe	3.5847s/sat	Clinozoisite	-1.2830
Ripidolit-14A	3.3191s/sat	Zoisite	-1.3291
Dolomite	3.0496s/sat	Dawsonite	-1.3362
Dolomite-ord	3.0495s/sat	Daphnite-14A	-1.4726
Beidellit-Ca	3.0339s/sat	Kalsilite	-1.4808
Beidellit-Mg	3.0306s/sat	Celestite	-1.5551
Heulandite	2.9381s/sat	Strengite	-1.5805
Petalite	2.9150s/sat	Enstatite	-1.5866
Kaolinite	2.8862s/sat	Minnesotaite	-1.6469
Mordenite-K	2.7629s/sat	Chamosite-7A	-1.6957
Beidellit-K	2.6018s/sat	Siderite	-1.7693
Clinochl-7A	2.5865s/sat	Bassanite	-1.7891
Laumontite	2.5495s/sat	Jadeite	-1.8396
Beidellit-Na	2.5066s/sat	CaS04^1/2H20(bet	-1.9657
Maximum Microcli	2.5055s/sat	Anthophyllite	-1.9983
K-feldspar	2.5043s/sat	Wairakite	-2.0684
Paragonite	2.3300s/sat	Spodumene-a	-2.1296
Fe(OH)3(ppd)	1.9993s/sat	Ferrosilite	-2.1715
Chrysotile	1.9727s/sat	CaHP04^2H2O	-2.2555
Pyrophyllite	1.9332s/sat	FeO(c)	-2.4969
Witherite	1.8916s/sat	Kyanite	-2.5278
Beidellit-H	1.7090s/sat	Nesquehonite	-2.7647
Sepiolite	1.6798s/sat	Andalusite	-2.8195
Dolomite-dis	1.4573s/sat	Brucite	-2.9104
Strontianite	1.3748s/sat		

(only minerals with log Q/K > -3 listed)

Appendix 7-9. Mineral saturation indices of seep water calculated by Geochemist's Workbench at Location G.

Mineral saturation states			
	log Q/K		log Q/K
CuFeO2(c)	13.2686s/sat	Epidote	0.3065s/sat
Nontronit-Ca	10.2874s/sat	Tridymite	0.2693s/sat
Nontronit-Mg	10.2598s/sat	Chalcedony	0.1640s/sat
Nontronit-K	9.9196s/sat	Saponite-Ca	0.1270s/sat
Nontronit-Na	9.7802s/sat	Saponite-Mg	0.1006s/sat
Ba3(AsO4)2(c)	8.2524s/sat	Cristobalite	-0.1298
Hematite	6.8274s/sat	Saponite-K	-0.2443
Cronstedt-7A	6.8142s/sat	Diaspore	-0.2668
Magnetite	6.3088s/sat	Greenalite	-0.3016
Smectite-Reykjan	4.8510s/sat	Saponite-Na	-0.3802
Muscovite	4.3748s/sat	Chamosite-7A	-0.4441
Clinoptil-K	4.3600s/sat	Talc	-0.5867
Ferrite-Cu	3.0307s/sat	Gypsum	-0.7042
Goethite	2.9516s/sat	Albite low	-0.7259
Ferrite-Zn	2.7781s/sat	Albite	-0.7260
Illite	2.6941s/sat	Lawsonite	-0.8198
Daphnite-14A	2.5622s/sat	Mordenite-Na	-0.8307
Kaolinite	2.5439s/sat	Ripidolit-14A	-0.8661
Clinoptil-Ca	2.5148s/sat	Andradite	-0.8944
Beidellit-Ca	2.4096s/sat	Daphnite-7A	-0.9075
Beidellit-Mg	2.3819s/sat	Petalite	-0.9103
Mordenite-K	2.1804s/sat	Saponite-H	-0.9231
Phengite	2.1455s/sat	Amorph [^] silica	-0.9284
Beidellit-K	2.0383s/sat	Anhydrite	-0.9860
Beidellit-Na	1.9023s/sat	Tenorite	-1.1330
Maximum Microcli	1.7825s/sat	Boehmite	-1.1677
K-feldspar	1.7810s/sat	Phlogopite	-1.2035
Pyrophyllite	1.7024s/sat	Ferrosilite	-1.2627
Annite	1.4867s/sat	Analcime	-1.3596
Smectite-low-Fe-	1.4218s/sat	Celestite	-1.4498
Beidellit-H	1.3567s/sat	Fe(OH)3(ppd)	-1.5554
Minnesotaite	1.2435s/sat	Bassanite	-1.6177
Heulandite	1.1762s/sat	Clinoptil-Na	-1.6560
Paragonite	0.9425s/sat	FeO(c)	-1.6722
Smectite-high-Fe	0.8258s/sat	CaSO4 [^] 1/2H2O(bet	-1.7995
Gibbsite	0.6188s/sat	Albite high	-2.1157
Laumontite	0.5810s/sat	Clinoptil-Mg	-2.2189
Sanidine high	0.5118s/sat	Kalsilite	-2.4034
Barite	0.4515s/sat	Jadeite	-2.7939
Quartz	0.4452s/sat	Ferrite-Mg	-2.8806
Epidote-ord	0.3073s/sat	Hercynite	-2.8878
(only minerals with log Q/K > -3 listed)			

Appendix 7-10. Mineral saturation indices of stream water calculated by Geochemist's Workbench at Location H.

Mineral saturation states			
	log Q/K		log Q/K
Antigorite	27.3453s/sat	Beidellit-K	1.0042s/sat
Nontronit-Mg	16.5851s/sat	Beidellit-Na	0.9859s/sat
Nontronit-Ca	16.5678s/sat	Paragonite	0.8019s/sat
Nontronit-K	16.0740s/sat	Magnesite	0.5843s/sat
Nontronit-Na	16.0540s/sat	Pyrophyllite	0.4399s/sat
Hematite	13.9312s/sat	Barite	0.3994s/sat
CuFeO2(c)	13.0789s/sat	Gibbsite	0.3982s/sat
Magnetite	12.6411s/sat	Lawsonite	0.3579s/sat
Ferrite-Zn	12.2204s/sat	Monohydrocalcite	0.3143s/sat
Cronstedt-7A	11.9263s/sat	Sanidine high	0.3121s/sat
Andradite	11.5103s/sat	Quartz	0.1876s/sat
Ferrite-Cu	11.4860s/sat	Beidellit-H	0.1649s/sat
Hydroxyapatite	10.1823s/sat	Tenorite	0.0865s/sat
Smectite-Reykjan	9.1876s/sat	Tridymite	0.0236s/sat
Epidote-ord	6.9482s/sat	Rhodochrosite	0.0087s/sat
Epidote	6.9482s/sat	Chalcedony	-0.0821
Ferrite-Mg	6.8389s/sat	Prehnite	-0.0827
Goethite	6.4840s/sat	Ripidolit-7A	-0.3217
Ferrite-Ca	6.4143s/sat	Cristobalite	-0.3595
Clinochl-14A	6.3667s/sat	Diaspore	-0.3774
Saponite-Mg	6.0341s/sat	Albite low	-0.5561
Saponite-Ca	6.0170s/sat	Albite	-0.5562
Saponite-K	5.5214s/sat	Diopside	-0.7116
Saponite-Na	5.5032s/sat	Anthophyllite	-0.7329
Tremolite	5.3556s/sat	Petalite	-0.7851
Phlogopite	5.1341s/sat	Gypsum	-0.8436
Talc	4.9582s/sat	Analcime	-0.9268
Saponite-H	4.6869s/sat	Anhydrite	-1.0036
Whitlockite	4.3767s/sat	Amrph [^] silica	-1.0879
Amesite-14A	4.3167s/sat	Mordenite-Na	-1.1581
Muscovite	3.7511s/sat	Boehmite	-1.2132
Phengite	3.7271s/sat	Annite	-1.2934
Dolomite	3.5165s/sat	Enstatite	-1.3361
Dolomite-ord	3.5164s/sat	Malachite	-1.3607
Ripidolit-14A	3.0384s/sat	Celestite	-1.4455
Clinochl-7A	3.0060s/sat	Smithsonite	-1.4698
Smectite-low-Fe-	2.9084s/sat	Dawsonite	-1.6201
Smectite-high-Fe	2.8904s/sat	Bassanite	-1.6327
Clinoptil-K	2.8363s/sat	Siderite	-1.7250
Chrysotile	2.5975s/sat	CaSO4 [^] 1/2H2O(bet	-1.7991
Illite	2.3737s/sat	Albite high	-1.8640
Fe(OH)3(ppd)	2.1119s/sat	Kalsilite	-2.0314
Dolomite-dis	1.9841s/sat	Ferrosilite	-2.2638
Sepiolite	1.7940s/sat	Minnesotaite	-2.2756
Witherite	1.7399s/sat	Clinoptil-Na	-2.3091
Clinoptil-Ca	1.7295s/sat	Clinozoisite	-2.3183
Kaolinite	1.6766s/sat	Margarite	-2.3279
Beidellit-Mg	1.5170s/sat	Zoisite	-2.3626
Maximum Microcli	1.5004s/sat	Jadeite	-2.3691
Beidellit-Ca	1.4997s/sat	FeO(c)	-2.3924
K-feldspar	1.4994s/sat	Nesquehonite	-2.4053
Strontianite	1.4964s/sat	Brucite	-2.4994
Mordenite-K	1.4169s/sat	Clinoptil-Mg	-2.5147
Huntite	1.3463s/sat	Strengite	-2.5154
Calcite	1.3133s/sat	Chamosite-7A	-2.5539
Laumontite	1.2874s/sat	Daphnite-14A	-2.6833
Heulandite	1.1634s/sat	Rhodonite	-2.8436
Aragonite	1.1489s/sat		

(only minerals with log Q/K > -3 listed)

Appendix 7-11. Mineral saturation indices of seep water calculated by Geochemist's Workbench at Location H.

Mineral saturation states			
	log Q/K		log Q/K
Nontronit-Mg	8.0010s/sat	Tridymite	0.2609s/sat
Nontronit-Ca	7.9740s/sat	Barite	0.2468s/sat
Nontronit-Na	7.4919s/sat	Clinoptil-Mg	0.2222s/sat
Nontronit-K	7.4592s/sat	Boehmite	0.1787s/sat
Muscovite	7.3125s/sat	Annite	0.1671s/sat
Clinoptil-K	5.3735s/sat	Chalcedony	0.1552s/sat
Beidellit-Mg	5.2174s/sat	Cristobalite	-0.1213
Beidellit-Ca	5.1904s/sat	Alunite	-0.1221
Illite	5.0006s/sat	Gypsum	-0.1679
Kaolinite	4.9171s/sat	Analcime	-0.2039
Beidellit-Na	4.7083s/sat	Ripidolit-14A	-0.3034
Smectite-Reykjan	4.6877s/sat	Kyanite	-0.3052
Beidellit-K	4.6737s/sat	Saponite-Mg	-0.3123
Paragonite	4.5312s/sat	Anhydrite	-0.3201
Hematite	4.4309s/sat	Saponite-Ca	-0.3390
Clinoptil-Ca	4.3925s/sat	Andalusite	-0.5738
Beidellit-H	4.2674s/sat	Celestite	-0.6399
Pyrophyllite	4.1611s/sat	Minnesotaitite	-0.6616
Magnetite	3.3671s/sat	Hercynite	-0.6929
Heulandite	3.1168s/sat	Saponite-Na	-0.8211
Cronstedt-7A	3.1030s/sat	Amrph [^] silica	-0.8455
Petalite	2.9407s/sat	Saponite-K	-0.8557
Mordenite-K	2.6854s/sat	Albite high	-0.8996
Laumontite	2.5287s/sat	Sillimanite	-0.9283
Phengite	2.3286s/sat	Bassanite	-0.9491
Maximum Microcli	2.2937s/sat	CaSO4 [^] 1/2H2O(bet	-1.1146
K-feldspar	2.2927s/sat	Saponite-H	-1.2572
Smectite-low-Fe-	2.1706s/sat	Phlogopite	-1.3411
Daphnite-14A	1.9085s/sat	Talc	-1.3668
Gibbsite	1.7791s/sat	Daphnite-7A	-1.4439
Goethite	1.7326s/sat	Prehnite	-1.5524
Smectite-high-Fe	1.3913s/sat	Jadeite	-1.6466
Margarite	1.2327s/sat	Kalsilite	-1.7025
Lawsonite	1.1234s/sat	Ferrosilite	-1.7992
Sanidine high	1.1105s/sat	Wairakite	-1.8050
Diaspore	1.0104s/sat	Corundum	-1.8058
Chamosite-7A	0.9052s/sat	FeO(c)	-2.1629
Epidote	0.7330s/sat	Spodumene-a	-2.1732
Epidote-ord	0.7330s/sat	Greenalite	-2.2095
Amesite-14A	0.6547s/sat	Clinochl-14A	-2.2629
Clinoptil-Na	0.5584s/sat	Clinozoisite	-2.3870
Quartz	0.4242s/sat	Zoisite	-2.4312
Albite low	0.4032s/sat	Fe(OH)3(ppd)	-2.6312
Albite	0.4031s/sat	Epsomite	-2.7988
Mordenite-Na	0.2756s/sat		

(only minerals with log Q/K > -3 listed)

Appendix 7-12. Mineral saturation indices of stream water calculated by Geochemist's Workbench at Location I.

Mineral saturation states			
	log Q/K		log Q/K
Nontronit-Ca	17.3830s/sat	Gibbsite	0.8044s/sat
Nontronit-Mg	17.3620s/sat	Sanidine high	0.8022s/sat
Nontronit-K	16.8772s/sat	Daphnite-14A	0.7539s/sat
Antigorite	16.8683s/sat	Petalite	0.6891s/sat
Nontronit-Na	16.8662s/sat	Annite	0.6189s/sat
Hematite	14.3760s/sat	Prehnite	0.4735s/sat
Magnetite	13.5663s/sat	Barite	0.4627s/sat
CuFeO2(c)	13.4666s/sat	Huntite	0.3208s/sat
Cronstedt-7A	13.3967s/sat	Sepiolite	0.2863s/sat
Ferrite-Zn	12.6601s/sat	Magnesite	0.2683s/sat
Ferrite-Cu	11.8922s/sat	Quartz	0.2661s/sat
Andradite	11.4338s/sat	Monohydrocalcite	0.2278s/sat
Smectite-Reykjan	9.2626s/sat	Ripidolit-7A	0.2239s/sat
Epidote	7.7320s/sat	Tridymite	0.1029s/sat
Epidote-ord	7.7320s/sat	Tenorite	0.0387s/sat
Ferrite-Mg	6.8214s/sat	Diaspore	0.0366s/sat
Goethite	6.7049s/sat	Chalcedony	-0.0029
Ferrite-Ca	6.6311s/sat	Albite low	-0.0378
Muscovite	5.0549s/sat	Albite	-0.0379
Clinochl-14A	4.9741s/sat	Rhodochrosite	-0.0612
Saponite-Ca	4.9211s/sat	Cristobalite	-0.2791
Saponite-Mg	4.8998s/sat	Mordenite-Na	-0.4814
Saponite-K	4.4135s/sat	Analcime	-0.4867
Saponite-Na	4.4043s/sat	Minnesotaitaite	-0.5331
Amesite-14A	4.1711s/sat	Chamosite-7A	-0.6930
Phlogopite	4.1453s/sat	Gypsum	-0.7242
Clinoptil-K	4.1235s/sat	Margarite	-0.7531
Talc	3.7958s/sat	Boehmite	-0.7946
Phengite	3.7926s/sat	Anhydrite	-0.8754
Saponite-H	3.6364s/sat	Clinoptil-Na	-0.9557
Ripidolit-14A	3.5768s/sat	Celestite	-1.0011
Smectite-low-Fe-	3.3913s/sat	Amrph^silica	-1.0028
Illite	3.3733s/sat	Siderite	-1.0714
Smectite-high-Fe	3.3477s/sat	Dawsonite	-1.1743
Dolomite	3.1109s/sat	Malachite	-1.2823
Dolomite-ord	3.1109s/sat	Diopside	-1.2906
Clinoptil-Ca	3.0875s/sat	Smithsonite	-1.3080
Tremolite	3.0300s/sat	Clinozoisite	-1.3334
Beidellit-Ca	2.7078s/sat	Albite high	-1.3399
Beidellit-Mg	2.6867s/sat	Clinoptil-Mg	-1.3724
Kaolinite	2.6522s/sat	Zoisite	-1.3775
Fe(OH)3(ppd)	2.3422s/sat	Bassanite	-1.5044
Heulandite	2.2861s/sat	CaSO4^1/2H2O(bet	-1.6697
Beidellit-K	2.2002s/sat	Kalsilite	-1.6942
Beidellit-Na	2.1909s/sat	Ferrosilite	-1.7030
Laumontite	2.1721s/sat	Enstatite	-1.7381
Paragonite	2.1419s/sat	Greenalite	-1.7651
Mordenite-K	2.0604s/sat	FeO(c)	-1.9084
Maximum Microcli	1.9847s/sat	Jadeite	-1.9295
K-feldspar	1.9837s/sat	Wairakite	-2.1585
Strontianite	1.7255s/sat	Hercynite	-2.3850
Clinochl-7A	1.6203s/sat	Kyanite	-2.4093
Witherite	1.5927s/sat	Jarosite-K	-2.4551
Dolomite-dis	1.5849s/sat	Daphnite-7A	-2.5976
Pyrophyllite	1.5809s/sat	Andalusite	-2.6776
Beidellit-H	1.4183s/sat	Nesquehonite	-2.7202
Chrysotile	1.2800s/sat	Brucite	-2.9822
Calcite	1.2290s/sat	Spodumene-a	-2.9822
Lawsonite	1.0827s/sat	Rhodonite	-2.9966
Aragonite	1.0647s/sat		

(only minerals with log Q/K > -3 listed)

Appendix 7-13. Mineral saturation indices of stream water calculated by Geochemist's Workbench at Location J.

Mineral saturation states			
	log Q/K		log Q/K
Antigorite	19.9745s/sat	Beidellit-H	1.0747s/sat
Nontronit-Ca	16.8227s/sat	Lawsonite	0.9733s/sat
Nontronit-Mg	16.8052s/sat	Gibbsite	0.7285s/sat
Nontronit-Na	16.3476s/sat	Sepiolite	0.6809s/sat
Nontronit-K	16.2978s/sat	Sanidine high	0.6012s/sat
Hematite	13.9632s/sat	Petalite	0.5328s/sat
CuFeO2(c)	13.1223s/sat	Barite	0.4694s/sat
Magnetite	12.8412s/sat	Prehnite	0.4500s/sat
Cronstedt-7A	12.3285s/sat	Huntite	0.4307s/sat
Ferrite-Zn	12.0021s/sat	Magnesite	0.3024s/sat
Ferrite-Cu	11.4053s/sat	Monohydrocalcite	0.2425s/sat
Andradite	11.2907s/sat	Quartz	0.2247s/sat
Hydroxyapatite	10.9084s/sat	Tridymite	0.0609s/sat
Smectite-Reykjan	9.2310s/sat	Tenorite	-0.0282
Epidote-ord	7.4981s/sat	Chalcedony	-0.0448
Epidote	7.4980s/sat	Diaspore	-0.0454
Ferrite-Mg	6.5441s/sat	Albite low	-0.0552
Goethite	6.4997s/sat	Albite	-0.0554
Ferrite-Ca	6.3307s/sat	Ripidolit-7A	-0.2110
Clinochl-14A	5.4760s/sat	Cristobalite	-0.3220
Saponite-Ca	5.2420s/sat	Rhodochrosite	-0.3615
Saponite-Mg	5.2243s/sat	Analcime	-0.4630
Whitlockite	4.9032s/sat	Annite	-0.5043
Saponite-Na	4.7668s/sat	Mordenite-Na	-0.5827
Saponite-K	4.7152s/sat	Gypsum	-0.7196
Muscovite	4.7009s/sat	Anhydrite	-0.8777
Phlogopite	4.4224s/sat	Boehmite	-0.8802
Amesite-14A	4.3874s/sat	Celestite	-1.0028
Talc	4.1064s/sat	Margarite	-1.0437
Saponite-H	3.9327s/sat	Amrph^silica	-1.0494
Tremolite	3.7461s/sat	Daphnite-14A	-1.0740
Phengite	3.7174s/sat	Diopside	-1.0898
Clinoptil-K	3.5615s/sat	Clinoptil-Na	-1.1583
Smectite-low-Fe-	3.1882s/sat	Dawsonite	-1.1820
Dolomite	3.1621s/sat	Albite high	-1.3619
Dolomite-ord	3.1620s/sat	Clinozoisite	-1.4504
Ripidolit-14A	3.1475s/sat	Zoisite	-1.4947
Smectite-high-Fe	3.1104s/sat	Siderite	-1.5061
Illite	3.0893s/sat	Bassanite	-1.5068
Clinoptil-Ca	2.6431s/sat	Chamosite-7A	-1.5182
Kaolinite	2.4127s/sat	Malachite	-1.5391
Beidellit-Ca	2.3887s/sat	Minnesotaite	-1.6258
Beidellit-Mg	2.3712s/sat	Enstatite	-1.6298
Fe(OH)3(ppd)	2.1296s/sat	Smithsonite	-1.6706
Clinochl-7A	2.1168s/sat	CaSO4^1/2H2O(bet	-1.6730
Laumontite	1.9777s/sat	Clinoptil-Mg	-1.8082
Heulandite	1.9657s/sat	Kalsilite	-1.8156
Paragonite	1.9652s/sat	Jadeite	-1.9054
Beidellit-Na	1.9136s/sat	Strengite	-2.0491
Beidellit-K	1.8620s/sat	Ferrosilite	-2.0582
Maximum Microcli	1.7882s/sat	FeO(c)	-2.2235
K-feldspar	1.7872s/sat	Wairakite	-2.3745
Mordenite-K	1.7794s/sat	Kyanite	-2.6263
Strontianite	1.7412s/sat	Nesquehonite	-2.6869
Chrysotile	1.6719s/sat	Anthophyllite	-2.7591
Dolomite-dis	1.6311s/sat	Greenalite	-2.7727
Witherite	1.6131s/sat	Brucite	-2.8307
Pyrophyllite	1.2521s/sat	Hercynite	-2.8710
Calcite	1.2420s/sat	Andalusite	-2.8964
Aragonite	1.0776s/sat	Spodumene-a	-2.9817
(only minerals with log Q/K > -3 listed)			

Appendix 7-14. Mineral saturation indices of stream water calculated by Geochemist's Workbench at Location K.

Mineral saturation states			
	log Q/K		log Q/K
Antigorite	20.5953s/sat	Gibbsite	1.0047s/sat
Hydroxyapatite	10.8981s/sat	Prehnite	0.9551s/sat
Nontronit-Ca	7.5465s/sat	Sanidine high	0.7693s/sat
Nontronit-Mg	7.5342s/sat	Petalite	0.7229s/sat
Nontronit-Na	7.0884s/sat	Sepiolite	0.6390s/sat
Nontronit-K	7.0184s/sat	Huntite	0.5746s/sat
Smectite-Reykjan	6.3837s/sat	Barite	0.4029s/sat
Clinochl-14A	6.2032s/sat	Magnesite	0.3446s/sat
Amesite-14A	5.6769s/sat	Monohydrocalcite	0.2498s/sat
Muscovite	5.4232s/sat	Diaspore	0.2395s/sat
Saponite-Ca	5.3508s/sat	Quartz	0.1823s/sat
Saponite-Mg	5.3382s/sat	Albite low	0.1752s/sat
Whitlockite	4.8960s/sat	Albite	0.1751s/sat
Saponite-Na	4.8927s/sat	Smectite-high-Fe	0.1722s/sat
Saponite-K	4.8209s/sat	Margarite	0.0597s/sat
Hematite	4.7569s/sat	Tridymite	0.0194s/sat
Phlogopite	4.7555s/sat	Chalcedony	-0.0863
Talc	4.1047s/sat	Analcime	-0.1898
Saponite-H	4.0403s/sat	Cristobalite	-0.3622
Phengite	3.8870s/sat	Rhodochrosite	-0.3879
Tremolite	3.7650s/sat	Mordenite-Na	-0.4353
Clinoptil-K	3.7207s/sat	Boehmite	-0.5902
Illite	3.6070s/sat	Clinozoisite	-0.6439
Epidote	3.4058s/sat	Zoisite	-0.6880
Epidote-ord	3.4057s/sat	Gypsum	-0.7638
Dolomite	3.2082s/sat	Dawsonite	-0.8530
Dolomite-ord	3.2082s/sat	Clinoptil-Na	-0.8635
Ferrite-Zn	2.9711s/sat	Anhydrite	-0.9121
Beidellit-Ca	2.8994s/sat	Magnetite	-0.9599
Kaolinite	2.8874s/sat	Celestite	-0.9838
Beidellit-Mg	2.8870s/sat	Diopside	-1.0767
Clinochl-7A	2.8518s/sat	Amrph^silica	-1.0843
Clinoptil-Ca	2.8192s/sat	Albite high	-1.1250
Paragonite	2.7586s/sat	Smithsonite	-1.5194
Beidellit-Na	2.4412s/sat	Bassanite	-1.5411
Laumontite	2.4053s/sat	Kalsilite	-1.5582
Beidellit-K	2.3695s/sat	Clinoptil-Mg	-1.5821
Heulandite	2.2690s/sat	Enstatite	-1.6034
Andradite	2.0553s/sat	Jadeite	-1.6328
Maximum Microcli	1.9499s/sat	CaSO4^1/2H2O(bet	-1.7061
K-feldspar	1.9489s/sat	Wairakite	-1.9161
Goethite	1.8949s/sat	Kyanite	-2.0823
Mordenite-K	1.8590s/sat	Andalusite	-2.3499
Strontianite	1.8015s/sat	Fe(OH)3(ppd)	-2.4648
Chrysotile	1.7569s/sat	Ferrite-Mg	-2.5732
Dolomite-dis	1.6843s/sat	Nesquehonite	-2.6437
Pyrophyllite	1.6516s/sat	Anthophyllite	-2.6528
Witherite	1.5931s/sat	Sillimanite	-2.7036
Beidellit-H	1.5841s/sat	Brucite	-2.7645
Lawsonite	1.4824s/sat	Anorthite	-2.7863
Smectite-low-Fe-	1.3756s/sat	Spodumene-a	-2.7961
Calcite	1.2519s/sat	Ferrite-Ca	-2.8160
Aragonite	1.0876s/sat		

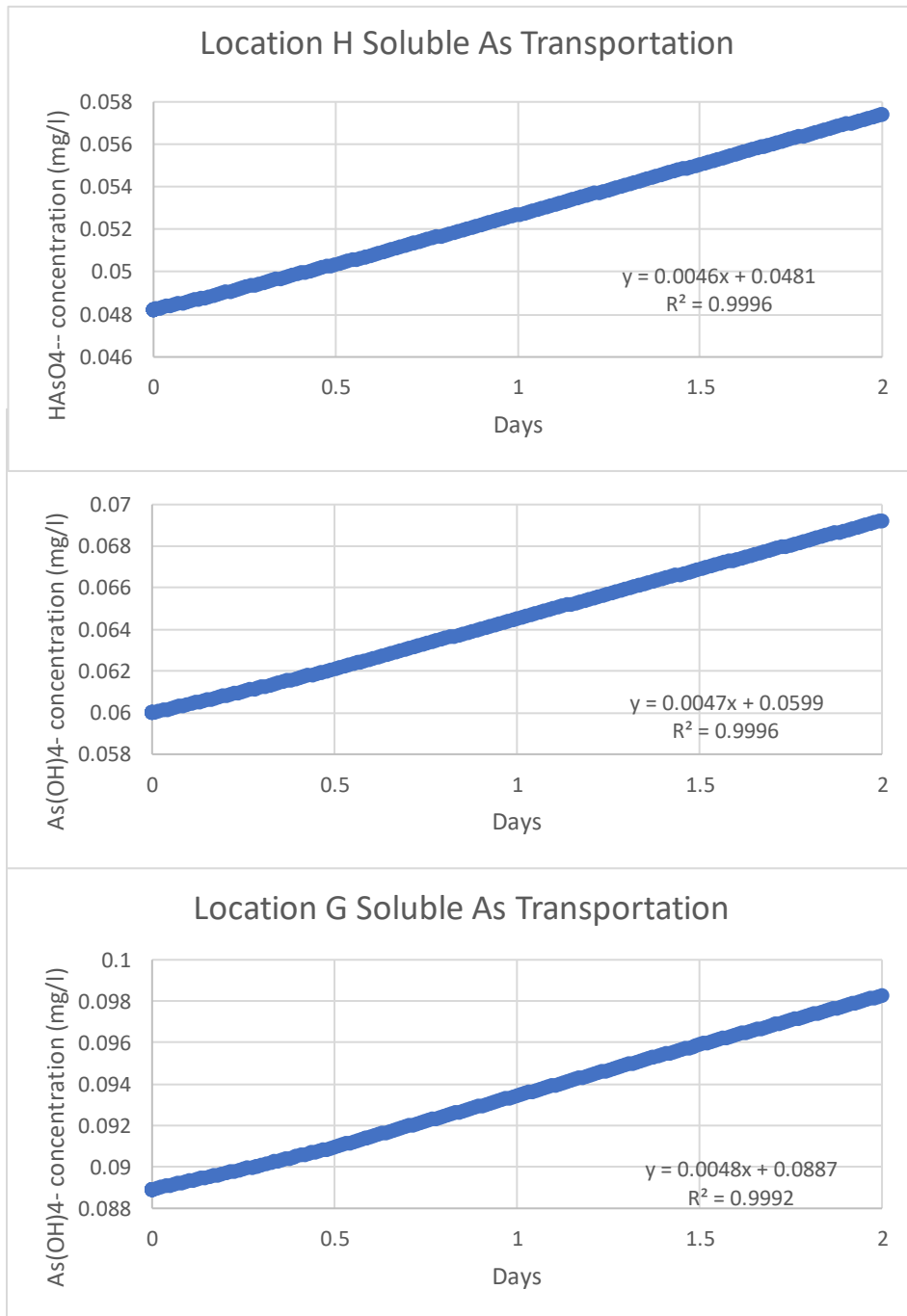
(only minerals with log Q/K > -3 listed)

Appendix 7-15. Mineral saturation indices of stream water calculated by Geochemist's Workbench at Location L.

Mineral saturation states		log Q/K	
	log Q/K		log Q/K
Antigorite	31.7481s/sat	Prehnite	5.7054s/sat
Clinoptil-K	28.7805s/sat	Kalsilite	5.6269s/sat
Nontronit-K	25.3292s/sat	Margarite	5.4425s/sat
Nontronit-Ca	24.1088s/sat	Lawsonite	5.3536s/sat
Nontronit-Mg	24.0830s/sat	Ba3(AsO4)2(c)	5.3433s/sat
Nontronit-Na	23.8397s/sat	Albite low	5.3040s/sat
Cronstedt-7A	18.0744s/sat	Albite	5.3039s/sat
Clinoptil-Ca	17.2904s/sat	Clinozoisite	4.8458s/sat
Muscovite	16.9515s/sat	Zoisite	4.8009s/sat
Andradite	16.1989s/sat	Wairakite	4.4774s/sat
Hematite	16.1958s/sat	Anthophyllite	4.4276s/sat
Magnetite	16.1655s/sat	Chamosite-7A	4.1487s/sat
CuFeO2(c)	15.2240s/sat	Albite high	3.9787s/sat
Ferrite-Zn	14.8873s/sat	Alunite	3.9468s/sat
Smectite-Reykjan	14.8104s/sat	Arcanite	3.6685s/sat
Clinoptil-Na	14.6935s/sat	Analcime	3.6094s/sat
Phengite	14.6454s/sat	Fe(OH)3(ppd)	3.2200s/sat
Ferrite-Cu	14.4719s/sat	Greenalite	3.1241s/sat
Mordenite-K	14.3893s/sat	Chrysotile	2.9767s/sat
Epidote-ord	13.8532s/sat	Jadeite	2.1686s/sat
Epidote	13.8530s/sat	Gibbsite	1.8425s/sat
Petalite	13.8152s/sat	Barite	1.7735s/sat
Phlogopite	13.1971s/sat	Cordier [^] hydr	1.6544s/sat
Illite	13.0649s/sat	Quartz	1.5105s/sat
Annite	12.8590s/sat	Tridymite	1.3440s/sat
Heulandite	12.7556s/sat	Chalcedony	1.2383s/sat
Clinoptil-Mg	12.7355s/sat	Spodumene-a	1.0709s/sat
Maximum Microcli	11.8341s/sat	Diaspore	1.0431s/sat
K-feldspar	11.8331s/sat	Jarosite-Na	0.9857s/sat
Tremolite	11.1054s/sat	Cristobalite	0.9574s/sat
Beidellit-K	10.8070s/sat	Anorthite	0.9521s/sat
Sanidine high	10.6283s/sat	Tenorite	0.8360s/sat
Smectite-low-Fe-	10.5720s/sat	Kyanite	0.7884s/sat
Daphnite-14A	10.5100s/sat	Gypsum	0.7040s/sat
Smectite-high-Fe	10.3125s/sat	Diopside	0.6403s/sat
Saponite-K	10.2212s/sat	Anhydrite	0.5177s/sat
Ripidolit-14A	10.1355s/sat	Andalusite	0.5109s/sat
Amesite-14A	9.6007s/sat	Celestite	0.4419s/sat
Beidellit-Ca	9.5884s/sat	Hercynite	0.3577s/sat
Beidellit-Mg	9.5625s/sat	Ferrosilite	0.3130s/sat
Paragonite	9.5221s/sat	Grossular	0.2596s/sat
Clinochl-14A	9.3949s/sat	Amrph [^] silica	0.2145s/sat
Beidellit-Na	9.3192s/sat	Boehmite	0.1935s/sat
Saponite-Ca	9.0025s/sat	Sillimanite	0.1499s/sat
Saponite-Mg	8.9768s/sat	Bassanite	-0.1118
Laumontite	8.9199s/sat	CaSO4 [^] 1/2H2O(bet	-0.2816
Saponite-Na	8.7333s/sat	Nepheline	-0.7648
Pyrophyllite	8.5750s/sat	Hedenbergite	-0.7751
Jarosite-K	8.4074s/sat	Enstatite	-0.8021
Beidellit-H	8.3273s/sat	Cordier [^] anhy	-0.8367
Ferrite-Mg	8.2593s/sat	Fayalite	-1.1046
Ferrite-Ca	8.0902s/sat	Analc-dehydr	-1.1162
Talc	7.9885s/sat	FeO(c)	-1.1435
Saponite-H	7.7460s/sat	CaSi2O5 [^] 2H2O	-1.5090
Goethite	7.6207s/sat	Corundum	-1.8165
Mordenite-Na	7.3433s/sat	Rhodonite	-2.0424
Kaolinite	7.1917s/sat	Epsomite	-2.1835
Daphnite-7A	7.1274s/sat	Hexahydrite	-2.4245
Minnesotait	6.8327s/sat	Fe(OH)2(ppd)	-2.6303
Ripidolit-7A	6.7534s/sat	Wollastonite	-2.6958
Sepiolite	6.7467s/sat	Pentahydrite	-2.7687
Clinochl-7A	6.0130s/sat	Wustite	-2.9355

(only minerals with log Q/K > -3 listed)

Appendix 7-16. Plots of soluble As being released from into stream water from 0.11% arsenopyrite dissolution calculated by Geochemist's Workbench at Whitewood Creek (Locations F, G, and H). The initial concentrations are the measured levels from Ji (2021).



Appendix 7-17. Plots of soluble As being released from into stream water from 15% arsenopyrite dissolution calculated by Geochemist's Workbench at Whitewood Creek (Locations F, G, and H). The initial concentrations are the measured levels from Ji (2021).

